NASA Contractor Report 165634

Advanced Manufacturing Development of a Composite Empennage Component for L-1011 Aircraft

Phase II - Final Report Design and Analysis

A.C. Jackson, J.F. Crocker, J.C. Ekvall, R.R. Eudaily, B. Mosesian, R.R. Van Cleave, J. Van Hamersveld

Lockheed Corporation
Lockheed-California Company
Post Office Box 551
Burbank, California 91520

CONTRACT NAS1-14000
APRIL 1981

National Aeronautics and Space Administration

Langley Research Center
Hampton, Virginia 23665

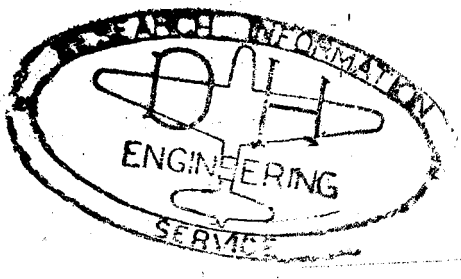

215

1. REPORT NO.	2. GOVERNMENT ACCESSION NO.	3. RECIPIENT'S CATALOG NO.
NASA - CR-165634		

4. TITLE AND SUBTITLE	5. REPORT DATE
ADVANCED MANUFACTURING DEVELOPMENT OF A COMPOSITE EMPENNAGE COMPONENT FOR L-1011 AIRCRAFT Phase II Final Report Design and Analysis	JANUARY 1981
	6. PERFORMING ORG. CODE: D76-23
7. AUTHOR(S) A.C. Jackson, J.F. Crocker, J.C. Ekvall, R.R. Eudaily, B. Mosesian, R.R. Van Cleave, J. Van Hamersveld	8. PERFORMING ORG. REPORT NO.: LR 29723
9. PERFORMING ORGANIZATION NAME AND ADDRESS Lockheed Corporation Lockheed-California Company P.O. Box 551 Burbank, California 91520	10. WORK UNIT NO.
	11. CONTRACT OR GRANT NO.: NAS1-14000
	13. TYPE OF REPORT, PERIOD COVERED: Contractor Report
12. SPONSORING AGENCY NAME AND ADDRESS National Aeronautics and Space Administration Washington, D.C. 20546	14. SPONSORING AGENCY CODE

15. SUPPLEMENTARY NOTES
Langley technical monitor: Dr. Herbert A. Leybold

16. ABSTRACT The activities documented in this report are associated with Phase II of the Advanced Composite Vertical Fin program. This phase included the detail design and analysis, material verification, producibility studies, process development and concept verification.

The composite fin design consists of two one-piece cocured covers, two one-piece cocured spars and eleven ribs. The lower ribs are truss ribs with graphite/epoxy caps and aluminum truss members. The upper three ribs are a sandwich design with graphite/epoxy face sheets and a syntactic epoxy core. The design achieves a 27% weight saving compared to the metal box. The fastener count has been reduced from over 40,000 to less than 7000.

The structural integrity of the composite fin is being verified by analysis and test. The static, fail-safe and flutter analyses have been completed. An extensive test program has established the material behaviour under a range of conditions and critical subcomponents have been tested to verify the structural concepts.

17. KEY WORDS (SUGGESTED BY AUTHOR(S))
Composites, Materials, Primary Structure, Design, Testing, Transport Aircraft, Graphite Epoxy

19. SECURITY CLASSIF. (OF THIS REPORT)	20. SECURITY CLASSIF. (OF THIS PAGE)	21. NO. OF PAGES	22. PRICE*
Unclassified	Unclassified	215	

FOREWORD

This report was prepared by Lockheed-California Company and Lockheed-Georgia Company under Contract NAS1-14000, Advanced Manufacturing Development of a Composite Empennage Component for L-1011 Aircraft. It is the final report for Phase II - Design and Analysis activity covering work completed between 1 February 1977 and 27 June 1980. This program is sponsored by the National Aeronautics and Space Administration (NASA) Langley Research Center. The program manager for Lockheed is Mr. Fred C. English. Mr. Herman L. Bohon is project manager for NASA Langley. The technical representative for NASA, Langley is Dr. Herbert A. Leybold.

Engineering Development activity (Phase I) has been reported previously in NASA CR-144986. Subsequent phases include fabrication and test of full-scale graphite-epoxy L-1011 vertical fin structural boxes.

The following Lockheed personnel were principal contributers to the program during Phase II:

At Lockheed California Company:

ENGINEERING:	A. M. James A. C. Jackson	- Engineering Managers
	S. I. Bocarsly	- Structural Test
	J. C. Ekvall	- Design Allowables
	R. Jusko	- Structural Test
	R. Lowe	- Structural Test
	D. C. Novelli	- Materials and Processes
	D. R. Pascal	- Design
	J. P. Pearson	- Stress
	J. C. Salvaggio	- Weights
	R. R. Van Cleave	- Stress
	J. Van Hamersveld	- Producibility
MANUFACTURING:	R. A. Short	- Manufacturing Manager
	G. R. Brozovic	- Manufacturing Research
	J. Henkel	- Planning
QUALITY ASSURANCE:	B. Mosesian	- Quality Assurance Manager
	J. F. Crocker	- Non-destructive Test
	F. W. Diggles	- Quality Assurance

At Lockheed Georgia Company:

ENGINEERING:	W. E. Harvill	- Program Manager
	R. R. Eudaily	- Engineering Manager
	R. E. Barrie	- Design
	D. P. Bierce	- Structural Analysis
	W. M. McGee	- Structural Test
	M. W. Lindsey	- Materials and Processes
	R. D. O'Brien	- Cost and Producibility
MANUFACTURING:	F. Blackton	- Manufacturing Manager
	R. B. Cantley	- Tooling and Fabrication Manager
	T. N. Bridges	- Tooling Design
	W. W. Barber	- Fabrication
QUALITY ASSURANCE:	G. A. Swain	- Quality Assurance Manager

TABLE OF CONTENTS

Section		Page
	FOREWORD	iii
	LIST OF FIGURES	ix
	LIST OF TABLES	xv
	SUMMARY	1
	INTRODUCTION	2
	SYMBOLS	5
1	COMPONENT DEFINITION	7
1.1	Design Configuration	7
1.1.1	Covers	7
1.1.2	Ribs	10
1.1.3	Spars	16
1.1.4	Box assembly	20
1.1.5	Fin installation	21
1.1.6	Weight status	21
1.2	Structural Analysis	21
1.2.1	Design loads	24
1.2.2	Analysis design allowables	24
1.2.3	Cover analysis	24
1.2.4	Rib analysis	34
1.2.5	Spar Analysis	43
1.2.6	Flutter analysis	50
2	MATERIAL VERIFICATION	51
2.1	Material Qualification	51
2.2	Laminate Durability-Test H13D	51
2.3	Defect and Damage Tolerance	51
2.3.1	Evaluation of defect tolerance in composites - H12B	51
2.3.2	Graphite/aluminum corrosion barrier - test H18	60

TABLE OF CONTENTS (Continued)

Section		Page
2.3.3	Environmental resistance of lightning protection techniques - test H19	61
2.3.4	Evaluation of crack tolerance in composites - test H12A1	61
2.3.5	Impact damage tolerance test H12A2	64
2.4	Design Allowables	76
2.4.1	Test program	76
2.4.2	Laminate strength prediction	77
2.4.3	Summary of test data	77
2.4.4	Calculation of "B" allowables	90
2.4.5	Laminate design allowables	93
2.4.6	Bearing strength and push-through strength	98
3	PRODUCIBILITY STUDIES	108
3.1	Ground Rules	108
3.2	Cost Reduction Candidate Matrix	108
3.2.1	Producibility/cost reduction, covers and ribs	115
3.2.2	Producibility/cost reduction, spars	115
3.2.3	Producibility/cost reduction, box assembly	115
3.3	Selected Configuration	115
3.3.1	Selected items - cover and ribs	115
4	PROCESS VERIFICATION	117
4.1	Covers - Manufacturing Process Development	117
4.1.1	Mandrel development	117
4.1.2	Processing studies	120
4.2	Ribs - Manufacturing Process Development	130
4.2.1	Truss rib process	131
4.2.2	Solid web rib process	133
4.3	Spars - Manufacturing Process Development	135
4.3.1	Tooling development	135

TABLE OF CONTENTS (Continued)

Section		Page
4.4	Quality Assurance.	143
4.4.1	Laboratory tests.	143
4.4.2	Nondestructive inspection	144
4.4.3	Conformity certification.	150
5	CONCEPT VERIFICATION.	151
5.1	Truss Rib Test (H20A).	151
5.2	Rear Spar Tests (H20B)	155
5.2.1	Room temperature static (H20B1)	157
5.2.2	Hot wet static (H20B2).	157
5.3	Spar Web Tests (H21).....	160
5.3.1	Room temperature dry static (H21A-1).	160
5.3.2	Hot wet static (H21A-2)	163
5.3.3	Fatigue (H21B).	165
5.4	Front Spar Test (H23).	166
5.5	Rudder Hinge to Rib Attachment Tests (H24A).	168
5.5.1	Truss rib (H24AT)	168
5.5.2	Solid web rig (H24AS)	168
5.6	Actuator to Rib Attachment Tests (H24B & H24C)	171
5.6.1	Static test (H24B1)	171
5.6.2	VSS 97.19 actuator rib test (H24C).	174
5.7	Surface Attachment to Fuselage Tests (H24)	175
5.7.1	Compression test (H25).	175
5.7.2	Tension test (H25A)	178
5.8	Stiffener Runout at Front Spar Tests (H26)	180
5.8.1	Static test (H26A).	180
5.8.2	Fatigue test (H26B)	182
5.9	Surface Panel Stability Tests (H27).	184
5.9.1	3 bay test (H27).	184

TABLE OF CONTENTS (continued)

Section		Page
5.9.2	2 bay test (H27A)	187
5.10	Surface Panel Fail-Safe Test (H28)	188
5.11	Lightning Strike Tests (H29)	193
6	CONCLUSIONS	193
	REFERENCES	196

LIST OF FIGURES

Figure	Title	Page
1	ACVF program master schedule.	3
2	Advanced composite vertical fin-design configuration.	8
3	Cover thickness	8
4	Skin ply build up	9
5	Stiffener spacing	9
6	Stiffener configuration	10
7	Actuator rib design	11
8	Truss rib design.	11
9	Typical solid web rib design.	13
10	Truss rib cap design evolution.	14
11	Solid web rib design evolution.	15
12	Design changes - spar web material change	17
13	Spar web access hold.	17
14	Spar web stiffener.	18
15	Rear spar assembly.	19
16	Front spar assembly	19
17	Auxiliary spar assembly	20
18	Fin assembly, showing rib stations.	22
19	Root splice	22
20	Cover design ultimate loads	25
21	Spar cap axial loads and web shear flows (ultimate) .	26
22	Loads on rib at VSS 97.199.	26
23	Loads on rib at VSS 145.71.	27
24	Loads on rib at VSS 299.97.	27
25	Cover ultimate gross area compression strain (μm/m) .	30
26	Idealized stiffener	31
27	Fin to afterbody root joint	32
28	Stress levels at design ultimate load - MPa (ksi) . .	33

LIST OF FIGURES (Continued)

Figure	Title	Page
29	Maximum design loads and fail-safe loads for cover.	34
30	VSS 97.19 rib station NASTRAN 2-D model, fail-safe analysis	42
31	VSS 145.71 rib station NASTRAN 2-D model, fail-safe analysis	42
32	VSS 299.97 rib station NASTRAN 2-D model, fail-safe analysis	43
33	Typical web panel geometry.	46
34	Spar cap geometry	47
35	Web stiffener geometry and required stiffness data.	48
36	Spar to fuselage joints	49
37	Defect tolerance specimen	59
38	Typical environmental cycle	59
39	Corrosion test panel representing cover assembly.	62
40	Center cracked tension (CCT) specimen	63
41	Three-bay subpanel in the universal test machine at 16 degrees to the gun.	67
42	Impact panel in the universal test machine with the hailstone gun barrel in position.	68
43	Four-hat stiffened panel no. 1 after hailstone impacting, showing visible damage at locations 2, 4 and 7. Damage at the other locations was detected by NDI.	69
44	Close-up view of the hat-stiffened side of panel no. 1 after impacting	70
45	Panel no. 1 (4 hats wide) showing NDI identified damage	71
46	Panel no. 2 (4 hats wide) showing NDI identified damage	71
47	Panel no. 3 (3 hats wide) showing NDI identified damage	71

LIST OF FIGURES (Continued)

Figure	Title	Page
48	Undamaged four-bay subpanel after static compression test.	72
49	Subpanel no. 1 after two lifetimes of flight spectrum fatigue loading, showing defect growth (numbers indicate flights in thousands where growth observed . .	72
50	Subpanel no. 2 showing damage growth after two lifetimes of flight spectrum fatigue loading.	73
51	Three-hat-stiffened panel after residual static failure (hatched areas are previously identified delaminations).	73
52	Four-hat-stiffened panel after residual static testing (hatched areas are previously identified delaminations).	74
53	Typical ultrasonic trace ("C" scan) showing damage before and after fatigue test in low speed impact specimens	75
54	Design allowables approach.	76
55	Schematic showing the relation of the "B" allowable factor, K_B to test and predicted strength values. . . .	92
56	T300/5208 tape tension strength predictions - room temperature dry	95
57	Tape T300/5208 compression strength predictions - room temperature dry.	95
58	Hole radius effects on tensile strength	97
59	Compression impact data	97
60	T300/5208 Unidirectional tape tensile strength design allowables	99
61	T300/5208 Unidirectional tape tensile modulus	99
62	T300/5208 Unidirectional tape Poisson's ratio	100
63	T300/5208 Unidirectional tape compression strength design allowables	100
64	T300/5208 Unidirectional tape compression modulus . . .	101
65	T300/5208 Unidirectional tape inplane shear strength design allowable.	101

LIST OF FIGURES (Continued)

Figure	Title	Page
66	T300/5208 Unidirectional tape inplane shear and modulus.	102
67	Double lap shear bolt bearing specimen (DB).	104
68	Single lap shear countersunk screw bearing specimen (SB).	104
69	Joint coupon, aileron program (DL)	105
70	Push-through specimen.	106
71	Typical push-thru test load-deflection behavior.	107
72	Thinning of hat flange attributed to pressure imbalance.	118
73	Foam mandrel system.	119
74	Viscosity versus temperature (5208).	121
75	Cross section of hat-stiffened panel	123
76	Caul plates and inflatable mandrels.	125
77	Cured part	125
78	End view of cured part	126
79	Bleeding system assembly - low resin content prepreg . .	128
80	Cure cycles.	129
81	Truss rib cap molding components	131
82	Bleeder/breather system for truss rib.	132
83	Placement of armalon strips for solid web rib.	134
84	Bleeder/breather system for solid web ribs	134
85	Spar simulation tool for developing cure cycle	136
86	Process development T test specimens (All dimensions in mm (in)).	138
87	Cure cycle	139
88	Tool cover being lowered on base	143
89	Cure cycle for L-1011 ACVF spars	144
90	Ultrasonic standards	147

LIST OF FIGURES (Continued)

Figure	Title	Page
91	Inspection techniques for cover panels.	148
92	Ultrasonic C-scans of single-stage cover specimens. . . .	149
93	H20A load summary	155
94	H20A pressure distribution - actual vs test	156
95	H20B1 spar assembled test specimen.	157
96	H20B1 critical loading condition test set-up.	159
97	H20B1 failed specimen	159
98	Diagram of environmental chamber for H20B2.	161
99	Failed H20B2 specimen	162
100	H21 "picture frame" test panel.	162
101	Spar web test set-up, failure mode and highest strains. .	163
102	Thermal chamber and thermal cycle	164
103	X-rays of crack tip in access hole edge at 1/2 and 1 lifetime.	167
104	Failure mode, ultimate loads and maximum strains for front spar.	169
105	Truce rib specimen.	170
106	Truss rib failure showing elongated holes at upper hinge attachment location , ...	170
107	Fail-safe test modifications - solid web rib specimen . .	172
108	Actuator rib test specimen.	173
109	Actuator rib test specimen after testing. (Note the saw servering the actuator attachment).	174
110	Actuator rib test specimen.	175
111	Cover root end test specimens	177
112	Closeup of cover root end specimen failure.	178
113	Shadow moire'pattern at 360 306 N (81 kips)	179
114	Compression panel following failure loading fixtures have been removed.	179
115	Closeup of root end tension test segment after removal from the compressor panel	180

LIST OF FIGURES (Continued)

Figure	Title	Page
116	Closeup of failed tension panel after removal from test fixture.	181
117	Stiffener runout specimen in environmental chamber. . .	181
118	Closeup of H-26A failed area as viewed from the hat side of the specimen.	182
119	Closeup of stiffener runout failed area as viewed from the skin side.	183
120	Stress and strain levels at failure load stiffener runout.	183
121	H26B failed surface	186
122	Schematic of stability test specimens	186
123	H27 failed specimen	187
124	H27A failed specimen.	188
125	Moire' pattern of skin deformation at 138% DUL 356 730N (80,200 lb) compression load just prior to failure	189
126	Surface panel fail safety specimen.	190
127	Cross section of hat/skin elements showing the areas cut during the test	191
128	H29 lightning strike test panels.	194
129	Surface damage from swept stroke test, and section photographs	195

LIST OF TABLES

Table	Title	Page
1	Current Weight Status	23
2	Design Load Conditions	25
3	Computer Program Input Data	28
4	Computer Programs Used in Cover Analysis	28
5	Computer Programs Used in Rib Analysis	35
6	Minimum Margins of Safety for Truss Members	40
7	Computer Programs Used in Spar Analysis	44
8	Summary of Fail-Safe Analysis at Critical Locations	50
9	Graphite/Epoxy Pre-Preg (NARMCO T300/5208) Material Qualification Test Results (SI Units)	52
10	Graphite/Epoxy Pre-Preg (NARMCO T300/5208) Material Qualification Test Results (Customary Units)	55
11	Test Laminates	58
12	H13D Test Plan	58
13	Laminate Residual Tension Strength	58
14	Through-the-Thickness Damage Test Matrix	63
15	Summary of Static Tension Fracture Test Results	65
16	Summary of Fatigue Test Results	65
17	Impact Area Damage - Before and After Two Lifetimes of Fatigue Testing	75
18	Tape Data - Tension (SI Units)	78
19	Tape Data - Compression (SI Units)	84
20	Tape Data - Shear (SI Unit)	88
21	Syntactic Epoxy ADX819 Cured Syntactic Sheet Properties	91
22	Syntactic Epoxy ADX819 Graphite/Syntactic Sandwich Properties	91
23	Determination of K_B Factors Assuming Distribution Function is Unknown	93
24	Hybrid Input for All Conditions	94
25	Notch/Environmental and Statistical Reduction Factors	96

LIST OF TABLES (Continued)

Table	Title	Page
26	0^{o} Ply Level Failure Strains.	96
27	Allowable Lamina Strains.	98
28	Mean Ultimate Bearing Strength.	103
29	Push-through Tests.	106
30	Producibility Candidate Items - Covers & Ribs).	109
31	Producibility/Cost Reduction Studies Summary - Spars. . . .	112
32	Mandrel Comparison.	120
33	Physical Properties Test Results for Panel No. 1, 2, and 3.	122
34	Resin Content of Trial Panels of Low Resin Content Prepreg.	127
35	Producibility Factors - Alternate No Bleed Fabrication Systems	130
36	Summary of Process Development "T" Specimen Test Results - SI Units.	140
37	T300/5208 Batch Acceptance Test Results (SI Units).	145
38	Concept Verification Test Results	152
39	Load Summary for H20B1 and H20B2.	158
40	Design vs Modified Case II Test Loads	161
41	Fatigue Spectrum for Spar Web Test.	165
42	Loading Sequence and Results for H24B1 Test	173
43	Summary of Static Tests of Actuator Rib Specimen H24C . . .	176
44	H25 Loading Sequence	177
45	Fatigue Test Spectrum	185

ADVANCED MANUFACTURING DEVELOPMENT OF A COMPOSITE EMPENNAGE COMPONENT FOR L-1011 AIRCRAFT

PHASE II FINAL REPORT
DESIGN AND ANALYSIS

A. C. Jackson, J. F. Crocker, J. C. Ekvall, R. R. Eudaily,
B. Mosesian, R. R. Van Cleave and J. Van Hamersveld

SUMMARY

This is the final report on Phase II technical activity conducted on the Advanced Composite Vertical Fin (ACVF) program. The significant tasks of this program phase include Task 1, Component Definition; Task 2, Material Verification; Task 3, Producibility Studies; Task 4, Process Verification; and Task 5, Concept Verification.

Phase I (Reference 1) consisted of preliminary design trade-off studies, material screening and selection of the composite material system to be used. Also plans were prepared for FAA certification, ancillary test program, quality control, and structural integrity control.

Phase II concentrated on the design and analysis of the full-scale box; the material testing for design allowables; producibility studies to identify the most cost effective fabrication techniques; process development for the covers, spars and ribs; and concept verification subcomponent testing.

The producibility program and process development work caused changes in the preliminary fin design and fabrication. The covers became one-piece cocured assemblies using low-resin-content material to minimize bleeding. The spars had detail changes to enhance their fabricability. The rib concepts changed from bead-stiffened members to plain C sections because of significant fabrication problems.

The material verification testing yielded design allowables and demonstrated that the material is tolerant to damage and defects in the strain range experienced by the fin.

The concept verification testing substantiated the design, analysis and demonstrated the structural integrity of the fin box.

The current indicated weight of the composite fin box is 282.3 kg (622.3 lb). This represents a weight savings of 102.2 kg (225.4 lb) or 26.8 percent in comparison with the existing metal fin.

INTRODUCTION

This is the final report of technical work conducted during the second phase of a multiphase program which provides for the design, development, and fabrication of advanced composite empennage components. This program is part of the Aircraft Energy Efficiency (ACEE) Composite Structures Program. The broad objective of the ACEE program is to accelerate the use of composite structures in new aircraft by developing technologies and processes for early progressive introduction of composite structures into production commercial transport aircraft. This program, as one of several which are collectively aimed toward accomplishing that goal, has the specific objective to develop and manufacture advanced composite vertical fins for L-1011 transport aircraft. Laboratory tests and analyses will be made to substantiate that the composite fin can operate safely and economically under service loads and environments, and that it will meet Federal Aviation Administration (FAA) requirements for installation on commercial aircraft. A limited quantity of units will be fabricated to establish manufacturing methods and costs. The Advanced Composite Vertical Fin (ACVF) will use advanced composite materials to the maximum extent practical and weigh at least 20 percent less than the metal fin it replaces. A method will be developed to establish cost/weight relationships for the elements of the composite and metal fins to establish cost-effective limits for composite applications. All of the above objectives have been met, or exceeded.

The ACVF developed under this program consists of the entire main box structure of the vertical stabilizer for the L-1011 transport aircraft. The box structure extends from the fuselage production joint to the tip rib and includes the front and rear spars. It is 7.62 m (25 ft) tall with a root box chord of 2.74 m (9 ft) and represents an area of 13.94 m^2 (150 ft^2).

The primary objective of this program is to gain a high level of confidence in the structural integrity and durability of advanced composite primary structures. An important secondary objective is to gain sufficient knowledge and experience in manufacturing aircraft structures of advanced composite materials to assess properly their cost effectiveness.

Lockheed-California Company, as the prime contractor, has overall program responsibility and has teamed with the Lockheed-Georgia Company in the development of the ACVF. Lockheed-California designed and fabricated the covers and the ribs, and is conducting the Production Readiness Verification Test (PRVT) program and the full-scale ground tests. Lockheed-Georgia designed and fabricated the front, rear, and auxiliary spars, and is assembling the composite fin at the plant in Meridian, Mississippi, where the present L-1011 vertical fins are assembled.

The duration of this program is 83 months, with completion scheduled for December 1983. The master schedule is shown on figure 1. The program is organized in four overlapping phases: Phase II, Design and Analysis;

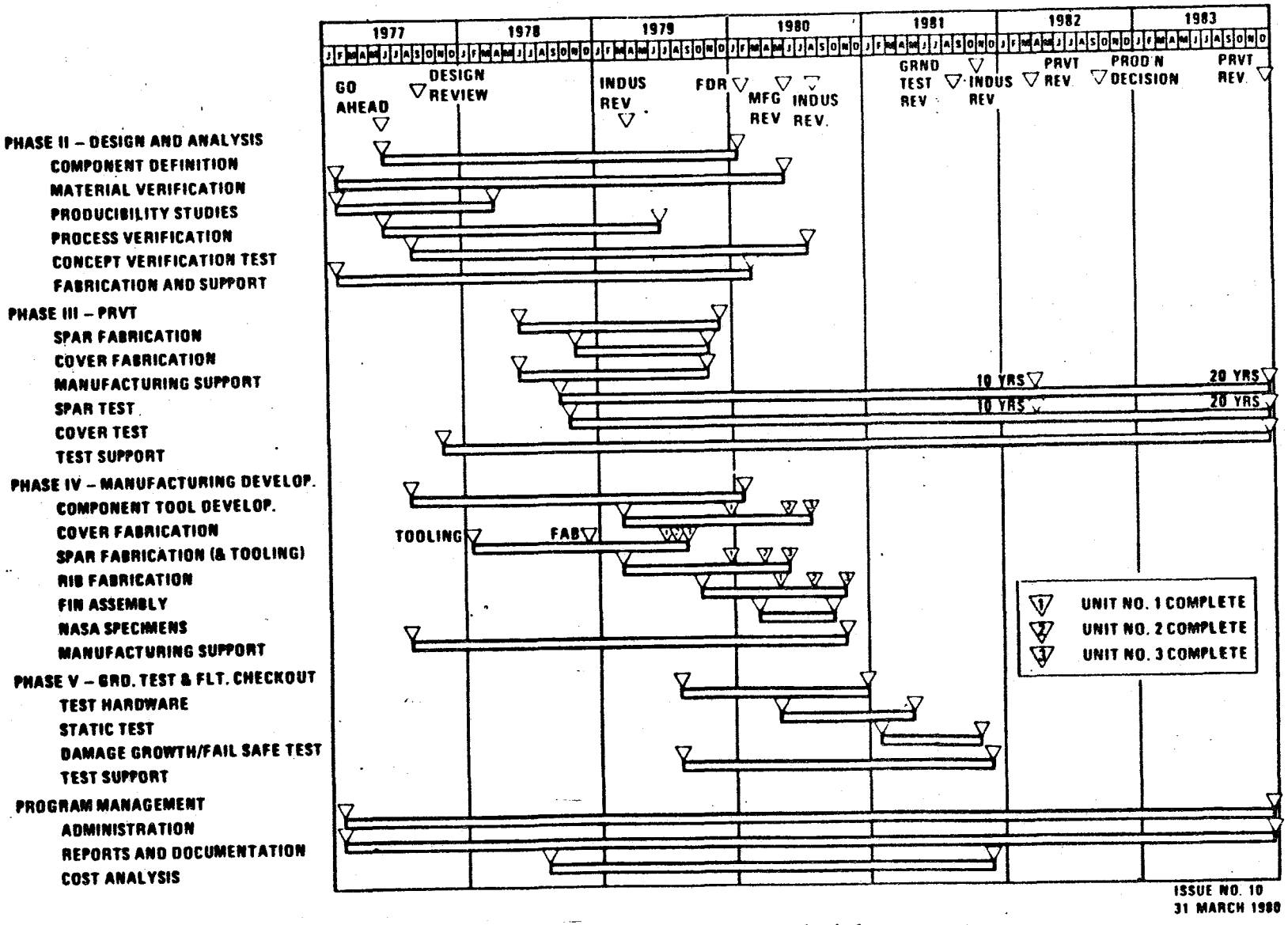

Figure 1. – ACVF program master schedule.

Phase III, Production Readiness Verification Tests (PRVT); Phase IV, Manufacturing and Development; and Phase V, Ground Tests. Phase I, Engineering Development, was completed in 1976; Phase II, has been completed and is reported herein; Phase IV Manufacturing Development has been completed; and Phases III, and V are currently in progress.

Phase III, PRVT is designed to provide information to answer the following questions:

- What is the range of production quantities that can be expected for components manufactured under conditions similar to those expected in production, and how realistic and effective are proposed quality levels and quality control procedures?

- What variability in static strength can be expected for production quality components? Are the margins sufficient to account for this variability?

- Will production quality components survive extended-time laboratory fatigue tests involving both load and environmental simulation of sufficient duration and severity to provide in-service confidence?

Ten static strength tests have been conducted and twelve durability tests are being conducted on each of two key structural elements on the ACVF. One element represents the front spar/fuselage attachment area, and the other element represents the cover/fuselage joint area. Two of the covers and two of the spars are being durability tested at strain levels 1.5 times those in the basic program.

Phase IV, Manufacturing Development, is complete. Two fins have been completed to prove the design, methods of manufacture and quality. Actual costs have been documented during fabrication and components were weighed to update cost and weight estimates. The manufacturing cost histories obtained through the fabrication of the PRVT specimens in a production environment have provided cost data for a starting point for this application of composite structure. Together, they form the basis for confident estimates of future production costs.

Ground tests will be conducted on one full-scale fin box beam structure mounted on simulated fuselage support structures during Phase V. The test plan will include static ultimate load, damage-growth test to one lifetime and fail-safe tests. Inspection and repair techniques for inservice maintenance will be employed throughout the tests. Test results will be used to verify the analytical, design, and fabrication procedures, and are essential inputs to the FAA for certification. Certification will be based on satisfying both static strength and damage tolerance requirements.

Throughout this program, technical information gathered during performance of the contract is being disseminated throughout the aircraft industry and to the government through quarterly reports that coincide with calendar quarters and final reports at the completion of each phase. All test and fabrication

data are being recorded on Air Force Data Sheets for incorporation in the Air Force Design Guide and Fabrication Guide for Advanced Composites. Oral reviews have been conducted to acquaint the aircraft industry and the government with progress of the program.

"Use of commercial products or names of manufacturers in this report does not constitute official endorsement of such products or manufacturers, either expressed or implied, by the National Aeronautics and Space Administration."

SYMBOLS

Measurement values used in this report are stated in SI units followed by customary units in parenthesis. All work was performed using customary units.

Symbol	Definition
A	Area
CV	Coefficient of Variation
D	Dry
D_{11}	Inplane bending stiffness in 0° direction
E	Youngs modulus
EI	Bending stiffness
F	Allowable stress
G	Shear modulus
GJ	Torsional stiffness
I	Second moment of area
K	Buckling coefficient, Reduction factor
KEAS	Knots Equivalent Air-Speed
L	Length
M	Mach No, Moment
MAC	Mean Aerodynamic Chord
M.S.	Margin of Safety
N	Applied load
OML	Outer Mold Line
P	Load
R	Stress ratio, Radius
RTD	Room Temperature Dry
SD	Standard Deviation

Symbol	Definition
V	Air speed, Shear load
VSS	Vertical Stabilizer Station
W	Wet
a	Panel length
b	Panel width
cg	Center of gravity
f	Stress
h	Altitude, Height
l	Length
m	Number of buckle half waves
t	Thickness
w	Width
α	Coefficient of thermal expansion
δ, Δ	Deflection
ϵ	Strain (Axial)
γ	Strain (Shear)
μ	Poisson's Ratio
Σ	Total
σ	Stress (axial)
τ	Stress (shear)

Subscripts

B	B basis statistical
BR	Bearing
BRU	Bearing ultimate
C	Compression
CR	Critical
CU	Compression ultimate
ET	Notched/environment
L	Longitudinal
N	Normalized

Subscripts

PL	Proportional limit
S	Shear
T	Tension, Transverse
X	Axial direction
Y	Transverse direction
XY	Shear direction

Superscripts

c	compression
t	tension

1. COMPONENT DEFINITION

This task covered the detail design and analysis of covers, ribs, spars, box assembly and installation.

1.1 Design Configuration

The fin box consists of two covers, two main spars, one stub spar and eleven ribs. Figure 2 shows an exploded view of box.

1.1.1 Covers. - The covers are designed primarily by stiffness. The fin box has to match the bending and torsional stiffness of the metal fin as closely as possible. Covers are nonbuckled until reaching design ultimate load (DUL). The root end has to match the existing joint to the afterbody, and all interfaces are unchanged. The cover skin tapers in steps from 34 plies at the root end to 16, 14 then 10. The edges are built up to 3.05 mm (0.12 in.) (24 plies) to allow for countersinking holes without feather edges. A thickness map is shown in figure 3 and the skin ply buildup is shown in figure 4. The 0^{o} ply is oriented parallel to the rear spar.

The closed hat section stiffener was selected because of its torsional stability and the fact that it did not have to be shear tied to each rib. The stiffener spacing and the hat configuration is shown in figures 5 and 6. The spacing at the forward end is established by the stiffener runout at rib stations. The stiffeners are terminated at the ribs adjacent to the front spar and the hat flanges continue under the rib caps to minimize any tendency to peel. Alternate ribs are rudder hinge support ribs. There are metal fittings attached to these ribs at the rear spar. The first stiffener was located to clear these fittings which thus established the aft spacing. The center three stiffener spacing was dictated based on the space remaining.

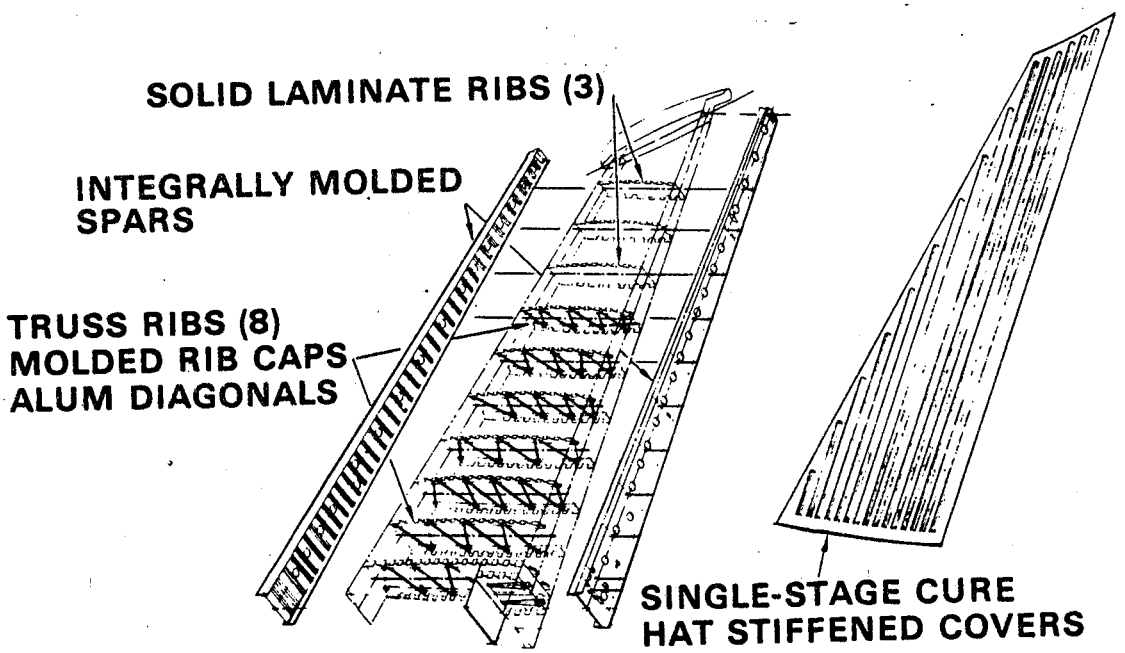

Figure 2. - Advanced composite vertical fin design configuration.

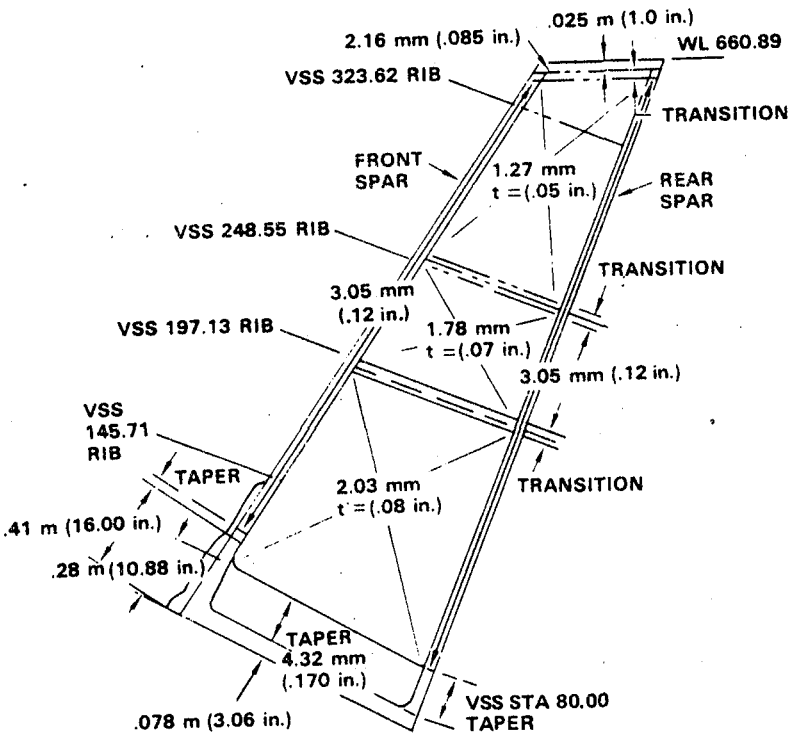

Figure 3. - Cover thickness.

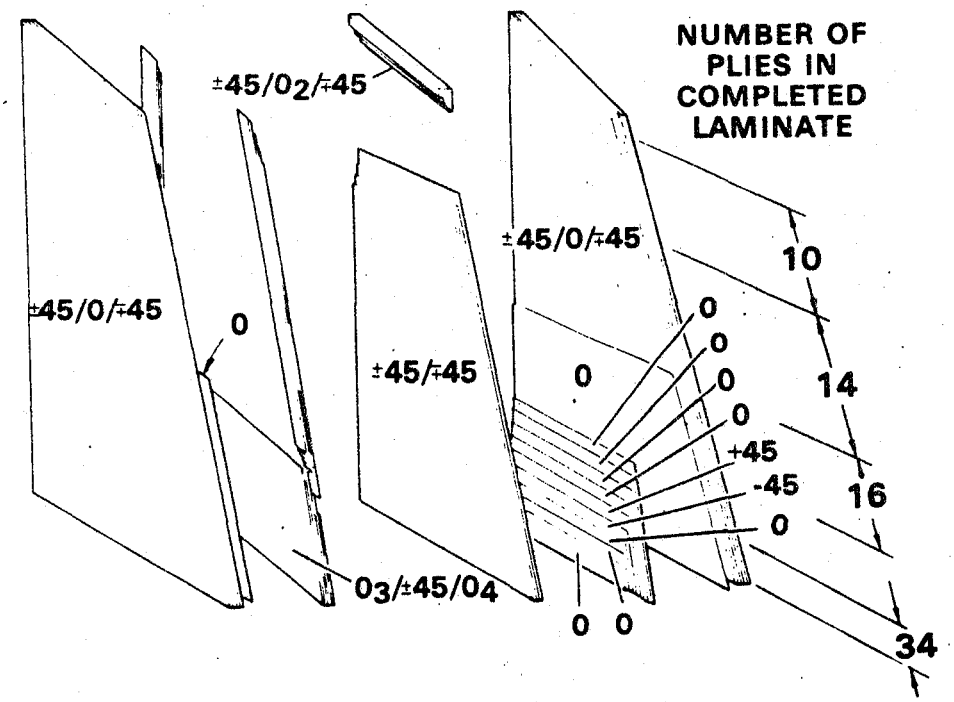

Figure 4. - Skin ply build up.

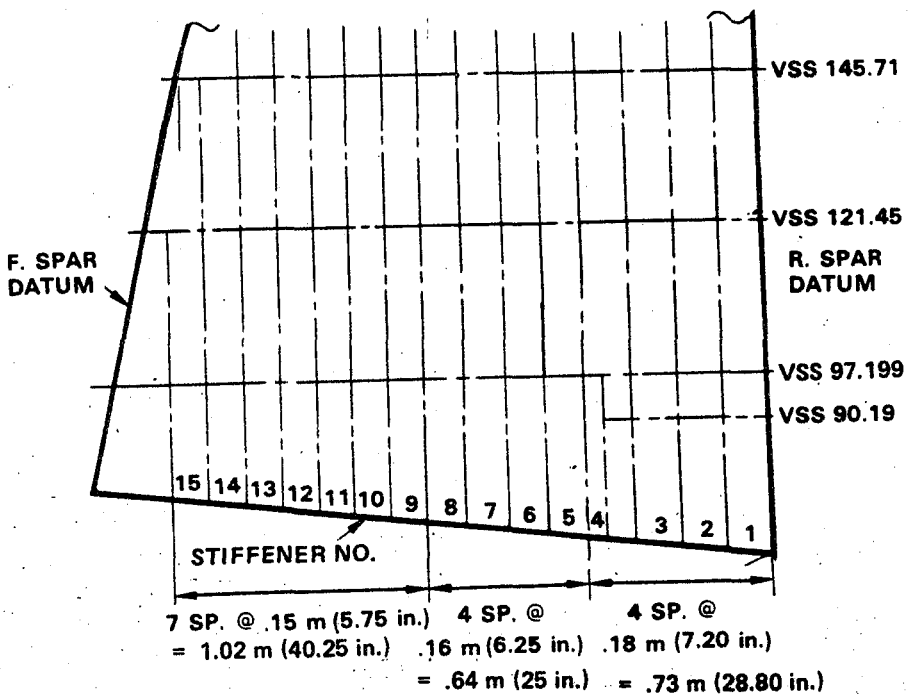

Figure 5. - Stiffener spacing.

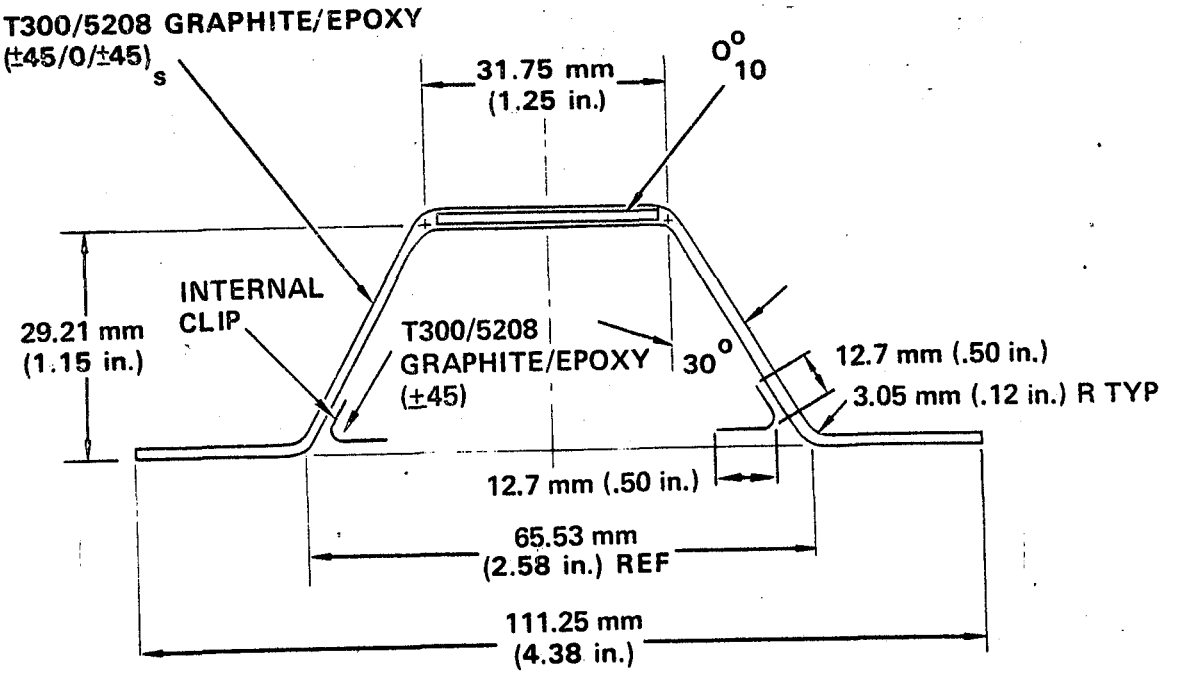

Figure 6. - Stiffener configuration.

The stiffener is built up of two 5-ply segments with a 10-ply segment sandwiched between them in the crown. A short segment of eight doubler plies is added at the root end only to stiffen the side walls for shearing out the crown loads. Internal clips consisting of two plies at ±45 degrees are added to prevent peel.

1.1.2 Ribs. - The eleven ribs fall into three basic categories: the two lower ribs are actuator ribs, the next six are truss ribs, and the upper three are solid web ribs.

The actuator ribs consist of a partial solid graphite/epoxy web at VSS 90.19 and a combination solid graphite/epoxy web and graphite/epoxy cap, aluminum truss rib at VSS 97.19 shown in figure 7. The solid web is a 16-ply layup $(+45/0/-45/90_2/-45/0/+45)_s$. The sides adjacent to the covers are flanged to provide part of the skin attachment. Additional cap is provided by a C section consisting of a 19-ply layup $(\pm 45/90/\mp 45/0/\pm 45/\bar{0}_3)_s$. This cap extends the full length on VSS 90.19. The forward portion of the VSS 97.19 rib consists of the graphite/epoxy C section caps and aluminum cruciform extruded truss members.

The truss rib caps are C section caps consisting of 19 plies with the same layup as the VSS 97.19 cap. The truss members are again aluminum cruciform extrusions. A typical truss rib is shown in figure 8.

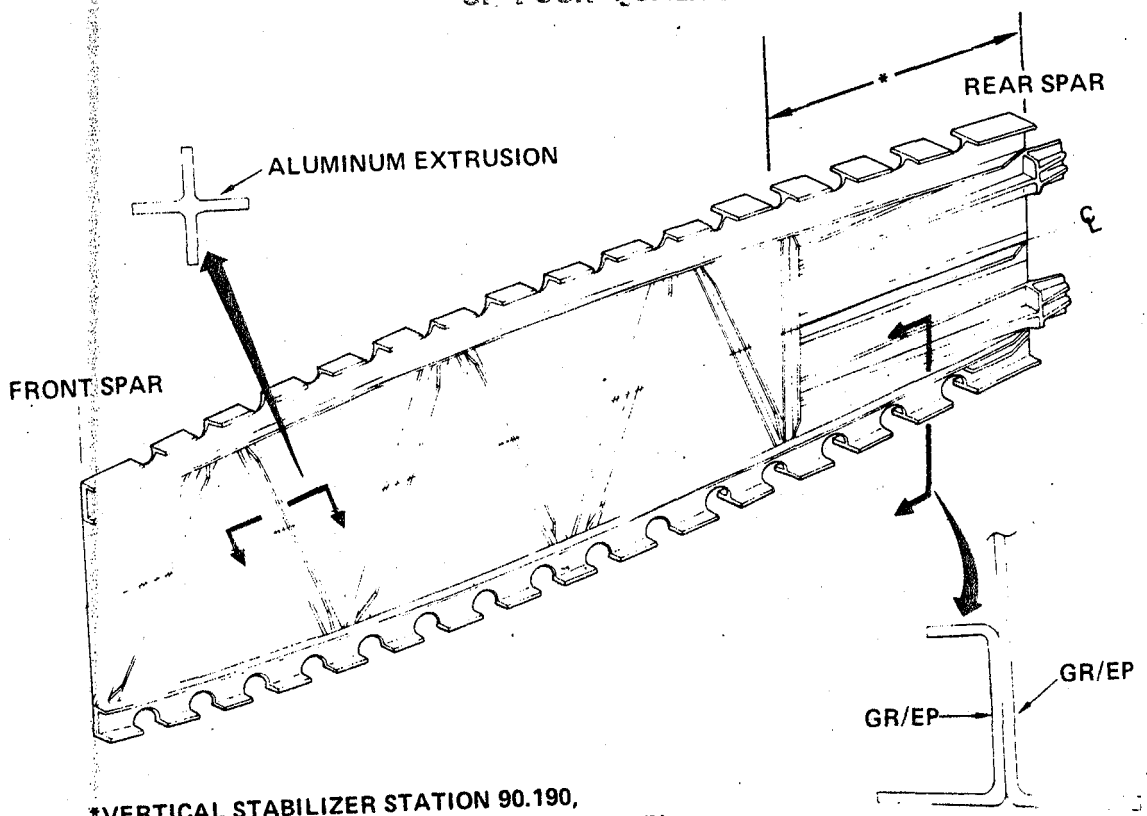

Figure 7. - Actuator rib design.

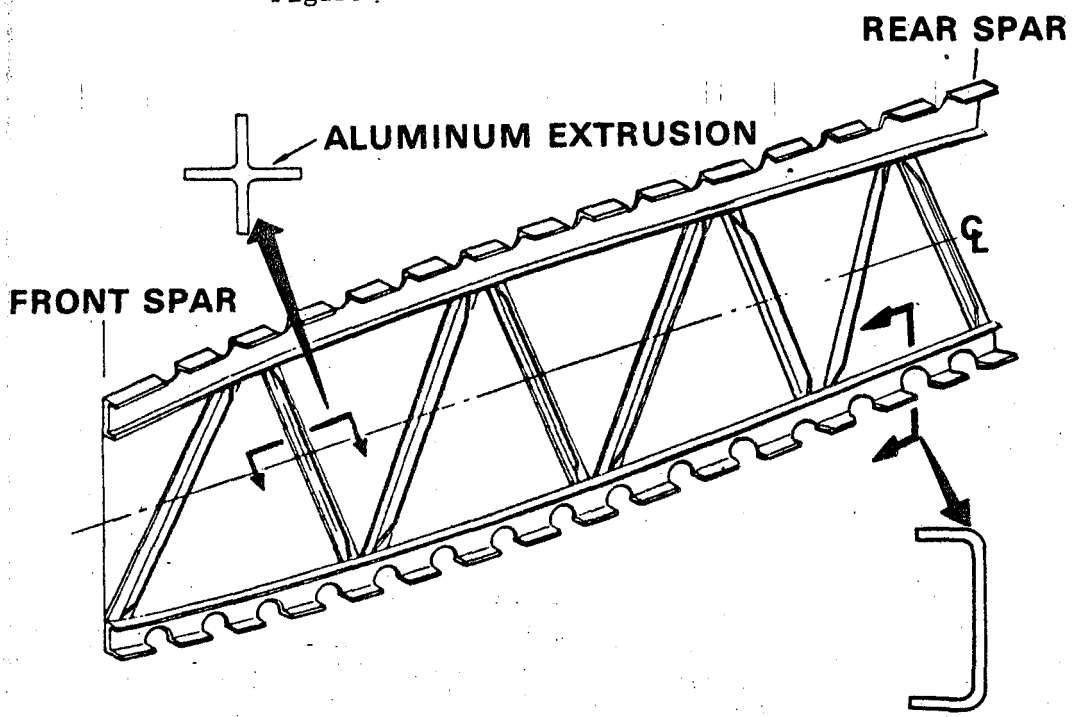

Figure 8. - Truss rib design.

The solid web ribs are a sandwich design. The fin box becomes too shallow near the tip to use the truss design efficiently. The most cost-effective design is one without stiffeners. Because of the size of the rib web, an all graphite/epoxy shear buckling resistant design would be heavy. Thus a syntactic epoxy core is used. Syntactic epoxy is an epoxy system filled with glass microballoons which has about half the density of graphite/epoxy. The face sheets consist of 7 plies laid up as $\pm 45/0/90/0/\mp 45$. The edges around the core are graphite/epoxy laid up as $\pm 45/0_2/\mp 45$. The uncured syntactic core is 0.95 mm (0.0375 in.) thick and compresses down to about 0.76 mm (0.03 in.) during cure. The configuration of the solid web rib is shown in figure 9.

1.1.2.1 Channel type rib development - rib redesign. - A brief history of the truss rib cap design evolution is shown in figure 10 and described below in chronological order:

- Concept A: This is the original rib cap configuration. The design turned out to be highly complex and not cost effective.

- Concept B: This concept is the baseline configuration for the comparison shown in figure 10, and represents what was considered a more producible design. In configuration, concept B is similar to concept A with the exception of a central bead which replaces the blade stiffener. The beads fabricated with this process contained severe microcracking.

- Concept C: In this concept an attempt was made to break up the large amount of 0° fibers in the bead by interleaving half of the existing 0° fibers in the outer flange. Although these changes produced a more efficient beam, they also created a loss of bead definition and did not solve the microcracking problem.

- Concept D: This concept is similar to concept C except for the extra ±45° plies added to the central bead to further break-up the concentration of 0° plies. This addition produced only slight improvement in over-all bead quality.

- Concept E: The shape of the rib cap in Concept E is a basic symmetric channel which is laid-up and cured on a single male tool. The loss in bending and axial stiffness is compensated for by distributing the 0° bead material of concept D evenly throughout the cross-section and by increasing the depth of the beam section. The small weight penalty experienced by this design was justified due to its greater producibility potential.

1.1.2.2 Solid web ribs. - The solid web ribs also underwent several design iterations aimed at making the ribs more producible. Figure 11 shows the design evolution of these ribs beginning with the earliest configuration.

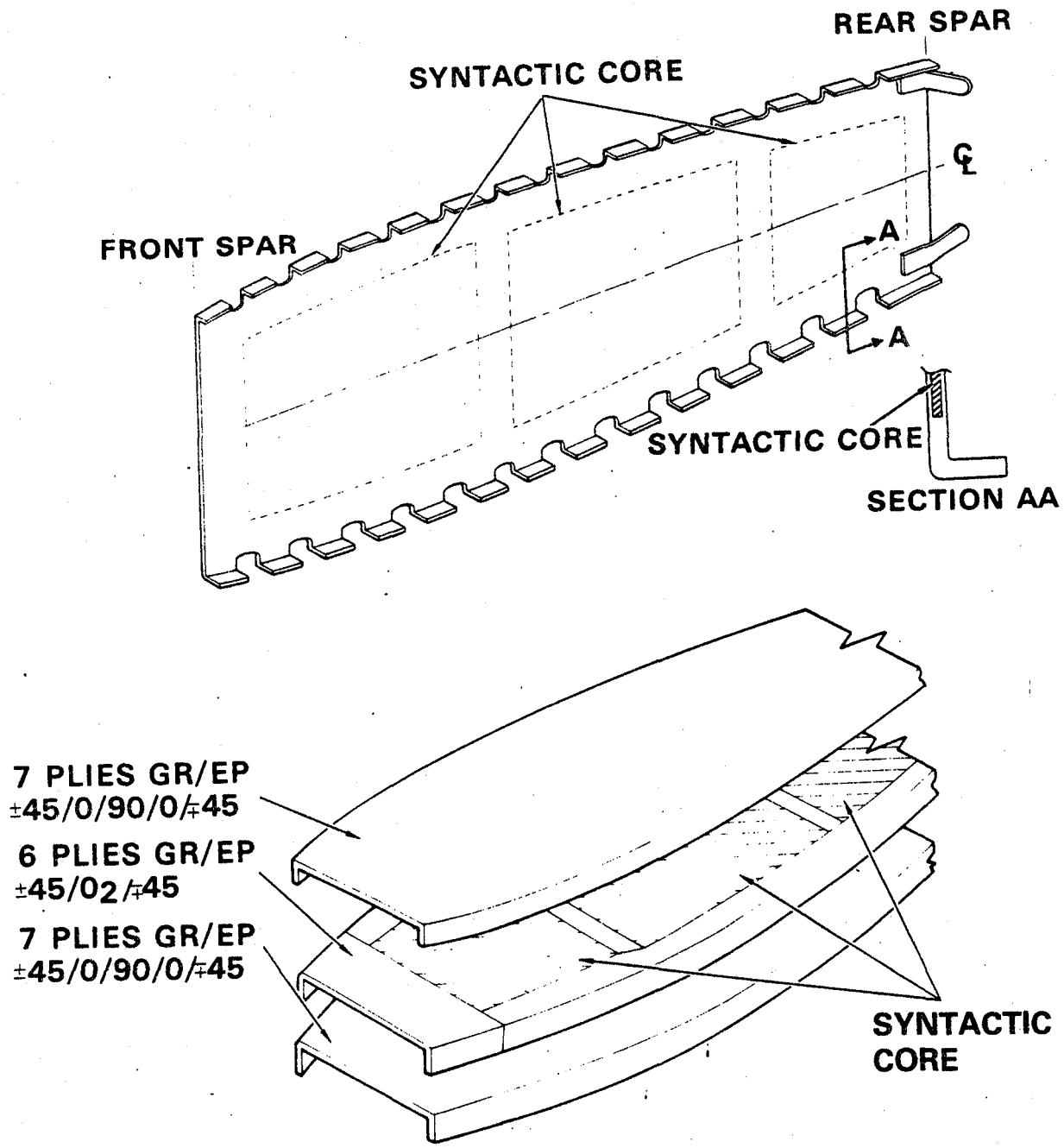

Figure 9. - Typical solid web rib design.

	Structural properties comparison		Weight comparison	Producibility rating 10-difficult 1-Easy
	Axial stiffness	Bending stiffness		
A 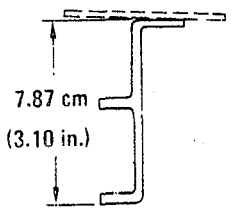 7.87 cm (3.10 in.)	1.00	1.20	1.62	10
B 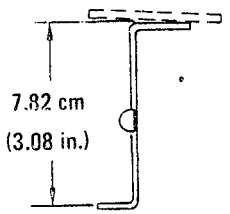 7.82 cm (3.08 in.)	1.00	1.00	1.00	3
	Baseline configuration			
C 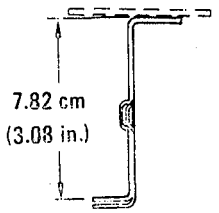 7.82 cm (3.08 in.)	1.03	1.35	1.06	7
D 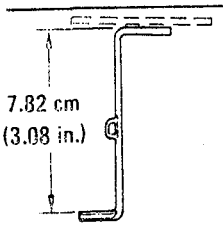 7.82 cm (3.08 in.)	Same as Concept C	Same as Concept C	Same as Concept C	5
E 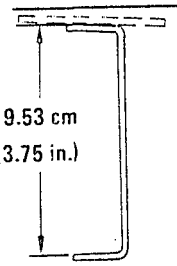 9.53 cm (3.75 in.)	1.00	2.05	1.14	1
	New selected configuration			

Figure 10. - Truss rib cap design evolution.

Design concept	Structural properties comparison		Weight comparison	Producibility rating 10-difficult 1-easy
	Torsional stiffness	Web buckling resistance		
A 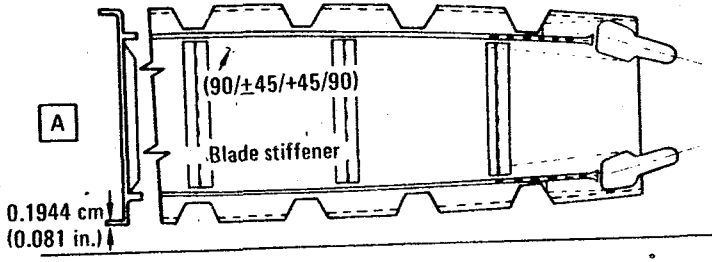	1.00	1.00	1.10	10
B 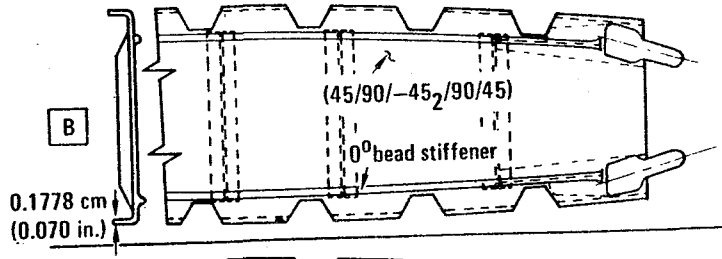	1.00	1.00	1.09	5
	Baseline configuration			
C 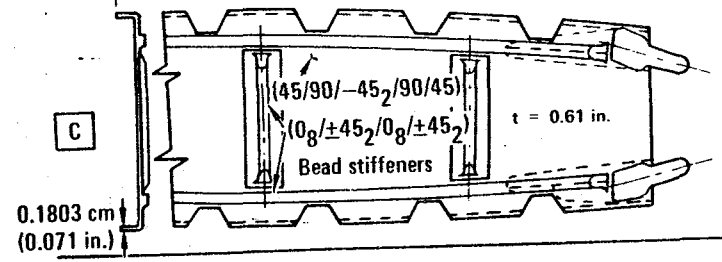	1.00	0.95	1.14	3
D 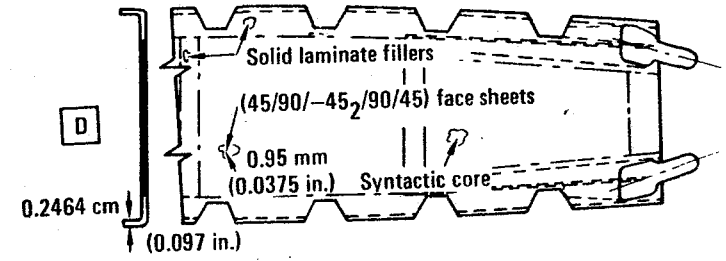	1.10	2.43	1.09	1
	New selected configuration			

Figure 11. - Solid web rib design evolution.

- Concept A: This was the original solid laminate rib design. The longitudinal web stiffeners were configured as integral blades while the transverse Z stiffeners were secondarily bonded to the web. This design was not cost-effective.

- Concept B: This is the baseline and was considered a more producible design. The rib featured 0° longitudinal bead stiffeners combined with transverse T shaped stiffeners co-cured to the web.

- Concept C: This concept was introduced to correct for several producibility problems encountered in the manufacturer of concept B. The principal problems concerned profile distortion, lateral shifting, and microcracking within the all 0° bead. To correct for these discrepancies, ±45° plies were interleaved between the 0° plies in the bead. In addition, the "T" stiffeners were replaced with bead stiffeners and relocated on the same side of the web as the longitudinal bead for producibility reasons. Despite some minor improvements obtained as a result of these changes, none of the process verification rib specimens satisfied design standards.

- Concept D: This configuration featured a 0.95 mm (0.0375 in.) syntactic core and precluded the need for beads or external stiffeners. It manifested the best structural and producibility characteristics of the four concepts at only a 9 percent weight penalty, approximately 0.45Kg (1 lb) per fin.

1.1.3 Spars. - Front and rear spars have been designed to comply with overall program objectives of providing a 20-percent weight savings over the metallic design, while maintaining production costs, and ensuring structural and functional interchangeability with the baseline article.

Numerous proposed design changes were evaluated for potential cost savings during the producibility studies and these, together with various tooling and manufacturing changes, are discussed in section 2. From these studies, three design changes from the Phase I design were recommended for incorporation:

- Kelvar cloth was originally used in the spar webs because of its lower material cost and the assumption that a thicker material (i.e., fewer plies) would be less expensive to lay up (figure 12). However, when the use of automated tape laying equipment was considered, together with revised projected material costs, unidirectional graphite/epoxy tape offered a substantial cost improvement.

- Detail analysis of the web access holes revealed high strain levels at the edge of the hole at 45° to the spar center line. On the original design using Kevlar, there was an insufficient number of ±45° plies in the web to withstand the strain, and unidirectional reinforcing rings were introduced (figure 13). When the change from Kevlar was made, however, additional ±45° graphite/epoxy plies were added and the reinforcing rings were no longer required.

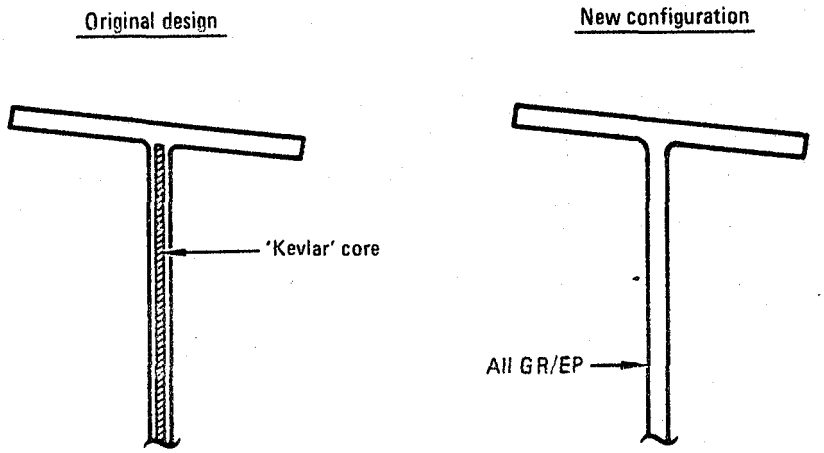

Figure 12. - Design changes - spar web material change.

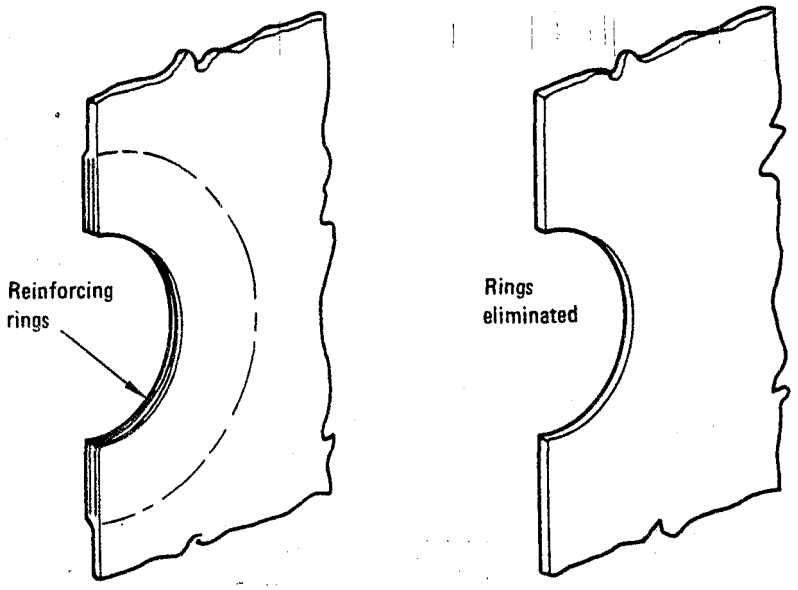

Figure 13.- Spar web access hole.

- Figure 14 shows the revised stiffener configuration resulting from the producibility studies. Analysis of this item indicated that a direct tie-in from stiffener to spar cap was not required to stabilize the web, and therefore the simpler stiffener configuration was incorporated.

The design concepts selected are the graphite/epoxy configurations shown in figures 15 and 16. The front and rear spars are similar in shape and size and are basically one-piece components with stiffeners, caps, and webs integrally molded in a single cocured operation. The front spar cap forward flange, rear spar cap aft flange and the fuselage joint areas have been configured to interface with the existing metallic structure and therefore, do not necessarily represent the most efficient designs for advanced composite structures. Another critical interface area is the attachment of rudder hinges to the rear spar. To ensure that these locations are accurately maintained, separate aluminum attachment angles are jig located on assembly and mechanically attached to the spar.

Strength and stiffness requirements are controlled by selecting ply layups with a sufficient number of $\pm 45^{\circ}$ plies in the webs to provide the required shear strength and 0° plies in the caps for axial loading. To facilitate fastener installation in the final assembly fixture, access holes have been provided in the spar webs. Two access holes are required in each rib bay and this dictates that three web stiffeners are added between ribs to ensure uniform hole spacing.

1.1.3.1 Auxiliary spar: The auxiliary spar shown in figure 17 is located between the aft fuselage closure rib and the rudder actuator rib, and has been retained as an aluminum assembly. This component cannot be attached until all fasteners in the fin-to-fuselage joint are installed and therefore has to be fabricated in small sections capable of passing through the root rib access hole. This involves a considerable amount of drilling and assembly of details

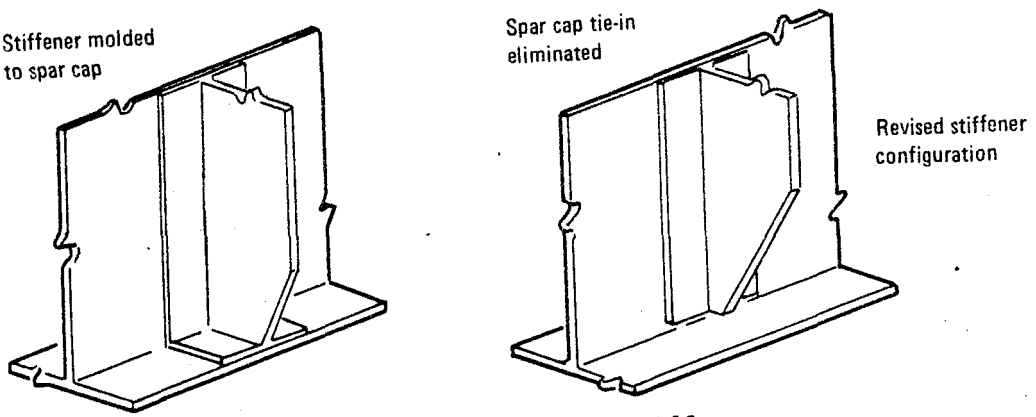

Figure 14. - Spar web stiffener.

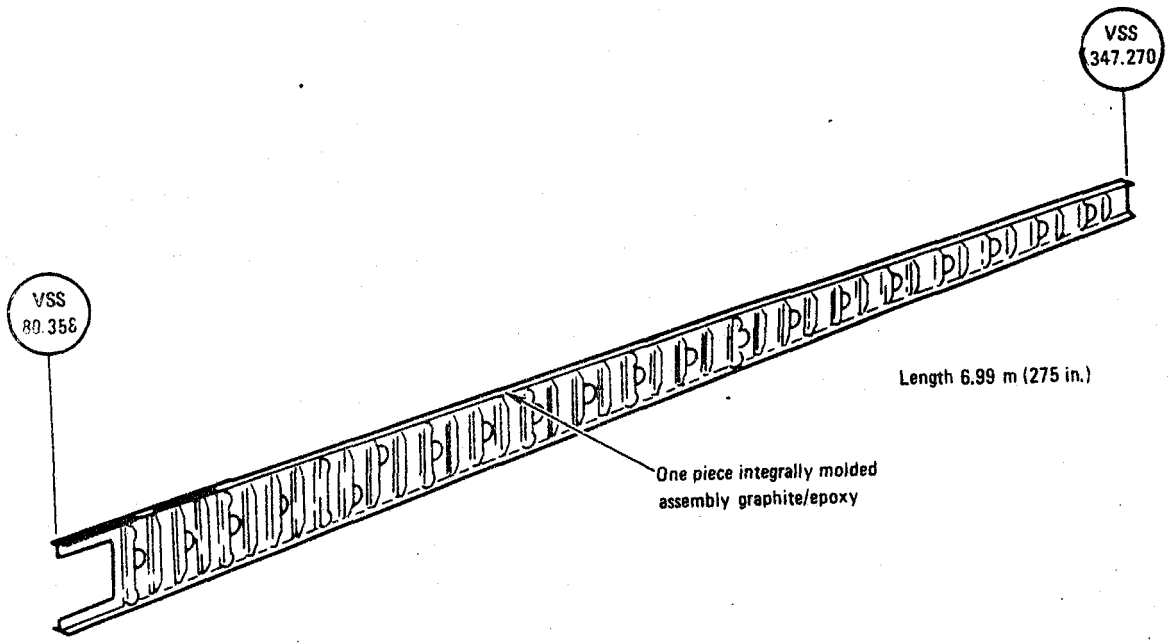

Figure 15. - Front spar assembly.

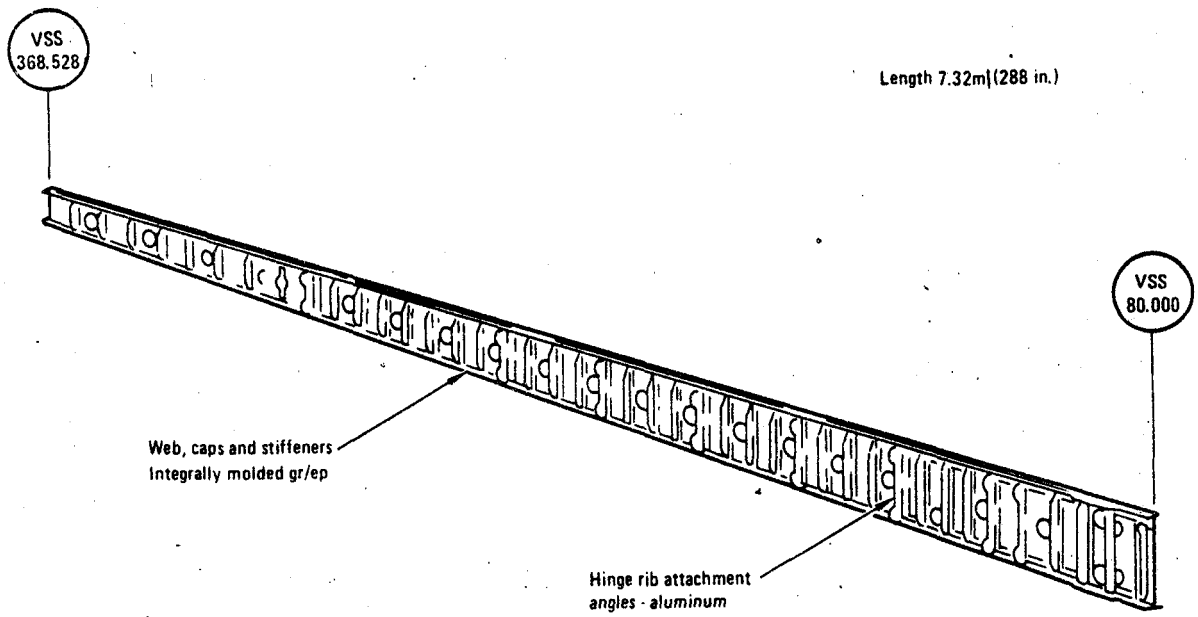

Figure 16. - Rear spar assembly.

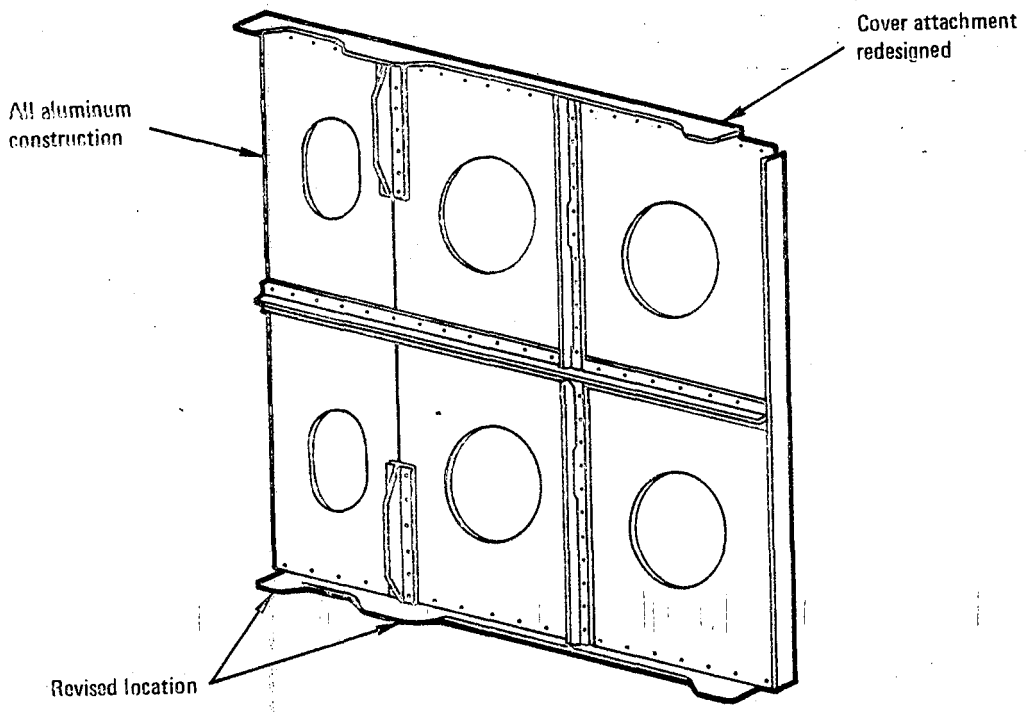

Figure 17. - Auxiliary spar assembly.

on location and was a major factor in the decision to avoid the use of composite materials. Minor changes have been made to this component with respect to redesigned ribs and cover assemblies.

1.1.4 Box assembly. - Fin assemblies for the ACVF program are manufactured at the Lockheed-Georgia Company facility in Meridian, Mississippi, using an existing assembly fixture suitably modified to accept the various advanced composite components. Use of this fixture, (where rudder hinges, rudder actuator and fuselage attachment control points have been retained) will ensure that all interchangeability requirements are met.

The fin box assembly is illustrated in figure 18. Parts of the skin are cut away to show details of cover hats, ribs, spars and joints used to assemble the L-1011 ACVF box. The fasteners selected for the assembly of major components are titanium hi-loks with stainless steel collars which are wet installed with sealant in close-tolerance, noninterference fit holes.

Access to the inside of the box is accomplished by the removal of rib truss members and entry from the fuselage joint area. Limited hand access is also available through the holes provided in the front and rear spar webs. This access allows hi-loks to be installed at approximately 95 percent of all fastener locations and at the remainder, blind fasteners are utilized.

Ribs, spars, and covers are designed to eliminate interference on assembly by assuming adverse tolerances at component interfaces. Where gaps in excess of 0.25 mm (0.010 in.) exist, Kevlar shims of the approximate thickness are installed.

1.1.5 Fin installation. - The fin box is installed in a similar manner to the metal fin it replaces. The root rib, which is part of the afterbody assembly, is unchanged. The outer splice plate shown in figure 19 has been increased in length to pick up two rows of fasteners in the cover above the root rib instead of one. The cover hat stiffeners are terminated above the root rib and are not tied to it with clips. Between the hats are finger plates to assist in reducing any offset bending going into the joint. These finger plates and the splice plate are aluminum.

Spar splices are the same as the metal fin consisting of angles to splice the caps and plates to splice the webs.

1.1.6 Weight status. - The goal for the weight savings was 20 percent from the structural box. Table 1 shows the weight status as of the end of Phase II. It can be seen that the weight-saving goal was exceeded and that in fact, 27.4 percent was saved.

1.2 Structural Analysis

The fin was designed to meet several structural criteria. The primary criterion was that the fin be designed to carry the design loads during and after exposure to the environmental conditions encountered in worldwide service. The fin must demonstrate the ability to carry design ultimate load without failure and design limit load without permanent deformation. The fin must also demonstrate the ability to carry design limit loads after the failure of single critical elements of the structure. The fin must be capable of being installed on an L-1011 aircraft without compromising the other structure or affecting interchangeability. The fin must be functionally compatible with the surrounding structure.

The fin bending stiffness (EI) and torsional stiffness (GJ) must closely match those of the metal fin box so as not to change the aeroelastic response. No buckling may occur below design limit load. This limitation on buckling was imposed because there was very little data available on post buckling behavior and it would have been a high risk. Because of the overall EI and GJ requirements buckling in fact does not occur until about 90% of design ultimate load.

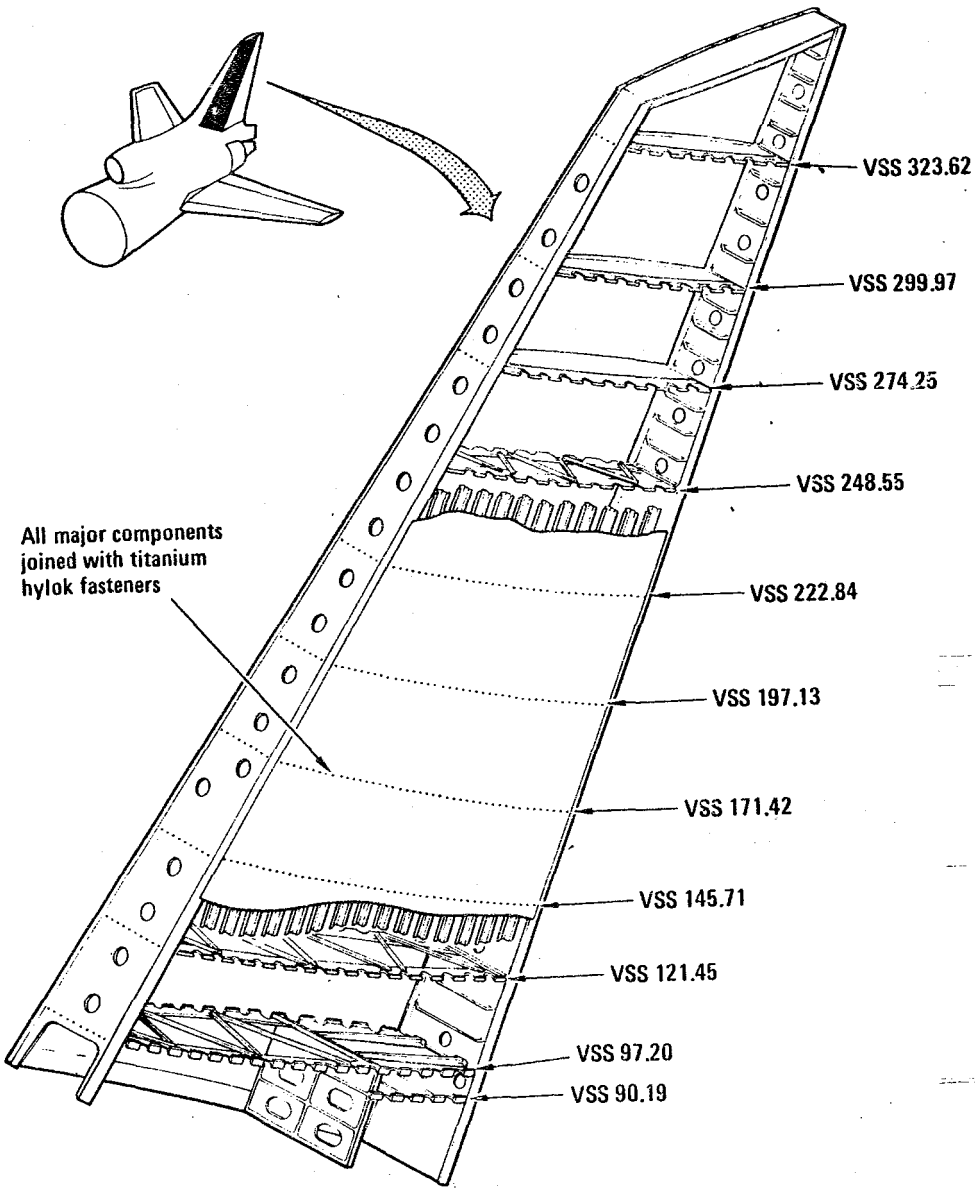

Figure 18. - Fin assembly, showing rib stations.

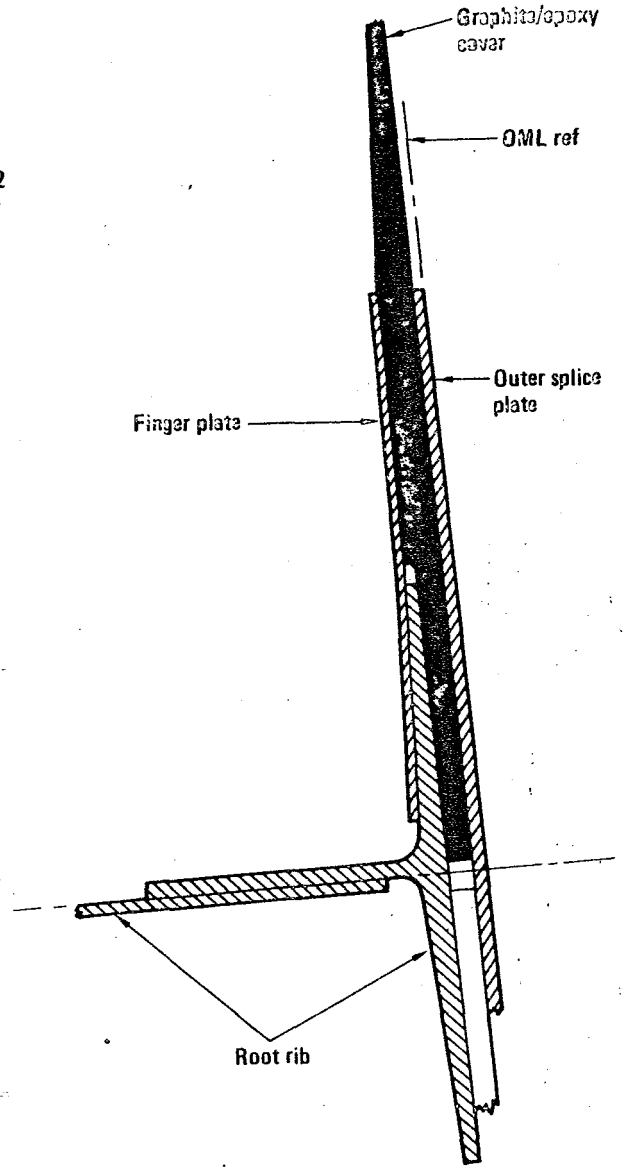

Figure 19. - Root splice.

TABLE I. - CURRENT WEIGHT STATUS

Item	Metal Design Total Weight		Composite Design					
			Target Weight		Total Weight		Composite Material Weight	
	kg	lb	kg	lb	kg	lb	kg	lb
Covers	208.8	460.4	167.1	368.4	162.5	358.2	154.4	340.4
Spars	90.3	199.0	59.9	132.0	51.6	113.8	38.3	84.5
Ribs	69.5	153.3	59.8	131.8	53.3	117.6	23.6	52.1
Assembly hardware	16.1	35.4	7.6	16.7	6.6	14.6	-	
Protective finish	4.4	9.6	4.4	9.6	4.4	9.6	-	-
Lightning protection	-	-	7.0	15.5	0.0	0.0	-	-
Installation penalty	-	-	5.5	12.2	3.9	8.5		
Total fin predicted	-	-	-	-	-	-	-	-
Delivery weight	389.0	857.7	-	-	282.3	622.3	216.3	477.0
Weight saving	-	-	-	-	106.7	235.4	-	-
Percent weight saved	-	-	-	-	27.4%	27.4%	-	-
Percent composite material	-	-	-	-	-	-	78.3%	78.3%

1.2.1 Design loads. - There are 3 primary design load conditions which are shown in table 2. It should be noted that condition 73 is a system failure condition. Structural design loads were generated using a NASTRAN finite element model. The model was described in reference 1. The cover design loads are shown in figure 20.

Loads on the fin are assumed to be applied in either direction, therefore the maximum absolute loads are used in the analysis. The axial loads on the spar caps and the shear flows on the webs were plotted and curves were faired through the data points. Discontinuities in shear flow occur at the rear spar due to concentrated loads input at the rudder hinge and actuator rib locations.

Shear flows in web panels containing cutouts were modified to account for the loss of area. The method used increased the shear flow by a factor of the ratio of the gross panel width to the net panel width. This net shear flow was then used in computing the margins in buckling as well as the margin at the critical location at the edge of the cutout. A plot of the front and rear spar maximum loads versus Vertical Stabilizer Station is shown in figure 21.

Three ribs were selected for detailed analyses: the main actuator rib at VSS 97.19, the highest loaded hinge rib at VSS 145.71, and the solid web hinge rib at VSS 299.97. The loads from the 3D model were applied to 2D models of these ribs to determine the design loads. The maximum design loads are shown in figures 22, 23, and 24.

1.2.2 Analysis design allowables. - The computer programs used for the analysis of stability, elastic properties, and stress concentrations require ply level input data. Based on the preliminary test data, properties were derived for room temperature dry (RTD), 355K (180°F) wet and 219K (-65°F) dry conditions. These properties are shown in table 3.

Analyses performed using the data in table 3 used the minimum value regardless of environmental condition.

1.2.3 Cover analysis

1.2.3.1 Analytical approach: The analysis of the covers was conducted using a series of computer programs (table 4). The cover was analyzed for panel stability using VIPASA. Individual elements such as cover, skin, hat flange, hat sidewall, and hat crown were then analyzed for local stability using COMAIN and strength. The load distribution was found using the equation

$$P_{(element)} = \frac{P_{(stiffener)} \times AE_{(element)}}{AE\ (stiffener)}$$

TABLE 2. - DESIGN LOAD CONDITIONS

Condition	Gross Weight		c.g.	V	M	h	
	kg	lb	% MAC	KEAS		m	ft
56 RM-2 (1)	211 374	466000	28.7	250	.38	0	0
59 Dyn. Lat. Gust	161 932	357000	24.5	320	.85	8534	28000
73 RM-2 (1)	191 416	422000	32.0	250	.38	0	0

(1) RM-2 Rudder Maneuver - Point in time at which the max sideslip angle occurs.

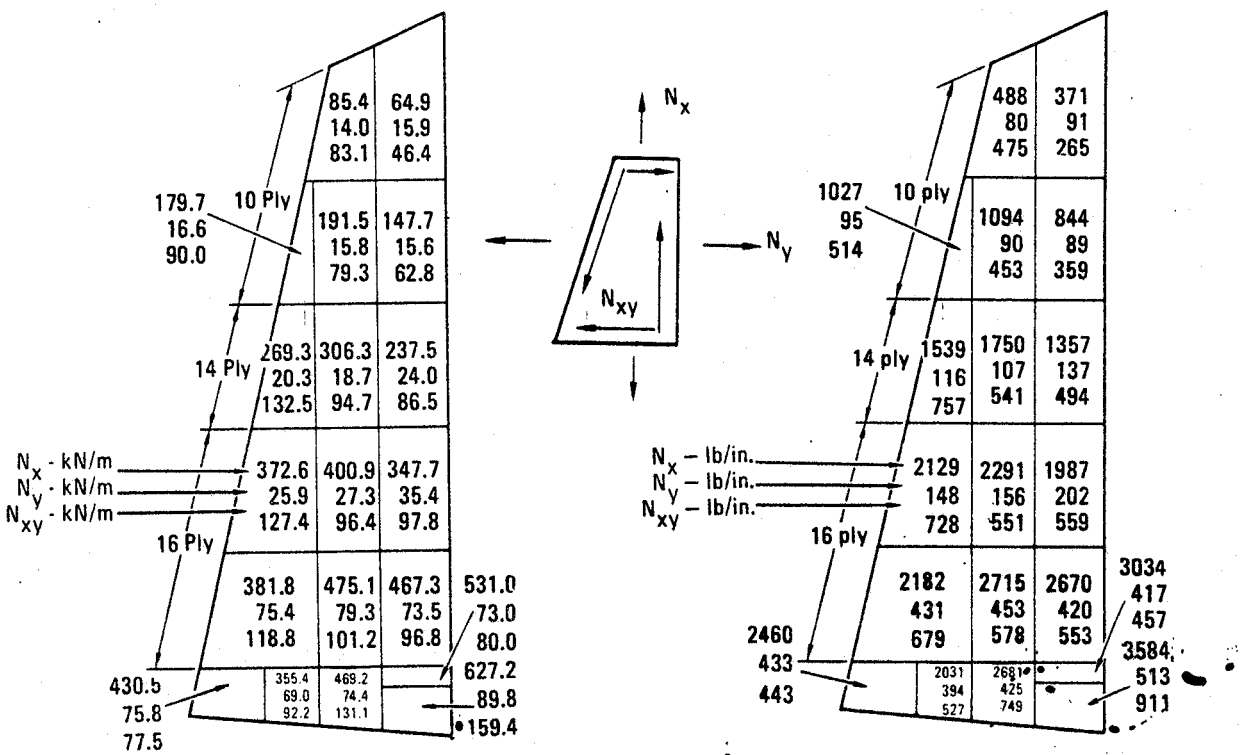

Figure 20. - Cover design ultimate loads.

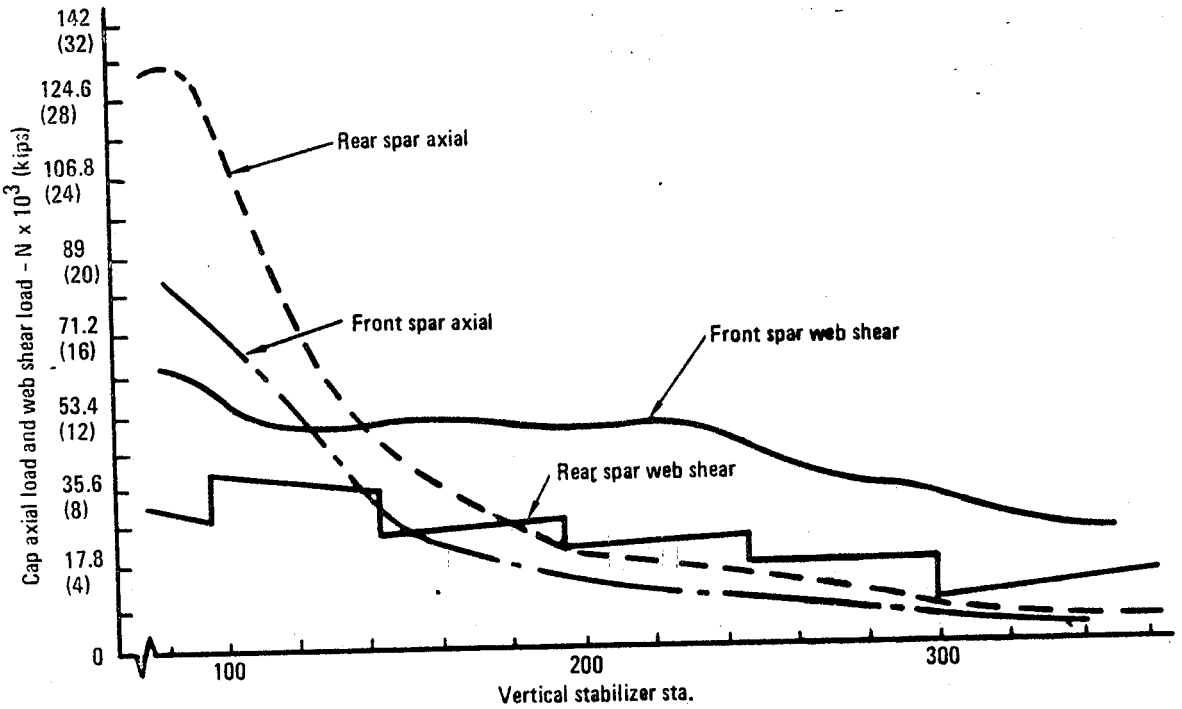

Figure 21. - Spar cap axial loads and web shear flows (ultimate).

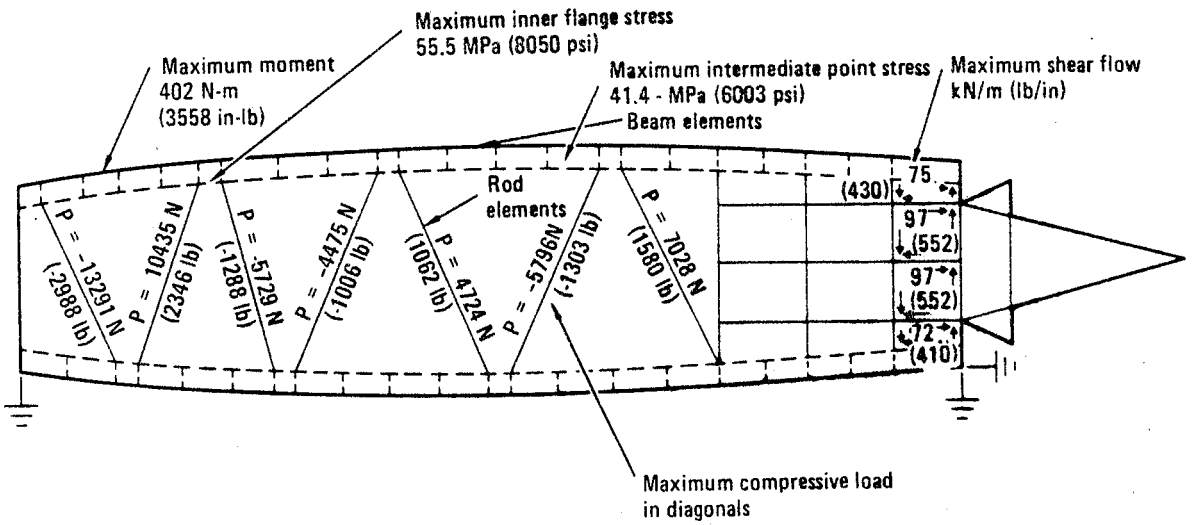

Figure 22. - Loads on rib at VSS 97.199.

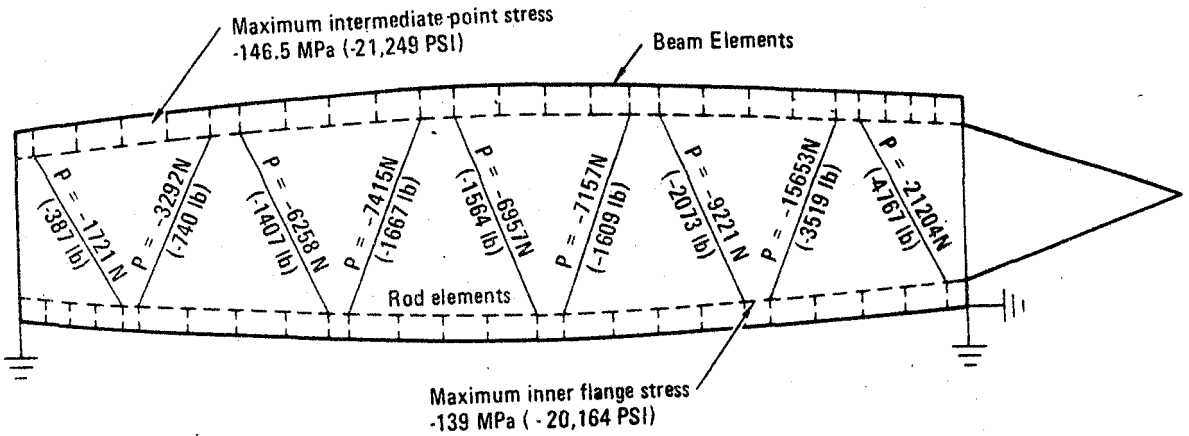

Figure 23. - Loads on rib at VSS 145.71.

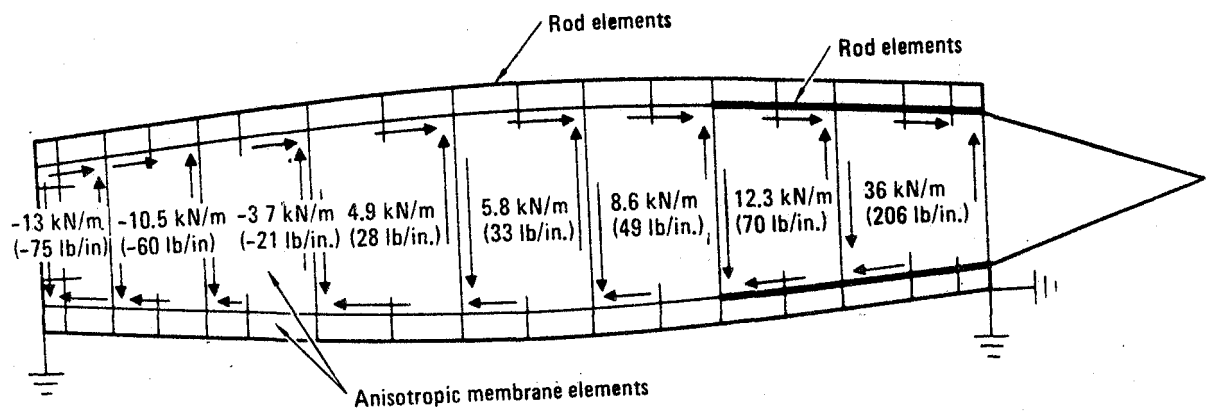

Figure 24. - Loads on rib at VSS 299.97.

TABLE 3. - COMPUTER PROGRAM INPUT DATA

Property	RTD		355K Wet	(180°F) Wet	219K Dry	(-65°F) Dry
E_{11} Tens GPa (msi)	138	20	140	20.3	134	19.5
E_{11} Comp. GPa (msi)	131	19	124	18	134	19.5
E_{22} Tens GPa (msi)	11.03	1.6	9.65	1.4	12.27	1.78
E_{22} Comp. GPa (msi)	10.76	1.56	9.38	1.36	12.07	1.75
G_{12} GPa (msi)	5.52	0.8	4.14	0.6	5.93	0.86
μ_{12} –	0.27		0.26		0.28	
α_1 μm/m/K (μin./in./°F)	0.43	0.24	0.50	0.28	0.36	0.20
α_2 μm/m/K (μin./in./°F)	29.2	16.2	33.9	18.8	27.2	15.1
Ultimate unnotched strains μm/m						
0° Tension	9 000		9 000		9 000	
0° Compression	8 100		7 500		6 000	
90° Tension	7 500		7 000		7 000	
90° Compression	12 000		12 000		12 000	
Shear	15 000		15 000		12 900	

TABLE 4. - COMPUTER PROGRAMS USED IN COVER ANALYSIS

Program	Function	Source
VIPASA	Stability analysis of stiffened plates constructed of advanced composite materials (Ref 4)	NASA
COMAIN	General purpose local stability analyses using orthotropic subroutines for compression, shear and combined loads. Calculates buckling for flanges and flat and curved plates.	Lockheed California Co.
SECPRO	Section properties of composite shape	Lockheed California Co.

When a skin local instability occured, panel failure was predicted on the basis that the stiffeners would continue to pick up load until one element became unstable at which time total collapse would occur or a strength cutoff was reached. Shear buckling stability was analyzed using COMAIN. Compression and shear buckling interaction was determined using the equation.

$$M.S. = \frac{1}{\sqrt{R_c + R_S^2}} - 1$$

where

$$R_c = \frac{N_x}{N_{x,\,cr}}, \quad R_s = \frac{N_{xy}}{N_{xy,\,cr}}$$

1.2.3.2 Strength and stability analysis: The covers are designed by either stability or impacted compression strength which is slightly lower than the notched tension strength. A strain map of the cover is shown on Figure 25. The allowable strain from table 27 is -4000 μm/m. There are three different hat stiffener spacings across the cover, the maximum being 0.18 m (7.2 in.) which is the critical area. The maximum load in this area (16 ply skin) is 475 kN/m (2715 lb/in) and the shear flow in that panel is 68.8 kN/m (393 lb/in.) (See figure 20.)

The VIPASA analysis showed initial buckling occurs in the skin at 473 kN/m (2704 lb/in.). The COMAIN analysis gave a skin shear buckling load of 170 kN/m (972 lb/in.). Initial buckling under combined loading would thus occur in the skin at

$$\frac{100}{\sqrt{\frac{475}{473} + \left(\frac{68.8}{170}\right)^2}} = \frac{100}{\sqrt{1.004 + .164}} = 92.5\% \text{ of design ultimate load}$$

Using the geometry of an idealized stiffener as shown in figure 26, the properties were calculated

$$A = 2x25.4x1.27 + 2x33.78x1.27 + 31.75x2.54 = 230.97 \text{ mm}^2 \ (0.358 \text{ in.}^2)$$

	A		E		AE	
	mm^2	$in.^2$	GPa	Msi	GPa mm^2	lb x 10^6
crown	80.65	.125	86.2	12.5	6952	1.563
flanges	64.52	.100	41.4	6.0	2671	0.600
webs	85.80	.133	41.4	6.0	3552	0.798
Σ	230.97	.358			13175	2.961
skin	371.61	.576	49.6	7.2	18441	4.147
Σ	602.58	.934			31616	7.108

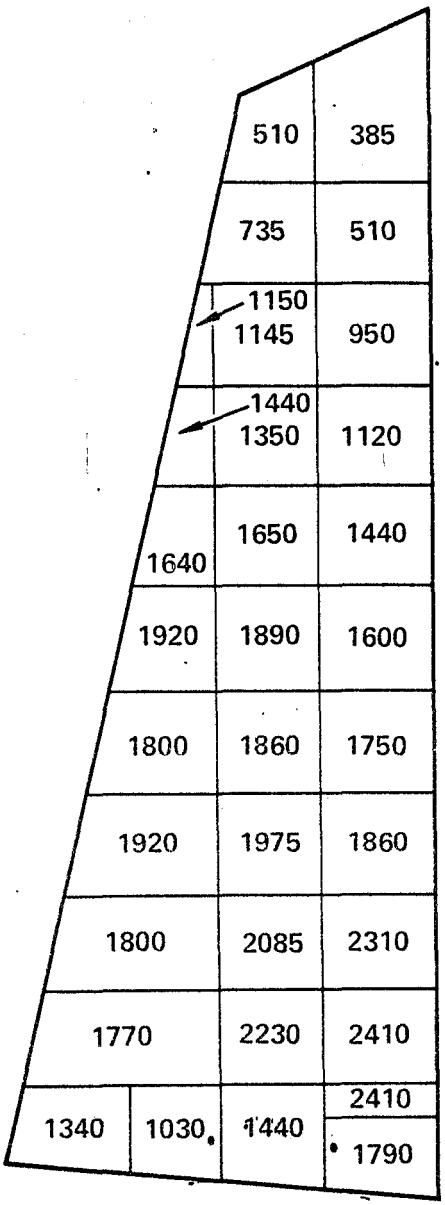

Figure 25. - Cover ultimate gross area compression strain (μm/m).

Total load in .183 m (7.2 in.) wide segment of skin and one hat = 473 x .183 = 86.6 kN (19 469 lb)

Distribution of load between elements

skin	86.6 x 18441/31616/.183	= 276 kN/m (1577 lb/in.)
crown	86.6 x 6952/31616/.032	= 595 kN/m (3400 lb/in.)
flanges	86.6 x 2671/31616/.051	= 143 kN/m (817 lb/in.)
webs	86.6 x 3552/31616/.068	= 143 kN/m (817 lb/in.)

Allowables:

skin	F_c = 193.1 MPa (28,000 psi)	N_x = 392 kN/m (2240 lb/in.)	Strength (Figure 63, Pg 100)
crown	F_c = 337.8 MPa (49,000 psi)	N_x = 858 kN/m (4900 lb/in.)	
flanges	F_c = 172.4 MPa (25,000 psi)	N_x = 219 kN/m (1250 lb/in.)	
webs	F_c = 172.4 MPa (25,000 psi)	N_x = 219 kN/m (1250 lb/in.)	
webs	F_c = 146.8 MPa (21,300 psi)	N_x = 186 kN/m (1065 lb/in.)	Stability (COMAIN) Table 4

$\text{Min} \frac{N_{x\,allow}}{N_x}$ = 1.303 for web stability

∴Failure will occur at 1.303 x 92.5% DUL
= 120%
∴MS = 0.20

It is assumed above that after the skin buckles, the hat will continue to pick up load until the sidewalls buckle at which time complete collapse will occur.

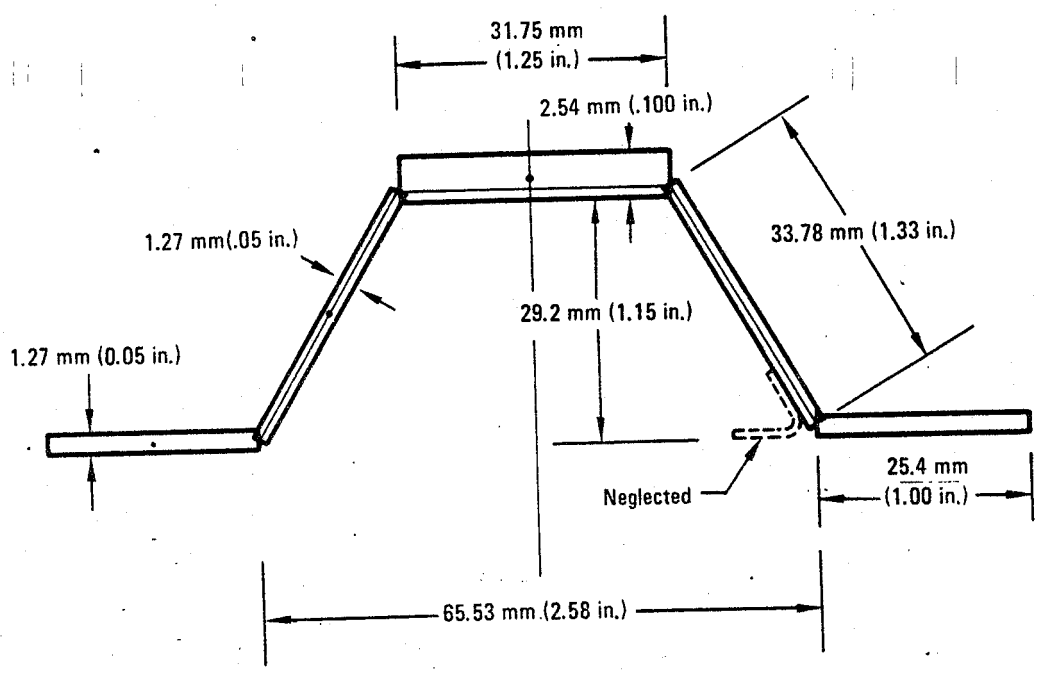

Figure 26. - Idealized stiffener.

1.2.3.3 Root joint analysis: The root end of the composite fin cover is attached to the L-1011 afterbody structure with a double shear joint as shown in figure 27. At the joint, the graphite/epoxy skin measures 4.32 mm (0.170 in.) thick and consists of 34 plies with a layup containing 18 plies at 0^{o} and 16 plies at $\pm 45^{o}$. The skin is joined to an aluminum root rib cap with a full-width aluminum outside splice plate in combination with a series of smaller inside splice plates. All cover loads are transferred to the afterbody through four rows of 4.76 mm (3/16 in.) diameter Hi-Lok fasteners. The root end joint is analyzed as an eccentrically loaded beam column loaded in compression. Bending stresses due to eccentricity are minimized by gradually reducing the hat stiffener effectiveness at the runout while at the same time increasing the skin thickness.

Structural analysis of this joint indicates high margins of safety for the ultimate loading conditions. The maximum axial stress in the joint is calculated to be 159.3 MPa (23.1 ksi) (Ref. figure 25) and exists in the graphite skin adjacent to the first row of fasteners. The margin of safety at this location is: (314.4/159.3) -1 = +.97 (Zone (A) figure 27). The notched compression allowable for this laminate is 314.4 MPa (45.6 ksi) (Ref. figure 63, page 100).

The maximum ultimate shear flow in the joint is 159 540 N/m (911 lb/in.) (Ref. figure 18) which is equivalent to a shear stress of 36.5 MPa (5.3 ksi). (This maximum shear flow does not act in combination with the above maximum axial force.) The minimum margin of safety is (151.7/36.5) -1 = + High (Zone (B) figure 24). The notch shear allowable is 151.7 MPa (22 ksi) (See figure 65, page 101).

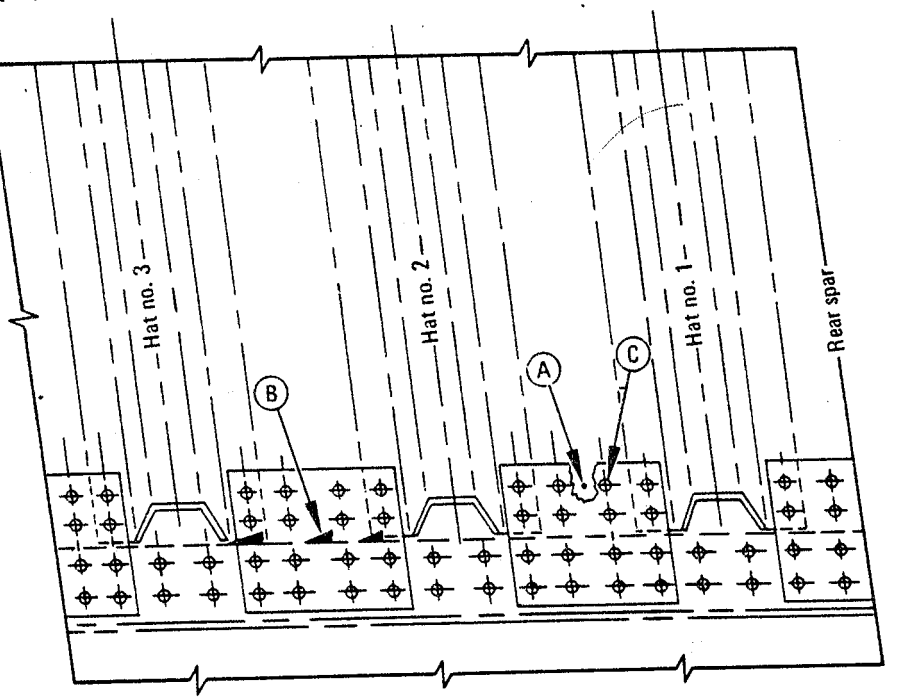

Figure 27. - Fin to afterbody root joint.

The maximum bearing stress in the composite skin is computed to be 479.9 MPa (69.6 ksi) and occurs in the first row of fasteners. Minimum margin of safety for this condition is (901.8/479.9) -1 = +.88 (Zone Ⓒ figure 27). The bearing allowable is 901.8 MPa (131 ksi) (table 28, page 103).

The fasteners in the joint are critical in shear. The maximum single shear force on any fastener is 4 564 N. (1026 lb). The margin is (11 965/ 4 564) - 1 = +1.62 (Zone Ⓒ figure 27). The single shear allowable for 4.32 mm (3/16 in.) Hi-Lok fastener is 11 965 N. (Ref. 3).

Figure 28 shows the stress distribution in the joint at ultimate load for Case 59.

1.2.3.4 Fail-Safe Analysis: A fail-safe load redistribution for the cover was made using the 3D NASTRAN model. A complete stiffened membrane element was removed. The element consisted of three stiffeners and skin approximately .46m (18 in.) wide and .43m (17 in.) long. Figure 29 shows the maximum N_x loads in the surrounding panels with no failure and with the failed panel. The load condition is #59.

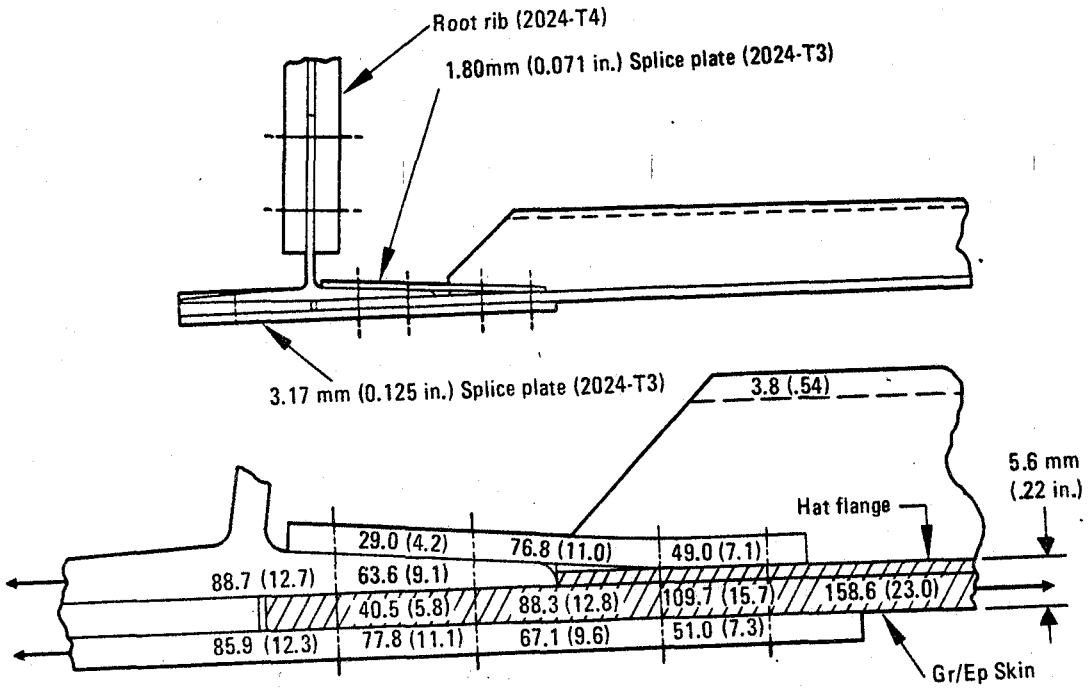

Figure 28. - Stress levels at design ultimate load - MPa (ksi).

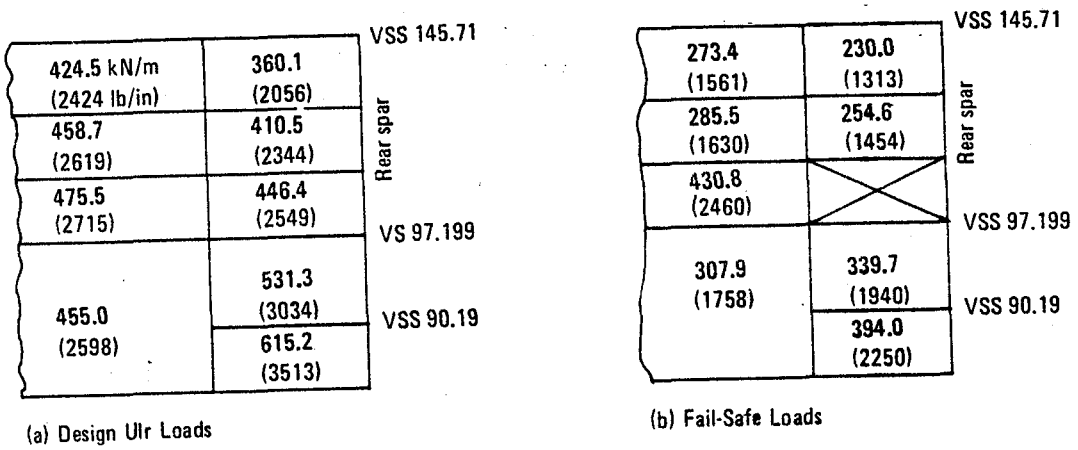

Figure 29. - Maximum design loads and fail-safe loads for cover.

The fail-safe loads are shown on the right hand side on figure 29. The maximum ratio of fail-safe load/design load is 430.5/475.1 = .906 so the minimum margin of safety was not affected.

This was a severe condition but the NASTRAN model would not allow for only one stiffener being cut because the element to be cut represents 3 stiffeners. The fail-safe characteristics of the cover were demonstrated by test H28 described in section 5.10.

1.2.4 Rib Analysis

1.2.4.1 Analytical approach: Analysis is conducted on the following rib assemblies:

- VSS 97.19 (Combination truss and solid web)
- VSS 145.71 (Truss type)
- VSS 299.97 (Solid web type)

These three stations are adequate coverage to satisfy any structural requirements associated with the other nine stations because they represent the highest loaded ribs of the three design concepts employed in the fin. Two dimensional finite element models were constructed for the above three stations. External loads (shell and hinge) were applied from the same load conditions used in the NASTRAN 3D model to design the spars and covers.

The stress analysis of the ribs is performed with the aid of a series of computer programs specifically designed for composite materials (table 5). The following is a summary of the potential failure modes investigated for each of the three structural components common to all rib assemblies:

- Rib Caps. - Inner flange stability, web shear strength, cap web buckling, lateral stability, maximum unsupported length, joint analysis.
- Cruciform Diagonals. - Tensile and compressive strength, column buckling, flange crippling, torsional instability, joint analysis.
- Shear Webs. - Tensile and compressive strength, combined axial and shear buckling, analysis of web stiffeners, joint analysis.

1.2.4.2 Actuator rib: The actuator rib at VSS 97.19 was chosen for analysis in order to represent a rib with shear webs as well as trusses. From an investigation of the analyses of all of the components, the most critical items have been chosen for this report.

TABLE 5. - COMPUTER PROGRAMS USED IN RIB ANALYSIS

Program	Function	Source
COMAIN	General purpose local stability analyses using orthotropic subroutines for compression, shear and combined loads. Calculates buckling for flanges and flat and curved plates.	Lockheed-California Co.
PLM	Critical buckling of orthotropic plates under combined loading including transverse shear deformations.	Lockheed-California Co.
AJOINT	Load distribution in joint fasteners including effects of bolt bending in double shear joints.	Lockheed-California Co.
SHEET	Instability of bent sheet stiffeners	Lockheed-Calofornia Co.
SM126	Crippling of metal stiffeners	Lockheed-California Co.
SECPRO	Section properties of composite shapes	Lockheed-California Co.

- Rib cap inner flange stability and strength: The maximum cap stress is $f_x = \pm 55.5$ MPa ($\pm$ 8050 psi) figure 20.

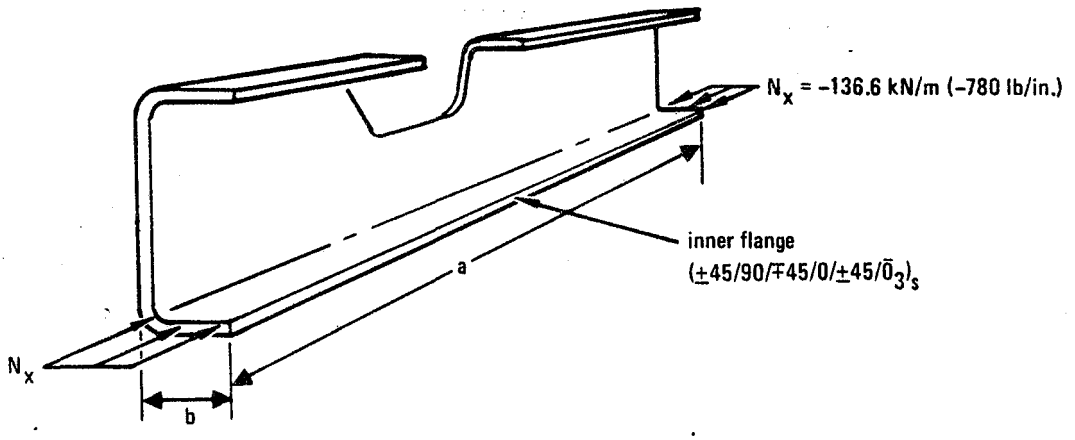

The inner flange contains 19 plies and is analyzed assuming the following conditions:

$a/b = \infty$

3 sides simply supported, 1 free

b = 25.4 mm (1.0 in.)

t/ply = .117 mm/ply (.0046 in./ply) (min. thickness allowed)

From the COMAIN program the buckling strength of this flange is calculated to be equal to N_{xcr} = -467.1 KN/m (-2667 lb./in.)

The maximum applied load (figure 22) is N_x = -136.6 kN/m (-780 lb./in.) or f_x = 55.5 MPa (8050 psi).

The margin of safety is:

$$M.S._{(stability)} = \frac{-467.1}{-136.6} - 1 = 2.42$$

For inner flange strength, the notched tension allowable is F_{TU} = 262.0 MPa (38,000 psi) Ref. fig. 56.

Margin of safety is:

$$M.S._{(notched\ tension)} = \frac{262.0}{55.5} - 1 = High$$

- Cap web shear strength

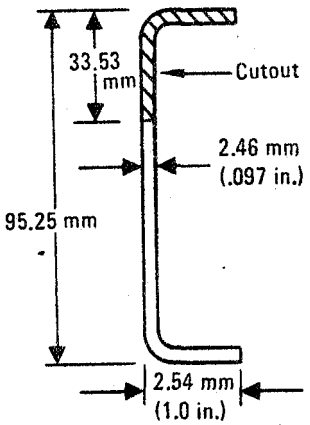

Standard rib cap

Maximum shear is

$V = -13\ 069N\ (-2938\ lb)$

$$f_{xy} = \frac{3}{2}\ \frac{V}{h\ t}$$

$h = 95.25 - 33.53 = 61.72$ mm (2.43 in.)

$$f_{xy} = \frac{3}{2}\ \frac{13\ 069}{.0617 \times .0025} = 129.16\ \text{MPa}\ (18{,}732\ \text{psi})$$

f_{xy} strength = 199.95 MPa (29,000 psi) (Notched shear strength) (Ref. figure 61)

$$M.S._{(Shear)} = \frac{199.95}{129.16} - 1 = 0.55$$

- Rib cap lateral stability: The method of analysis used is from page 94 of reference 2.

In this analysis, the maximum axial load that will cause rib cap lateral buckling is determined. The rib cap material between the hat cutouts is not considered in the analysis except to provide lateral restraint, and the cap is conservatively assumed to be pinned at the truss members.

ℓ' is the distance of the centroid of the cap below the cutout from the skin (the elastic foundation)

Δ is deflection

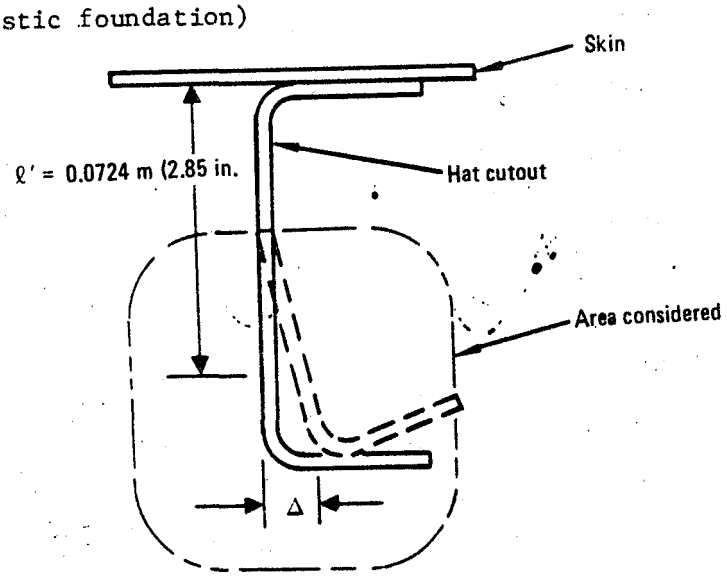

The laterial stiffness for this configuration is the same as a cantilevered beam.

$$\Delta = \frac{P(\ell')^3}{3EI_x}$$

or $K' = \frac{P}{\Delta} = \frac{3E_y I_x}{(\ell')^3}$ where I_x is equal to the moment of inertia/unit length of the rib cap web.

$$I_x = \frac{(25.4)(2.46)^3}{12} = 3.15 \times 10^{-11}\ m^4\ (7.606 \times 10^{-5}\ in^4)$$

also,

E_y = 38.13 GPa (5.53×10^6 psi)
E_x = 54.88 GPa (7.96×10^6 psi) [Calculated values using COMAIN program (Table 5)]

Solving for the spring constant K'

$$K' = \frac{3(38.13 \times 10^9)\ 3.15 \times 10^{-11}}{(0.0724)^3} = 9486\ N/m\ (54.17\ lb/in)$$

The reduced cap stiffness K due to the hat cutouts is:

$$K = K'\left(\frac{d - s}{d}\right)$$

where

d = spacing of cutouts = .159m (6.25 in)
s = width of cutouts = 0.074m (2.92 in)

$$K = 9495\left(\frac{.159 - .074}{.159}\right) = 5047\ N/m\ (28.82\ lb/in)$$

from reference 2

$$\beta = \frac{K\ell^4}{16(EI)_{min}} \quad \text{and} \quad P_{cr} = \frac{\pi^2 (EI)_{min}}{L^2}$$

ℓ = actual length of rib cap = .643m (25.3 in.) between diagonal supports

L = reduced length of rib cap between diagonal supports.

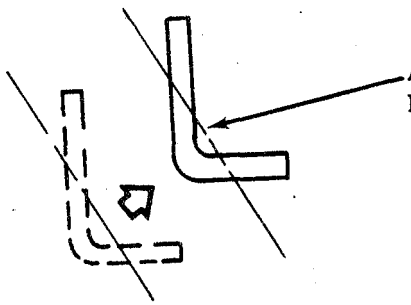

$(EI)_{min} = 336\ N\text{-}m^2\ (.1171 \times 10^6)\ lb\text{-}in^2$

$$\beta = \frac{5047\ (.642)^4}{16\ (336)} = .1595m\ (6.28\ in)$$

from Ref. 2 pg 97 the L/ℓ ratio is .708

therefore

$L = .708\ \ell$

$L = .708\ (.642)$

$L = .454\ m\ (17.87\ in)$

Laterial buckling of the rib cap due to an axially applied load is:

$$P_{CR} = \frac{\pi^2\ (336)}{(.454)^2} = 16\ 088N\ (3616\ lb)$$

The maximum applied load over the portion of rib cap is 12 170N (2736 lb).

$$M.S._{(Lateral\ Stability)} = \frac{16\ 088}{12\ 170} - 1 = +.32$$

- Truss members: Table 6 summarizes the minimum margins of safety for the various failure modes. The truss joint consists of five fasteners, three in one row, and two in the other. By using the (AJOINT) program, the percentages of load per fastener are 40.73 percent for the row with three fasteners, and 50.92 percent for the row with two fasteners. The maximum load per fastener is calculated as follows:

$$P_{MAX} = \frac{3}{5} \times 13\ 290N \times .4073 = 3248\ N\ (730\ lb)/fastener\ (figure\ 22).$$

The lowest allowable is for the composite in bearing: (Ref. table 28).

$F_{BR} = 1124\ MPa\ (163\ ksi)\ t = 2.461\ mm\ (.0969\ in)$

$d = 3.969\ mm\ (.156\ in)$

$P_{BR} = 10\ 979\ N\ (2464\ lb)/fastener$

TABLE 6. - MINIMUM MARGINS OF SAFETY FOR TRUSS MEMBERS

Failure Mode	Length	Max. Load	Allow. Load	M.S.
Tension	.503 m (19.81 in.)	13290 N (2,988 lb)	49304 N (11,084 lb)	2.71
Crippling	.503 m (19.81 in.)	13290 N (2,988 lb)	28197 N (6,339 lb)	1.12

Using a fitting factor of 1.15,

$$M.S._{(Bearing)} = \frac{10\ 979}{(1.15)(3248)} - 1 = +1.94$$

Aft solid web stability: The shear web buckling analysis uses the COMAIN (Table 5) program. The most critical panel, has an applied shear load of:

$$\text{Max } N_{XY} = 97.20 \text{ N/mm (552 lb/in) (Figure 22).}$$

$$\text{or } \tau_{XY} = 47.21 \text{ MPa (6847 psi)}$$

from the COMAIN program with

$$a = 0.237 \text{ m (9.34 in.) and } b = 0.157 \text{ m (6.20 in.)}$$

$$N_{XY,CR} = 84.76 \text{ N/mm (484 lb/in.) with simply supported edges}$$

$$N_{XY,CR} = 138.0 \text{ N/mm (788 lb/in.) with fixed (clamped) edges}$$

Assuming that the end fixity is half way between simply supported and fixed,

$$N_{XY,CR} = \frac{84.76 + 138.0}{2} = 111.38 \text{ N/mm (636 lb/in.)}$$

$$M.S._{(Shear\ buckling)} = \frac{111.38}{97.20} - 1 = .15$$

1.2.4.3 Truss ribs: The truss rib selected for analysis was the most critical truss rib which is located at VSS 145.71. This stress analysis was similar to that described previously. The minimum margins of safety were +.11 for cap lateral stability and +.36 for flange buckling.

1.2.4.4 Solid web rib: The top three ribs are designed with shear-resistant solid webs. Rib internal loads were generated using the VSS 299.97 hinge rib which is the highest loaded station. All three ribs are constructed from a 20-ply laminate containing an orientation of 30 percent 0°, 60 percent ±45°, and 10 percent 90°. In the center of the rib, the webs are reinforced against buckling with a sheet of 0.95 mm (0.0375 in.) syntactic core located at the mid-plane of the laminate. To accommodate the core, six plies of the laminate are removed. All strength margins on the solid web ribs were high.

- Solid web buckling analysis: The portion of the web subjected to the highest buckling loads is located adjacent to the rear spar and between the two hinge fitting stiffeners. For the purposes of analysis this web element conservatively is assumed to be loaded as follows:

  Web margin analysis under combined N_x and N_{xy} loading:

  For the above loading distribution the following allowable loads were calculated using (PLM) program (ref. Table 5).

  $$N_{X,CR} = 74\ 954 \text{ N/m}, \ (428 \text{ lb/in})$$

  $$N_{XY,CR} = 85\ 812 \text{ N/m}, \ (490 \text{ lb/in})$$

  The maximum applied loads are:

  $$N_X = 41\ 154 \text{ N/m} \ (235 \text{ lb/in})$$

  $$N_{XY} = 36\ 076 \text{ N/m} \ (206 \text{ lb/in})$$

  $$R_C + R_S{}^2 = 1$$

  therefore,

  $$\text{M.S.(Web Buckling)} = \left[(41\ 154/74\ 954) + (36\ 076/85\ 812)^2\right]^{-1/2} - 1$$

  $$\text{M.S.} = +0.17$$

1.2.4.5 Fail-safe analyses. - Fail-safe analyses were performed on the three typical ribs VSS 97.19, VSS 145.71 and VSS 299.97. The fail-safe cases considered for each rib are shown in figures 30, 31, and 32. In no case did the stresses exceed the allowables. Each case was run separately using the 2D NASTRAN models. The resulting limit loads for the fail-safe cases were compared with the design ultimate loads.

For VSS 97.19 only Cases I and III showed any fail-safe loads which were in excess of the design loads. For Case 1 the stress in the inner flange of the left-hand rib cap at the intersection of the failed truss member is -164 MPa (-23800 psi) which gives a margin of safety of 217/164 - 1 = 0.32. For Case III the lowest margin was for shear buckling in the bay forward of the failed panel, this margin is 0.11.

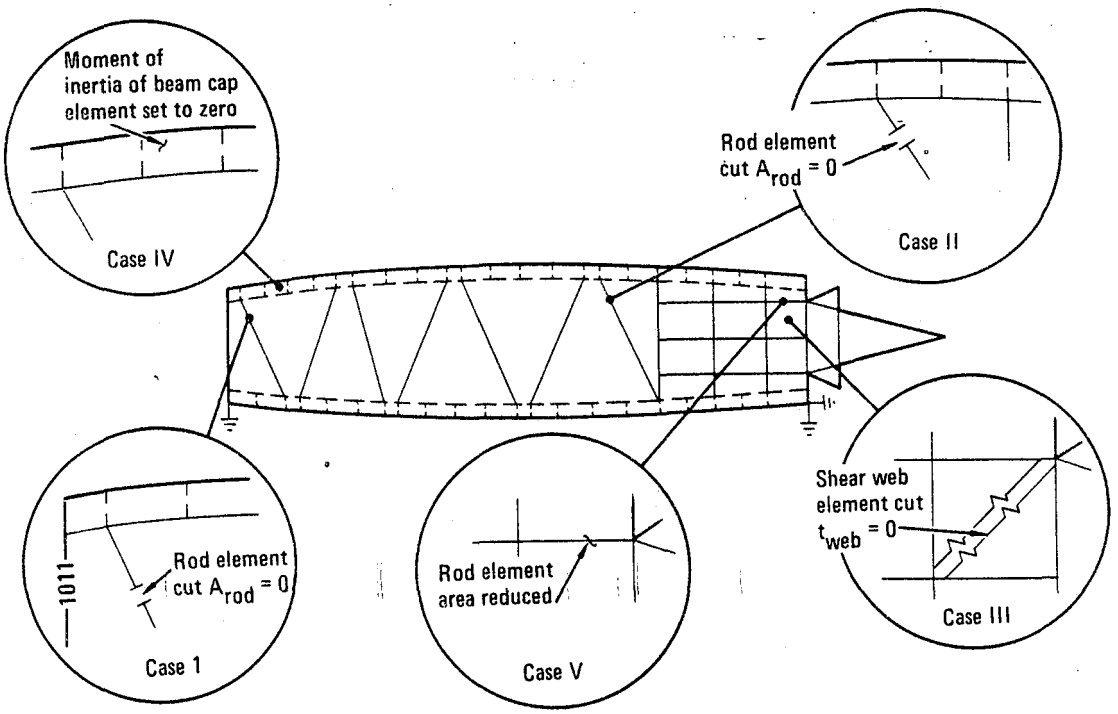

Figure 30. - VSS 97.19 rib station NASTRAN 2-D model, fail-safe analysis.

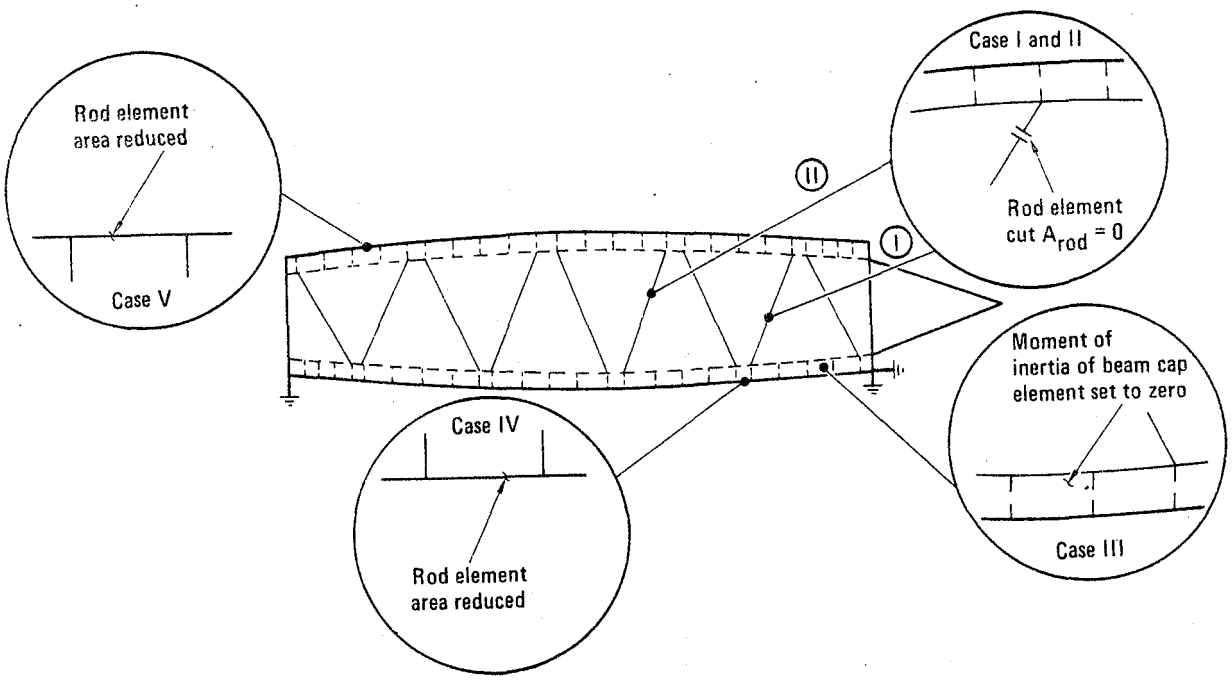

Figure 31. - VSS 145.71 rib station NASTRAN 2-D model, fail-safe analysis.

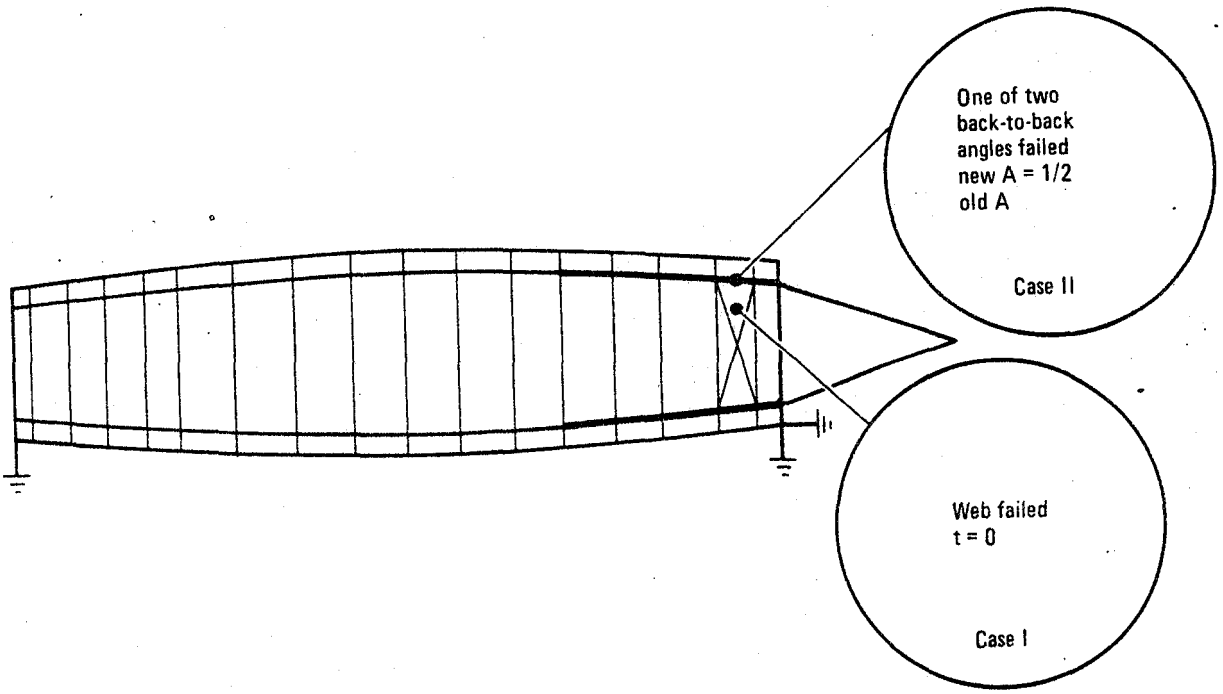

Figure 32. - VSS 299.97 rib station NASTRAN 2-D model, fail-safe analysis.

For VSS 145.71 only Cases I, IV and V showed fail-safe loads in excess of the design loads. Case I is similar to Case V for the VSS 97.19 rib and the corresponding minimum margin is 0.22 for the inner cap flange. Case IV gave a maximum inner cap flange stress of 175 MPa and a margin of safety of 217/175-1 = 0.24. Case V similarly gave a minimum margin in the cap flange of 0.18.

For VSS 299.97 no fail-safe loads in excess of design loads occurred.

1.2.5 Spar Analysis

1.2.5.1 Analytical approach: The analysis of the spars was conducted using primarily a series of Lockheed-Georgia computer programs developed under company funding for the express purpose of providing analysis methods for use in advanced composite material designs and are therefore proprietary. The unidirectional properties and allowables for the T300/5208 graphite/epoxy are stored in a data bank which is a library program for this series of programs. All programs in the series use linear stress-strain relationships. The program designations, their individual functions, and their specific use in the spar analysis are shown in table 7.

TABLE 7. - COMPUTER PROGRAMS USED IN SPAR ANALYSIS

Program	Function	Source
LG-001	Calculates average elastic properties and stiffness matrices for composite laminates.	Lockheed-Georgia Co.
LG-004	Calculates section properties of composite sections providing EA, EI, and neutral axis location.	Lockheed-Georgia Co.
LG-011	Calculates ply level stresses and strains and laminate margins of safety for in-plane loads.	Lockheed-Georgia Co.
LG-031	Calculates buckling loads of simply supported orthotropic plates subject to biaxial and shear loads.	Lockheed-Georgia Co.
LG-033	Calculates buckling load of rectangular orthotropic plate with three edges simply supported and one edge free, subject to axial load.	Lockheed-Georgia Co.
LG-080	Calculates tangential, radial, and shear stresses at 5^0 intervals around circular or elliptical cutouts at variable distances from the edge of the cutout for general in-plane loads.	Lockheed-Georgia Co.

The spar web panels were analyzed first for shear buckling using the LG-031 program. The shear flows used were gross shears in panels without cutouts and net shears in panels with cutouts. The program computes an allowable shear flow based on the panel dimensions, thickness, and ply orientation.

The panels with cutouts were then analyzed using the LG-080 program to calculate the value and location of the peak stresses around the edge of the cutout. These peak stresses were then converted to running loads and input to the LG-011 program which calculates the minimum margin of safety in the laminate.

The web stiffeners were then analyzed to determine that they provided adequate bending stiffness to prevent buckling from progressing from one panel to the next. Data from reference 2 were used to determine the required bending stiffness. The bending stiffness of the web (D_{11}) was calculated using the LG-011 program. The LG-004 program was then used to calculate the actual bending stiffness of the stiffeners.

The spar caps were analyzed using the axial loads previously shown. The caps were checked for net section tension using the notched allowables. They were also checked for local compression instability of the critical flange using the LG-033 program.

Web panel buckling margins were calculated as the allowable buckling shear flow over the gross or net shear flow depending on whether the panel contained a cutout. The margins at the edge of a panel cutout were calculated using the LG-011 program and the lowest ply margin is quoted. The method of determining the minimum margin in the program is as described above, except that strains were compared rather than loads.

The margins for the web stiffeners were calculated as the actual bending stiffness over the required bending stiffness. Cap margins were calculated by summing up the allowable load for each component of the cap and comparing to the applied load. The lowest allowable total load, either net tension or flange crippling was used in the margin calculation.

1.2.5.2 Strength and stability analysis: The front and rear spars are structurally similar in that each have tee caps, webs with 4-inch-diameter circular access hole cutouts in approximately every other stiffener bay and generally three blade stiffeners on the web between ribs. The rear spar is different in that it has several significant additional cutouts in the web at the lower end of the spar. These are for the rudder actuators and rudder actuator support ribs to extend through the spar. The cutouts for the actuators are 4-inch diameter circular holes while the holes for the support ribs are D-shaped holes 0.091 m (3.6 in.) long by 0.05 m (1.95 in.) wide. The 'D' shaped holes are treated as ellipses. In addition, smaller holes occur in the rear spar at each rudder hinge rib location.

The rib-to-spar clips are cocured to the front spar and mechanically attached on the rear spar. Preliminary analysis showed that the shear flows were low compared to the joint allowables and all margins were high. The auxiliary spar extends up to VSS 97.199 and serves to close out the VSS 90.19 stub rib. It carries no primary loads, therefore no analysis was conducted on it. The rudder damper fitting forms a part of the rear spar web at VSS 307.68 and is identical to the existing fitting. There are no damping loads unique to the composite fin, therefore no analysis of the part was warranted.

1.2.5.3 Typical web analysis: The typical web panel selected is located on the front spar at VSS 100.2. The panel geometry is shown in figure 33.

The gross shear flow at this location is 226 kN/m (1290 lb/in). The net shear flow is [50.8/(50.8-10.2)] x 226 = 282 kN/m (1613 lb/in). The LG-031 program was run using the geometry shown and the allowable buckling shear flow was calculated and was 314 kN/m (1795 lb/in). The margin of safety in shear buckling is (314/282) -1 = +0.11 M.S.

The LG-080 program was then run to determine the stresses around the edge of the access hole. The maximum tangential tensile stress occurred at an angle of 130 degrees from the reference axis and was 404.72 MPa (58.7 ksi). Preliminary analysis showed that the location of the minimum margin occurs at the edge of the hole where the tangential stresses are maximum and the radial and shear stresses are essentially zero. The local ply orientation at Point C is $[(-85.5)_4, 50_2, -40, 50]_s$. The web thickness is 24 x 0.129 mm = 3.1 mm (0.122 in.) $N_x = \sigma t$ = 404.85 x 0.0031 = 1.255 MN/m (7174 lb/in.).

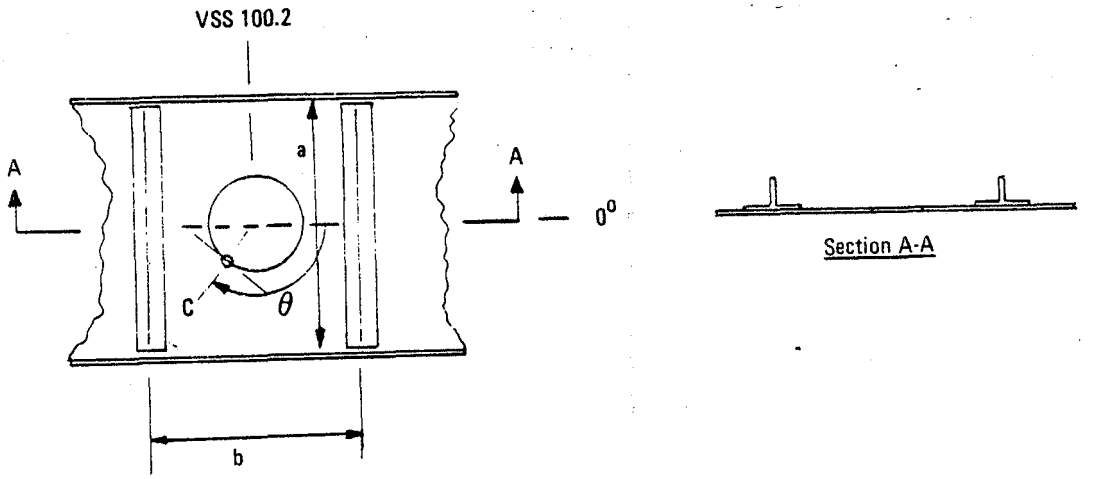

a = .508m (20.0 in.) b = .16m (6.3 in.) θ = 130°

Web ply orientation is $(\pm 45_4, 0_2, 90, 0)_s$ a total of 24 plies.

Figure 33. - Typical web panel geometry.

The LG-011 program was then run using the local ply orientation at Point C as 0° in the tangential direction. The maximum ratio of applied strain to allowable strain occurred as transverse tension in the -85° plies and was 0.951.

The minimum margin is then (1.0/.951) - 1 = +.05

1.2.5.4 Typical cap analysis: The typical cap section selected is located on the front spar between VSS 99.82 and 115.94. Geometry of the cap is shown in figure 34. The maximum load at this location is 74282 N (16700 lb). Each portion of the cap is analyzed separately and then the lowest allowable strain is taken as the critical strain for the cap.

- Forward flange

The ply layup is $(\pm 45_3/+45/0_6)_s$. The gross area is A = 39.9 x 3.38 = 135 mm^2 (.209 in^2). From figure 59 F_c = 285.4 MPa (41.4 ksi). From figure 60 E_c = 69.64 GPa (10.1 msi). The strain ε_c = -285.4/69.64 = -4098 μm/m. From LG-033 $N_{x,cr}$ = -717 kN/m (-4098 lb/in).

$\therefore$ P_{cr} = -.03988 x 717 = -28.59 kN (-6434 lb)

$\therefore$ ε_{cr} = -28.59/.000135/69.64 = -3041 μm/m

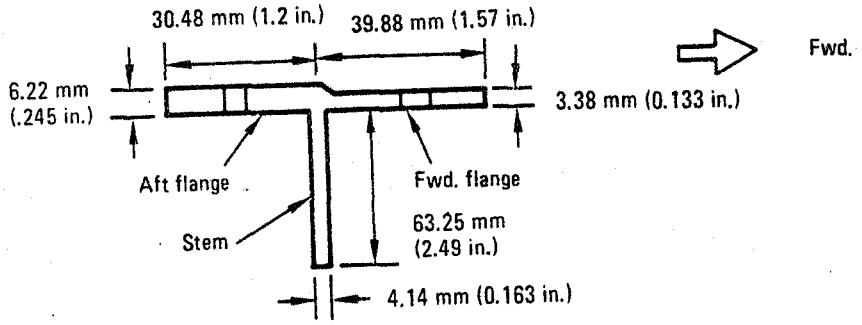

Forward flange ply layup is $(\pm 45_3/45/0_6)_s$ = 26 plies = 3.38 mm (.133 in.)

Aft flange ply layup is $(\pm 45_3/0_6/\pm 45_3/0_6)_s$ = 48 plies = 6.22 mm (.245 in.)

Stem ply layup is $(\pm 45_3/0_4/\pm 45/0_2/90/0)_s$ = 32 plies = 4.14 mm (.163 in.)

NOTE: Above VSS 127.69 on the front spar and above VSS 140.25 on the rear spar, the reinforcing of the web to create the stem terminates. The cap is then assumed to be the flanges only.

Figure 34. - Spar cap geometry.

- Aft flange

  The ply layup is $(\pm 45_3/0_6/\mp 45_3/0_6)_s$. The gross area is A = 30.5 x 6.22 = 189.7 mm^2 (.294 in^2). From figure 63 F_c = 303.4 MPa (44 ksi). From figure 64 E_c = 75.84 GPa (11 Msi). The strain ε_c = -303.4/75.84 = -4000 μm/m. $N_{x,cr}$ is considerably higher than for the forward flange. Hence the forward flange is critical.

- Stem

  The ply layup is $(\pm 45_3/0_4/\mp 45/0_2/90/0)_s$. The gross area is A = 6.325 x 4.14 = 262 mm^2 (0.406 in^2). From figure 63 F_c = 275.8 MPa (40 ksi). From figure 64 E_c = 68.95 GPa (10 Msi). The strain ε_c = -275.8/68.95 = -4000 μm/m.

  The minimum strain is in the forward flange for buckling. The allowable compressive loads in each component are as follows:

Forward flange		= -28 590 N (6434 lb)
Aft flange	.897 x 3041 x 75.84	= -43 750 N (9836 lb)
Stem	.262 x 3041 x 68.95	= -54 940 N (12350 lb)
Total		127 280 N (28 620 lb)

  ∴ Margin of Safety = (127 280/74 287) - 1 = .71

1.2.5.5 Typical web stiffener analysis: The typical group of web stiffeners selected is located on the front spar between VSS 97.199 and 121.45. Figure 35 shows the panel and stiffener geometry and also a set of curves used to determine the required stiffness of the stiffener to prevent buckling from progressing from one web panel to the next.

There are three stiffeners between the ribs with the stiffener spacing being .16 m (6.3 in.). The two stiffener curve (figure 31) was conservatively used to determine the required stiffness. The 'a' dimension was taken as 3 x 16 = .48 m (18.9 in.). The 'b' dimension was taken as the average of the four bays between ribs and was .50 m (19.55 in.). a/b = 48/50 = .967 γ = 41.5. The D_{11} of the skin was calculated using the LG-001 program and was 113.7 N/m (1007 lb/in.). The required EI of the stiffener is the 41.5 x 113.7 x 48 = 2265 N/m^2 (789,333 lb/in^2). The actual EI of the stiffener was then calculated using the LG-004 program including a section of effective skin equal to the length of the skin flanges 0.038m (1.5 in.). The calculated value of EI was 4349 N/m^2 (151,559 lb/in^2). The margin of safety is therefore (4 349/2 265)-1 = +.92 M.S.

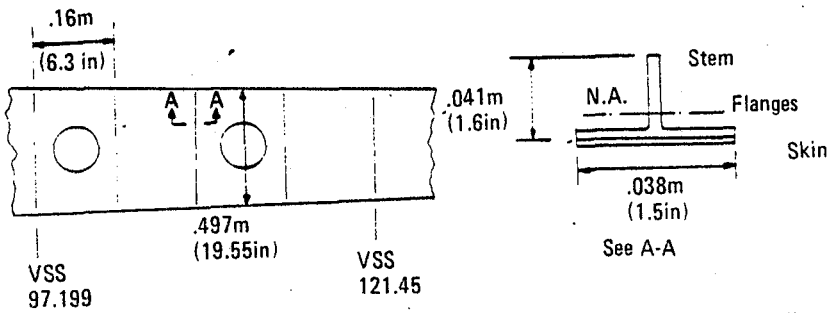

The stem ply orientation is $(\pm 45_2, 0_6, \mp 45_2, 0_3)_s$ = 34 plies

The flange ply orientation is $(\pm 45_2)_s$ = 8 plies

The skin ply orientation is $(\pm 45_4, 0_2, 90,0)_s$ = 24 plies

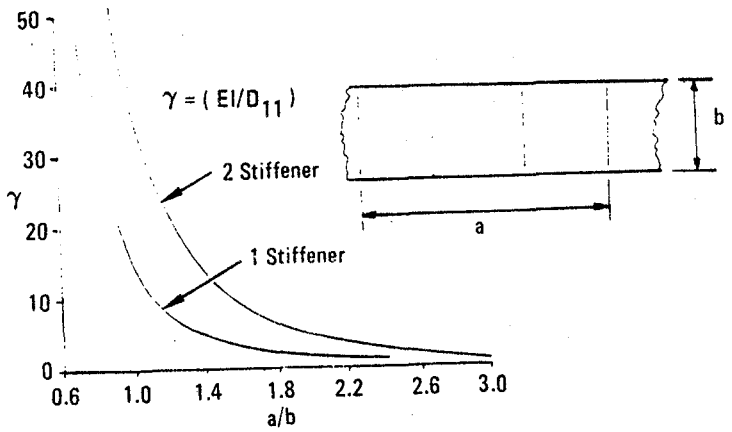

Figure 35. - Web stiffener geometry and required stiffness data.

1.2.5.6 Spar to fuselage joint analysis: The front spar caps and web are attached to the fuselage structure by a system of aluminum splice fittings and mechanical fasteners as shown in figure 36. The caps are spliced by two angle fittings nesting on the inside of the composite tee cap and a plate fitting on the outside. The composite spar web is spliced to the aluminum web by a single lap splice plate with two rows of fasteners. Preliminary analysis showed that the fasteners were critical in bearing in the composite as opposed to being critical in shear in the fastener. The total allowable bearing load in the cap splice fasteners was 522 177 N (177,396 lb). The applied cap load was 91 184 N (20 500 lb). The margin is (522 177/91 184) -1 = High. The allowable load per inch in the web splice was 673 400 N/m (3848 lb/in.). The applied shear flow was 244 650 N/m (1398 lb/in.). The margin is (673 400/244 650)-1 = High.

The rear spar caps and web are also attached to the fuselage structure by a system of aluminum splice fittings and mechanical fasteners as shown in figure 12. The caps are spliced by two angle fittings meeting on the inside of the composite tee cap. The web composite spar web is spliced to the aluminum web by a single lap splice plate with two rows of fasteners. Fasteners through the cap stem are critical in double shear while fasteners through the flanges and web are critical in bearing. The total allowable fastener load in the cap splice was 52 6452N (11,8357 lb). The applied cap load was 133 400 N (30 000 lb). The margin is (526 452/133 440)-1 = High. The allowable load per inch in the web splice is 914 500 N/m (5226 lb/in.). The applied shear flow is 124 250 N/m (710 lb/in.). The margin is (914 550/ 124 250)-1 = High.

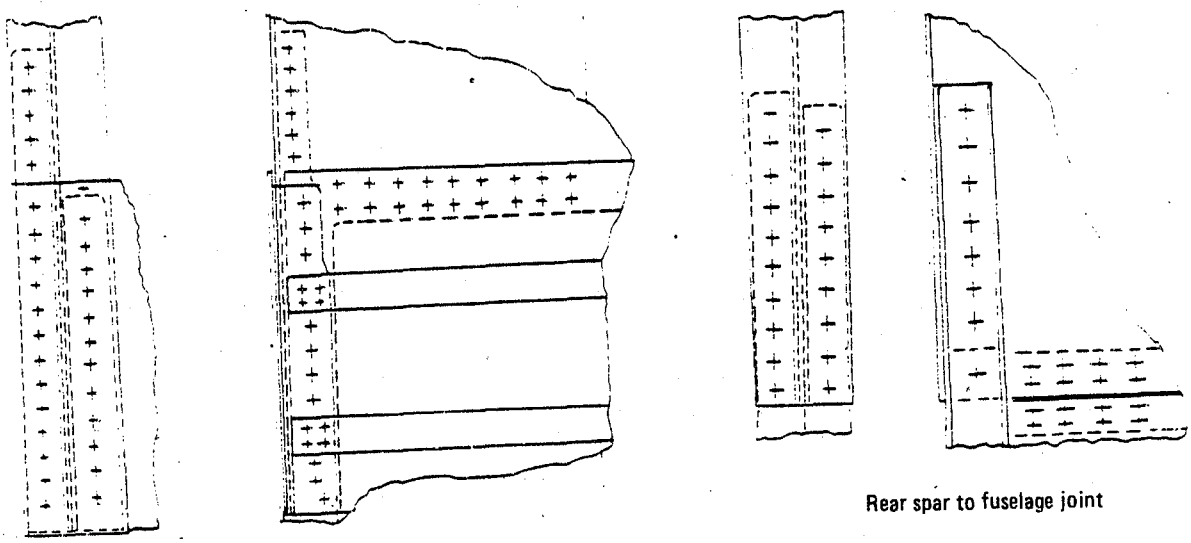

Figure 36. - Spar to fuselage joints.

1.2.5.7 Fail-safe analysis: Four separate fail-safe load cases were developed by Lockheed-California using the finite element NASTRAN model. The method used was to reduce the stiffness of a member to near zero to simulate a failure in that member in the model. The loads in the remaining members were then examined to determine their value relative to the design loads. This process was repeated until the critical failure members had been identified. The four critical cases include a failed cap in the front spar, a failed cap in the rear spar, a failed web in the front spar, and a failed web in the rear spar.

A comparison of the fail-safe loads and the design loads shows that the fail-safe loads exceeded the design loads at three locations. An examination of the margins shows that there was sufficient extra strength at these locations to prevent the margins from becoming negative. A summary of the analysis at the critical locations is shown in table 8.

1.2.6 Flutter Analysis

A flutter analysis was performed using the L-1011-1 antisymmetric airplane flutter model with the composite fin. Mach 0.88 aerodynamics was used with Kernel Function aero for the wing and double lattice aerodynamic theory for the fuselage and empennage.

No flutter was found below the required 1.2Vd/M30 for the intact, full fuel case.

TABLE 8. - SUMMARY OF FAIL-SAFE ANALYSIS AT CRITICAL LOCATIONS

Location	Element	① Design Loads	Fail-Safe Loads ②	Ratio ②/①	Design M.S.	Fail-Safe M.S.
Front Spar	Cap	38.45 kN (8 643 lb.)	42.47 kN (9 547 lb.)	1.10	High	High
VSS 133	Cap	-38.80 kN (-8 723 lb.)	-40.31 kN (-9 063 lb.)	1.04		
Front Spar	Cap	26.64 kN (5 990 lb.)	28.25 kN (6 350 lb.)	1.06		
VSS 157		-27.18 kN (-6 110 lb.)	-29.10 kN (-6 542 lb.)	1.06	High	High
Rear Spar	Web	-38.92 N (-875 lb.)	-46.93 N (-1 055 lb.)	1.21	+ 0.21	0.00
VSS 110.						

2. MATERIAL VERIFICATION

This task included material qualification, durability, damage and defect tolerance, and material allowables.

2.1 Material Qualification

A material specification was developed during Phase I, reference 1. After selection of the T300/5208 system the material was qualified by the Quality Assurance Laboratory to this specification. The results are shown in tables 9 and 10. Although two compression and three short beam shears fell slightly below the requirement, the material was qualified to the specification.

2.2 Laminate Durability-Test H13D

The purpose of this test activity was to determine the durability of T300/5208 graphite/epoxy laminates typical of the L-1011 ACVF application. The four layups tested are shown in table 11. Specimens were prepared from these laminates and tests were conducted as shown in table 12.

The fatigue tests were run for two lifetimes in the cyclic environment shown in figure 33. All specimens survived the two-lifetime fatigue exposure. The specimens were then residual strength tested in the laboratory environment. Results are presented in table 13. The notch factors vary from 0.495 for layup 2 to 0.704 for layup 3. The fatigue and cyclic environment had a negligible effect on the static strengths. The notch was a 4.76 mm (3/16 in.) hole.

2.3 Defect and Damage Tolerance

2.3.1 Evaluation of defect tolerance in composites - test H12B. - Test H12B had the objective of assessing the tolerance to defects in T300/5208 composite laminates. Starting with 25.4 mm(1in) diameter defects, the plan was to work progressively down in size to find the maximum size tolerable defect.

Eight specimens of the configuration shown in figure 37 successfully completed four lifetimes of fatigue loading with no propagation of the imbedded defects. Four specimens were tested at room temperature in ambient air, and four specimens, preconditioned to 1 percent moisture weight gain, were tested under the environmental cycle shown in figure 38.

TABLE 9. - GRAPHITE/EPOXY PRE-PREG (NARMCO T300/5208) MATERIAL QUALIFICATION TEST RESULTS (SI UNITS) (1 of 3)

Specification Requirements			Results of Test					
			1	2	3	4	5	Avg.
Aeral Wt	130 – 149 g/m^2		139	141	147	141		142
Infrared Spectrophotometric Analysis			Conforms					
Volatiles (60±5 Minutes at 450K)	3% Max		Edge	Center				
			2.45	2.56				
Dry Resin Content	38 – 44%	Left	43.2	43.9				43.2
		Right	43.1	42.7				
Flow at 450K at 486 kPa	15 – 29 %		20.0	19.5				
Gel Time at 450K	Info Only, Minutes		26.5					
Cured Fiber Volume 2mm Panel	60 – 68%		67	67	67			67
Cured Fiber Volume 1.5mm Panel	60 – 68%		64	65	64			65
Cured Fiber Volume 1mm Panel	60 – 68%		63	64	64			64
Cured Fiber Volume 0.76mm Panel	60 – 68%		67	67	67			67
Specific Gravity 2mm Panel	1.55 – 1.62		1.59	1.59	1.59			1.59
Specific Gravity 1.5mm Panel	1.55 – 1.62		1.56	1.57	1.57			1.57
Specific Gravity 1mm Panel	1.55 – 1.62		1.57	1.55	1.56			1.56
Specific Gravity 0.76mm Panel	1.55 – 1.62		1.59	1.58	1.59			1.59
Thickness Per Ply 2mm Panel	0.117 – 0.142 mm							0.119
Thickness Per Ply 1.5mm Panel	0.117 – 0.142 mm							0.132
Thickness Per Ply 1mm Panel	0.117 – 0.142 mm							0.124
Tensile, Longitudinal at 297K (1mm)	1172 MPa min. ind.		1386	1345	1441	1551	1489	1441
Tensile Modulus (Longit.) at 297K	138 GPa min. ind.		157	157	165	175	164	163
Tensile Longit. at 218K	1172 MPa min. ind.		1544	1813	1558	1627	1627	1634
Tensile Modulus (Longit.) at 218K	138 GPa min. ind.		150	161	152	166	155	157
Tensile, Longit. at 355K	1172 MPa min. ind.		1558	1655	1675	1793	1710	1675
Tensile Modulus (Longit.) at 355K	138 GPa min. ind.		161	142	143	145	145	148
Tensile, Transverse at 297K (1mm)	41 MPa min. ind.		85	77	85	84	90	84
Tensile Modulus Transverse at 297K	8 GPa min. ind.		13.1	12.4	12.4	12.4	12.4	12.4

Note: min. ind. = minimum individual

TABLE 9. - GRAPHITE/EPOXY PRE-PREG (NARMCO T300/5208) MATERIAL QUALIFICATION TEST RESULTS (SI UNITS) (2 of 3)

Specification Requirements		Results of Test					
		1	2	3	4	5	Avg.
Tensile, Transverse at 218K	48 MPa min. ind.	92	59	75	72	72	74
Tensile Modulus at 218K	10 GPa min. ind.	14.5	13.1	14.5	14.5	13.8	13.8
Tensile, Transverse at 355K	34 MPa min. ind.	53	50	57	38	58	51
Tensile Modulus at 355K	7.6 GPa min. ind.	11.7	12.4	11.7	11.7	11.7	11.7
Tensile, Trans. Strain at Fail	0.50% min. ind.	0.7	0.6	0.7	0.7	0.7	0.7
Tensile, 45 Degree at 297K (1.5mm)	158 MPa min. ind.	201	188	197	200	191	195
Tensile Modulus, 45 Degree at 297K	13.8 GPa min. ind.	22.8	21.4	20.7	23.4	20.7	22.1
Tensile, 45 Degree at 218K	158 MPa min. ind.	219	205	205	212	225	213
Tensile Modulus, 45 Degree at 218K	13.8 GPa min. ind.	16.5	19.3	20.7	22.1	20.7	20.0
Tensile, 45 Degree at 355K	131 MPa min. ind.	156	164	161	157	154	158
Tensile Modulus, 45 Degree at 355K	13.8 GPa min. ind.	20.7	20.0	20.0	19.3	18.6	20.0
Tensile, 45 Degree at 355K Wet	117 MPa min. ind.	161	168	165	154	149	159
Tensile Modulus, 45 Deg. at 355K Wet	12.4 GPa min. ind.	16.5	15.9	18.6	17.2	17.2	17.2
Compressive at 297K (0.76mm)	1310 MPa min. ind.	1634	1324	1655	1524	1476	1524
Compressive Modulus 297K	124 GPa min. ind.	123	123	125	125	129	125
Compressive at 218K	1310 MPa min. ind.	1703	1744	1675	1586	1538	1648
Compressive at 355K	1310 MPa min. ind.	1427	1365	1220	1241	1345	1317
Compressive Modulus at 355K	124 GPa min. ind.	123	121	123	129	124	124
Flexural Strength at 297^{0}K (2mm)	1448 MPa min. ind.	1972	1779	1751	1924	1841	1855
Flexural Modulus at 297^{0}K	124 GPa min. ind.	138	143	141	145	148	143
Flexural Strength at 218^{0}K	1517 MPa min. ind.	1862	1827	1855	1820	1820	1834
Flexural Modulus at 218^{0}K	124 GPa min. ind.	153	149	141	137	143	145
Flexural Strength at 355^{0}K Wet	1379 MPa min. ind.	1586	1620	1544	1669	1655	1613
Flexural Modulus at 355^{0}K Wet	110 GPa min. ind.	131	135	132	130	135	132
Flexural Strength at 355^{0}K	1379 MPa min. ind.	1786	1669	1731	1675	1917	1758
Flexural Modulus at 355^{0}K	110 GPa min. ind.	144	146	148	150	163	150

Note: min. ind. = minimum individua

TABLE 9. - GRAPHITE/EPOXY PRE-PREG (NARMCO T300/5208) MATERIAL QUALIFICATION TEST RESULTS (SI UNITS) (3 of 3)

Specification Requirements		Results of Test					
		1	2	3	4	5	Avg.
Short Beam Shear at 297K (2mm) Panel	90 MPa min. ind.	128	129	130	121	121	125
Short Beam Shear at 256K	138 MPa min. ind.	135	145	133	129	145	137
Short Beam Shear at 356K	83 MPa min. ind.	97	101	109	100	105	103
Short Beam Shear at 355K Wet	75 MPa min. ind.	103	104	103	101	97	102
Water Absorption (2mm) Panel	1.5% Max. Avg.	0.01	0.06	0.04			0.04
Water Absorption (1.5mm) Panel	1.5% Max. Avg.	0.16	0.09	0.13			0.13
Water Absorption (1mm) Panel	1.5% Max. Avg.	0.03	0.13	0.05			0.07
Water Absorption (0.76mm) Panel	1.5% Max. Avg.	0.04	0.00	0.16			0.10
Thickness per ply (0.76mm) Panel	0.117 – 0.142 mm						0.140
Compressive Modulus 218K	124 GPa min. ind.	140	125	125	129	125	129
Alignment, Gaps, Width, Bend Radius, Tack		Okay					

Note: min. ind. = minimum individual

Visual Inspection Results:

Roll No. 9 appeared uniform in quality and condition, clean and free of foreign material and defects exceeding specified tolerances. The carrier width appears to be within tolerances and is easily removed from the prepreg without transfer of resin or distantion of fiber. The pre-preg did not split, springback, or break when bent around a 25.4mm dia. mandrel. Tackiness is satisfactory for ease of handling.

TABLE 10. - GRAPHITE/EPOXY PRE-PREG (NARMCO T300/5208) MATERIAL QUALIFICATION TEST RESULTS (CUSTOMARY UNITS) (1 of 3)

Specification Requirements		Results of Test					
		1	2	3	4	5	Avg.
Areal Wt	139 – 149 g/m^2	139	141	147	141		142
Infrared Spectrophotometric Analysis		Conforms					
Volatiles (60±5 Minutes at 350^{0}F)	3% Max	Edge	Center				
		2.45	2.56				
Dry Resin Content	38 – 44% Left	43.2	43.9				43.2
	Right	43.1	42.7				
Flow at 350^{0}F at 85 psi	15 – 29%	20.0	19.5				
Gel Time at 350^{0}F	Info Only, Minutes	26.5					
Cured Fiber Volume 0.080 In. Panel	60 – 68%	67	67	67			65
Cured Fiber Volume 0.060 In. Panel	60 – 68%	64	65	64			65
Cured Fiber Volume 0.040 In. Panel	60 – 68%	63	64	64			64
Cured Fiber Volume 0.030 In. Panel	60 – 68%	67	67	67			67
Specific Gravity 0.080 In. Panel	1.55 – 1.62	1.59	1.59	1.59			1.59
Specific Gravity 0.060 In. Panel	1.55 – 1.62	1.56	1.57	1.57			1.57
Specific Gravity 0.040 In. Panel	1.55 – 1.62	1.57	1.55	1.56			1.56
Specific Gravity 0.030 In. Panel	1.55 – 1.62	1.59	1.58	1.59			1.59
Thickness Per Ply 0.080 In. Panel	.0046 – .0056 (")						.0047
Thickness Per Ply 0.060 In. Panel	.0046 – .0056 (")						.0052
Thickness Per Ply 0.040 In. Panel	.0046 – .0056 (")						.0049
Tensile, Longitudinal at 75^0 (.040")	170 ksi min. ind.	201	195	209	225	216	209
Tensile Modulus (Longit.) at 75^{0}F	20 Msi min. ind.	22.7	22.8	23.9	25.4	23.8	23.7
Tensile Longit. at -67^{0}F	170 ksi min. ind.	224	263	226	236	236	237
Tensile Modulus (Longit.) at -67^{0}F	20 Msi min. ind.	21.8	23.4	22.0	24.1	22.5	22.8
Tensile, Longit. at +180^{0}F	170 ksi min. ind.	226	240	243	260	248	243
Tensile Modulus (Longit.) at 180^{0}F	20 Msi min. ind.	23.3	20.6	20.8	21.1	21.0	21.4
Tensile, Transverse at 75^{0}F (0.040")	6 ksi min. ind.	12.4	11.2	12.3	12.2	13.0	12.2
Tensile Modulus, Transverse at 75^{0}F	1.2 ksi min. ind.	1.9	1.8	1.8	1.8	1.8	1.8

Note: min. ind. = minimum individual

TABLE 10. - GRAPHITE/EPOXY PRE-PREG (NARMCO T300/5208) MATERIAL QUALIFICATION TEST RESULTS (CUSTOMARY UNITS) (2 of 3)

Specification Requirements		Results of Test					
		1	2	3	4	5	Avg.
Tensile, Transverse at -67°F	7 ksi min. ind.	13.4	8.6	10.9	10.5	10.4	10.7
Tensile Modulus at -67°F	1.5 Msi min. ind.	2.1	1.9	2.1	2.1	2.0	2.0
Tensile, Transverse at 180°F	5 ksi min. ind.	7.7	7.3	8.3	5.5	8.4	7.4
Tensile Modulus at 180°F	1.1 Msi min. ind.	1.7	1.8	1.7	1.7	1.7	1.7
Tensile, Trans Strain at Fail. (0.040")	0.05% min. ind.	0.7	0.6	0.7	0.7	0.7	0.7
Tensile, 45 Degree at 75°F (0.060")	23 ksi min. ind.	29.2	27.2	28.6	29.0	27.7	28.3
Tensile Modulus, 45 Degree at 75°F	2 Msi min. ind.	3.3	3.1	3.0	3.4	3.0	3.2
Tensile, 45 Degree at -67°F	23 ksi min. ind.	31.8	29.7	29.8	30.8	32.6	30.9
Tensile Modulus, 45 Degree at -67°F	2 Msi min. ind.	2.4	2.8	3.0	3.2	3.0	2.9
Tensile, 45 Degree at 180°F	19 ksi min. ind.	22.6	23.8	23.3	22.7	22.3	22.9
Tensile Modulus, 45 Degree at 180°F	2 Msi min. ind.	3.0	2.9	2.9	2.8	2.7	2.9
Tensile, 45 Degree at 180°F, Wet	17 ksi min. ind.	23.3	24.4	23.9	22.3	21.6	23.1
Tensile Modulus, 45 Deg. at 180°F Wet	1.8 Msi min. ind.	2.4	2.3	2.7	2.5	2.5	2.5
Compressive at 75°F (0.030")	190 ksi min. ind.	237	192	240	221	214	221
Compressive Modulus 75°F	18 Msi min. ind.	17.9	17.9	18.1	18.1	18.7	18.1
Compressive at -67°F	190 ksi min. ind.	247	253	243	230	223	239
Compressive at 180°F	190 ksi min. ind.	207	198	177	180	195	191
Compressive Modulus at 180°F	18 Msi min. ind.	17.8	17.6	17.8	18.7	18.0	18.0
Flexural Strength at 75°F (0.080")	210 ksi min. ind.	286	258	254	279	267	269
Flexural Modulus at 75°F	18 Msi min. ind.	20.0	20.8	20.5	21.0	21.4	20.7
Flexural Strength at -67°F	220 ksi min. ind.	270	265	269	264	264	266
Flexural Modulus at -67°F	18 Msi min. ind.	22.2	21.6	20.4	19.9	20.8	21.0
Flexural Strength at 180°F	200 ksi min. ind.	259	242	251	243	278	255
Flexural Modulus at 180°F	16 Msi min. ind.	20.9	21.2	21.4	21.7	23.7	21.8
Flexural Strength at 180°F Wet	200 ksi min. ind.	230	235	224	242	240	234
Flexural Modulus at 180°F Wet	16 Msi min. ind.	19.0	19.6	19.1	18.9	19.4	19.2

Note: min. ind. = minimum individual

TABLE 10. - GRAPHITE/EPOXY PRE-PREG (NARMCO T300/5208) MATERIAL QUALIFICATION TEST RESULTS (CUSTOMARY UNITS) (3 of 3)

Specification Requirements		Results of Test					
		1	2	3	4	5	Avg.
Short Beam Shear at 75°F (0.080")	13 ksi min. ind.	18.6	18.7	18.8	17.5	17.6	18.2
Short Beam Shear at -67°F	20 ksi min. ind.	19.6	21.0	19.3	18.7	21.0	19.9
Short Beam Shear at 180°F	12 ksi min. ind.	14.1	14.7	15.8	14.5	15.2	14.9
Short Beam Shear at 180°F Wet	11 ksi min. ind.	15.0	15.1	15.0	14.6	14.1	14.8
Water Absorption (0.080") Panel	1.5% Max. Avg.	.01	.06	.04			.04
Water Absorption (0.060") Panel	1.5% Max. Avg.	.16	.09	.13			.13
Water Absorption (0.030") Panel	1.5% Max. Avg.	.03	.13	.05			.07
Water Absorption (0.030") Panel	1.5% Max. Avg.	.04	.00	.16			.10
Thickness per ply (0.030") Panel	.0046 - .0056						.0055
Compressive modulus -67°F	18 Msi min. ind.	20.3	18.1	18.2	18.7	18.2	18.7
Alignment, Gaps, Width, Bend Radius, Tack		Okay					

Visual Inspection Results:

Roll No. 9 appeared uniform in quality and condition, clean and free of foreign material and defects exceeding specified tolerances. The carrier width appears to be within tolerances and is easliy removed from the prepreg without transfer of resin or distantion of fiber. The pre-preg did not split, springback, or break when bent around a 1" dia. mandrel. Tackiness is satisfactory for ease of handling.

Note: min. ind. = minimum individual

TABLE 11. - TEST LAMINATES

Panel No.	Layup	No. of Plies
1	$(\pm 45/0/\mp 45/\pm 45)_s$	14
2	$(\pm 45/0/\mp 45/\pm 45/0)_s$	16
3	$(\pm 45/0_3)_s$	10
4	$(0/+45/90/-45)_{2s}$	16

TABLE 12. - H13D TEST PLAN

Layup	Static Tension (RTD)		Fatigue Notched	Totals
	Unnotched	Notched		
1	5	5	10	20
2	5	5	10	20
3	5	5	10	20
4	5	5	10	20
Σ	20	20	40	80

TABLE 13. - LAMINATE RESIDUAL TENSION STRENGTH

Layup	No. Plies		Static Unnotched Control		Static Notched Control		Fatigued Notched Residual	
			MPa	ksi	MPa	ksi	MPa	ksi
1	14	AVE ①	389	56.4	208	30.1	213	30.9
		SD ②	12.7	1.84	3.5	0.51	4.7	0.68
		CV% ③	3.26	3.26	1.68	1.68	2.21	2.21
2	16	AVE	591	85.7	292	42.4	301	43.6
		SD	17.4	2.52	4.8	0.70	12.1	1.76
		CV%	3.00	3.00	1.66	1.66	4.05	4.05
3	10	AVE	1 148	166.5	807	117.1	776	112.5
		SD	32.6	4.73	40.9	5.93	69.8	10.13
		CV%	2.84	2.84	5.06	5.06	9.00	9.00
4	16	AVE	556	80.6	295	42.8	298	43.2
		SD	16.5	2.39	11.6	1.68	14.6	2.12
		CV%	2.96	2.96	3.93	3.93	4.91	4.91

① AVE – Average ② SD – Standard Deviation ③ CV – Coefficient of Variation

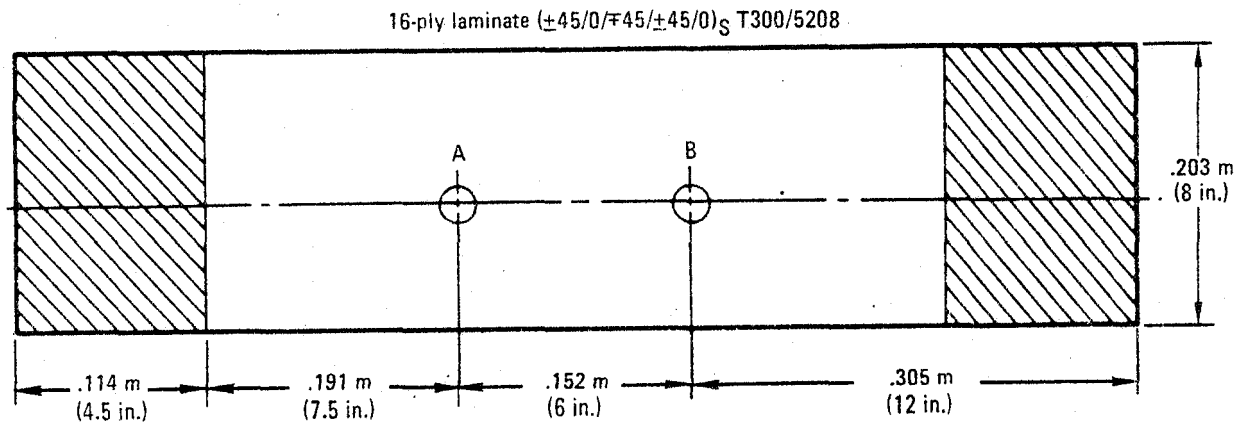

Defect: 25.4 mm (1 in.) dia. .0.13 mm (0.0005 in.) thick kapton
Defect A located between 2nd and 3rd plies
Defect B located between 8th and 9th plies
Cross-hatched region: fiberglass end tabs

Figure 37. - Defect tolerance specimen.

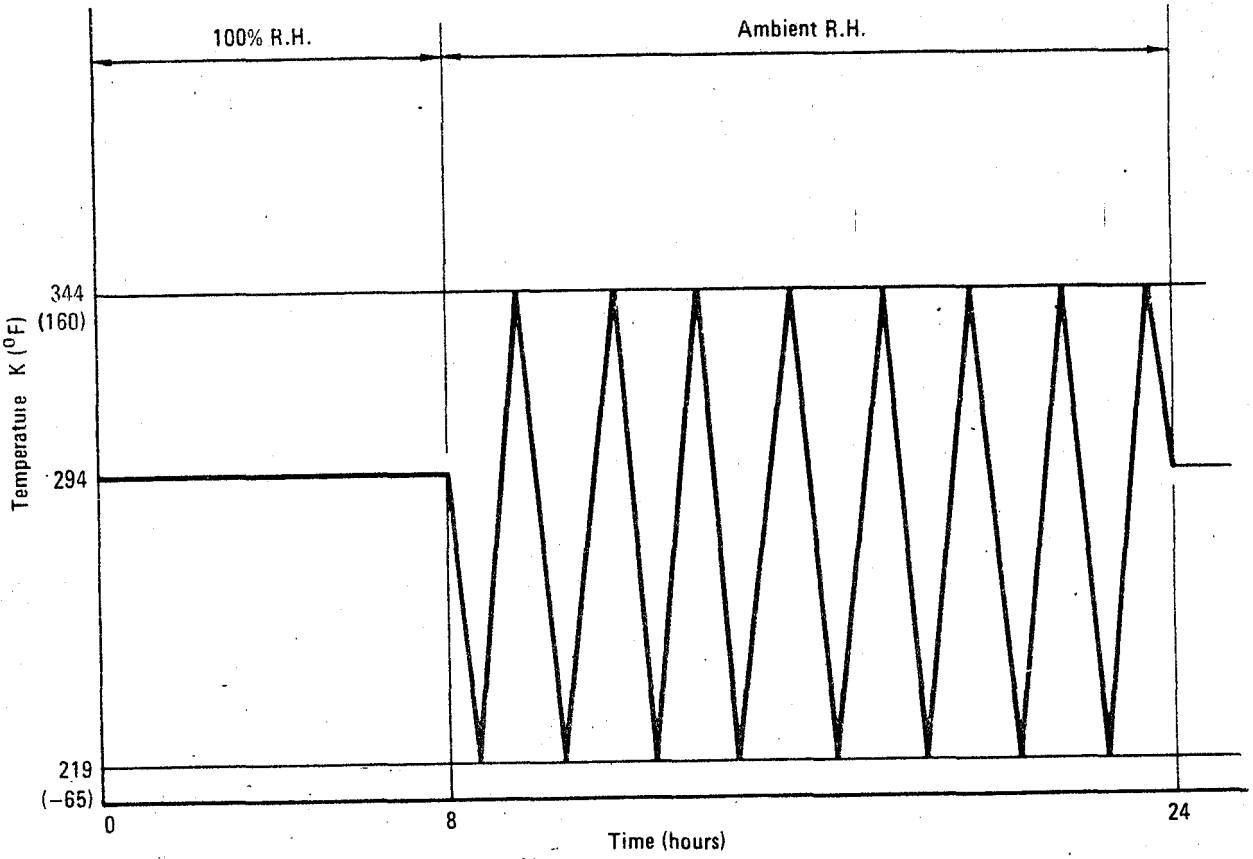

Figure 38. - Typical environmental cycle.

Because the 25.4 mm(1in) diameter defect survived the fatigue tests no smaller defects were run. All defects larger than this will be repaired.

The laminate tested represented the 16 ply area of the cover which is the most highly loaded cover area.

2.3.2 Graphite/aluminum corrosion barrier - test H18.- The purpose of this test program was to evaluate the corrosion inhibiting effectiveness of various faying surface treatments in mechanical joints between aluminum and graphite/epoxy composite laminates. Two sets of coupons, incorporating five faying surface corrosion protection barriers, were fabricated. These were:

- Faying surface sealant only
- Pressure-sensitive tape (Fed. Spec. L-T-1G0A)
- One ply of 120 Kevlar 49, cocured to the graphite/epoxy
- One ply of 120 Kevlar 49, cocured to the graphite/epoxy, with faying surface sealant
- Polyurethane primer and finish coat on both the aluminum and graphite components with faying surface sealant between the aluminum and graphite.

One set of coupons were exposed to a salt spray test (ASTM-B117) for one week, then to a weatherometer for 300 hours, and finally to the salt spray test for an additional 23 days. Throughout the salt spray test, the aluminum surface of the test coupons was exposed to the flow of the salt fog; throughout the weatherometer test, the aluminum was exposed to illumination from the carbon arc. The coupons were periodically removed, examined and photographed. At the completion of the test, the coupons were disassembled, examined, and photographed. The second set of coupons was sent to Point Loma for seacoast exposure which began on September 21, 1977.

Based on the examination of the laboratory exposed coupons, the following observations were made:

- With the exception of the painted coupon, the external aluminum surfaces of the test coupons were corroded after 64 hours of salt spray exposure. A corrosion blister approximately 6.35 mm (0.25 in.) in diameter was noted on the painted coupon after one week of salt spray exposure. The corrosion damage and blistering became increasingly severe with continued exposure.
- The corrosion of the unpainted aluminum surfaces on the test coupons was fairly uniform over the external portions of the unpainted coupons and was independent of the method of faying surface protection.
- No corrosion of the fasteners was noted.

- In the faying surface region, the painted coupon showed no degradation, the unpainted coupons with faying surface sealant showed corrosion only on the edges of the faying surface and the coupons with no sealant were corroded throughout the faying surface. The presence of the Kevlar ply and the pressure-sensitive tape had no corrosion inhibiting effect.

2.3.3 Environmental resistance of lightning protection techniques - test H19.- The purpose of this test was to determine if the need existed for a fiberglass interface between an aluminum wire mesh lightning protection and graphite composite and the effectiveness of paint coatings in preventing corrosion of the aluminum. Based on H29 described later the cover surface aluminum mesh was found to be unnecessary.

Salt-spray and sea-coast exposure are being used to evaluate the protective measures and determine the extent of the corrosion problem. The accelerated salt spray provided quick results for design decisions, while the long-term (up to five years) sea-coast exposure will simulate service conditions and show any problems that may occur with age.

The panels tested were 0.3 m (12 in.) x 0.3 m (12 in.), 10-ply construction $(\pm 45/0/\mp 45)_s$ made of T300/5208 prepreg tape. The panels were cured using the single-stage 450K (350°F) cure process. The lightning protection was 150 x 150 mesh aluminum screen that has been cleaned and coated with a corrosion inhibiting primer, BR-127A (American Cyanamid Co., Bloomingdale Division). Panels were fabricated with and without a 105 style fiberglass fabric layer between the aluminum screen and the graphite. For both combinations, tests were run on unpainted, painted and panels with conductive aluminum strips and titanium fasteners installed as shown in figure 39. Control panels were made by cocuring aluminum screen to 5-ply, 181 style fiberglass laminates.

The following summary describes the condition of the test specimens after approximately 1000 hours exposure to the salt spray environment.

Results of salt-spray exposure indicated that the amount of wire corrosion can be related to the extent that the aluminum wire mesh is encapsulated by resin. This is evidenced by the extent of corrosion: least being the fiberglass control (greatest encapsulation) to most corrosion being the mesh to graphite (least encapsulation). The graphite panels were considerably more corroded than the fiberglass control, indicating extensive galvanic acceleration. Painted panels showed excellent resistance in undamaged areas and moderate protection at the scribe line.

2.3.4 Evaluation of crack tolerance in composites - test H12A1.- The objective of this test was to develop data on the damage tolerance of the T300/5208 composite material and structural elements. These tests deal with

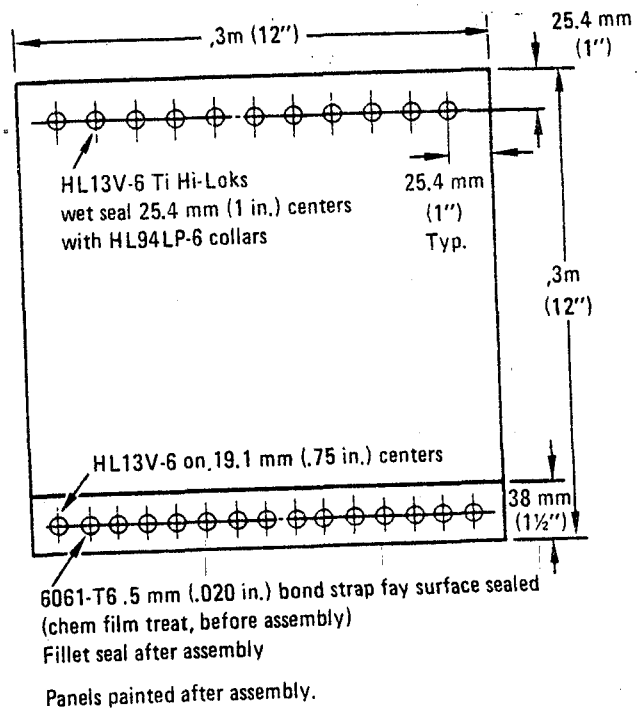

Figure 39. - Corrosion test panel representing cover assembly.

the degradation of strength in the presence of thru-the-thickness (full-penetration) damage. A 16-ply layup $(\pm 45/0/\mp 45/\pm 45/0)_s$ was used.

The test matrix is presented in table 14. A Center Cracked Tension (CCT) specimen patterned after the R-curve fracture test specification ASTM-E 561-76T was used and is shown in figure 40.

All specimens were stabilized as per ASTM-E561-76T to prevent out-of-plane buckling. For specimens run at 355K (+180°F), an environmental chamber was placed around the specimen and hot air blown through a water bath, the hot, wet air then entering the chamber. Temperature was controlled by thermocouples attached to the specimen surface. For tests conducted at 219K (-65°F), the same equipment was used except that the hot-air system was replaced with a solenoid operated LN_2 tank to cool the specimen. The specimen crack-opening displacement (COD) was monitored during test by 2 MTS clip gages attached across the center slot, one on the front and one on the back. Load versus COD was measured to failure for each test.

All fatigue tests were conducted under spectrum loading in closed-loop electrohydraulic MTS test machines using tape spectrum load control. The three tests used the thermo-humidity cycle, shown in figure 38, and were encased in an environmental chamber.

TABLE 14. - THROUGH-THE-THICKNESS DAMAGE TEST MATRIX

Test Condition	219K (-65°F) Wet	219K (-65°F) Dry	R.T. Dry	355K (+180°F) Wet	Thermo Humidity Cycle	Total Spec.
Static Tension	3*	3	3	3*	-	12
Fatigue (R=-1)	-	-	3	-	3*	6
	3	3	6	3	3	18

*Specimens pre-conditioned to 1% minimum weight gain by exposing to 95 to 100% relative humidity at 339K (150°F)

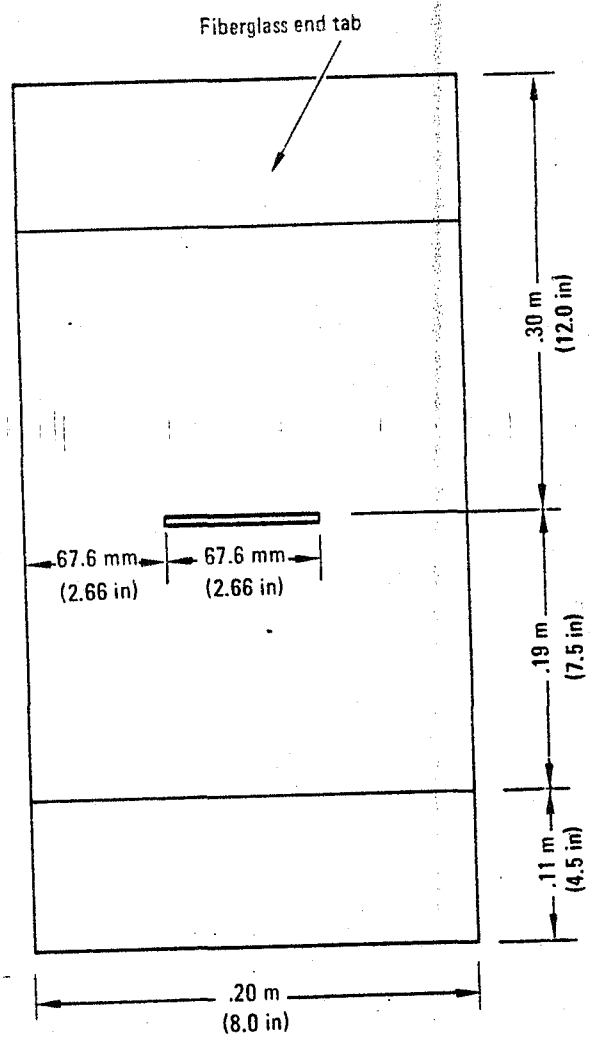

Figure 40. - Center cracked tension (CCT) specimen.

Temperature was controlled by a switching system using timers to adjust the LN_2 supply for cool down and the hot, wet air supply on heat-up to maintain the desired thermo cycle period. During nights and weekends, a bubbler arrangement maintained a humid environment in the test chamber. Those specimens that survived two lifetimes were removed, inspected by Quality Assurance (QA), and residual-tension-strength tested at room temperature using the static fracture test procedure. In these tests, a third slip gage was attached to the specimen well away from the slot to measure the far field strain.

The results of the static fracture tests are presented in table 15. The apparent critical fracture toughness was computed as:

$$K_c = \frac{P}{A}\sqrt{\pi c \sec\left(\frac{\pi c}{w}\right)}$$

where

P = max load

c = ½ slot length

A = gross area

w = specimen width

The results show very little scatter among the results of a given test condition. No major effect of either prior moisture conditioning or test temperature was observed on the critical fracture toughness.

Results of the spectrum fatigue tests and subsequent residual tension strength tests are presented in table 16. All but one specimen survived two lifetimes of fatigue cycling without failure with a slot one third the width in the specimen. Since all stresses were based on gross area, it should be noted that the maximum load cycle of 103 MPa (15 ksi) gross area stress is exceeded by the residual strength of all surviving specimens. Strength of the specimens after fatigue cycling two lifetimes showed no effect on the residual static strength.

2.3.5 Impact damage tolerance test H12A2.- The objective of this program was to determine the damage tolerance characteristics of the T300/5208 graphite/epoxy material system.

The program had two phases: the first covered damage caused by high-speed impacts typical of a hailstone 25.4 mm (1 in.) in diameter, traveling at 271 m/s (890 ft/s), and the second covered damage typical of tool drops.

The high-speed impact tests were performed on three panels, two had 4-hat stiffeners and one had 3-hat stiffeners. The two 4-hat panels were conditional to 1 percent moisture weight gain prior to impacting, and the

TABLE 15. - SUMMARY OF STATIC TENSION FRACTURE TEST RESULTS

Test Condition	Failure Load		k_c		Gross Failure Stress	
	kN	kips	MPa $\sqrt{m}$	ksi $\sqrt{in.}$	MPa	ksi
R.T. Dry	53.8	12.1	44.2	40.2	126	18.3
	52.0	11.7	40.2	36.6	124	18.0
	54.7	12.3	44.4	40.4	128	18.5
219K Dry (-65°F)	52.9	11.9	44.2	40.2	127	18.4
	52.5	11.8	42.8	39.0	123	17.8
	49.8	11.2	42.1	38.3	120	17.4
355K Wet (180°F)	56.5	12.7	46.3	42.1	133	19.3
	57.8	13.0	46.7	42.5	134	19.4
	56.9	12.8	46.1	42.0	137	19.9
219K Wet (-65°F)	55.6	12.5	44.6	40.6	129	18.7
	53.4	12.0	43.4	39.5	125	18.1
	55.6	12.5	46.1	42.0	133	19.3

TABLE 16. - SUMMARY OF FATIGUE TEST RESULTS

Test Condition	Failure Load		k_c		Gross Failure Stress	
	kN	kips	MPa $\sqrt{m}$	ksi $\sqrt{in.}$	MPa	ksi
R.T. Dry	51.6	11.6	41.5	37.8	119	17.3
	53.4	12.0	44.8	40.8	128	18.6
	58.3	13.1	46.9	42.7	136	19.7
Spectrum Conditioned	55.6	12.5	44.9	40.9	129	18.7
	*	*	–	–	–	–
	52.0	11.7	43.3	39.4	124	18.0

*Failed after 1.1 lifetimes of spectrum fatigue

3-hat panel was impacted in the as-fabricated condition. All impacting was performed in normal laboratory air.

The panels were installed in the test machine, and the hail gun was located so that the impact would be at 0.28 radians (16 degrees) to the surface, as shown in figure 41. The panels were loaded in compression to approximately 193 kN/m (1100 lb/in.), which is limit load for the flight condition in which hail impact might occur. Figure 42 shows the hail gun in position for test.

The impact criterion was for a gust penetration in cruise flight at 32 000 m (35,000 ft). The true airspeed is 271 m/s (890 ft/s). The impact angle consisting of the yaw angle due to the dutch roll and the slope of the cover relative to the centerline of the fin is 0.28 radians (16 degrees) measured from the surface of the cover.

Impacting was performed at predetermined locations, either at the hat flange between the hats or under the hats. Impacting at the hat flange location caused the most severe damage. Figure 43 shows the visible damage at three locations on the outside of panel No. 1 which was impacted at hat flange locations. Some surface damage is evident at several of the impact zones. Figure 44 shows the inner surface of panel No. 1 at the location marked 7. Delamination in the skin and at the flange is shown. All panels sustained full load throughout impacting.

At the completion of impacting, the three panels were ultrasonically inspected, and the extent of the damage marked at each location. The damaged zones are shown in figures 45, 46, and 47. The panels shown in figure 45 was the most severely damaged. The large damaged area marked at the left-hand side of the panel shown in figure 46 was caused by impacting the panel between the outermost hat flange and the panel edge.

One 4-hat panel that had not been impacted was tested in static compression to failure as a baseline. This panel failed at 543 kN (122,000 lb) (8000 μm/m strain). The failure, shown in figure 48 was typical compression failure.

The three impacted panels were then tested in spectrum fatigue for two lifetimes and damage growth, if any, was noted and marked on the specimen. The most badly damaged panel incurred growth of the delaminations. Figures 49 and 50 show the growth as a function of the number of flights in thousands. All three panels survived the fatigue testing and sustained design limit load. Panel Nos. 2 and 3 were then static tested to determine the residual strength.

The 3-hat-stiffened panel No. 3 failed at 286 kN (64,400 pounds), which is 112 percent of design ultimate. This panel is shown in figure 51 after failure. The white cross-matched areas were the delaminations identified by A-scan after two lifetimes of spectrum fatigue.

Figure 52 shows the 4-hat-stiffened panel No. 2 after residual static failure, which occurred at 278 kN (62,500 pounds), which is 82 percent of design ultimate.

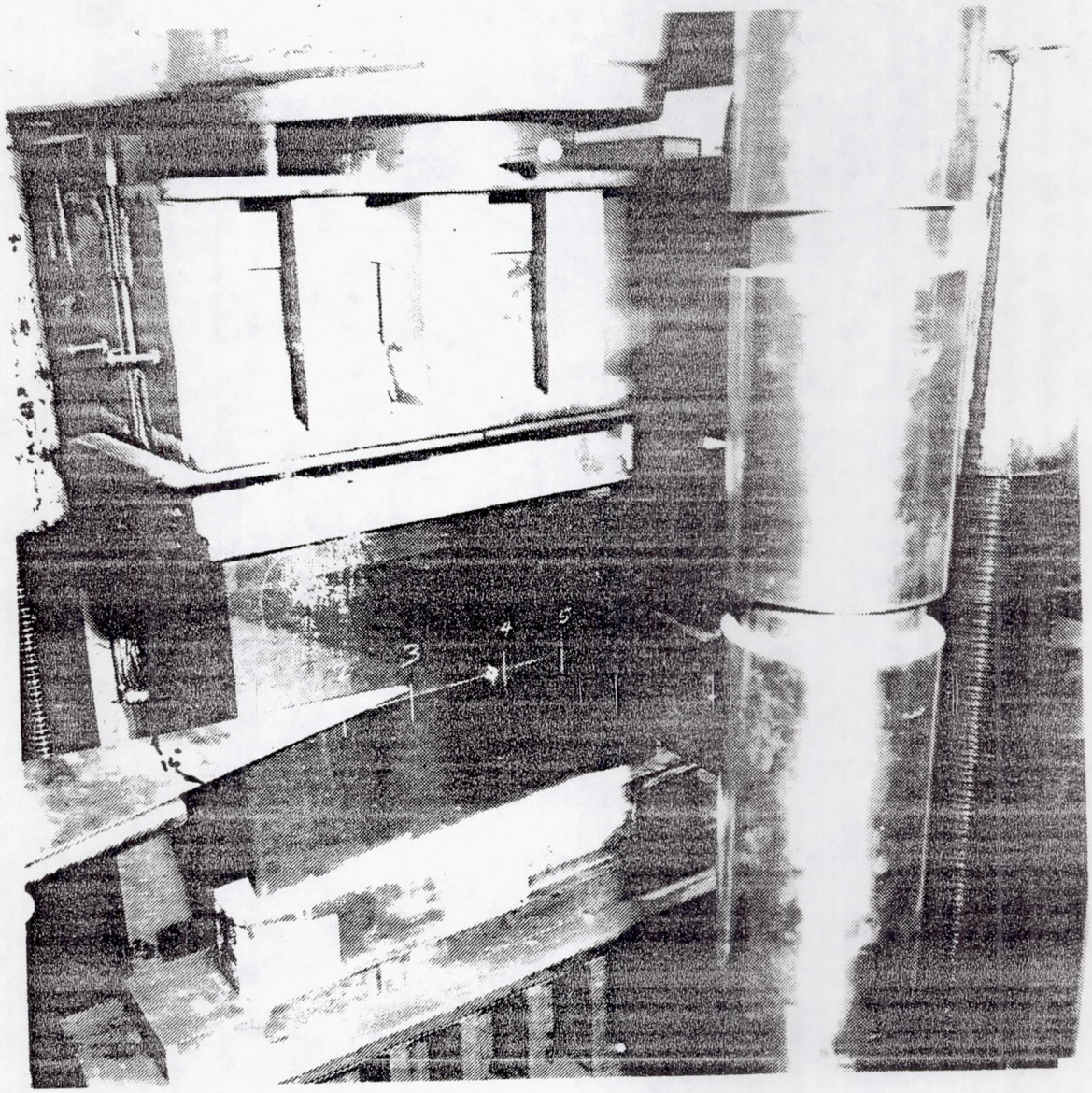

Figure 41. - Three-bay subpanel in the universal test machine at 16 degrees to the gun.

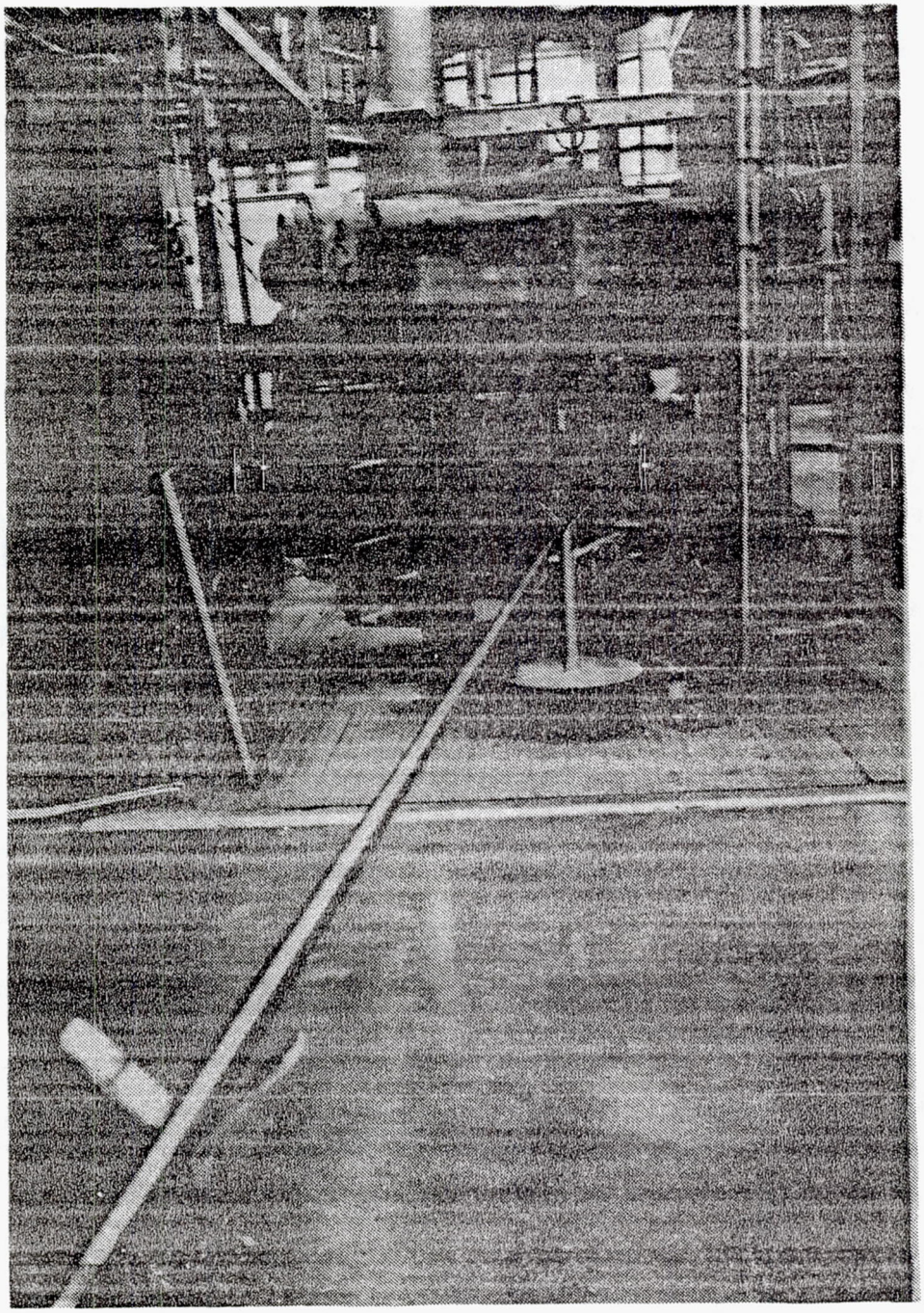

Figure 42. - Impact panel in the universal test machine with the hailstone gun barrel in position.

Figure 43. - Four-hat stiffened panel no. 1 after hailstone impacting, showing visible damage at locations 2, 4 and 7. Damage at the other locations was detected by NDI.

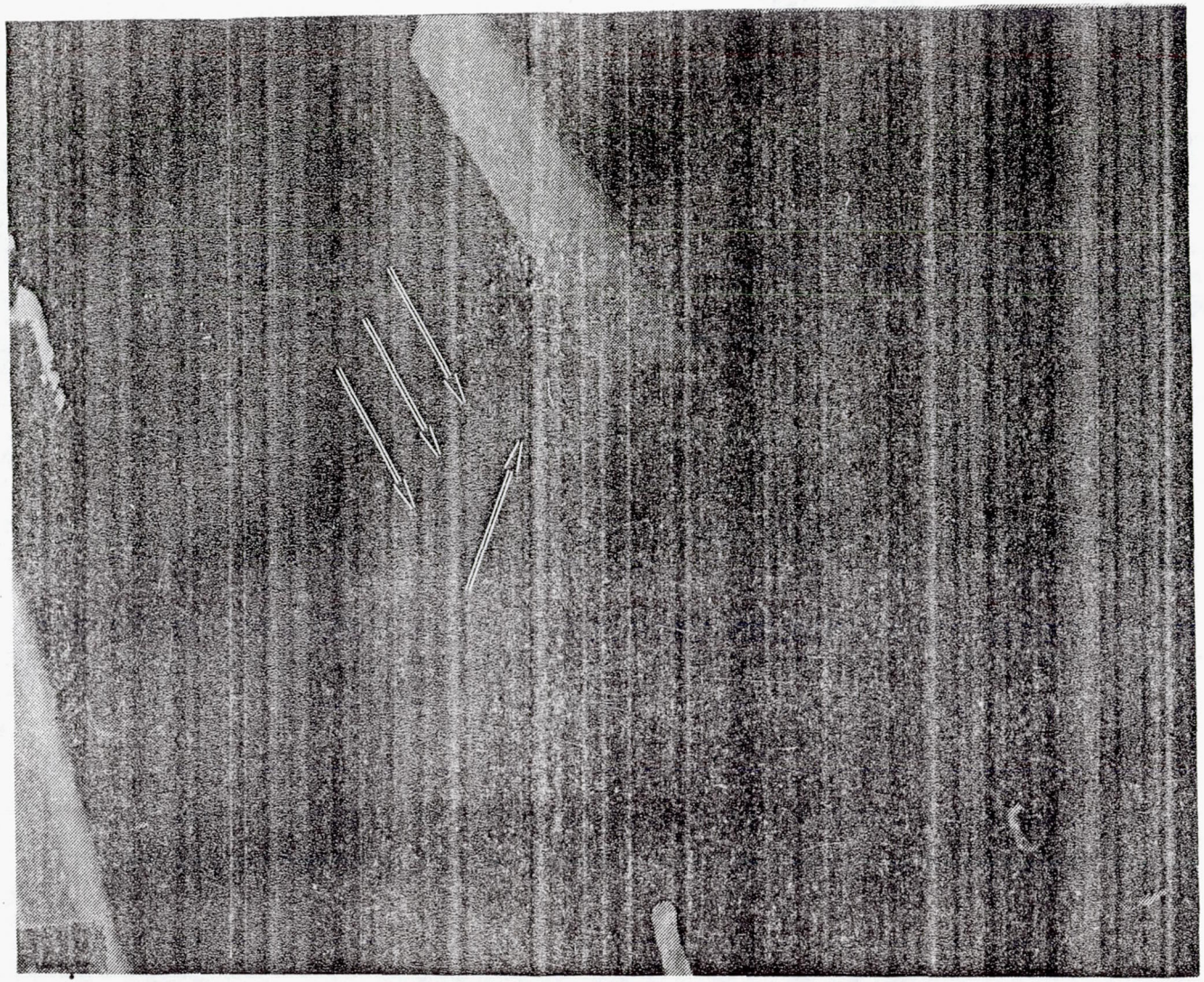

Figure 44. - Close-up view of the hat-stiffened side of panel no. 1 after impacting.

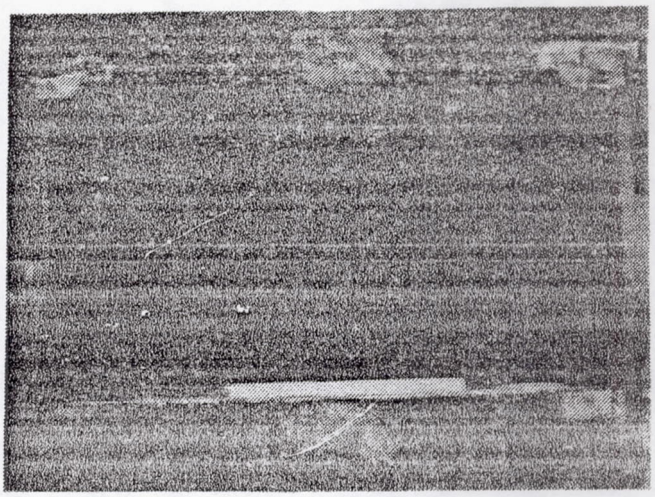

Figure 45. - Panel no. 1 (4 hats wide) showing NDI identified damage.

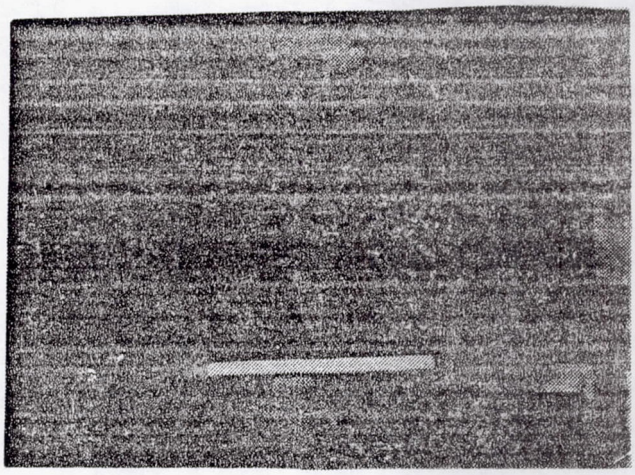

Figure 46. - Panel no. 2 (4 hats wide) showing NDI identified damage.

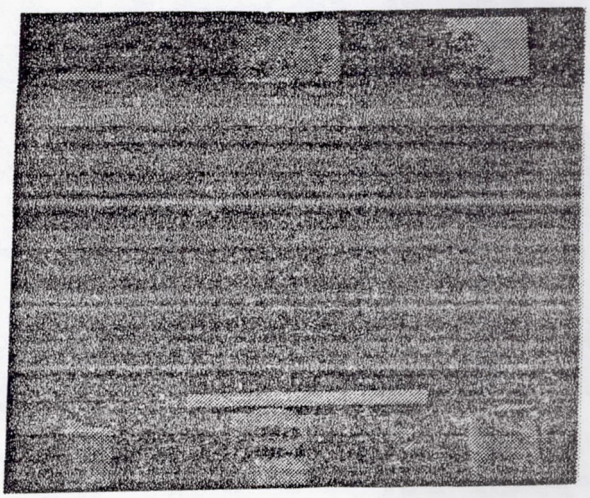

Figure 47. - Panel no. 3 (3 hats wide) showing NDI identified damage.

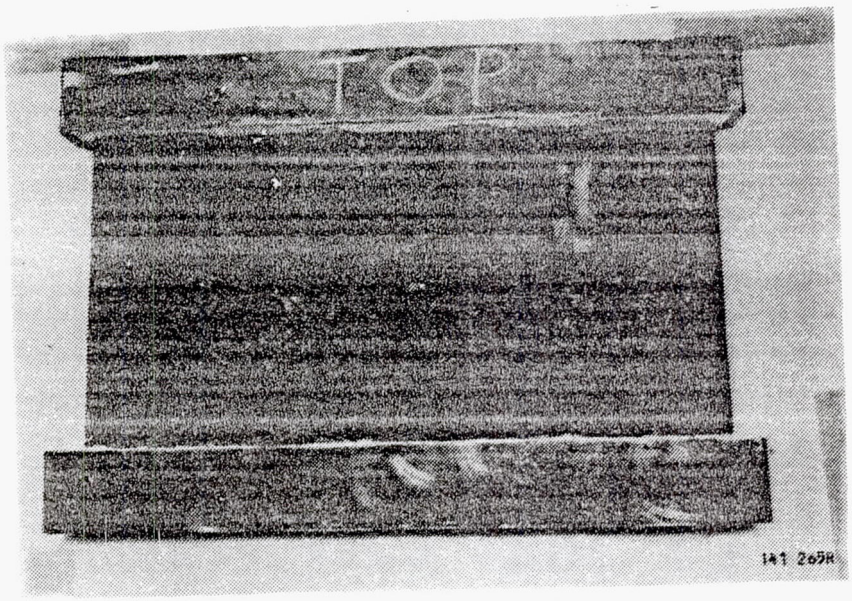

Figure 48. - Undamaged four-bay subpanel after static compression test

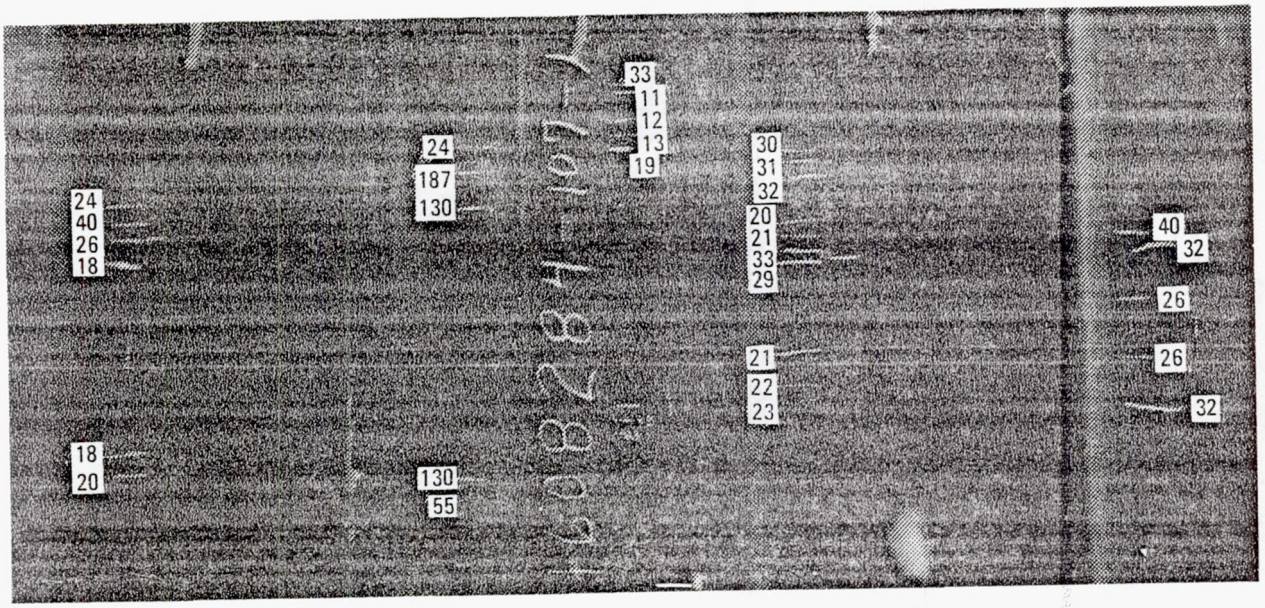

Figure 49. - Subpanel no. 1 after two lifetimes of flight spectrum fatigue loading, showing defect growth (numbers indicate flights in thousands where growth observed).

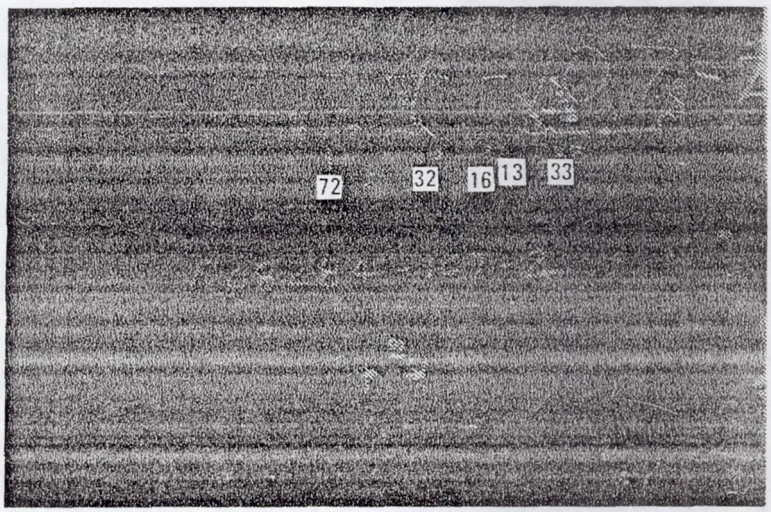

Figure 50. - Subpanel no. 2 showing damage growth after two lifetimes of flight spectrum fatigue loading.

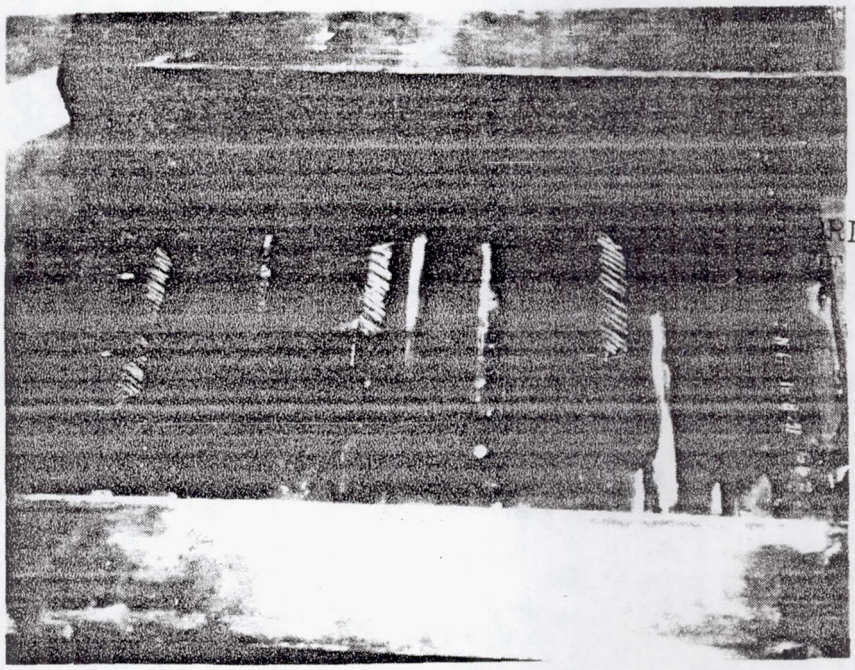

Figure 51. - Three-hat-stiffened panel after residual static failure (hatched areas are previously identified delaminations).

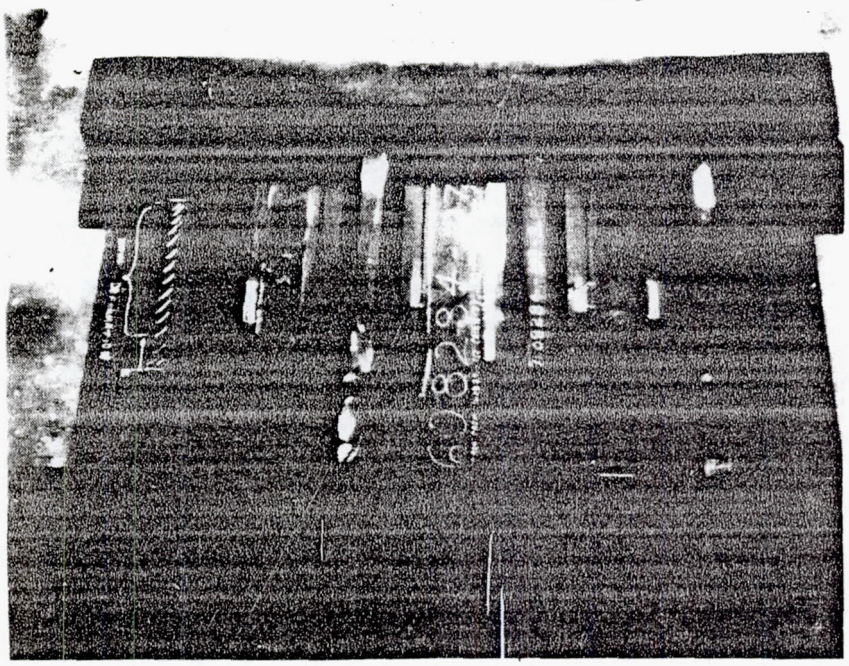

Figure 52. - Four-hat-stiffened panel after residual static testing (hatched areas are previously identified delaminations).

The low-speed (drop) impacting was performed by dropping a 1.2 kg (2.65 lb) rounded nose steel mass from a 1.35 m (53 in.) height, guided through a teflon tube, onto a panel laying on wooden 2 x 4's on a cement floor. The 1.35 m (53 in.) height gave an impact velocity of 0.38 m/s (15 ft/s) accounting for air resistance. This was calibrated using high-speed photography. This mass and velocity were selected because based on prior experience it was known to cause damage to panels of comparable thickness. This damage was not visible but could be readily detected by ultrasonic inspection.

The 2 x 4's were approximately 0.3 m (12 in.) apart. Impacts were performed on the flat panel side at sites between the hats and at the hat flanges. Specimens were then machined for static and fatigue testing.

The impacted coupons were spectrum fatigue tested for two lifetimes in a cyclic environment ranging from 219K (-65°F) to 339K (150°F), 95 percent RH. All 10 coupons completed the spectrum testing without visual evidence of damage growth. The specimens were ultrasonically inspected before and after fatigue testing. This showed that the original damage zones had increased in size. A typical area is shown in figure 53. The measured areas are shown in table 17.

Static compression tests on coupons which had not been fatigued and on fatigued specimens showed considerable scatter in both instances, so no conclusions on the residual strength could be drawn.

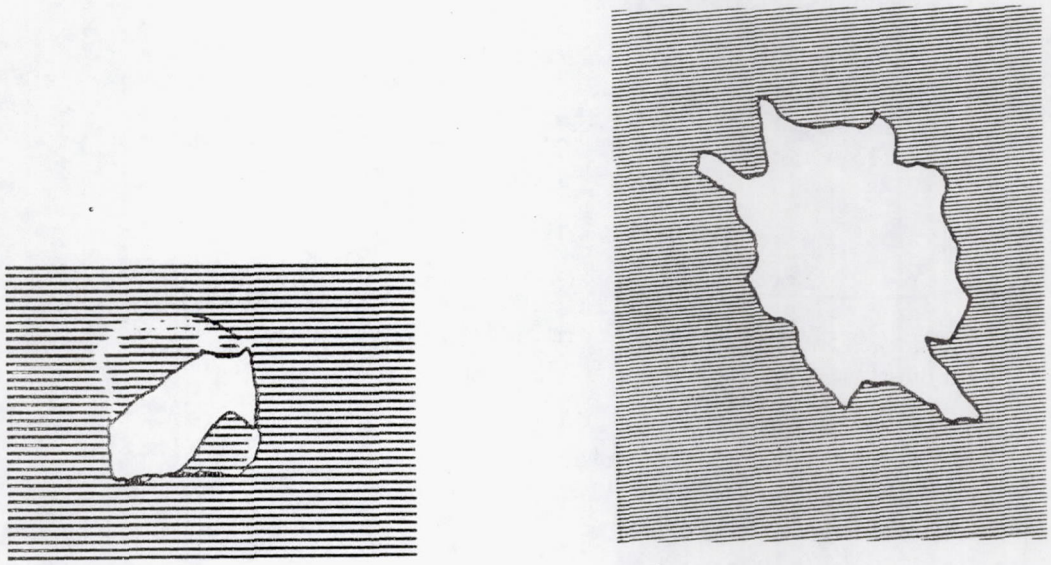

Figure 53. - Typical ultrasonic trace ("C" scan) showing damage before and after fatigue test in low speed impact specimens.

TABLE 17. - IMPACT AREA DAMAGE - BEFORE AND AFTER TWO LIFETIMES OF FATIGUE TESTING.

Test Coupon ID	Area of Damage Before Fatigue Test		Area of Damage After Fatigue Test	
	cm^2	$in.^2$	cm^2	$in.^2$
1F	5.29	0.82	7.87	1.22
2F	5.03	0.78	8.71	1.35
3F	5.48	0.85	10.84	1.68
4F	7.94	1.23	9.35	1.45
5F	0.52	0.08	0.52	0.08
12B	6.97	1.08	12.58	1.95
13B	0.19	0.03	10.39	1.61
14B	5.94	0.92	6.90	1.07
15B	2.19	0.34	8.52	1.32
16B	0.71	0.11	9.03	1.40

2.4 Design Allowables

The approach used to establish the design allowables for graphite/epoxy composites is illustrated in figure 54. The following paragraphs discuss the various steps involved to obtain the design allowables. Tape test data on 0.19 mm (7.5 mil) tape from the L-1011 Advanced Composite Aileron program is included.

2.4.1 Test program. - The physical and mechanical properties of the T300/5208 graphite/epoxy materials being used to construct the advanced composite vertical fin have been determined by coupon tests. The configurations of the coupons are shown in the Appendix.

Tests were conducted on 0°, 90°, and ±45° laminates to formulate ply level properties. These properties are the basis of analytical predictions of laminate properties. Crossplied laminates were tested with and without notches at various environmental conditions. These data were used to verify analytical predictions of laminate strength and stiffness and to establish factors to account for notch and environmental effects.

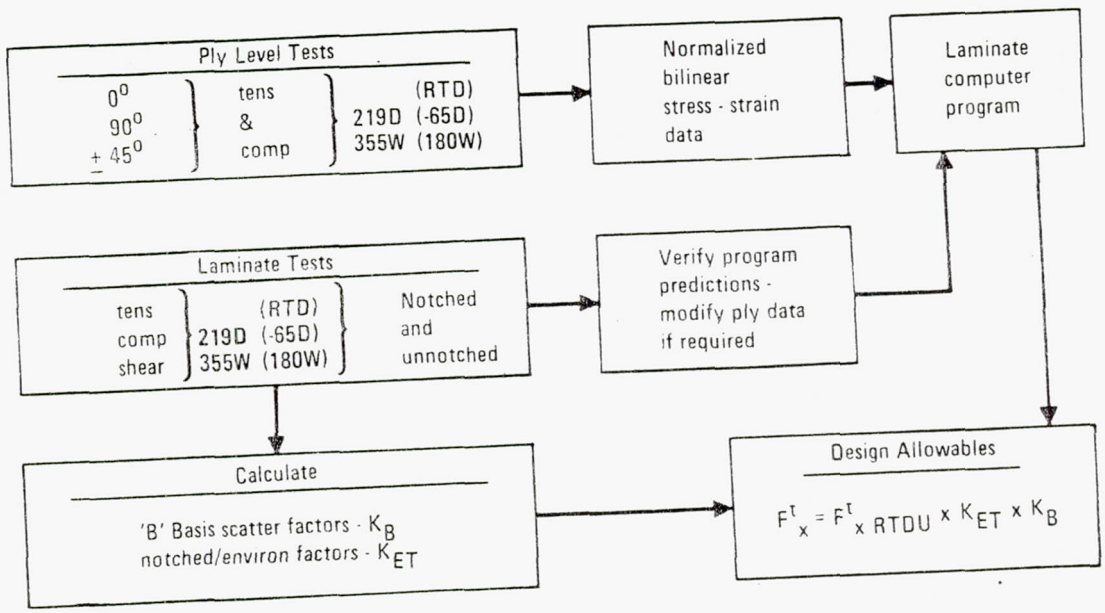

Figure 54. - Design allowables approach.

The notch size used for the laminate test was 4.76 mm (3/16 in.) diameter holes. This notch size was selected since most of the fasteners used for assembly of the fin or aileron are 4.76 mm (3/16 in.) diameter or smaller.

Laminate tests were conducted at temperatures ranging from 219K (-65°F) to 355K (180°F). Many of these tests were conducted on laminates which had been moisture conditioned to a weight gain of 1 percent prior to the tests. Analysis of the thermal environment of the vertical fin and aileron led to the selection of the 219K (-65°F) and 355K (180°F) temperatures as the most extreme conditions. Graphite/epoxy materials absorb moisture when exposed to humid environments. This absorbed moisture reduces the mechanical properties of the composite, particularly for tests conducted at elevated temperatures. To account for the detrimental effect of moisture on laminate properties some of the test coupons were moisture conditioned to a weight gain of 1 percent, which is 67 percent of the moisture saturation level in T300/5208 graphite/epoxy composites.

The design allowables for a given laminate will conservatively be based on the worst combination of environmental condition and notch for a given type of load, regardless of the actual environmental condition of the structure associated with the external load condition.

2.4.2 Laminate strength prediction.- To design a composite material laminate, four primary variables must be considered; 1) orientation of the plies, 2) stacking sequence of the plies, 3) reinforcement form to each ply (fabric or tape) and 4) the number of plies of each material at a given orientation. Considering these variables it is obvious that an infinite number of materials may be created. Consequently a laminate property prediction computer program is used.

The laminate prediction computer program 'HYBRID' calculates the strength and failure steps of hybrid composite laminates under uniaxial or combined loading. Inputs to the program include the tension and compression stress-strain behavior of a lamina in the orthotropic axis, inplane shear stress-strain behavior, and coefficients of thermal expansion for each material within the laminate. Orientation and thickness of each lamina are also input. The program uses lamination theory to predict the inplane stresses in each ply. A maximum strain theory of failure is employed.

2.4.3 Summary of test data. All of the test data for the tension, compression, and inplane shear tests conducted are summarized in tables 18, 19 and 20. The data summarized includes the strength, modulus, failure strain and the normalized values of strength and modulus. Normalization of the data based on the thickness ratios where the normal thickness for tape is 0.12 mm (5 mils) and 0.19 mm (7.5 mils) per ply.

Testing of the syntactic/epoxy material included physical and mechanical properties of cast syntactic sheet specimens. The syntactic epoxy used is

TABLE 18. - TAPE DATA - TENSION (SI UNITS) (1 of 6)

Laminate & Cond. ①	③ N	F_{AVE} ④ (Mpa)	CV (%)	N	E_{AVE} (MPa)	CV (%)	N	ϵ_{AVE} (10^{-3} mm/mm)	CV (%)	Normalized F_N (MPa)	Normalized E_N (MPa)
0^o RT D UN	30	1 360.68	10.14	15	137 688	1.04	10	10.162	7.96	1 455.48	147.55
219K D UN	30	1 217.82	11.30	15	140 170	3.28	10	8.941	12.47	1 303.11	149.62
355K D UN	10	1 333.38	8.55	6	130 725	1.56	10	9.968	12.60	1 447.21	138.58
355K W UN	21	1 422.11	8.99	16	139 412	2.49	10	10.042	11.95	1 541.60	151.00
90^o RT D UN	7	51.09	11.64	7	11 238	8.68	7	4.592	14.7	52.33	11.51
219K D UN	10	59.02	5.41	10	11 859	3.19	10	4.987	6.3	61.23	12.27
355K W UN	8	32.06	16.53	8	9 446	3.05	5	3.825	9.2	32.13	9.45
$\pm 45^o$ RT D UN	10	174.02	2.09	5	19 512	6.22	*	*	*	184.78	20.75
219K D UN	10	176.92	6.46	5	18 478	3.41	*	*	*	189.67	19.79
355K W UN	10	150.24	2.25	5	20 546	9.91	*	*	*	158.65	21.72
$(\pm 45/0/\pm 45/0_3)s$											
RT D UN	20	863.05	6.469	20	81,537	3.112	20	10.609	6.155	911.49	86.12
RT D N	5	444.71	9.844	5	76,070	1.656	4	5.564	2.542	470.50	80.46
219K D UN	10	770.01	4.151	10	84,033	12.005	5	9.221	3.706	813.10	88.74
219K D N	5	399.47	7.552	5	81,000	1.252	5	4.934	8.157	423.41	85.84
355K W UN	20	844.54	4.505	20	81,324	8.542	20	10.478	5.545	898.59	86.53
355K W N	5	489.89	6.924	5	76,394	1.297	5	6.413	6.864	528.07	82.32
$(\pm 45/0_3/\pm 45/0)s$											
RT D UN	20	836.51	9.327	20	81,551	4.224	20	10.290	8.081	873.29	85.15
219K D N	11	428.23	8.597	11	84,557	2.859	11	5.076	7.058	447.06	88.25
355K W N	5	568.13	22.202							605.64	
219K W N	5	404.58	2.611	5	83,758	5.937	4	4.963	3.999	434.51	89.98
$(\pm 45/0_3/\pm 45/0)s$ ②											
RT D UN	5	887.36	3.46							908.04	
219K D N	5	399.21	5.14							417.82	
$(45/90/-45/0_2)s$ ②											
RT D UN	5	546.06	3.13							577.78	
219K D N	5	349.56	5.25							372.32	
$(\pm 45/0/\pm 45_2)s$											
RT D UN	10	348.89	5.376	10	32 971	5.714	10	11.387	10.059	366.32	34.61
RT D N	5	223.36	1.615	5	34 612	2.842	5	6.486	3.323	234.56	36.34
219K D UN	10	376.32	5.620	10	39 100	8.257	9	9.972	7.884	386.86	40.20
219K D N	5	231.58	2.012	5	37 645	4.328	5	6.069	3.975	244.56	39.78
355K W UN	10	312.13	3.368	9	33 371	8.988	8	10.692	4.434	327.09	34.96
355K W N	5	203.31	1.046	5	33 412	1.260	5	6.278	1.557	208.98	34.34

TABLE 18. - TAPE DATA - TENSION (SI UNITS) (2 OF 6)

Laminate & Cond. ①	③ N	F_{AVE} ④ (Mpa)	CV (%)	N	E_{AVE} (MPa)	CV (%)	N	ϵ_{AVE} (10^{-3} mm/mm)	CV (%)	Normalized F_N(MPa)	Normalized E_N (MPa)
$(\pm 45/0/\mp 45/\pm 45)_S$											
RT D UN	5	388.78	3.263							402.79	
RT D N	5	207.30	1.682							214.77	
$(\pm 45/0/\pm 45/\pm 45/0)_S$											
RT D UN	5	591.21	3.001							577.02	
RT D N	5	292.54	1.653							284.34	
$(\pm 45/0/\mp 45)_S$											
RT D UN	20	415.13	6.900	20	39,610	2.149	20	11.228	7.156	449.19	42.89
219K D N	11	226.09	3.996	11	42 803	2.181	11	5.347	4.468	246.42	46.68
355K W N	5	236.90	3.036	5	40 789	9.300	5	5.970	10.695	254.90	43.92
219K W N	5	234.56	3.979	5	43 954	1.974	4	5.519	7.945	255.66	47.92
$(0/\pm 45/90)_{2S}$											
RT D UN	5	499.29	6.332	5	50 925	1.980	5	9.981	5.126	544.20	55.50
(0/+45/90/−45)s											
RT D UN	5	555.73	2.961							580.19	
RT D N	5	295.08	3.983							305.71	
$(45/90/-45/0_2)_S$											
RT D UN	20	648.07	7 220	20	67 279	2.463	20	9.857	8.049	703.82	73.08
219K D N	11	373.07	15 040	11	69 878	3.557	11	5.220	8.502	405.14	75.91
355K W N	5	561.10	5.517	5	69 085	5.347	1	5.875		612.74	75.43
219K W N	5	384.87	11 747	5	69 871	2.560	5	5.575	10.250	422.58	76.74
(45/0/−45/0/90)s ②											
RT D UN	5	591.31	10 360	5	66 328	1.747	5	9.424	12.270	627.56	70.40
RT D UN	30	362.10	6.345	30	65 735	3.941	30	5.973	12.391	408.10	74.12
219K D UN	5	549.53	10.042	5	66 741	3.197	5	8.866	12.071	581.02	70.53
219K D N	10	326.69	5.667	10	65 100	1.965	10	5.018	6.186	341.50	68.05
335K W UN	5	627.01	8.722	5	69 637	3 501	4	9.357	9.802	664.65	73.84
335K W N	10	379.56	3.792	10	66 624	2.913	9	5.738	4.769	397.76	69.84
(45/0/−45/90/0)s ②											
RT D UN	5	530.69	6.79							580.19	
RT D N	5	339.77	1.47							373.76	
219K D N	5	329.71	4.27							362.66	
$(\pm 45/90_3/\mp 45/90)_S$											
RT D UN	21	150.66	8.653	21	20 222	2.919	21	9.247	15.109	166.92	22.41
219K D N	11	123.88	5.668	11	22 311	7.216	11	5.561	3.078	137.00	24.68
335K W N	5	132.66	4.814	4	19 133	3.450	4	7.616	7.192	145.41	20.96
219K W N	5	129.90	1.619	5	22 615	3.340	5	5.442	5.523	142.38	24.75

TABLE 18. - TAPE DATA - TENSION (SI UNITS) (3 of 6)

Laminate & Cond. ①	③ N	F_{AVE} ④ (Mpa)	CV (%)	N	E_{AVE} (MPa)	CV (%)	N	$\bar{\epsilon}_{AVE}$ (10^{-3} mm/mm)	CV (%)	Normalized F_N(MPa)	Normalized E_N (MPa)
$(\pm 45/90/\pm 45_2)_S$											
RT D UN	5	204.22	1.195	5	23 139	2.463	5	9.987	1.944	207.60	23.99
RT D N	5	178.86	1.884	5	24 421	2.674	5	8.199	2.691	185.68	25.30
219K D UN	5	228.46	2.988	5	25 717	5.230	5	10.114	4.477	236.97	26.68
219K D UN	5	198.25	1.541	5	26 862	6.188	5	8.1296	2.074	207.39	28.13
355K W UN	5	166.69	1.645	5	21 381	2.680	5	9.626	5.941	174.99	22.48
355K W UN	5	148.28	1.943	5	21 898	4.861	5	8.066	2.841	152.17	22.48
$(0_2/+45/0_2/-45/0_2)_S$											
RT D UN	5	1144.53	3.7				5	10.350	3.1	1217.75	
RT D UN	5	561.92	7.5				5	5.390	4.9	602.95	
$(\pm 45/0/\pm 45/\pm 45)_S$											
RT D UN	5	321.30	7.5				5	10.420	8.6	344.32	
RT D N	5	204.77	3.7				5	6.460	1.6	220.36	
$(0/45/90/-45)_{2S}$											
RT D UN	5	541.93	6.0				5	10.800	5.6	577.16	
RT D N	5	269.58	3.2				5	5.490	2.8	290.48	

TABLE 18. - TAPE DATA - TENSION (CUSTOMARY UNITS) (4 of 6)

Laminate & Cond ①		③ N	F_{AVE} ④ (ksi)	CV (%)	N	E_{AVE} (Msi)	CV (%)	N	ϵ_{AVE} (10^{-3} in/in)	CV (%)	Normalized F_N (ksi)	Normalized E_N (Msi)
0^0	RTD UN	30	197.35	10.14	15	19.97	4.04	10	10.162	7.96	211.1	21.4
	−65D UN	30	176.63	11.30	15	20.33	3.28	10	8.941	12.47	189.0	21.7
	180D UN	10	198.39	8.55	6	18.96	1.56	10	9.968	12.60	209.90	20.1
	180W UN	21	206.26	8.99	16	20.22	2.49	10	10.042	11.95	223.59	21.9
90^0	RTD UN	7	7.41	11.64	7	1.63	8.68	7	4.592	14.7	7.59	1.67
	−65D UN	10	8.56	5.41	10	1.72	3.19	10	4.987	6.3	8.88	1.78
	180W UN	8	4.65	16.53	8	1.37	3.05	5	3.825	9.2	4.66	1.37
$\pm 45^0$	RTD UN	10	25.24	2.09	5	2.83	6.22	*	*	*	26.80	3.01
	−65D UN	10	25.66	6.46	5	2.68	3.41	*	*	*	27.51	2.87
	180W UN	10	21.79	2.25	5	2.98	9.91	*	*	*	23.01	3.15
$(\pm 45/0/\pm 45/0_3)_S$												
	RTD UN	20	125.17	6.469	20	11.83	3.112	20	10.609	6.155	132.2	12.49
	RTD N	5	64.5	9.844	5	11.03	1.656	4	5.564	2.542	68.24	11.67
	−65D UN	10	111.68	4.151	10	12.19	12.005	5	9.221	3.706	117.93	12.87
	−65D N	5	57.94	7.552	5	11.75	1.252	5	4.934	8.157	61.41	12.45
	180W UN	20	122.49	4.505	20	11.80	8.542	20	10.478	5.545	130.33	12.55
	180W N	5	71.05	6.924	5	11.08	1.297	5	6.413	6.864	76.59	11.94
$(\pm 45/0_3/\pm 45/0)_S$												
	RTD UN	20	121.32	9.327	20	11.83	4.224	20	10.290	8.081	126.66	12.35
	−65D N	11	61.11	8.597	11	12.26	2.859	11	5.076	7.058	64.84	12.80
	180W N	5	82.40	22.202							87.84	
	−65W N	5	56.68	2.611	5	12.15	5.937	4	4.963	3.999	63.02	13.05
$(\pm 45/0_3/\mp 45/0)_S$ ②												
	RTD UN	5	128.7	3.46							131.7	
	−65D N	5	57.9	5.14							60.6	
$(45/90/-45/0_2)_S$ ②												
	RTD UN	5	79.2	2.13							83.8	
	−65D N	5	50.7	5.25							54.0	
$(\pm 45/0/\pm 45_2)_S$												
	RTD UN	10	50.60	5.376	10	4.78	5.714	10	11.39	10.059	53.13	5.02
	RTD N	5	32.40	1.615	5	5.02	2.842	5	6.49	3.323	34.02	5.27
	−65D UN	10	54.58	5.620	10	5.67	8.257	9	9.97	7.884	56.11	5.83

TABLE 18. - TAPE DATA - TENSION (CUSTOMARY UNITS) (5 of 6)

Laminate & Cond ①	③ N	F_{AVE} ④ (ksi)	CV (%)	N	E_{AVE} (Msi)	CV (%)	N	ϵ AVE (10^{-3} in/in)	CV (%)	Normalized F_N (ksi)	Normalized E_N (Msi)
−65D N	5	33.59	2.012	5	5.46	4.328	5	6.07	3.975	35.47	5.77
180W UN	10	45.27	3.368	9	4.84	8.988	8	10.69	4.434	47.44	5.07
180W N	5	29.49	1.046	5	4.85	1.260	5	6.28	1.557	30.31	4.98
$(\pm 45/0/\mp 45/\pm 45)_S$											
RTD UN	5	56.39	3.263							58.42	
RTD N	5	30.07	1.682							31.15	
$(\pm 45/0/\mp 45/\pm 45/0)_S$											
RTD UN	5	85.75	3.001							83.69	
RTD N	5	42.43	1.653							41.24	
$(\pm 45/0/\mp 45)_S$											
RTD UN	20	60.21	6.900	20	5.74	2.149	20	11.228	7.156	65.15	6.22
−65D N	11	32.79	3.996	11	6.21	2.181	11	5.347	4.468	35.74	6.77
180W N	5	34.36	3.036	5	5.92	9.300	5	5.970	10.695	36.97	6.37
−65W N	5	34.02	3.979	4	6.37	1.974	4	5.519	7.945	37.08	6.95
$(0/\pm 45/90)_{2S}$											
RTD UN	5	72.42	6.332	5	7.39	1.980	5	9.981	5.126	78.93	8.05
$(0/+45/90/-45)_S$											
RTD UN	5	80.60	2.961							84.15	
RTD N	5	42.80	3.983							44.34	
$(45/90/-45/0_2)_S$											
RTD UN	20	93.99	7.220	20	9.76	2.463	20	9.857	8.049	102.08	10.60
−65D N	11	54.11	15.040	11	10.13	3.557	11	5.220	8.502	58.76	11.01
180W N	5	81.38	5.517	5	10.02	5.347	1	5.875		88.87	10.94
−65W N	5	55.82	11.747	5	10.13	2.560	5	5.575	10.250	61.29	11.13
$(45/0/-45/0/90)_S$ ②											
RTD UN	5	85.76	10.360	5	9.62	1.747	5	9.424	12.270	91.02	10.21
RTD N	30	52.52	6.345	30	9.53	3.941	30	5.973	12.391	59.19	10.75
−65D UN	5	79.70	10.042	5	9.68	3.197	5	8.866	12.071	84.27	10.23
−65D N	10	47.38	5.667	10	9.44	1.965	10	5.018	6.186	49.53	9.87
180W UN	5	90.94	8.722	5	10.10	3.501	4	9.357	9.802	96.40	10.71
180W N	10	55.05	3.792	10	9.66	2.913	9	5.738	4.769	57.69	10.13

TABLE 18. - TAPE DATA - TENSION (CUSTOMARY UNITS) (6 of 6)

Laminate & Cond ①	③ N	F_{AVE} ④ (ksi)	CV (%)	N	E_{AVE} (Msi)	CV (%)	N	ϵ_{AVE} (10^{-3} in/in)	CV (%)	Normalized F_N (ksi)	Normalized E_N (Msi)
$(45/0/-45/90/0)_S$ ②											
RTD UN	5	76.97	6.79							84.15	
RTD N	5	49.28	1.47							54.21	
−65D N	5	47.82	4.27							52.60	
$(\pm 45/90_3/\mp 45/90)_S$											
RTD UN	21	21.85	8.653	21	2.93	2.919	21	9.247	15.109	24.21	3.25
−65D N	11	17.97	5.668	11	3.24	7.216	11	5.561	3.078	19.87	3.58
180W N	5	19.24	4.814	4	2.77	3.450	4	7.616	7.192	21.09	3.04
−65W N	5	18.84	1.619	5	3.28	3.340	5	6.163	5.442	20.65	3.59
$(\pm 45/90/\pm 45_2)_S$											
RTD UN	5	29.06	1.195	5	3.36	2.463	5	9.987	1.944	30.11	3.48
RTD N	5	25.94	1.884	5	3.54	2.674	5	8.199	2.691	26.93	3.67
−65D UN	5	33.14	2.988	5	3.73	5.230	5	10.114	4.477	34.39	3.87
−65D N	5	28.75	1.541	5	3.90	6.188	5	8.1296	2.074	30.08	4.08
180W UN	5	24.18	1.645	5	3.01	2.680	5	9.626	5.941	25.38	3.26
180W N	5	21.51	1.943	5	3.18	4.861	5	8.066	2.841	22.07	3.26
$(0_2/+45/0_2/-45/0_2)_S$											
RTD UN	5	166.0	3.7				5	10.350	3.1	176.62	
RTD N	5	81.5	7.5				5	5.390	4.9	87.45	
$(\pm 45/0/\pm 45/\pm 45)_S$											
RTD UN	5	46.6	7.5				5	10.420	8.6	49.94	
RTD N	5	29.7	3.7				5	6.460	1.6	31.96	
$(0/45)90/-45)_{2S}$											
RTD UN	5	78.6	6.0				5	10.800	5.6	83.71	
RTD N	5	39.1	3.2				5	5.490	2.8	42.13	

① Condition
- D = Dry
- W = Wet (1% moisture by weight)
- UN = Unnotched
- N = 4.76 mm (3/16 in) dia hole

② 0.19 mm (7.5 ml) ply tape
③ N = Number of coupon
④ F = Failure Stress

TABLE 19. - TAPE DATA - COMPRESSION (SI UNITS) (1 of 4)

Laminate & Cond. (1)	(3) N	F_{AVE} (4) (MPa)	CV (%)	N	E_{AVE} (MPa)	CV (%)	N	ϵ_{AVE} (10^{-3} mm/mm)	CV (%)	Normalized F_N (MPa)	Normalized E_N (MPa)
0^0											
RT D UN	10	1 596.96	8.04	10	127 967	1.48	7	14.250	5.51	1 606.55	128.24
219K D UN	10	1 459.28	7.10	10	135 551	4.07	2	11.450	*	1 488.44	138.24
219K W UN	15	1 804.36	6.95	15	131 897	6.46	11	16.000	13.22	1 937.91	141.69
355K W UN	7	1 393.43	5.33	7	137 757	1.91	6	11.030	7.64	1 373.92	135.83
90^0											
RT D UN	9	186.02	6.88	10	10 756	1.42	9	18.355	7.07	194.91	11.24
219K D UN	10	200.91	7.51	10	11 859	6.03	9	17.446	4.52	214.15	12.62
355K W UN	8	138.24	8.37	10	9 377	2.27	8	18.173	10.93	146.24	9.93
$(\pm 45/0/\pm 45/0_3)_s$											
RT D UN	23	757.82	7.500	23	73 257	6.613	22	11.748	13.035	795.72	76.95
RT D N	5	550.37	6.309	5	77 345	1.473	5	7.551	13.148	564.68	79.36
219K D UN	10	865.22	6.486	5	75 208	3.166	5	12.856	8.616	918.86	79.84
219K D N	5	599.97	11.149	5	76 449	1.805	5	8.725	15.454	639.56	81.50
355K W UN	15	675.50	11.025	15	71 533	3.321	14	10.846	13.231	716.02	75.84
355K W N	5	568.83	8.725	5	74 767	0.784	5	9.175	10.875	592.74	29.65
$(\pm 45/0_3/\pm 45/0)_s$											
RT D UN	20	684.10	18.361	20	72 602	4.508	20	10.341	23.264	714.30	75.77
219K D N	4	681.72	14.024	4	75 325	2.521	3	9.649	25.058	734.91	81.22
355K W N	11	628.55	10.233	10	77 842	7.693	2	10.425	9.021	653.69	80.94
219K W N	4	698.61	20.322	4	70 154	1.237	2	10.125	36.648	753.11	75.64
$(\pm 45/0/\pm 45_2)_s$											
RT D UN	8	408.60	8.024	8	33 612	3.561	8	17.544	15.289	431.47	35.51
RT D N	5	290.64	2.055	5	37 190	0.766	5	9.022	3.166	304.61	38.96
219K D UN	10	498.10	6.726	10	39 273	6.593	9	17.543	20.982	516.00	40.68
219K D N	5	309.81	1.654	5	38 031	2.334	5	8.874	1.846	329.64	40.47
355K W UN	10	363.60	8.881	10	32 998	5.413	10	17.562	17.077	375.21	34.06
355K W N	5	259.41	6.796	5	34 736	2.185	5	9.207	9.080	264.62	35.44
$(\pm 45/0/\pm 45)_s$											
RT D UN	20	439.44	18.545	20	36 990	6.227	18	14.195	28.128	476.36	40.13
219K D N	5	346.53	3.059	5	40 955	2.817	4	9.080	5.690	374.94	44.33
355K W N	11	291.34	8.305	11	36 639	4.763	10	9.178	10.648	316.40	39.78
219K W N	5	310.68	6.959	5	38 473	3.885	4	8.875	8.350	338.05	41.85
$(0/\pm 45/90)_2$											
RT D UN	5	627.42	4.115	5	51 118	1.566	5		5.423	658.79	53.64
$(45/90/-45/0_2)_s$											
RT D UN	20	644.52	13.708	19	61 129	4.361	14		14.650	697.40	66.12
219K D N	4	587.26	3.632	4	64 638	2.937	3		7.800	648.31	71.36
355K W N	10	449.68	10.602	10	64 328	4.977	7		13.477	488.36	69.84
219K W N	4	524.35	12.861	4	64 466	4.142	3		17.310	568.40	69.91

TABLE 19. - TAPE DATA - COMPRESSION (SI UNITS) (2 of 4)

Laminate & Cond. (1)			(3) N	F_{AVE} (4) (MPa)	CV (%)	N	E_{AVE} (MPa)	CV (%)	N	ϵ_{AVE} (10^{-3} mm/mm)	CV (%)	Normalized F_N (MPa)	Normalized E_N (MPa)
(45/0/-45/0/90)s (2)													
RT	D	UN	5	714.02	7.397	4	62 191	0.941	4		8.510	754.98	65.78
RT	D	N	5	478.77	9.682	5	63 128	0.763	5		10.495	508.14	67.02
219K	D	UN	5	724.91	5.759	4	61 660	4.732	4		6.711	765.52	65.09
355K	W	UN	5	581.78	13.078	5	62 315	0.826	5		12.800	615.91	65.98
(45/0/-45/90/0)s (2)													
RT	D	UN	5	636.25	6.13	5	62 191	4.32	5		9.67	700.71	68.46
355K	W	N	5	409.55	5.21	5	60 122	9.42	5		8.84	451.06	66.19
(±45/90/∓45/90)s													
RT	D	UN	20	266.96	5.698	20	19 292	3.039	19	14.420	5.221	296.34	21.44
219K	D	N	5	285.58	9.547	5	20 753	3.272	5	14.144	9.220	313.02	22.75
355K	W	N	11	206.09	13.829	11	18 926	6.111	9	11.522	12.231	228.35	20.96
219K	W	N	5	249.18	4.013	5	20 450	3.049	5	12.392	5.232	275.10	22.55

TABLE 19. - TAPE DATA - COMPRESSION (CUSTOMARY UNIT) (3 of 4)

Laminate & Cond (1)	(3) N	F_{AVE} (4) (ksi)	CV (%)	N	E_{AVE} (Msi)	CV (%)	N	ϵ_{AVE} (10^{-3} in/in)	CV (%)	Normalized F_N (ksi)	Normalized E_N (Msi)
0^o											
RTD UN	10	231.62	8.04	10	18.56	1.48	7	14.250	5.51	233.01	18.67
−65D UN	10	211.65	7.10	10	19.66	4.07	2	11.450	–	215.88	20.05
−65W UN	15	261.70	6.95	15	19.13	6.46	11	16.000	13.22	281.07	20.55
180W UN	7	202.10	5.33	7	19.98	1.91	6	11.030	7.64	199.27	19.70
90^o											
RTD UN	9	26.98	6.88	10	1.56	1.42	9	18.355	7.07	28.27	1.63
−65D UN	10	29.14	7.51	10	1.72	6.03	9	17.446	4.52	31.06	1.83
180W UN	8	20.05	8.37	10	1.36	2.27	8	18.173	10.93	21.21	1.44
$(\pm 45/0/\pm 45/0_3)_S$											
RTD UN	23	109.91	7.500	23	10.62	6.613	22	11.748	13.035	115.41	11.16
RTD N	5	79.82	6.309	5	11.22	1.473	5	7.551	13.148	81.90	11.51
−65D UN	10	125.49	6.486	5	10.91	3.166	5	12.856	8.616	133.27	11.58
−65D N	5	87.02	11.149	5	11.09	1.805	5	8.725	15.454	92.76	11.82
180W UN	15	97.97	11.025	15	10.37	3.321	14	10.846	13.231	103.85	11.00
180W N	5	82.50	8.725	5	10.84	0.784	5	9.175	10.875	85.97	11.30
$(\pm 45/0_3/\pm 45/0)_S$											
RTD UN	20	99.22	18.361	20	10.53	4.508	20	10.341	23.264	103.6	10.99
−65D N	4	98.87	14.024	4	10.92	2.521	3	9.649	25.058	106.59	11.78
180W N	11	91.16	10.233	10	11.29	7.693	2	10.425	9.021	94.81	11.74
−65W N	4	101.32	20.322	4	10.17	1.237	2	10.125	36.648	109.23	10.97
$(\pm 45/0/\pm 45_2)_S$											
RTD UN	8	59.26	8.024	8	4.87	3.561	8	17.544	15.289	62.58	5.15
RTD N	5	42.15	2.055	5	5.39	0.766	5	9.022	3.166	44.18	5.65
−65D UN	10	72.24	6.726	10	5.70	6.593	9	17.543	20.982	74.84	5.90
−65D N	5	44.93	1.654	5	5.52	2.334	5	8.874	1.846	47.81	5.87
180W UN	10	52.74	8.881	10	4.79	5.413	10	17.562	17.077	54.42	4.94
180W N	5	37.62	6.796	5	5.04	2.185	5	9.207	9.080	38.38	5.14
$(\pm 45/0/\mp 45)_S$											
RTD UN	20	63.73	18.545	20	5.36	6.227	18	14.195	28.128	69.09	5.82
−65D N	5	50.26	3.059	5	5.94	2.817	4	9.080	5.690	54.38	6.43
180W N	11	42.25	8.305	11	5.31	4.763	10	9.178	10.648	45.89	5.77
−65W N	5	45.06	6.959	5	5.58	3.885	4	8.875	8.350	49.03	6.07
$(0/\pm 45/90)_2$											
RTD UN	5	91.00	4.115	5	7.41	1.566	5	13.329	5.423	95.55	7.78

TABLE 19. - TAPE DATA - COMPRESSION (CUSTOMARY UNIT (4 of 4)

Laminate & Cond (1)	(3) N	F_{AVE} (4) (ksi)	CV (%)	N	E_{AVE} (Msi)	CV (%)	N	ϵ_{AVE} (10^{-3} in/in)	CV (%)	Normalized F_N (ksi)	Normalized E_N (Msi)
$(45/90/-45/0_2)_S$											
RTD UN	20	93.48	13.708	19	8.87	4.361	14	11.243	14.650	101.15	9.59
−65D N	4	85.17	3.632	4	9.37	2.937	3	9.464	7.800	94.03	10.35
180W N	10	65.22	10.602	10	9.33	4.997	7	8.635	13.477	70.83	10.13
−65W N	4	76.05	12.861	4	9.35	4.142	3	8.397	17.310	82.44	10.14
$(45/0/-45/0/90)_S$ (2)											
RTD UN	5	103.56	7.397	4	9.02	0.941	4	12.514	8.510	109.50	9.54
RTD N	5	69.44	9.682	5	9.16	0.763	5	7.853	10.495	73.70	9.72
−65D UN	5	105.14	5.759	4	8.94	4.732	4	12.747	6.711	111.03	9.44
180W UN	5	84.38	13.078	5	9.04	0.826	5	10.071	12.800	89.33	9.57
$(45/0/-45/90/0)_S$ (2)											
RTD UN	5	92.28	6.13	5	9.02	4.32	5	11.424	9.67	101.63	9.93
180W N	5	59.40	5.21	5	8.72	9.42	5	7.098	8.84	65.42	9.60
$(\pm 45/90_3/\mp 45/90)_S$											
RTD UN	20	38.72	5.698	20	2.80	3.039	19	14.420	5.221	42.98	3.11
−65D N	5	41.42	9.547	5	3.01	3.272	5	14.144	9.220	45.40	3.30
180W N	11	29.89	13.829	11	2.74	6.111	9	11.522	12.231	33.12	3.04
−65W N	5	36.14	4.013	5	2.97	3.049	5	12.392	5.232	39.90	3.27

(1) Condition D = Dry
W = Wet (1% moisture by weight)
UN = Unnotched
N = 4.76 mm (3/16 in) dia hole

(2) 0.19 mm (7.5 m.l) 1 ply tape

(3) N = Number of coupons

(4) F = Failure stress

TABLE 20. - TAPE DATA - SHEAR (SI UNIT) (1 of 2)

Laminate & Cond. (1)	(3) N	(4) τ_{AVE} (MPa)	CV (%)	N	G_{AVE} (MPa)	CV (%)	N	γ_{AVE} (10^{-3} mm/mm)	CV (%)	Normalized τ_N (Mpa)	Normalized G_N (MPa)
$(\pm 45/0/\pm 45_2)s$											
RT D UN	5	348.71	5.429	4	29 303	9.410	4	12.053	4.266	362.66	30.47
RT D N	5	279.43	4.722	5	27 193	3.082	5	11.427	5.379	289.51	28.20
219K D UN	5	385.95	7.257	5	30 889	7.630	5	13.163	9.307	399.83	31.99
219K D N	5	280.08	8.882	5	29 289	4.255	4	10.331	11.872	290.75	30.41
355K W UN	5	223.85	13.398	5	28 227	16.733	5	8.573	34.384	234.15	29.51
355K W N	5	187.95	32.823	4	27 131	6.058	3	8.603	31.886	196.22	28.34
$(\pm 45/0/\pm 45)s$											
RT D UN	23	396.94	7.973	23	26 262	4.542	23	16.333	9.414	431.89	28.54
219K D N	10	300.54	16.277	10	24 642	6.052	10	12.555	15.117	310.95	26.34
$(\pm 45/0_3/\mp 45/0)s$											
RT D UN	22	286.10	16.518	22	19 057	5.740	18	17.574	14.189	300.96	20.06
219K D N	10	207.41	9.356	10	16 940	7.078	9	13.339	5.413	222.36	18.13
$(45/90/-45/0_2)s$											
RT D UN	21	305.31	6.571	21	18 071	20.597	21	21.831	9.220	328.54	19.44
219K D N	9	205.06	5.214	9	15 699	5.913	9	14.861	14.933	219.39	16.82
(45/0/-45/0/90)s (2)											
RT D UN	5	297.47	7.169	5	16 920	8.014	5	19.462	6.040	307.37	17.51
RT D N	5	214.65	4.123	5	14 038	8.777	5	15.936	14.216	219.80	14.34
219K D UN	5	252.87	11.843	5	16 272	5.748	4	15.605	8.094	262.00	16.82
355K W UN	5	281.72	2.714	5	15 555	7.802	5	19.704	7.512	292.27	16.13
$(\pm 45/90_3/\mp 45/90)s$											
RT D UN	21	245.98	11.304	21	18 726	3.843	21	14.101	12.291	274.55	20.90
219K D N	10	236.84	9.666	10	17 492	3.951	10	16.383	13.296	262.90	19.44

TABLE 20. - TAPE DATA - SHEAR (CUSTOMARY UNITS) (2 of 2)

Laminate & Cond. (1)	(3) N	(4) τ_{AVE} (ksi)	CV (%)	N	G_{AVE} (Msi)	CV (%)	N	γ_{AVE} (10^{-3} in/in)	CV (%)	Normalized τ_N (ksi)	Normalized G_N (Msi)
$(\pm 45/0/\pm 45_2)_S$											
RT D UN	5	50.58	5.429	4	4.25	9.410	4	12.053	4.266	52.60	4.42
RT D N	5	40.53	4.722	5	3.94	3.082	5	11.427	5.379	41.99	4.09
-65 D UN	5	55.98	7.257	5	4.48	7.630	5	13.163	9.307	57.99	4.64
-65 D N	5	40.62	8.882	5	4.25	4.255	4	10.331	11.872	42.17	4.41
180 W UN	5	32.47	18.398	5	4.09	16.733	5	8.573	34.384	33.96	4.28
180 W N	5	27.26	32.823	4	3.93	6.058	3	8.603	31.886	28.46	4.11
$(\pm 45/0/\mp 45)_S$											
RT D UN	23	57.57	7.973	23	3.81	4.542	23	16.333	9.414	62.64	4.14
-65 D N	10	43.59	16.277	10	3.57	6.052	10	12.555	15.117	46.55	3.82
$(\pm 45/0_3/\mp 45/0)_S$											
RT D UN	22	41.49	16.518	22	2.76	5.740	18	17.574	14.189	43.65	2.91
-65 D N	10	30.08	9.356	10	2.46	7.078	9	13.339	5.413	32.25	2.63
$(45/90/-45/0_2)_S$											
RT D UN	21	44.28	6.571	21	2.62	20.597	21	21.831	9.220	47.65	2.82
-65 D N	9	29.74	5.214	9	2.28	5.913	9	14.861	14.933	31.82	2.44
$(45/0/-45/0/90)_S$ (2)											
RT D UN	5	43.14	7.169	5	2.45	8.014	5	19.462	6.040	44.58	2.54
RT D N	5	31.13	4.123	5	2.04	8.777	5	15.936	14.216	31.88	2.08
-65 D UN	5	36.68	11.843	5	2.36	5.748	4	15.605	8.094	38.00	2.44
180 W UN	5	40.86	2.714	5	2.26	7.802	5	19.704	7.512	42.39	2.34
$(\pm 45/90_3/\mp 45/90)_S$											
RT D UN	21	35.68	11.304	21	2.72	3.843	21	14.101	12.291	39.82	3.03
-65 D N	10	34.35	9.666	10	2.54	3.951	10	16.383	13.296	38.13	2.82

(1) Condition
- D = Dry
- W = Wet (1% moisture by weight)
- UN = Unnotched
- N = 4.76mm (3/16 in) dia. hole

(2) 0.19mm (7.5 mil) 1 ply tape

(3) N = Number of coupons

(4) γ = Failure Stress

0.95 mm (0.0375 in.) thick and is made by Hysol Corp. A summary of the cured syntactic sheet properties is presented in table 21.

Tests were also run on graphite/syntactic sandwich test panels representative of the end application. These specimens incoporate the T300/5208 graphite tape prepreg which is cocured with the syntactic epoxy as the core material. Interlaminar tensile and short-beam shear were the principal mechanical tests run on the sandwich. The test values show that syntactic epoxy used as core material provides an order of magnitude improvement in compression and shear properties over conventional honeycomb. A summary of the test data is shown in table 22.

2.4.4 Calculation of "B" allowables.- Since it is impractical to conduct tests for all laminates, properties, and environmental conditions, the allowables must be related to the analytical predictions. Sufficient tests are then conducted to cover the range of laminates and test conditions that are applicable to the structure. It is assumed that each test group represents a sample from the population for which the allowable is being derived. Tests must cover a range of laminate layups, or environmental conditions, and batches.

For establishing the "B" allowable, the data can be pooled by relating the test strength to the predicted strength as shown in figure 55. If there is a perfect correlation between predicted strength and test strength the test data would fall on the line with a slope of 1.0. Based on the analysis of the data, the scatter is proportional to the strength; i.e., the coefficient of variation is the same for all test groups. Therefore, the data are distributed within a scatterband represented by the slope of lines through the minimum and maximum test results. The data can be pooled by considering that each test result gives an independent assessment of the relation between the test strength and predicted strength.

For establishing "B" allowables the individual results must be considered. The B value for the slope, K_B, is the value that is equal or exceeded by 90 percent of the population with a 95 percent confidence. If the probability distribution of values is known or can be determined, then the K_B value can be determined using the appropriate statistical analysis procedure. Rather than perform an analysis of the probability distribution for individual values of test/prediction, however, a nonparametric statistical analysis procedure for an unknown distribution was used (see 9.2.8 of reference 3).

The nonparametric procedure ranks the values of test/prediction from the lowest to the highest including all data points. The K_B value is then determined by counting down to the r^{th} calculated value which is a function of the total number of test data points as given in reference 3 table 9.6.4.2. A summary of these calculated values are given in table 23. Therefore, the "B" allowable can be determined from the predicted strength using the following equation:

$$F_B = F_{RTDU} \times K_{ET} \times K_B$$ (Note. Laminate must contain 0° plies)

TABLE 21. - SYNTACTIC EPOXY ADX819 CURED SYNTACTIC SHEET PROPERTIES

Properties	Test Results Average	Test Results Average
Density	609 kg/m^3	0.022 lb./in.^{3}
Thickness	5.49 mm	0.216 in.
Mositure wt. gain*	8.5 %	8.5 %
Flatwise compressive str. at 297K (75^{0}F)	60 MPa	8 701 psi
Flatwise compressive str. at 218K (-67^{0}F)	72 MPa	10 428 psi
Flatwise compressive str. at 355K (180^{0}F)	55 MPa	7 928 psi
Flatwise compressive str. at 355K (180^{0}F) wet	29 MPa	4 208 psi
Tensile strength at 297K (75^{0}F)	23 MPa	3 407 psi
Tensile strength at 218K (-67^{0}F)	18 MPa	2 643 psi
Tensile strength at 355K (180^{0}F)	18.5 MPa	2 677 psi
Tensile strength at 355K (180^{0}F) wet	12 MPa	1 688 psi
Tensile ult. strain at 297K (75^{0}F)	0.0093 m/m	0.0093 in./in.
Tensile ult. strain at 218K (-67^{0}F)	0.0073 m/m	0.0073 in./in.
Tensile ult. strain at 355K (180^{0}F)	0.0077 m/m	0.0077 in./in.
Tensile ult. strain at 355K (180^{0}F)	0.0071 m/m	0.0071 in./in.

*19 days at 339 K (150^{0}F) 95-100% relative humidity

TABLE 22. - SYNTACTIC EPOXY ADX819 GRAPHITE/SYNTACTIC SANDWICH PROPERTIES

Properties	Test Results Average	Test Results Average
Density	26 572 kg./m^3	0.96 lb./in.^{3}
Thickness	3 mm	0.121 in.
Moisture wt. gain *	2.7%	2.7%
Interlaminar tensile strength at 297K (75^{0}F)	12 MPa	1 768 psi
Interlaminar tensile strength at 218K (-67^{0}F)	11 MPa	1 635 psi
Interlaminar tensile strength at 355K (180^{0}F)	8 MPa	1 116 psi
Interlaminar tensile strength at 355K (180^{0}F) wet	13 MPa	1 926 psi
Short beam shear str. at 297K (75^{0}F)	15 MPa	2 208 psi
Short beam shear str. at 218K (-67^{0}F)	17 MPa	2 508 psi
Short beam shear str. at 355K (180^{0}F)	18 MPa	2 557 psi
Short beam shear str. at 355K (180^{0}F) wet	17 MPa	2 472 psi

*19 days at 339K (150^{0}F) 95-100% relative humidity

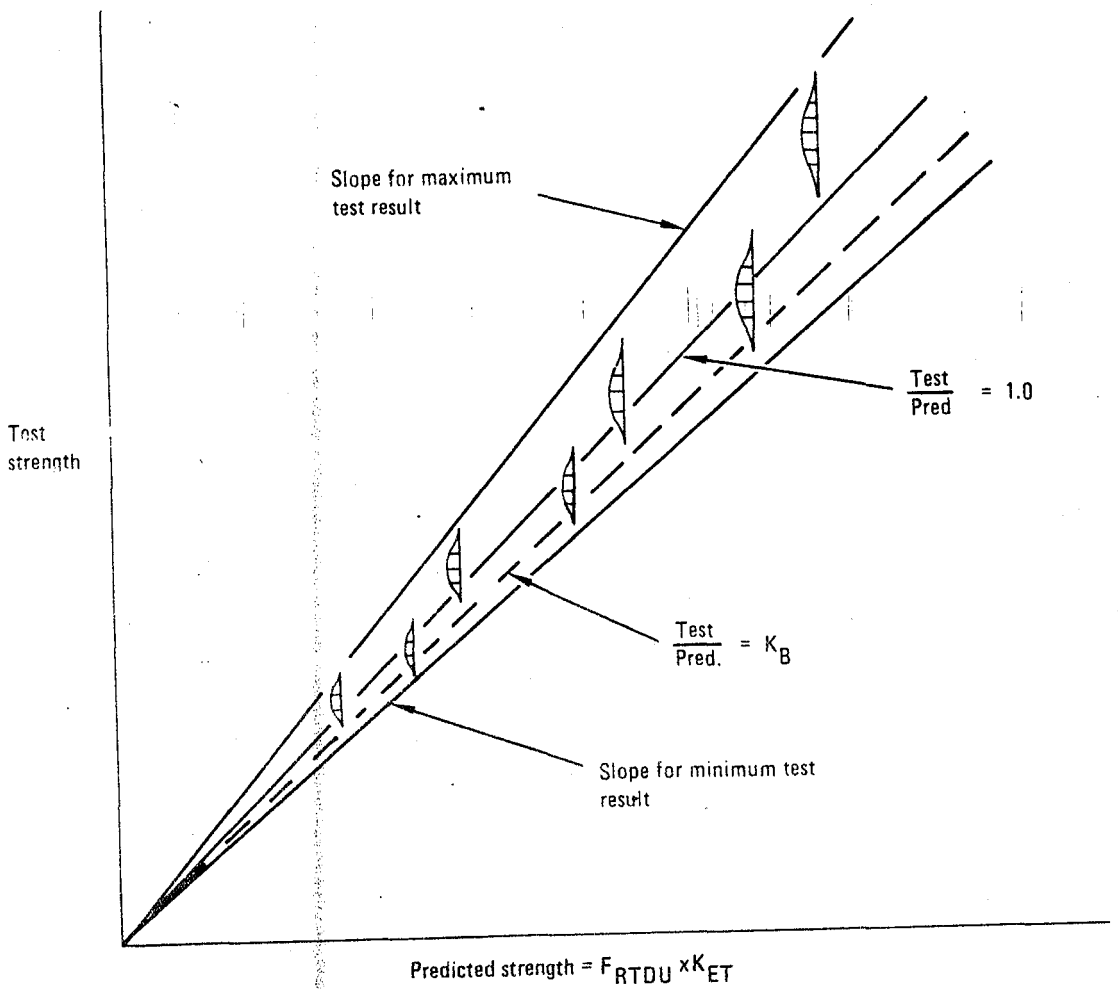

Figure 55. - Schematic showing the relation of the "B" allowable factor, K_B to test and predicted strength values.

TABLE 23. - DETERMINATION OF K_B FACTORS ASSUMING DISTRIBUTION FUNCTION IS UNKNOWN

Rank Order, r	Tape Tension n = 158	Tape Compression n = 76
1	0.903	0.821
2	0.939	0.920
3	0.958	0.924
4	0.962	0.940
5	0.965	0.947
6	0.974	
7	0.975	
8	0.983	
9	0.987	
10	0.987	
11	0.988	

n = number of tests performed

where

F_{RTDU} = predicted unnotched room temperature dry strength

K_{ET} = reduction factor

K_B = 0.99 tape, tension; 0.94 tape, compression.

2.4.5 Laminate design allowables. - The ply level data presented in table 24 were used in a laminate strength prediction computer program named HYBRID to determine the laminate property carpet plots for the 0°/±45°/90° family. Carpet plots for tape room temperature dry, unnotched tension and compression strengths are presented in figures 56 and 57. For laminates with fibers in the direction of loading, failure was assumed when laminate strain exceeded the ply level 0° failure strain. For laminates which contained only ±45°/90° plies and which are loaded in tension in the 0° direction, failure was conservatively assumed to occur when the 90° tensile strain was exceeded. When the ±45°/90° laminates were loaded in compression, failure was

TABLE 24. - HYBRID INPUT FOR ALL CONDITIONS

Property	SI Units	RTD	Customary Units	RTD
E^t_{L1}	GPa	141	10^6 psi	20.5
E^c_{L1}	GPa	128	10^6 psi	18.5
E^t_{L2}	GPa	141	10^6 psi	20.5
E^c_{L2}	GPa	99	10^6 psi	14.3
E^t_{T1}	GPa	11.5	10^6 psi	1.67
E^c_{T1}	GPa	11.3	10^6 psi	1.64
E^t_{T2}	GPa	11.5	10^6 psi	1.67
E^c_{T2}	GPa	9.8	10^6 psi	1.42
G_{LT1}	GPa	6	10^6 psi	0.87
G_{LT2}	GPa	1.8	10^6 psi	0.26
μ_{LT}	–	0.30	–	0.30
α_L	10^{-6} m/m/K	0.43	10^{-6} in./in./°F	0.24
α_T	10^{-6} m/m/K	29.2	10^{-6} in./in./°F	16.2
ϵ^t_{L1}	10^{-6} m/m	9 800	10^{-6} in./in.	9 800
ϵ^t_{T1}	10^{-6} m/m	5 000	10^{-6} in./in.	5 000
ϵ^t_{L2}	10^{-6} m/m	9 800	10^{-6} in./in.	9 800
ϵ^t_{T2}	10^{-6} m/m	5 000	10^{-6} in./in.	5 000
ϵ^c_{L1}	10^{-6} m/m	6 200	10^{-6} in./in.	6 200
ϵ^c_{T1}	10^{-6} m/m	9 900	10^{-6} in./in.	9 900
ϵ^c_{L2}	10^{-6} m/m	11 200	10^{-6} in./in.	11 200
ϵ^c_{T2}	10^{-6} m/m	18 400	10^{-6} in./in.	18 400
γ_{LT1}	10^{-6} m/m	10 300	10^{-6} in./in.	10 300
γ_{LT2}	10^{-6} m/m	27 500	10^{-6} in./in.	27 500
t	mm	0.127 – 0.191	in.	0.0050 – 0.0075

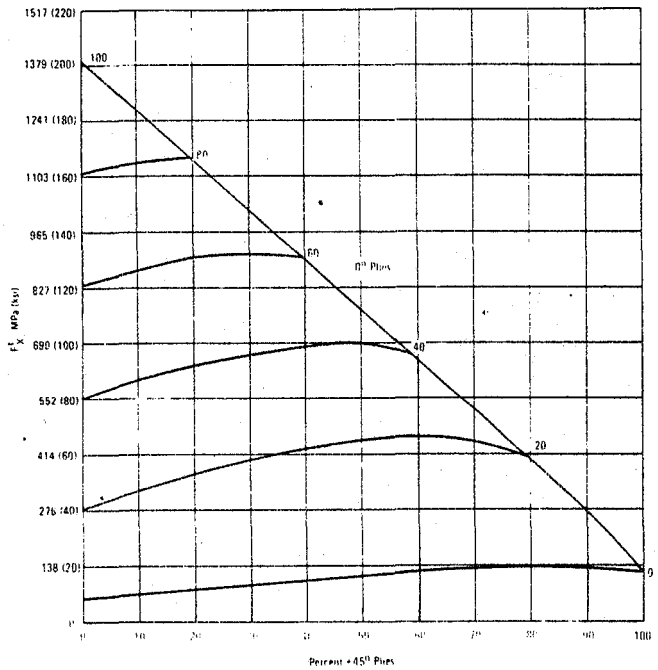

Figure 56. - T300/5208 tape tension strength predictions - room temperature dry.

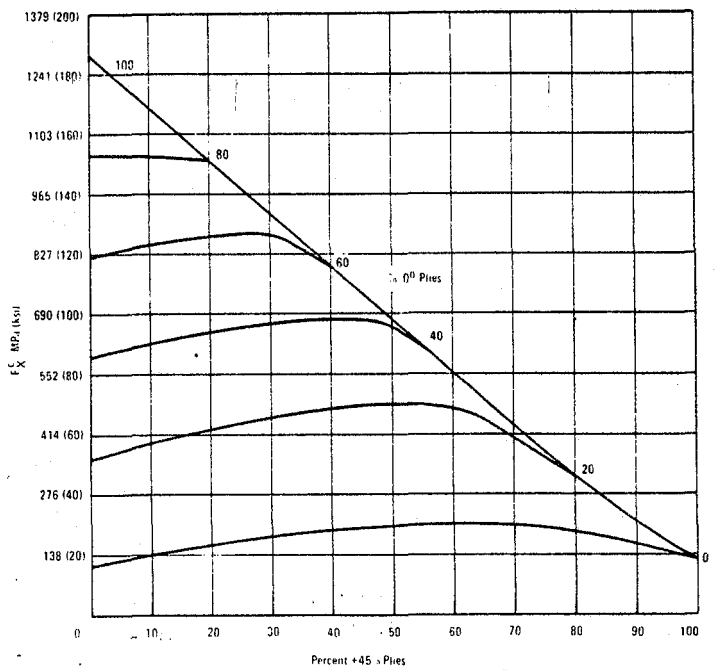

Figure 57. - Tape T300/5208 compression strength predictions - room temperature dry.

conservatively assumed to occur when the shear-strain in the ±45° plies exceeded the ply level yield shear strain.

The values of K_{ET} and K_B are tabulated in table 25. Using these values the 0° ply level failure strains have been computed and are presented in table 26.

Note that the design allowables are based on notched strength where the notch is a 4.76 mm (3/16 in.) diameter hole. For a structure having holes greater than 4.76 mm (3/16 in.) diameter the tensile strength must be further reduced to account for the greater notch size. The curve presented in figure 58 should be used for this purpose. This modification should be accomplished as follows:

$$K_{ET} \text{ for 4.76 mm (3/16 in.) dia holes} = K_{ET} \times \frac{K_T \text{ for large dia}}{K_T \text{ for 4.76 mm (3/16 in.) dia}}$$

Advanced composite structures are vulnerable to impact damage. Compression tests have been conducted on coupons containing both nonvisible and visible impact damage - some of the data are summarized in figure 59. Note that the

TABLE 25. - NOTCH/ENVIRONMENTAL AND STATISTICAL REDUCTION FACTORS

Material	Loading	K_{ET} Condition			K_B
		219K (-65°F) Dry	RT Dry	355K (180°F) Wet	
Tape	Tension	0.49	0.52	0.59	0.99
	Compression	0.84	0.71	0.68	0.94

TABLE 26. - 0° PLY LEVEL FAILURE STRAINS

Material	Loading	Failure Strain μm/m Condition		
		219K (-65°F) Dry	RT Dry	355K (180°F) Wet
Tape	Tension	4750	5050	5720
	Compression	8460	6870	6500

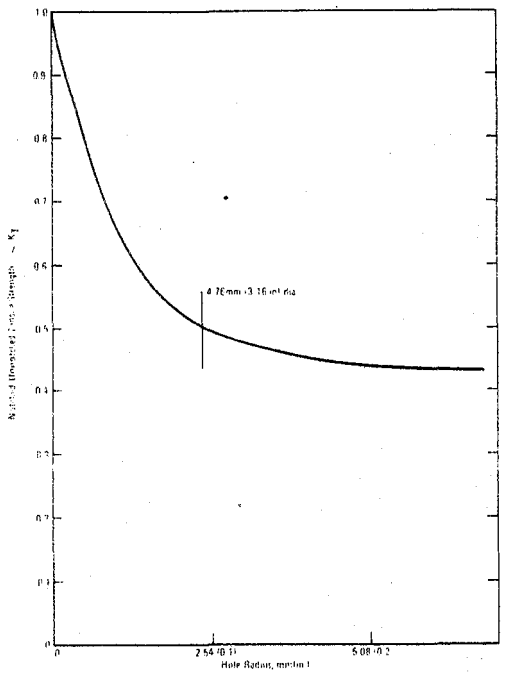

Figure 58. - Hole radius effects on tensile strength.

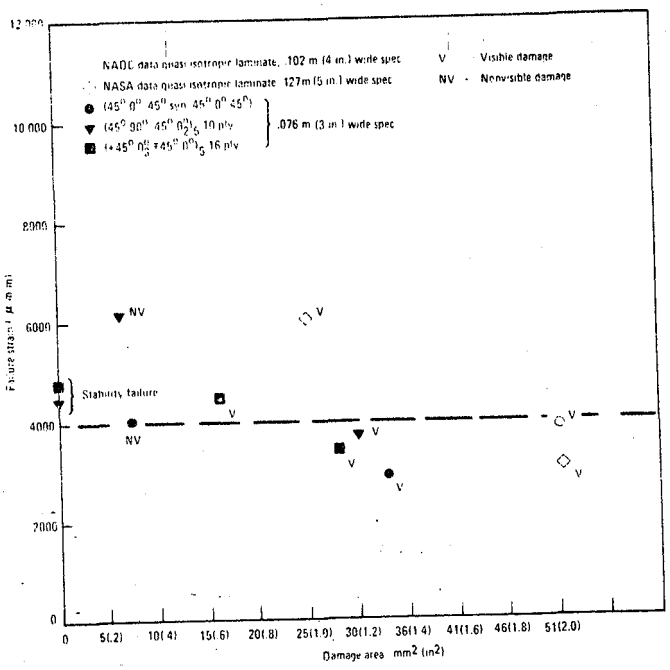

Figure 59. - Compression impact data.

failure strain for nonvisible impact damage is generally lower than previously reported for a laminate containing a 4.76 mm (3/16 in.) diameter hole. Thus to account for the effect of nonvisible impact damage on the compressive strength of a laminate, a maximum strain or 4000 μm/m (4000 μ in/in) is used for all environmental conditions for both tape and fabric laminates.

The design allowables used for analysis reflect the worst environmental condition in combination with a 4.76 mm (3/16 in.) diameter notch (greater if required) or nonvisible impact damage. The allowables are conservatively used for all loading conditions irrespective of associated environmental conditions.

The allowable lamina level strains in the direction of the fiber are shown in table 27. The carpet plots based on lamina level strains are presented in figures 60 through 66.

2.4.6 Bearing strength and push-through strength.- The bearing tests are summarized in table 28. Tests included cylindrical bolt bearing (figures 67 and 68) and countersunk screw bearing (figure 69). The test specimens had an edge distance ratio of 5.3 to ensure bearing failures rather than shear-tear out failures. The countersunk single lap shear bearing specimen was attached to an aluminum extruded channel to minimize the rotation of fastener and specimen due to the eccentric load for single shear. To prevent fastener failure, a 1517 MPa (220 ksi) heat-treated screw was used. The 4.76 mm (3/16 in.) diameter fasteners were installed with standard torques of 2.83 to 3.39 N/m (25 to 30 lb/in).

Tests were conducted for T300/5208 tape laminates, fabric laminates, and tape laminates cocured to a syntactic core for various combinations of 0°, ±45°, 90° plies. Tests included dry, 219K (-65°) dry and 365K (180°F) wet environmental conditions.

TABLE 27. - ALLOWABLE LAMINA STRAINS

Material	Loading	Allowable Strain μm/m (μin./in.)
Tape	Tension	4750*
	Compression	-4000

*4.76 mm (3/16 inch) dia. notch or less

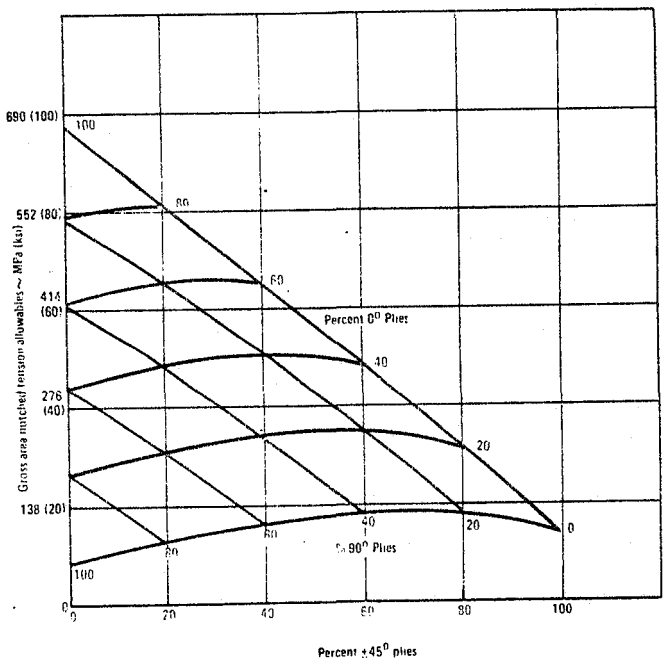

Figure 60. - T300/5208 Unidirectional tape tensile strength design allowables.

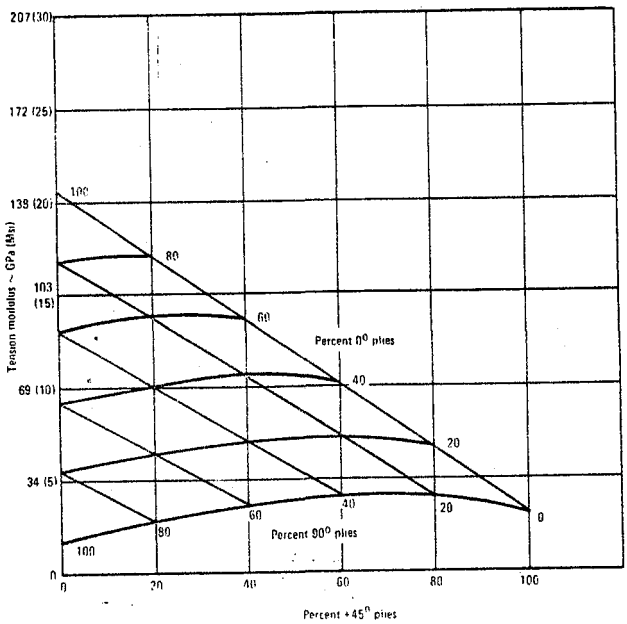

Figure 61. - T300/5208 Unidirectional tape tensile modulus.

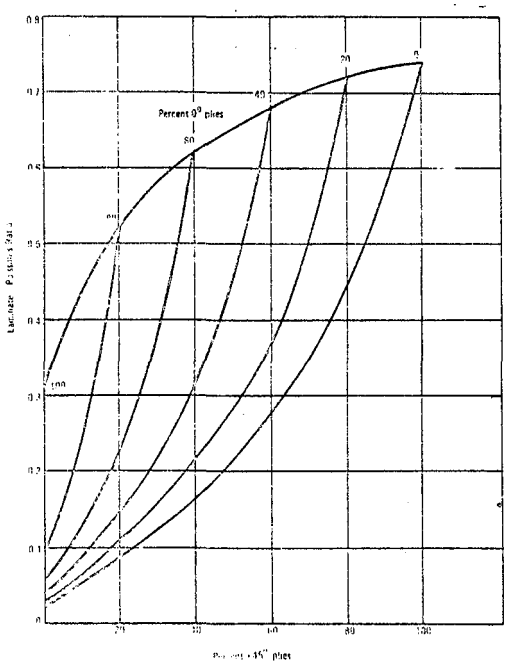

Figure 62. - T300/5208 Unidirectional tape Poisson's ratio.

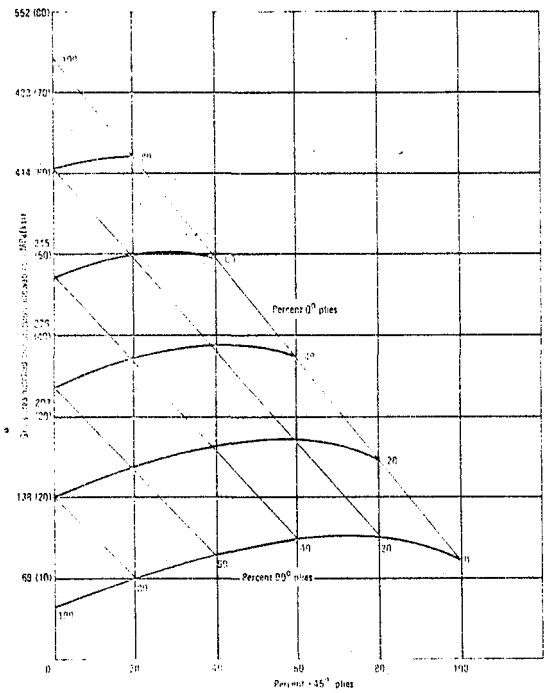

Figure 63. - T300/5208 Unidirectional tape compression strength design allowables.

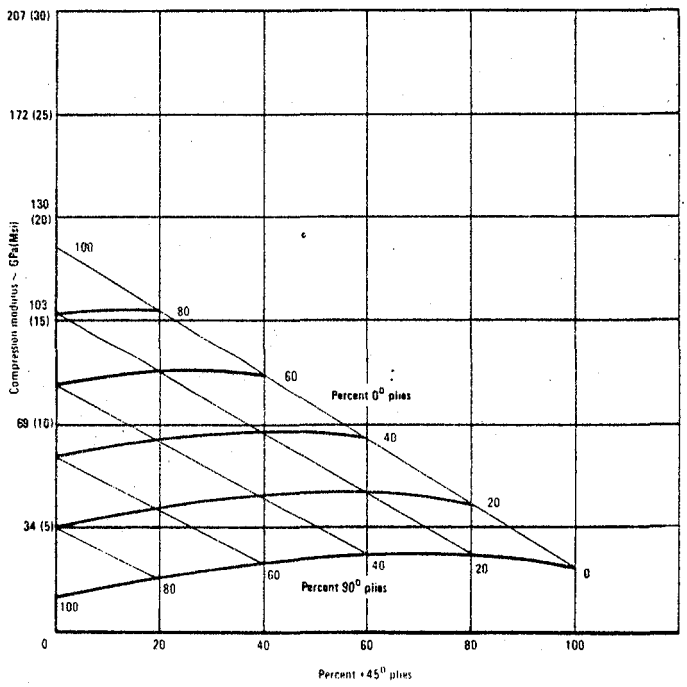

Figure 64. - T300/5208 Unidirectional tape compression modulus.

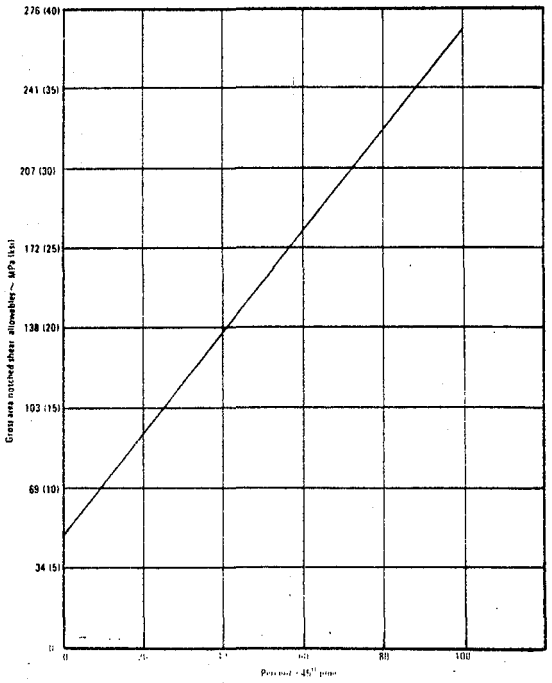

Figure 65. - T300/5208 Unidirectional tape inplane shear strength design allowable.

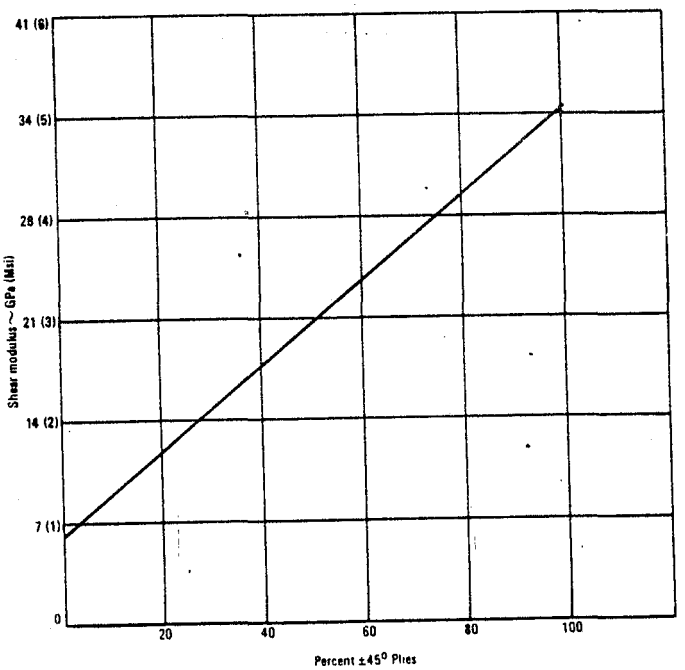

Figure 66. - T300/5208 unidirectional tape inplane shear and modulus.

Table 28 gives the mean ultimate bearing strength for each test group along with the standard deviation. This bearing strength was determined from the ultimate load recorded during test divided by the nominal bearing area [4.8 mm (0.19 in) x t].

The proportional limit load P_{PL} was determined from the autographic load-deflection curves for each specimen and divided by the ultimate load P_{BRU} to obtain the (P_{PL}/P_{BRU}) ratios given in table 28. The proportional limit load is the maximum load that can be applied without causing permanent deformation in the bearing area of the composite material. In general the proportional limit load was at least two thirds of the ultimate bearing load.

TABLE 28. - MEAN ULTIMATE BEARING STRENGTH

Percent 0°/±45°/90°	Thickness mm	Thickness in.	(5) Type	Condition	No. of Test	Load Direction	Mean Ultimate Bearing Stress MPa	Mean Ultimate Bearing Stress ksi	Standard Deviation MPa	Standard Deviation ksi	(4) P_{PL}/P_{BRU}	Comments
0/50/50	3.175	0.123	DB	RTD	5	90°	934	135.4	60.7	8.81	0.69	5 Mil Tape Laminates
0/50/50	3.150	0.124	SB	RTD	5	90°	650	94.3	24.3	3.53	0.68	
0/90/10	2.642	0.104	DB	RTD	5	90°	1163	168.7	38.1	5.53	0.67	5 Mil Tape Laminates
0/90/10	2.616	0.103	SB	RTD	5	90°	820	118.9	29.0	4.20	0.79	
25/50/25	2.134	0.084	DB	RTD	5	0°	1129	163.8	34.0	4.93	0.79	5 Mil Tape Laminates
25/50/25	2.134	0.084	SB	RTD	5	0°	849	121.1	43.4	6.29	0.83	
56/44/0	4.648	0.183	DB	RTD	5	0°	1049	152.1	14.1	2.05	0.71	5 Mil Tape Laminates
56/44/0	4.597	0.181	SB	RTD	5	0°	651	94.4	40.3	5.84	0.75	
50/50/0	3.100	0.122	DL	RTD	5	0°	1149	166.6	30.3	4.39	0.74	5 Mil Tape Laminates
50/50/0	3.100	0.122	SB	RTD	5	0°	848	123.0	24.4	3.54	0.72	
50/50/0	3.100	0.122	DL	RTD	3	0°	1216	176.3	73.6	10.68	0.79	(1) 5 Mil Tape Laminates
50/50/0	3.073	0.121	DL	RTD	3	0°	1203	174.5	29.9	4.34	0.73	(2)
40/40/20	2.159	0.085	DB	RTD	4	0°	994	144.1	22.3	3.23	0.68	7.5 Mil Tape Laminates
40/40/20	2.083	0.082	DB	356K (180°F) Wet	3	0°	856	124.1	5.7	0.83	0.72	
40/40/20	2.070	0.085	DB	219K (-65°F) Dry	3	0°	1473	213.6	28.6	4.15	0.68	
40/60/0	1.956	0.077	DB	RTD	3	0°	868	125.9	14.3	2.07	0.70	Fabric Laminates
40/60/0	1.956	0.077	DB	356K (180°F) Wet	3	0°	796	115.5	8.7	1.26	0.83	
40/60/0	1.956	0.077	DB	219K (-65°F) Dry	3	0°	1063	154.2	53.0	7.69	0.76	
33/67/0 (3)	1.219	0.048	DB	RTD	3	0°	1051	152.4	44.2	6.41	0.70	3 Plies of 7.5 Mil Tape on Each Side of Syntactic Core
33/67/0	1.219	0.048	DB	356K (180°F) Wet	3	0°	858	124.5	79.9	11.59	0.75	
33/67/0	1.219	0.048	DB	219K (-65°F) Dry	3	0°	1334	193.5	126.5	18.35	0.76	

(1) Bearing Holes Drilled at 4° Angle

(2) Bearing Holes Drilled W/O Back-Up

(3) Thickness Does Not Include 0.0375 In. Syntactic Core

(4) Proprotional Limit Load Divided by Ultimate Bearing Load

(5) See Figures 67 thru 69

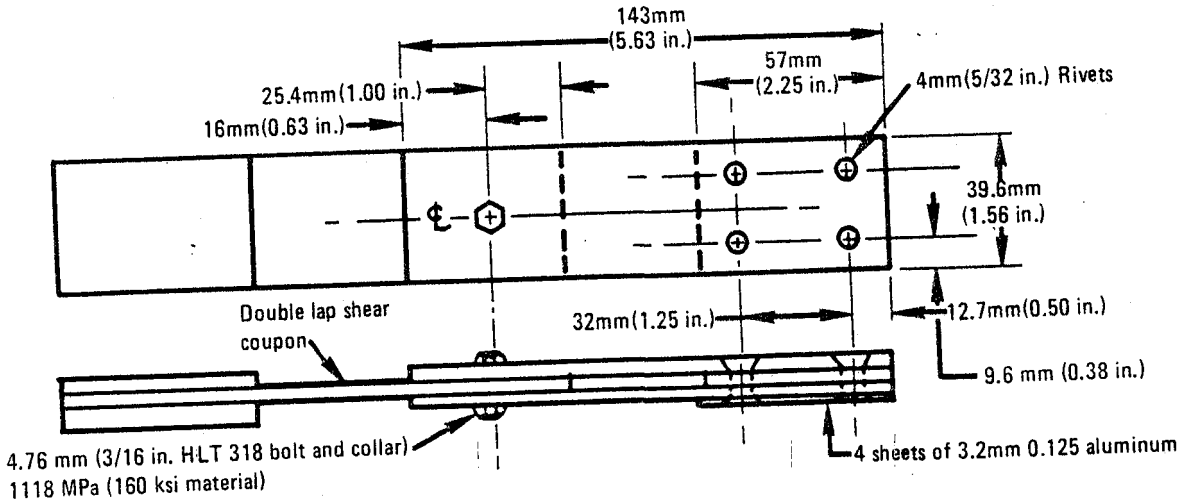

Figure 67. - Double lap shear bolt bearing specimen (DB).

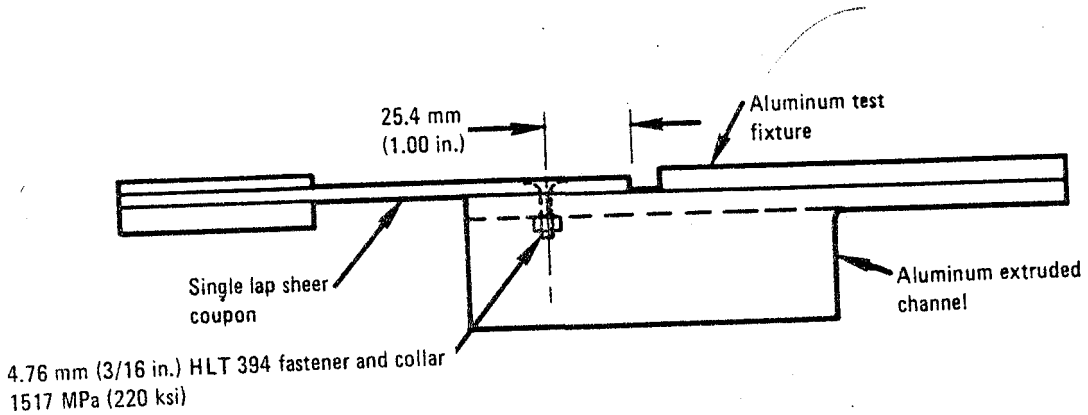

Figure 68. - Single lap shear countersunk screw bearing specimen (SB).

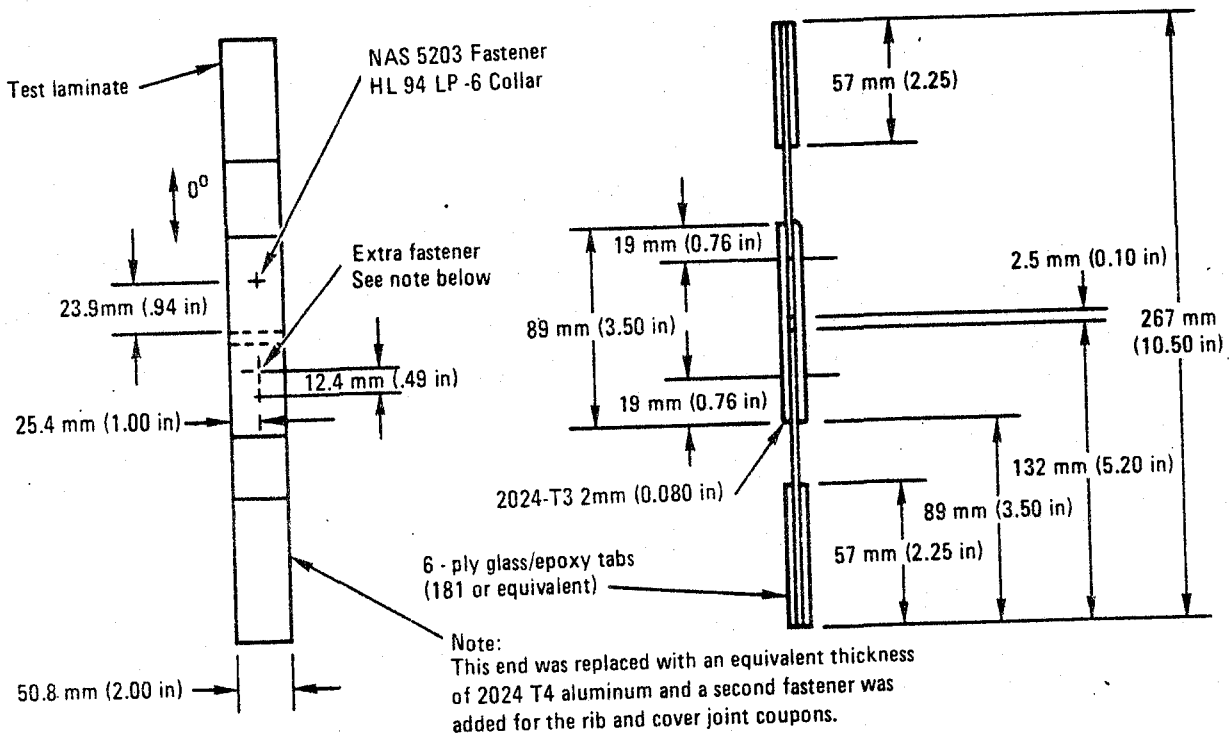

Figure 69. - Joint coupon, aileron program (DL).

The effect of manufacturing errors on the cylindrical bearing strength was evaluated for a hole drilled slightly oversize 5.05 to 5.13 mm (0.199 to 0.202 in.) at an angle of 0.07 radians (4 degrees) off the perpendicular to the load direction and for a hand drilled hole without using a backup for a (50%/50%/0%) tape laminate. The results given in table 32 indicate no detrimental effect of the manufacturing errors on the bearing ultimate strength.

Push-thru tests, were conducted to evaluate the effect of fastener head configuration on out-of-plane load capacity of typical composite joints. The test technique, shown in figure 70, measures the load required to push the fastener head through the composite material. The test results are summarized in table 29. The composite aileron cover tests, showed that loads obtained from push-thru tests were equivalent to the loads obtained from pull-thru tests, so only push-thru data are reported here.

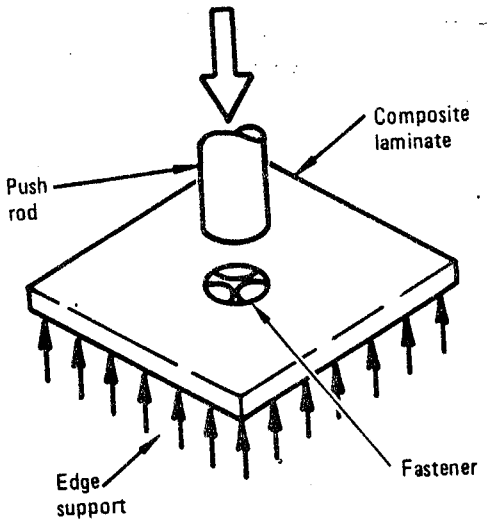

Figure 70. - Push-through specimen.

TABLE 29. - PUSH-THROUGH TESTS

	Initial Failure Load		Max Failure Load	
	N	lb	N	lb
4.76 mm (3/16 in.) Countersunk, 3 mm (0.12 in.) GR/EP	2455	552	4484	1008
	3309	744	4666	1049
	2669	600	3790	852
Ave	2811	632	4313	970
4.76 mm (3/16 in.) Countersunk and Dimpled Washer, 3 mm (0.12 in.) GR/EP	5168	1162	6992	1572
	5996	1348	7099	1596
	4933	1109	6810	1531
Ave	5365	1206	6967	1566
4.76 mm (3/16 in.) Pan Head, 3 mm (0.12 in.) GR/EP	4377	984	6063	1363
	5284	1188	6138	1380
	5765	1296	6138	1380
Ave	5142	1156	6113	1374

Three types of 4.76 (3/16 in) diameter fastener configurations (countersunk screw, pan-head screw and countersunk screw with a dimpled washer) were investigated for push-thru strength of the solid laminate material. Only the 3.97 mm (5/32 in) diameter countersunk screw configuration was tested for the aileron cover material. For each specimen, the fastener was installed with sufficient torque to shear off the external wrenching portion of the collar.

The push-thru specimens were tested statically to failure at a deflection rate of 1.4 mm/min (0.050 in/min). The load-deflection characteristics of each specimen were similar. Typical load-deflection curves are shown in figure 71.

The load deflection curves for the solid laminates exhibited a bimodal failure characteristic, as shown in figure 71. The initial failure was a localized crushing of the laminate under the head of the laminate followed by a final shear-tear out failure of the composite material around the periphery of the fastener head. The average value of the initial failure was from 65 to 84 percent of the final failure. The combination of a countersunk fastener with a dimpled washer yielded the greatest push-thru capability.

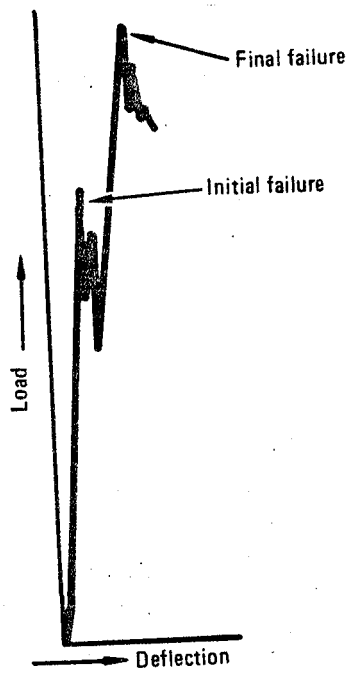

Figure 71. - Typical push-thru test load-deflection behavior.

3. PRODUCIBILITY STUDIES

A producibility and design-to-cost, cost reduction program was implemented to identify the indicated production costs of composite fin assemblies and high cost drivers and to develop and evaluate producibility cost reduction concepts to minimize or eliminate these drivers. A list of candidate cost-reduction items was compiled for analysis and evaluation.

3.1 Ground Rules

The following ground rules, developed and coordinated between the Lockheed-California and Lockheed-Georgia Companies, were in effect during the producibility studies:

- The composite fin will be interchangeable with the metallic L-1011 fin.
- A production run of 100 fin boxes was used. The first unit began in February 1981 with first delivery in November 1981, the second delivery was January 1982, third delivery was February 1982, and the rate was 2 per month thereafter.
- Lot size was 12 aircraft, but this was not restricted if set-up or other considerations warranted different lot sizes for component parts.
- Material Costs

Graphite-epoxy tape	$44.09/kg ($20/lb)
Graphite-epoxy bi-directional cloth	$55.12/kg ($25/lb)
Kevlar-epoxy bi-directional cloth	$35.27/kg ($16/lb)

- Projected labor rates at the approximate mid-span of the production program (March 1983) were used for cost estimates.
- An automated facility that reduces production costs on this 100 ship-set run was assumed since it would also be applicable to other composite programs.

3.2 Cost Reduction Candidate Matrix

A series of producibility candidate items was accumulated from Engineering, Manufacturing, and Tooling. Tables 30 and 31 show a list of these items collected for detail studies to find the items which would produce the lowest cost approach and meet the structural requirements.

TABLE 30. - PRODUCIBILITY CANDIDATE ITEMS - COVERS & RIBS (1 of 3)

Item	Description	Potential Savings* Cum. Total for 100	Weight		Cost to Implement	**	Status			
		Dollars	kg	lb	Dollars	Risk	Go Now	Go Prod	Cancel	Process Verif. Required
1.1.2√	Eliminate Interleaving Doublers	– 606 421		0	–	L	x	x		
1.2.1	Low Resin Content Prepreg	– 22 699		0	–	L				x
1.2.2	Use 6000 Filament Tow	–		–	–				x	
1.2.3	Use 3501-6 Resin System	–		–	–				x	
1.2.4	Raw Material Quality	–		–	–					x
1.2.5	Optimize Tape Width	–		0	–					x
1.2.6	Use Transparent Backing	–		0	–					x
1.3.1	Delete "How To" From Specs.	–		0	–					x
1.3.2√	Relax Gap/Overlap Tolerances	– 100 828		0	–	L	x	x		x
1.3.4	Relax Wrinkle Requirements	–		–	–	L			x	
1.3.5√	Prebleed Laminate/Hats	–1 075 349		0	–	L	x	x		x
1.4.2√	Reusable Rubber Bag	–		0	–	L		x		x
1.5.1	Mech. Cutting Prepreg	In item 1.3.5 & 3.5.3		0	–	L				x
1.6.2√	QA Procedure Flexibility	– 155, 551		0	–	L		x		
1.6.3	Relax Porosity Requirement	–		–	–					x
1.6.4√	Prod. Stamp Ply Identity	–1 064 009		0	–	L		x		
1.6.5	Upgrade Material Dispensing Machine	–		0	62 848				x	
1.6.6√	N/C Automated Machine	See item 4.3.7 - 4.3.9		0	7 082 800			x		
2.5.2	Layup on Flat Plate	– 942,184		0	–	L	x			
2.6.3	Use Gr/Ep Fabric for Covers	– 3 299 716	+29.7	+66.0	–	L			x	
2.6.3A	Use Gr/Ep Fabric & Uni-Tape	– 2 623 762	+2.7	+5.0	–	L			x	
2.6.4√	New Fillers – Rib to Cover Config.	–860 979	+0.8	+1.8	–	L	x	x		
2.6.5√	Lightning Protection Flame Spray in lieu of Alum. Screen	+6 497	+1.6	+3.5	247 000	M	–	–		x
3.1.3√	Const. Sect. Hat/External Doublers	In item 1.3.5 & 3.5.3	+0.05	+0.1	–		x	x		x
3.2.1	Fabric for Hat Stiffeners	–1 695 883	+2.31	+5.1	–	H			x	

*negative sign means cost saving

√Item selected for incorporation

** L Low
M Medium
H High

TABLE 30. - PRODUCIBILITY CANDIDATE ITEMS - COVERS & RIBS (2 of 3)

Item	Description	Potential Savings* Cum. Total for 100	Weight		Cost to Implement	**	Status			
		Dollars	kg	lb	Dollars	Risk	Go Now	Go Prod	Cancel	Process Verif. Required
3.3.2	Press Molded Hats	−1 535 775		0	–	L			x	
3.3.4	Pultruded 0° Cap Strip	+98 929		0	–	H			x	
3.3.5	Preplied Tape Hat Stiffeners	−2 793 144		0	–	H		x		
3.4.2	Redesign Hat Tools – Single-Stage Cure	–		0					x	
3.4.3	Redesign Hat Tools – Cocure	–		0	–				x	
3.5.2	Roll Form Hat	−1 441 412		0	–	M				x
3.5.3	Layup Hat Flat-Drape Drape on Tool	−1 109 352		0	–	L				x
3.5.4	Eliminate Net Trim – Relax Trim Tolerance	–		TBD	–					x
3.5.5	Cocured Cap Strip to Web	+212 328	+4.3	+9.4	–				x	
3.5.6√	Automated Continuous Roll From Hats – Preplied Material	−3 358 014		0	243,363	L		x		x
3.5.7	Precured Hats	−2 118 243		0	–	L			x	
3.5.8	Prestaged Hats	–		0	–				x	
3.5.9	Preplied Prepreg – Powered Dispensing Machine	–		0	–				x	
3.6.0√	Decrease Hat Flange Radius	−1 350 845	+0.1	+0.2	–	L	x	x		
3.6.1	Hats – Preplied – Roll Form – Press Mold	−2 937 360		0	–	L				x
3.6.3√	Improved Ultrasonic Inspection	– 328 700		0	40 000	L	x	x		
4.1.1	Call Out Recessed Head Flush Screws	–		TBD	–				x	
4.1.2	Relax Finish Tolerance and Assembly Requirements	–		TBD	–					x
4.1.3	Relax Hole Spec. Requirements	–		0	–					x
4.3.1	Single-Stage Cure Skin to Hat	−4 483,276		Replaced by 4.3.7		H			x	
4.3.1A	Single-Stage Cure Prebled Skin and Hat	−4 445 212		Replaced by 4.3.7		H			x	
4.3.2	Cocure Skin and Precured Hat	–		Replaced by 4.3.7					x	
4.3.4	Cocure Hats/Inflatable Mandrel	−4 396 242		Replaced by 4.3.7		H			x	

TABLE 30. - PRODUCIBILITY CANDIDATE ITEMS - COVERS & RIBS (3 of 3)

Item	Description	Potential Savings* Cum. Total for 100	Weight		Cost to Implement	**	Status			
		Dollars	kg	lb	Dollars	Risk	Go Now	Go Prod	Cancel	Process Verif. Required
4.3.4A	Cocure Hats/Open Ended Mandrel	–		0	–				x	
4.3.5	Cocure Hats/Segmented Alum. Mandrel	–		0	–				x	
4.3.6	Single-Stage Cure – Skin to Hat Male MBF Tool	– 6 441 302	-2.3	-5.0	–	H			x	
4.3.7√	Single-Stage Cure Skin to Hat Assembly – Modified Female Tool	–12 641 744	+2.6	+5.7	7 640 752	L	x	x		x
4.3.8	Single-Stage Cure Skin to Hat Assembly – Male Mold Concept	–13 222 525	+2.6	+5.7	8 057 449	H			x	
4.3.9	Single-Stage Cure Prepreg Skin to Prepreg Hat – Male Mold Concept	–12 989 081	+2.6	+5.7	8 102 249	H			x	
4.5.1	Pressure Pads for Bond	+116 970		0	–	L			x	
4.5.2√	Alt. Peel Ply Material	–		0	–					x
4.6.1√	NDT Inspection – Single-Stage Cure Process	+156 859		0	–	H		x		x
5.1.1	Use Fabric on Ribs	–		–	–				x	
5.1.4√	Beaded Web on Solid Web Rib	–332 381	-0.5	-1.1	–	L	x	x		x
5.1.5A1	Change Ribs to Alum.	– 4 414 097		–					x	
5.1.5A2	Alum. Ribs vs. New Composite Design	– 479 047		–	–				x	
5.1.5A2.1	Composite and Alum. Rib Combination	–392,037		–		M			x	
5.1.5A2.2	Composite and Alum. Rib Combination	–452,884		–		M			x	
5.1.5A2.3	Composite and Alum. Rib Combination	–358 898		–		M			x	
5.1.7	Composite and Alum. Rib Combination	–		–					x	
5.1.12√	Redesign Ribs vs. Phase I Design	– 3 671 316	-9.5	-20.9			x	x		x
5.5.3√	Rib Cap Machining			0						x
6.1.1√	Eliminate Kevlar	– 64 070	-3.8	-8.3			x	x		
6.1.3	Single-Stage Cure Skin, Hat and Rib Assembly	–		–					x	
6.1.4	Cocure Skin, Hat and Rib Assembly	–		–					x	
6.1.5	Cocure Skin and Precured Hats and Ribs	–		–						

TABLE 31. - PRODUCIBILITY/COST REDUCTION STUDIES SUMMARY - SPARS (1 OF 3)

Item	Description	Potential Savings* Cum. Total for 100	Weight		Cost to Implement	** Risk	Status			
		Dollars	kg	lb	Dollars		Go Now	Go Prod	Cancel	Process Verif. Required
GA✓	Incorporate Production Tools	−4 222 700	N/C	N/C	643 664		X			
GB ✓	Automated Lay-up and Cut of Spar	−567 300	N/C	N/C	1 007 854		X			
GS1✓	Replace Web Kevlar with ±45° / Graphite Tape (in GS12B)	+28 400	+1.2	+2.6	–					
GS1	Replace Web Kevlar with Graphite Graphite Cloth	−28 100	+1.2	+2.6	5 630				X	
GS1	Replace Web Kevlar with Fiberglass Cloth	−126 700	+3.4	+7.5	–				X	
GS2✓	Cut Access Holes After Bond	Negligible	–	–	Neglibile		X			
GS3	Replace Integrally Molded Rib Attach Angles with Aluminum Angles and Mechanically Attach	Large Increase	+1.4	+3.0	162 006	L			X	
GS4✓	Delete Reinforcing Rings (in GS12B)	−153 100	−0.7	−1.6	24 826	L				
GS6✓	Shorten Web Stiffeners	−59 900	−0.2	−0.5	5 147	L	X			
GS12	Provide Commonality of Plies in Caps, Stiffeners & Webs (Net Change Includes GS1, 2 & 4) (See GS12B)	−206 100 (−24 900)	+3.4 (+2.9)	+7.5 (+6.5)	102 881 Includes GS1 & 4	L			X	
GS14	Prebleed Kits Used to Assemble Spar	Large Increase	N/C	N/C	Large; Requires Additional Tools & Cure Cycles				X	X

TABLE 31. - PRODUCIBILITY/COST REDUCTION STUDIES SUMMARY - SPARS (2 of 3)

Item	Description	Potential Savings* Cum. Total for 100	Weight		Cost to Implement	** Risk	Status			
		Dollars	kg	lb	Dollars		Go Now	Go Prod	Cancel	Process Verif. Required
GA3	Eliminate "C" Stiffener and Angle Drill	-400	N/C	N/C	2 288				X	
GS5	Change Spar Cap width to eliminate wide tabs	-18 000	N/C	N/C	7 020				X	
GS16	Automate inspection	-6 800	N/C	N/C	150 000				X	
GS20 √	Purchase Low Resin Content Cloth and Tape Prepregged	-18 600	+2.3	+5.0	Negligible				X	X
GA2	Use Liquid Shims to Close Out	-29 200	N/C	N/C	1 560	H			X	
GA1	Locate Rib Attach Angles for rear spar	-6 000	N/C	N/C	15 652				X	
GS9	Relax Spar Web Finish Acceptance Criteria	-9 000	N/C	N/C	40	L	X			
GS11√	Standardize Ply Direction	-54 300	N/C	N/C	2 312	L		X		
GA4	Assemble Truss Rib Caps to Cover Surface Assembly	Large Increase	N/C	N/C	Large; Requires Additional Tools	H			X	X
GA7√	Review Corrosion Protection Requirements	-101 500	N/C	N/C	2 338	L	X			
GA8	Review Finish Requirements	-56 000	N/C	N/C	1 144	L	X			
GS23	Purchase Pultruded Stiffeners & Rib Attach Angles		+0.2	+0.4		H			X	X

TABLE 31. - PRODUCIBILITY/COST REDUCTION STUDIES SUMMARY - SPARS (3 of 3)

Item	Description	Potential Savings* Cum. Total for 100	Weight		Cost to Implement	** Risk	Status			
		Dollars	kg	lb	Dollars		Go Now	Go Prod	Cancel	Process Verif. Required
GS24	Purchase Pultruded Spar Caps	Not feasible for Spar Caps because of tape in thickness and lay-up of web into spar cap							X	X
GS12A	Provide Commonality of Plies; Use Cloth & Tape & Maintain Thickness		+0.5	+1.0					X	
GS7	Design Spars and Box Assembly with Optimized Application of CADAM	Drawing Status Minimized Potential Saving	N/C	N/C	–				X	
GS15	Provide Wire Mesh Bleed Within Spar Tools								X	X
GS14	Redesign Aux. Spar to 1-piece G/E								X	
GS22 √	Pre-assemble in Lot Quantities In GA						X			
GS12B	Provide Commonality of Plies in Spar Web. Use All Tape	–250 000	+0.5	+1.0	102 283	L	X			

*N/C No change

√ Item selected for incorporation

Neg Negligible

* Negative sign means cost saving

** L Low

M Medium

H High

3.2.1 Producibility/cost reduction, covers and ribs. - The study items are listed in table 30. Each of these items was analyzed as to weight conditions, cost to implement, manufacturing risk, go/no-go production/cancel, and process verification requirements. The results of the studies from a potential cost savings and weight impact are summarized for each item. All incorporated items saved money except 4.6.1. The cost of implementing this item and the risk involved was negligible when compared to the overall savings of 4.3.7.

3.2.2 Producibility/cost reduction, spars. - The study items are listed in table 31. The studies on the spar fabrication and ACVF box assembly at the Lockheed-Georgia Company were closely paralleled with studies of the covers and ribs at the Lockheed-California Company. A coding system of GS for Georgia spar fabrication items and GA for Georgia assembly items was applied for identification.

3.2.3 Producibility/cost reduction, box assembly. - Since the composite box structure assembly was to be interchangeable with the metal fin box structure, the decision was made to assemble the composite box in the same existing fixture. This provided the most producible method to use. Only slight modifications were necessary for material thickness and positioning. Production spacematic drilling was planned to drill the majority of the fastener holes.

3.3 Selected Configuration

The anticipated result of the incorporation of the selected producibility items was a significant reduction in the manufacturing costs of the production fin box without compromising the composite weight objectives. Assembly costs for the composite box are less than assembly costs for the metallic box because of the reduction in parts and fasteners. The covers and spars are fabricated as one piece units, thus dramatically reducing the number of parts. The fasteners were reduced from 40,870 to 6300.

The selection process consisted of evaluating together the cost avoidance potential, the costs to implement, the technical feasibility, weight effects and manufacturing risk assessment.

3.3.1 Selected items - cover and ribs. - Most of the items that were selected for incorporation had a degree of process development to verify the feasibility of achieving the low-cost approach for fabrication. Items in tables 30 and 31 that were selected are designated by a check mark (√).

The key item selected to produce the lowest cost approach for the fin box structure in comparison to the metal structure was item 4.3.7, Single-Stage Cure Skin-to-Hat Assembly - Rubber Mandrel - Modified Female Tool Concept, which had a low risk and shorter development time. Also, item 5.1.12 Redesign Composite Ribs vs the Phase I design, was considered to have a low risk.

4. PROCESS VERIFICATION

Analysis of the cost estimates for candidate items in the producibility program indicated that significant savings would result from their incorporation into the ACVF program, both individually and in combination with other candidate items. Other candidates offered savings potential which could only be realized nominally in a production program, such as use of fully automated layup equipment and continuous hat stiffener forming. Initial priority was given to those alternates which would affect design configuration. Using this premise, preliminary manufacturing operation sequences were developed for each component as it was defined by the producibility configuration alternates. The process verification task was to apply these sequences in the shop, using development tooling as indicated, to ensure that the selected combination of configuration and manufacturing process could be translated into quality components and that the indicated cost savings would ultimately result.

Outgrowth of the producibility program involved major reorientation of the baseline manufacturing plan for ACVF covers; producing them in a single stage cure versus the former method of adhesive bonding of cured hats and skins. The manufacturing process development activity on the cover assemblies became a program-pacing task. Redesign of the composite ribs for the new rib shapes resulting from the producibility studies obviated most of the previous manufacturing development on ACVF ribs and focused additional importance on process verification in manufacturing development of rib components.

4.1 Covers - Manufacturing Process Development

The primary approach selected for single stage cure of ACVF covers was to use a female molding fixture, that is the tool side coincident with the external skin surface, and position prebled hats over mandrels on the inside skin surface.

4.1.1 Mandrel development

Three types of mandrel were investigated. The first type was a solid rubber mandrel, the second a foam mandrel and the third was an inflatable mandrel. Each type of mandrel was evaluated by fabricating single hat stiffened panels initially and then scaling up to panels with three hat-stiffeners.

4.1.1.1 Solid rubber mandrel: This concept has the advantages of being reusable, difficult to damage, easy to repair, easy to store and handle and easy to remove from the cured part. It does not require a special vacuum bag seal and it can be easily fabricated by extruding.

It has several disadvantages. Because it produces pressure by expansion, it must be very precisely sized to fill the cavity when autoclave pressure is applied. The continued expansion as the temperature is increased causes a pressure imbalance trying to lift off the hat. The result is a thinning of the hat flange as shown in figure 72. Because of this a two-stage cure is necessary. The part is cured in the autoclave at 394K (250°F). The mandrels are then removed and the part postcured in an oven at 450K (350°F).

4.1.1.2 Foam rubber mandrel: This concept has the advantage that it allows an uninterrupted single-stage cure to 450K (350°F). It does not require precise sizing, it allows equalized pressure on all surfaces and a uniform heat-up rate.

It has a major disadvantage in that it requires wrapping with release film, a nylon film as a vacuum bag and a bleeder cloth as illustrated in figure 73. It has to be machined from a cast bun to open up the foam cells so that it is porous. It is fragile and is not reusable as it shrivels during the cure cycle. Because of the wrapping it can be difficult to remove without tearing.

4.1.1.3 Inflatable bladder mandrel: This concept has the advantages that it is reusable, repairable, handles and stores easily, it is easy to locate on the part and to remove after cure. It is easily cleaned, it can be extruded, it allows for uninterrupted part cure at 450K (350°F) and for uniform heat-up. It does not require precise sizing and it allows for equalized pressure on all part surfaces.

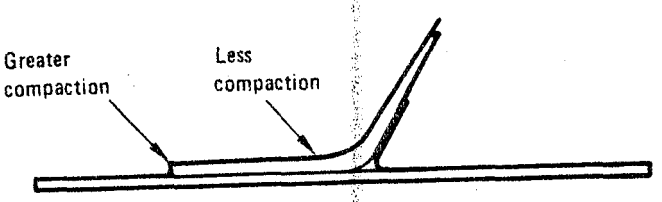

Figure 72. - Thinning of hat flange attributed to pressure imbalance.

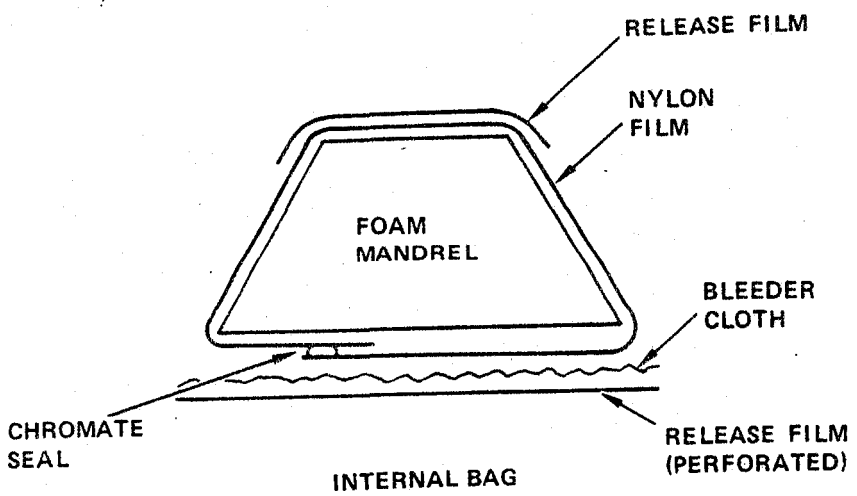

Figure 73. - Foam mandrel system.

The disadvantages are that there is an increased chance of leakage due to the multiplicity of parts requiring sealant and it can be easily damaged during removal.

4.1.1.4 Mandrel selection: The features of the three concepts are summarized in table 32.

The foam mandrel was eliminated first as it was considerably more expensive because it was not reusable and it required wrapping.

A cost review of the remaining two concepts showed that the cost differential was too small to be a decisive factor. The inflatable mandrel was selected because it offered more manufacturing flexibility by not requiring a two-stage cure cycle.

TABLE 32. - MANDREL COMPARISON

Feature	Solid	Foam	Inflatable
Reusable	Yes	No	Yes
Repairable	Yes	No	Yes
Handling	Easy	Fragile	Easy
Fabricate	Extrude	Cast & machine	Extrude
Cure Cycle Effect	Two Stage	Single Stage	Single Stage
Heat-up	Uneven	Even	Even
Installation	Easy	Complex	Easy
Removal	Easy	Fair	Easy
Damage Resistance	Yes	No	Yes
Precise & Sizing	Yes	No	No

4.1.2 Processing Studies

The early process studies were performed on the high resin content prepeg which was readily available. This prepeg was purchased with a resin content of 41 percent ±3 percent. Because of the amount of resin which had to be removed to reach the 26 to 32 percent range specified for the finished parts, prebleeding was necessary.

Two basic prebled cycles were evaluated: Cycle A - 15 minutes at 394K (250°F) with full vacuum and Cycle B - 30 minutes at 381K (225°F) with full vacuum. Figure 74 shows that viscosity of the 5208 resin is higher at 381K (225°F) than at 394K (250°F). This increased viscosity tends to reduce resin loss and prebled porosity without significant resin advancement. Cycle B, the lower temperature cycle was selected.

Prebleeding large panels of the order of 3m (100 in.) in length resulted in wrinkling of the prebled stack. This was attributed to interface thermal expansion between the bagging materials and the tool surface. This problem did not however have any effect on the physical and mechanical properties of the cured panels. A cured panel was deplied and no evidence of wrinkling was found.

Cost studies indicated that prebleeding would be an expensive operation for production. Therefore, it was decided to pursure the low resin content prepreg of 34 ±3 percent by weight and thus eliminate the need for prebleeding.

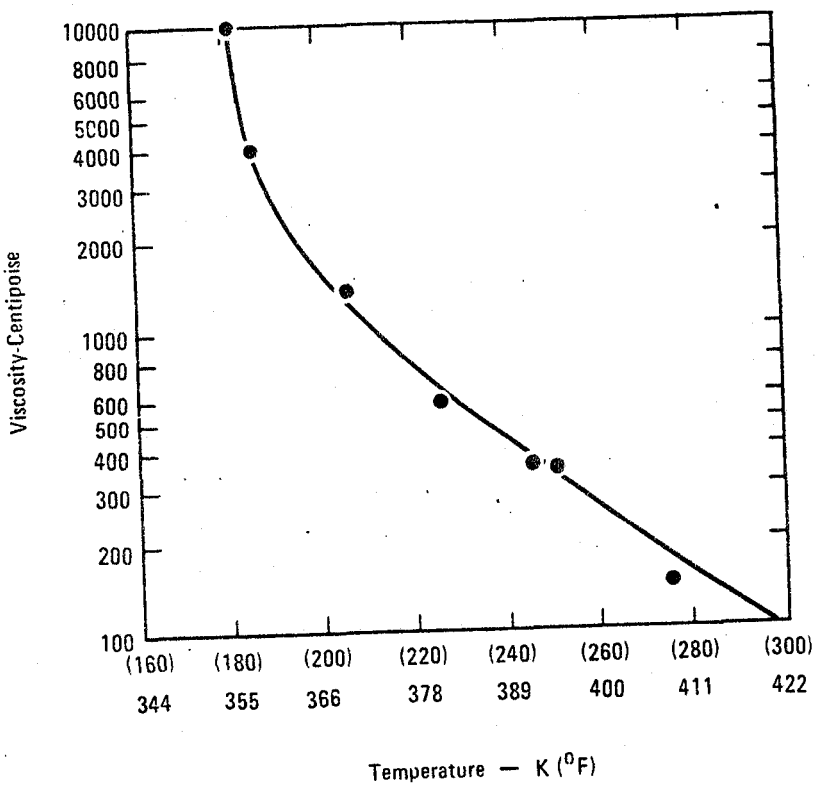

Figure 74. - Viscosity versus temperature (5208).

The approach to this task basically consisted of fabricating and testing flat laminated panels and simulated structural panels to verify known processing techniques relative to end-laminate quality. The flat panels were used to determine air bleeding arrangement and required cure cycle. Single and multihat-stiffened panels were fabricated using the air bleeding arrangement and cure cycle developed from flat panel studies.

4.1.2.1 Flat panel studies: Three panels were fabricated using an air bleeding systems developed for 16- and 32-ply panels.

Bleeding and bagging sequence:

- Panel No. 1

1. Tool plate
2. A4000 release film
3. Porous Armalon
4. Nylon peel ply
5. Laminate panel
6. Nylon peel ply
7. Porous Armalon
8. Glass boat cloth strips ground panel periphery
9. One ply nonporous Armalon
10. One ply 181 glass breather
11. Nylon vacuum bag.

- Panels No. 2 and 3: Same as Panel No. 1 except one-ply of Nexus was added between porous Armalon and A4000 release film and one-ply Nexus to extend 25.4 mm (1 in.) beyond laminate between porous Armalon and nonporous Armalon

All three panels averaged 0.124 mm (4.9 mils) per ply and the ultrasonic check indicated satisfactory panels. The physical properties of the three panels based on a .051 m (2 inch) edge strip cut from the 0.61 m (24 in.) length of the panels, are shown in table 33. Resin contents for Panels No. 1 and 2 were low, indicating that the bleeding system removed too much resin, and with the extra Nexus bleeder ply in Panel No. 2, the resin content was below specification value. Panel No. 3, using the same bleeder system as Panel No. 2, showed excellent resin content for a 32-ply laminate with no voids and very low moisture pickup.

TABLE 33. - PHYSICAL PROPERTIES TEST RESULTS FOR PANEL NO. 1, 2, AND 3.

Panel No.	Resin Wt. % Average	% Voids	Moisture 2-Hr. 355°K (180°F)
1 (16 ply)	26.04	0.34	0.75
2 (16 ply)	25.32	0.49	0.13
3 (32 ply)	32.40	0.0	0.09

4.1.2.2 Single hat-stiffened panel No. 1: The detail preplied laminates for the skin and hat were laid up in kit form ready for assembly. The preplied segments of the hat readily formed to shape on the male tool with hand forming and with minimum rub in place. Straps worked well in holding the assembly in the caul plate as it was rotated and placed in position on the skin laminate. The turnover straps (nonporous armalon were positioned spanwise at approximately every 0.25 m (10 in) to 0.30 m (12 in). The air bleeding materials used for this panel were similar to flat panel no. 1 surface:

Top Surface (Laminate)	Low Surface (Laminate)
• Nylon peel ply	• Nylon Peel ply
• Porous armalon	• Porous armalon
• Vac Pak film (PVF)	• Vac Pac film (PVF)

Upon completion ot the cure, a review of the bagged assembly indicated the breather plies (181 glass) had absorbed a certain amount of resin that edge bled from the part.

Removal of the bagging material and the peel ply showed a very good part surface with no resin-rich areas on the part. Good definition of the hat configuration was achieved. Removal of the inflatable rubber mandrel caused the rubber to tear. Apparently, the previous rough spots on the mandrel surface adhered to the resin causing added resistance to the removal process. A cross section cut at the end of the panel is shown in figure 75. The ultrasonic examination of the skin and the hat flange/skin areas showed no problems.

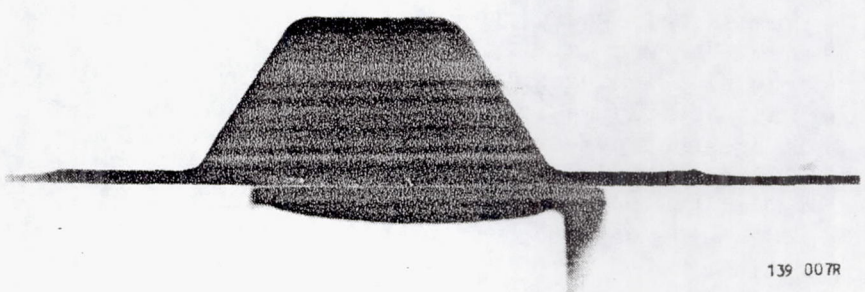

Figure 75. - Cross section of hat-stiffened panel.

4.1.2.3 Hat-stiffened panel 2: This panel was assembled from preplied kit materials, which had been in the freezer for about 10 days. The surface tack of the material was good and the hat shape was easily formed on the tools using hand pressure and rubbing (Teflon) tools.

The air bleeding system was modified for this panel to eliminate the peel ply on the hat surface of the panel assembly and to use a gas-porous film (A4000P3). This film has very small-diameter pin holes spaced at 9.5 mm (0.375 in.) centers to allow gas volatiles to escape. Additionally, silicone edge dams were used to control edge bleeding during cure. Removal of the peel ply from the hat surface of the panel would eliminate the cost of removing it and eliminate the possibility of damaging the surface during removal, particularly on the full scale covers. The panel was cured using the same cure cycle as for panel no. 1.

A considerable amount of resin was collected in the breather ply. The film did not stop the resin from flowing through the tiny pin holes into the porous armalon ply. The silicon edge dams restricted the edge bleeding but also contributed to forcing the resin to flow through the film pin holes. The top surface of the panel had a shiny finish with a few mark-off areas caused by the difficulty of smoothing out the film during the bagging operation. The ply thickness averaged slightly higher than panel 1 which indicated increased resin content. Resin contents were above the specified maximum value of 30%. The mechanical properties were very good, however. No additional cure time at 453K (355°F) and/or post cure was used.

4.1.2.4 Multihat-stiffened panel no. 1: Two kits of preplied material were laid up for the skin, hat webs, hat crown and rib doublers. The prepreg material had an average resin content of 33.4 percent in weight by weight. The process air bleeding system and cure cycle were similar to the single hat-stiffened panel 1. However, since some of the mechanical properties of panel 1 were on the low side, the cure cycle for the multihat panel 1 was increased by 1 hour at 435K (355°F). Figure 76 shows the tools. They were composed of two steel hat caul plates and two inflatable silicone rubber mandrels. The assembly was composed of the steel caul plate with the air bleeding system (Vac Pac barrier film, porous armalon and nylon peel ply) over the hat section laminate layup. The armalon strips were pulled out as soon as the hat assembly was properly positioned. The bagged assembly with the 181 glass breather plies over the top of the assembly and the vacuum bag was cured. All corner edges were check for bridging. Figure 77 shows the cured top view of the panel. Figure 78 is an end view close up of one of the hat sections, showing very good internal and external tool definition of the hat configuration.

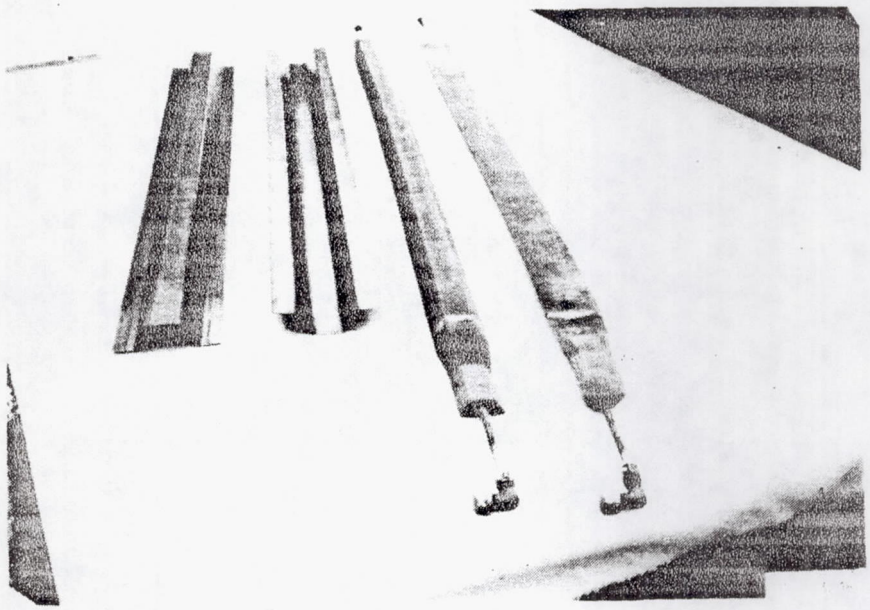

Figure 76. - Caul plates and inflatable mandrels.

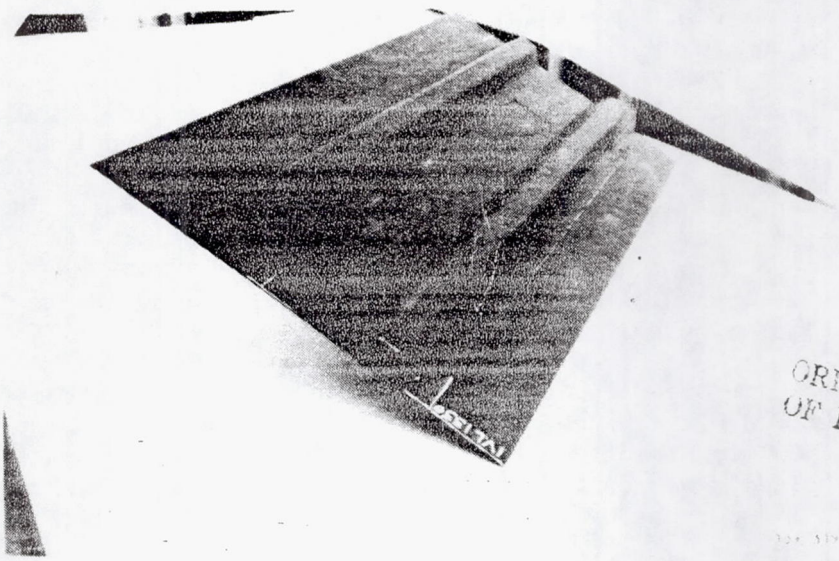

Figure 77. - Cured part.

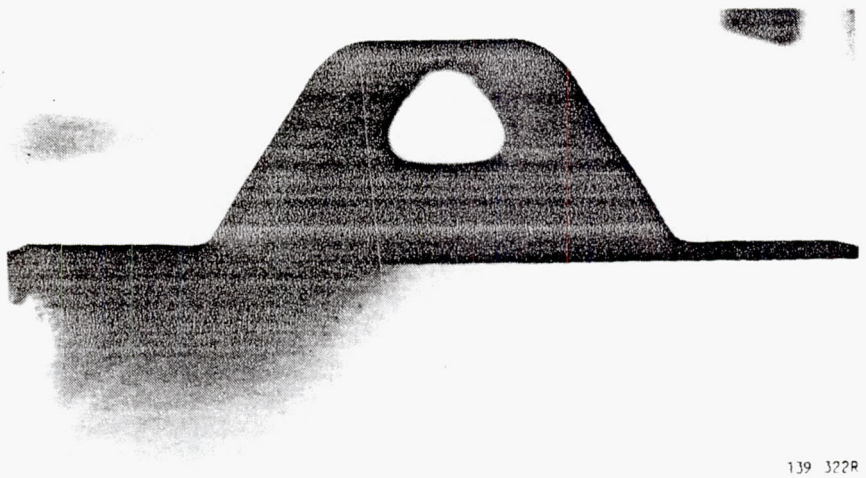

Figure 78. - End view of cured part.

The overall quality of this panel was good, indicating that the basic process for the low-resin content single cure system could be reproduced for this size panel configuration. Ultrasonic check showed that the panel was good except for three very small spots on the hat flanges. The average thickness was 0.12 mm (4.7 mils/ply) which was similar to the thickness per ply achieved in the single hat-stiffened panel no. 1 except that resin content was 24.2 percent. A review of the bleeder system after cure did show considerable edge bleeding.

Two 16-ply flat panel tests were made with the following change to the air bleeding system to increase the resin content.

- Panel No. 1 Air Bleeding Method I - Incorporated a performated barrier film (A4000P3) between the nylon peel ply and the porous armalon for both the upper and lower surface bleeding systems of the laminate. Also, the edge bleeder was changed back to 1-ply mochburg. Average resin content 29.47 percent by weight.

- Panel No. 2 Air Bleeding Method II - The nylon peel was removed from the upper surface bleeding system and replaced with film (A4000P3). The lower surface bleeding system was kept the same as panel no. 1. Average resin content 30.92 percent by weight.

4.1.2.5 Multihat panel no. 2: This panel was laid up on the tools using the laminate segment preplied materials. The method I air bleeding system which had shown by flat panel studies to achieve a resin content of approximately 29 to 30 percent by weight was used. The cured panel had good visual appearance and the ultrasonic check indicated an acceptable panel. Panels No. 1 and 2 were on the minimum side of the specification requirements. However, the mechanical properties were considered acceptable and a degree of uniformity was achieved for the skin edges, skin under the hat, and skin in between the hats using this selected bleeding system.

The multihat panel studies indicated that further refinement to the bleeding system would be required to increase the resin content of the panel. A series of flat panels were fabricated to evaluate bleeding arrangements. These panels included ply thickness variations and different bleeding arrangements as shown in table 34. Based on the results shown in this table the bleeding arrangement identified as number three (3) was selected for further evaluation for scale-up panel configurations.

4.1.2.6 Scale-up M25 (three) hat stiffened panel development: A series of hat stiffened panels were fabricated representing the root end section of the skin cover. Each panel contained three hat stiffeners 1.52 m (60, in.) long. Panels were made both from standard (41 percent) and low (34 percent) resin content material. No prebleeding of any of these panels was performed prior to cure. The low resin content panels (identified as M25-3 and M25-5) used a stacking sequence which was a modified method (3) and is illustrated in figure 79. The A4000P3 perforated film was changed to A4000P (larger perforations).

TABLE 34. - RESIN CONTENT OF TRIAL PANELS OF LOW RESIN CONTENT PREPREG

Panel No.	No. Plies	Bleeding Method No.	Bleeding Method Description		Resin Wt. %
			Bottom	Top	
Flat 1	10	1	Laminate Nylon Peel Ply A4000 P3 Perf. Film Porous Armalon	Porous Armalon A4000 P3 Perf. Film Nylon Peel Ply Laminate	26.33
Flat 2	10	2	Laminate Nylon Peel Ply Porous Armalon	Porous Armalon A4000 P3 Perf. Film Laminate	25.23
Flat 3	16	1	Same as Described Above for Method 1		29.47
Flat 4	16	3	Laminate Peel Ply A4000 P3 Perf. Film Porous Armalon	Porous Armalon A4000 P3 Perf. Film Laminate	30.92
Tapered 1	(16)-(34)	1	Same as Described Above for Method 1		27.38
Tapered 2	(16)-(34)	3	Same as Described Above for Method 3		30.4

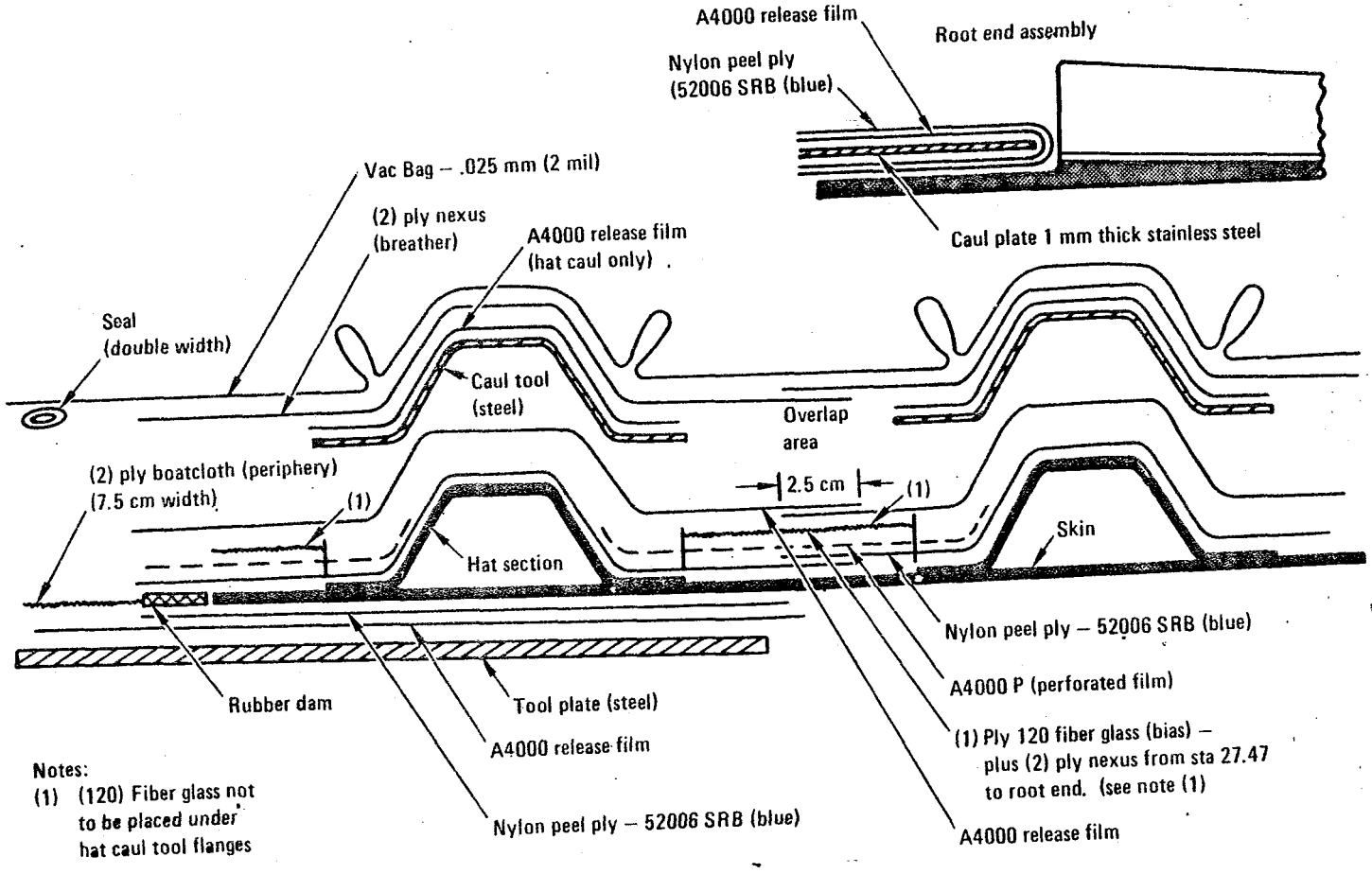

Figure 79. - Bleeding system assembly - low resin content prepreg.

Two cure cycle alternates were carried into this final phase of cover development. These included (a) the cure cycle developed for 41 percent resin content material without prebleed, and (b) an alternate cure cycle which utilized less time at 400K (260°F) and a faster heatup rate from 311K (100°F). These cure cycles are shown in figure 80. The longer cure cycle (a) was felt to offer improved volatile evacuation and assure temperature uniformity in the cover and supporting tooling.

All three panels produced results within acceptable limits, demonstrating that the properties required for the covers could be satisfactorily achieved by use of either high or low-resin-content material. Fabrication of specimens for ancillary test was able to proceed on that basis with available (41 percent) resin content material.

A comparison of the producibility aspects of cover fabrication was made and a recommendation to proceed using low resin prepreg material was adopted. A brief outline of the producibility factors considered and conclusions drawn is shown in table 35.

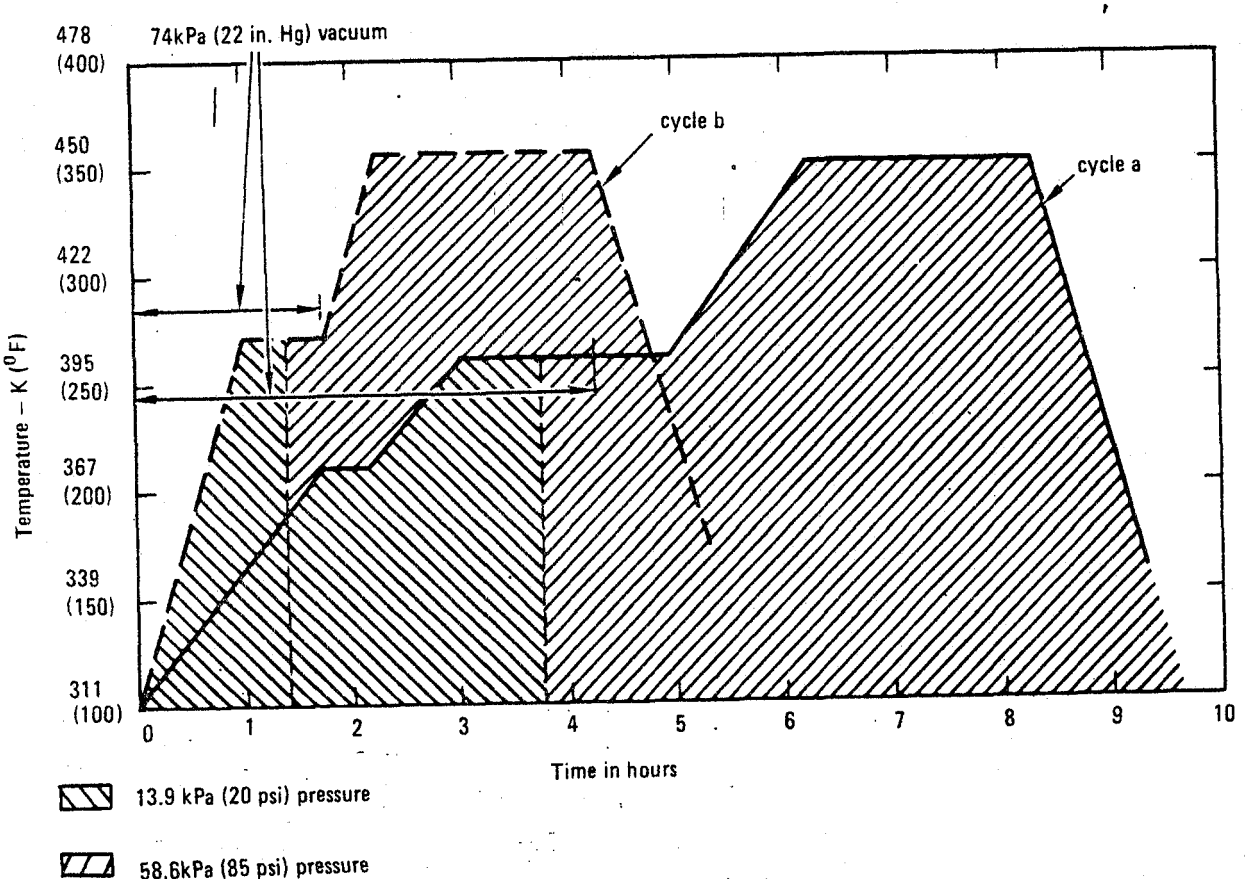

Figure 80. - Cure cycles.

TABLE 35. - PRODUCIBILITY FACTORS - ALTERNATE NO BLEED FABRICATION SYSTEMS

Factor		Preference
1.	Resin removal during cure	Low resin
2.	Preparation of stack for cure	Low resin
3.	Material handling, layup	No preference
4.	Trim of uncured layup	Low resin
5.	Control of resin flow	Low resin
6.	Cure cycle	No preference
7.	Tooling cleanup	Low resin
8.	Trim cured laminate	Low resin
9.	Part cleanup	Low resin
10.	Tooling requirements	No preference
11.	Repeatability confidence	Low resin

4.2 Ribs – Manufacturing Process Development

The evolution of the rib design concepts is discussed in Section 1.1.2.1. The Phase I concept A shown on figure 10 was dropped in favor of concept B because the producibility study showed it was not cost effective.

Concept B tooling for the truss rib cap is shown on figure 81. The tools were designed as matched tools capable of being used either in hot platen hydraulic presses or autoclaves. The laminates were prebled prior to assembly in the tools. It proved difficult to obtain uniform thickness in the flanges and webs because of the tool mass heat-up rates were low causing long cure cycles. Assembly of the tool was awkward, and tooling costs were projected to be high for a production program.

To alleviate some of these problems, the upper half of the tool was removed and replaced by a flexible caul. Fiberglass cauls were tried first but resulted in low resin content because of excessive edge bleeding. Although this condition was improved by the use of silicone rubber straps as edge dams, and modification of the cure cycle, the resin content remained on the low end of the specification requirements.

A formed silicone rubber bag acting as a caul was then developed. The bag was molded net to the aluminum tool. With this tooling concept acceptable resin content was achieved, but bead definition was poor and microcracks and cast resin problems occurred.

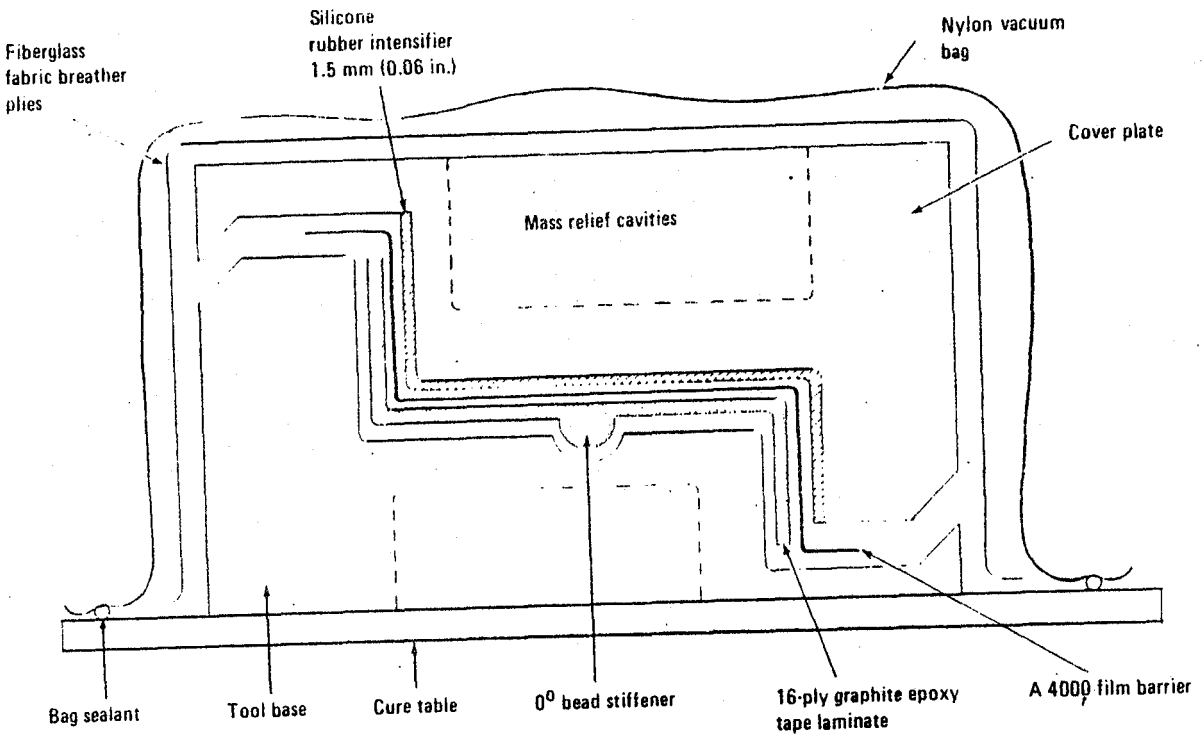

Figure 81. - Truss rib cap molding components.

The design development described in Section 1.1.2.1 led to configuration E the easily producible "C" section being selected.

The solid web ribs went through similar problems and the design was changed as described in Section 1.1.2.2 to a sandwich of graphite/epoxy and syntactic/epoxy.

4.2.1 Truss rib process. - The material for the ribs is cut and preplied in three of four ply stacks. These stacks are placed on the warmed aluminum tools which have baked-on release coat. After positioning each preplied stack the material is vacuum debulked. At the completion of layup the flanges are trimmed back to be 12.7mm (0.5 in.) above the tool base plate. The laminate is then lifted off the tool and a barrier film is draped over the tool. The laminate is then replaced on the tool and damming tape is butted up to its edges to minimize edge bleeding. The prepreg is then covered with Armalon (a teflon-coated cloth) which is trimmed net to the edge dams. An 0.05mm (0.002 in.) thick perforated barrier film is placed over the armalon to reduce resin bleed while allowing volatiles to escape. This film is also trimmed net to the edge dam. An Armalon breather ply is then placed in position and it extends 0.1m (4 in.) beyond the edge of the

part. A 2.3mm (0.009 in.) thick formed silicone rubber bag is then fitted over the assembly. Finally two plies of a polyester breather cloth are draped over the caul, and a nylon vacuum bag is sealed over the assembly to a tooling plate. This bleeder/breather system is illustrated in figure 82.

The parts are cured in a space heated autoclave. The autoclave was pressurized with CO_2. All ribs are cured by the following cycle.

1. Raise the autoclave pressure to 103 kPa (15 psi).
2. Heat the parts at a rate of .83K (1.5°F) to 1.94K (3.5°F) per minute to 394K (250°F).
3. Hold the parts at 394K (250°F) for 30 to 45 minutes.
4. Raise the autoclave pressure to a range of 586 kPa (85 psi) to 689 kPa (100 psi).
5. Raise the temperature of the part to 450K (350°F) at a rate of .83K (1.5°F) to 1.94K (3.5°F) per minute.
6. Hold the temperature of the part at 450K (350°F) for 120 minutes.
7. Cool the parts to 333K (140°F) at a rate of 1.94K (3.5°F) per minute.

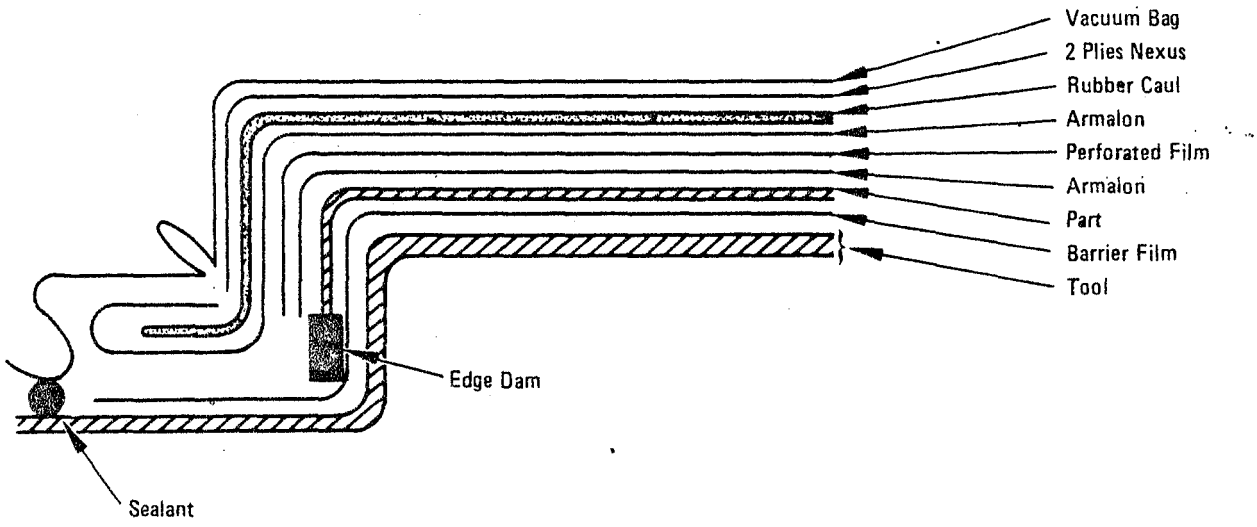

Figure 82. - Bleeder/breather system for truss rib.

A pressure cam and a temperature cam control the cure with a minimum of manual override. The leading thermocouple is recognized as that determining part temperature.

The hat section cutouts are made in the rib caps using a hand router block. This tool is located to the tooling holes or center line of the cutouts and guides an air-powered hand router. A 6.35mm (0.25 inch) diameter carbide diamond-cut ball nose router bit gives a good cut with reasonable tool life. Masking tape is placed on break-out surfaces as a precautionary measure to eliminate splintering.

The flanges are trimmed to width using a 76.2mm (3 inch) diameter abrasive wheel in a Bridgeport mill. The wheel is set at the proper dimension above the surface of the table and the part is passed under it. All sharp edges are removed using fine emery paper.

4.2.2 Solid web rib process. - The solid web rib process initially had a nylon peel ply placed on both the top and bottom faces of the laminate and a bleeder/breather stack. These ribs are a sandwich structure containing six-ply tape face sheets and a 0.95mm (0.0375 in.) thick syntactic resin core sheet. Volatiles from the graphite epoxy face sheets cannot pass through the core; so, breather material must be placed against the skins. Resin content of the ribs has been in the 26 to 27 percent range which is acceptable but low. Therefore, porous Armalon was substituted for the peel ply and then trimmed net to the edge dam. However, the volatile escape is prevented in the lower face sheet by the short trim. Armalon strips 25.4mm (1 in.) wide were then placed under the lower Armalon at .30m (12 in.) intervals extending into the breather plies. This method is shown in figures 83 and 84. It is a modification of the method developed for similar parts on the Advanced Composite Aileron for L-1011 Aircraft program. Reference NASA Contract NAS1-15069.

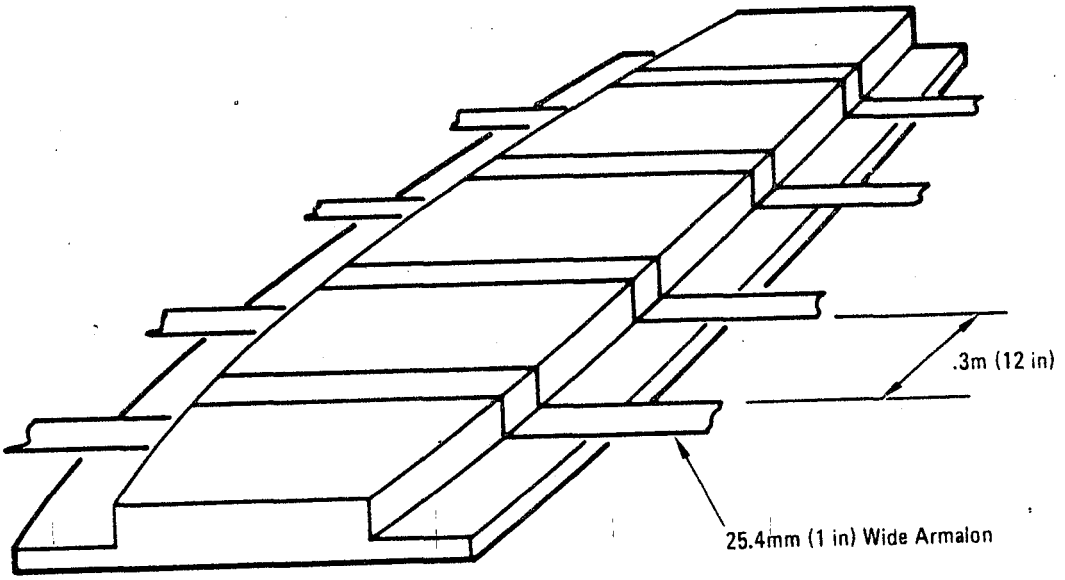

Figure 83. - Placement of armalon strips for solid web rib.

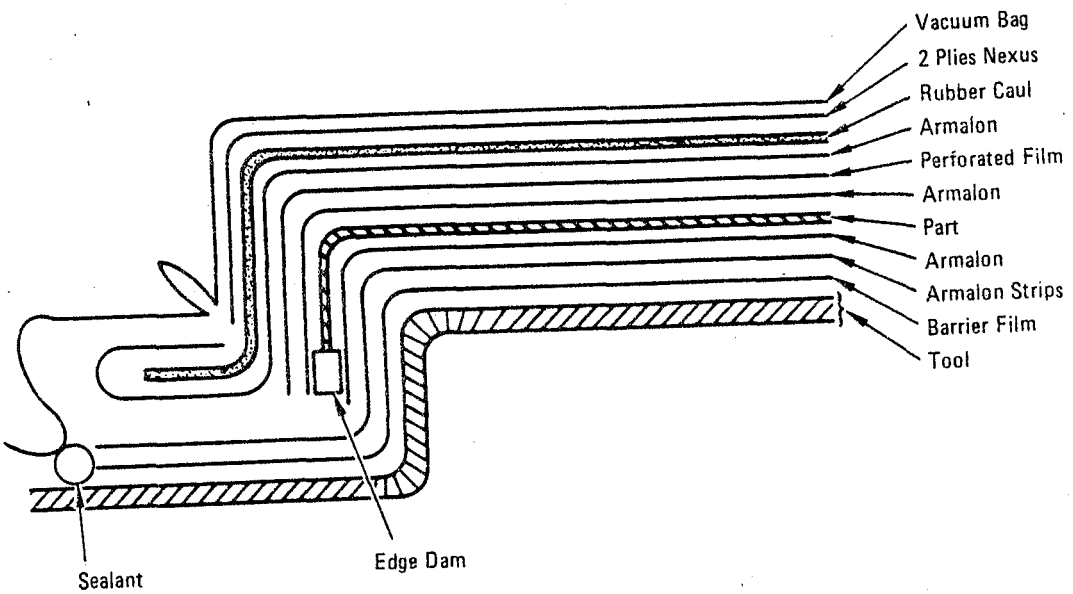

Figure 84. - Bleeder/breather system for solid web ribs.

4.3 Spars – Manufacturing Process Development

Spar tooling for molding the spars with the T300/5209 system was partially complete when the material was changed to the T300/5208 system. The spar tools were "moth balled" while the change over to the 5208 was engineered. The processing procedures developed for the 5209 resin required extensive changes before they could be applied to the 5208 resin. In addition to the higher curing temperature, the 5208 resin became very fluid in the 344 - 366K (160-200°F) range of the slow, heat-rise cure cycle used with the massive spar tools. The high pressure that was applied to the 5209 resin in this temperature range could not be used for the 5208 resin. A complete modification of the time-temperature-pressure schedule was necessary to adapt the 5208 resin to the spar tool concepts.

The purpose of the process verification task was to allow use of the T300/5208 system with minimum impact on the spar design and tool concepts and to verify that the selected cure cycle and processing would develop the mechanical and physical properties expected of the T300/5208 material. A tentative cure cycle was developed by processing numerous 0.076 by 0.076 m (3 by 3 in.) flat specimens during the material system change. Also, a rough draft of the process bulletin for molding the spars was prepared, and a small tool simulating the characteristics of the full size tools was designed and fabricated. Process verification began with fabricating approximately 20 "T"'s simulating the spar cap and web in the small tool and evaluating the effects of process variables.

4.3.1 Tooling development.- The small tool shown in figure 85 contained the basic elements used in the full size tool. The outer steel plates simulated the cover and base plate. The rubber blocks had approximately the same cross sections and offsets as those planned for the full size tool. Island blocks and cap rails had bleed hole patterns similar to those planned for the bull size tool.

4.3.1.1 Spar T section: A representative section of the spar cap and web was designed, and tests were defined for evaluating cure cycle and process variables. The T dimensions, layup, and test speciments are shown in figure 86. Lay-up of the cap was similar to the lay-up of the full size spars. Six ±45° and twelve 0° plies were laid in the steel rails. The web lay-up had the six °45° plies on its outer faces that also formed the inner flange surfaces of the spar caps.

The inner web lay-up was $(\pm 45, \pm 45, 0_2, 90, 9)_s$ as shown on the figure. A total of 28 plies were in the web part of the T and 24 plies were in the cap. Thickness tolerances were set equivalent to those that would be used on the spar drawings.

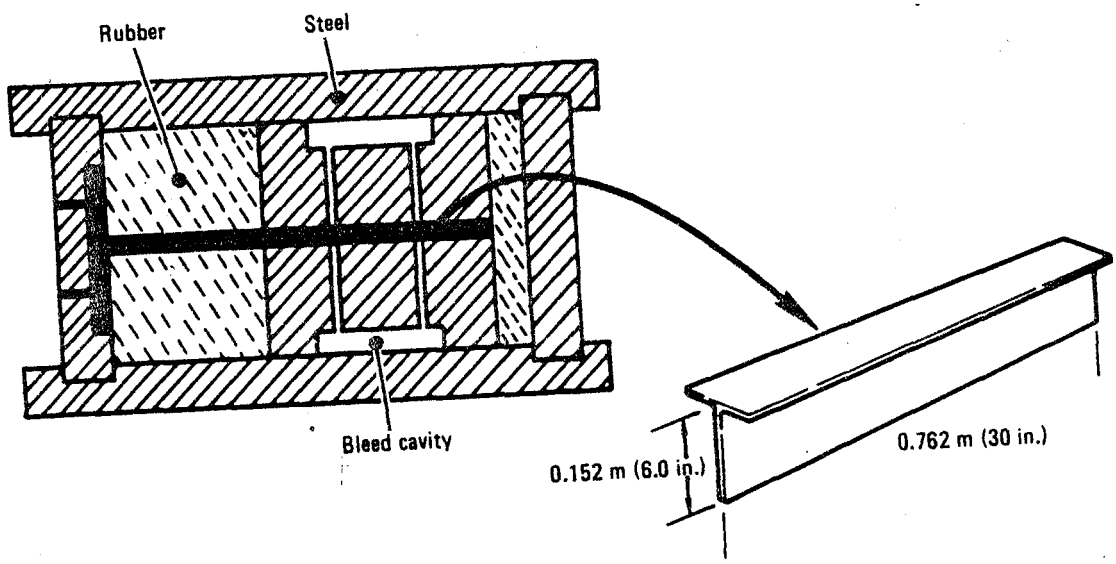

Figure 85. - Spar simulation tool for developing cure cycle.

Thirty-seven specimens were located on the T for use in mechanical and physical property tests. These specimens were used to measure the fiber volume, specific gravity, porosity, back-to-back interlaminar tension, flexural strength, compression in total cap flange and in sections of cap, web and short beam shear.

4.3.1.2 Variations in cure cycle and processing: A basic cure cycle was defined using information obtained from numerous experimental runs on 0.076 m by 0.076 m (3 by 3 in.) and 0.10 by 0.15 m (4 by 6 in) flat laminates. Isothermal gel times were obtained for the 394K (250°F) to 450K (350°F) range from NARMCO, and these extrapolated back to room temperature. The extrapolated gel time versus temperature was used to estimate the progress of the resin toward gel during the initial heat rise.

Early experiments with small 0.076 m by 0.076 m (3 by 3 in.) laminates indicated the time of pressure application during the long time (9 hours) required to reach 394K (250°F) in the spar tool was very critical. If pressure was applied too early, the result was a dry, porous laminate with unacceptable properties. If pressure was applied too late, the resin would gel before the laminate was compacted and properly bled. The objective was to apply pressure while the resin was still fluid and sufficiently viscious to

resist over bleeding. The extrapolated gel time versus temperature was used to set the time for applying pressure in the initial cure cycle.

The cure cycle and other processing procedures were refined by fabricating Ts in the simulated spar tool with controlled variations in the cure cycle and after the estimated time in the initial cure cycle. Bleed holes were varied in size and density. The effect of bleeding with and without armalon between the T and the tool was evaluated. Experiments were conducted on the use of armalon, rubber seals and/or edge wrapping to prevent fiber wash. Stops built into the tool were evaluated for control of bleed and T thickness. Details of the rubber to steel and rubber sizing were varied to control mark-off.

Each T was laid-up, cured in the autoclave and either rejected or accepted for further processing and testing after removal from the small tool. If a T was dimensionally and visually acceptable, it was post cured, inspected and cut into a limited number of test specimens. If the T was unacceptable, the process or cure cycle was adjusted and another T was made. When a satisfactory T was produced, all the test specimens indicated in figure 86 were cut out and sent to the structural test laboratory for testing. Figure 87 illustrates the cure cycle developed for the T test specimens.

4.3.1.3 Test data for process development "T's:" The test data accumulated from those Ts with acceptable processing is tabulated in table 36. The properties listed are fiber volume, specific gravity, porosity, flexural strip compression, cap compression and short beam shear.

A good laminate should have a fiber volume between 59 and 68 percent according to the material specifications and design allowables available at the time the Ts were fabricated. The processing and cure cycle was adjusted and refined until this requirement was achieved. Later in the program, resin content by weight was used in place of fiber volume. A nominal density fiber volume range of 59 to 68 percent converts to a resin content of approximately 25 to 33 percent by weight.

A specific gravity of an acceptable laminate is between 1.54 and 1.60. A nominal density of resin and resin fiber will fall in this range. The lower fiber volume (higher resin content) will approach the lower specific gravity of 1.54 and the higher fiber volume (lower resin content) will approach a specific gravity of 1.60. Comparison of these values is a good indication of the accuracy of the physical property measurements, but usually require additional information on porosity to determine the overall qualify of the laminate.

Porosity measurements are difficult to qualify in absolute terms. Ultrasonic inspections give an indication of voids in the laminate. Fiber volume, resin content and specific gravity measurements give an indication of void content. Polished cross sections observed under a high powered microscope

SYM	SPECIMEN	SIZE	NO.	
			CAP	WEB
FV	FIBER VOLUME	25.4 X 25.4 (1 X 1)	3	2
SG	SPECIFIC GRAVITY	25.4 X 25.4 (1 X 1)	3	2
P	POROSITY	6.35 (.25) X T	4	-
BTOB	BONDED BACK TO BACK	25.4 (1) X T	2	-
FLEX	FLEXURAL	12.9 X 127 (.5 X 5)	4	2
COMP	COMPRESSION STRIP	12.7 X 76.2 (.5 X 3)	4	2
COMP T	COMPRESSION 'T'	102 X 61 X 19.1 (4 X 2.4 X .75) LEG	3	-
SBS	SHORT BEAM SHEAR	12.7 X 25.4 (.5 X 1)	4	2

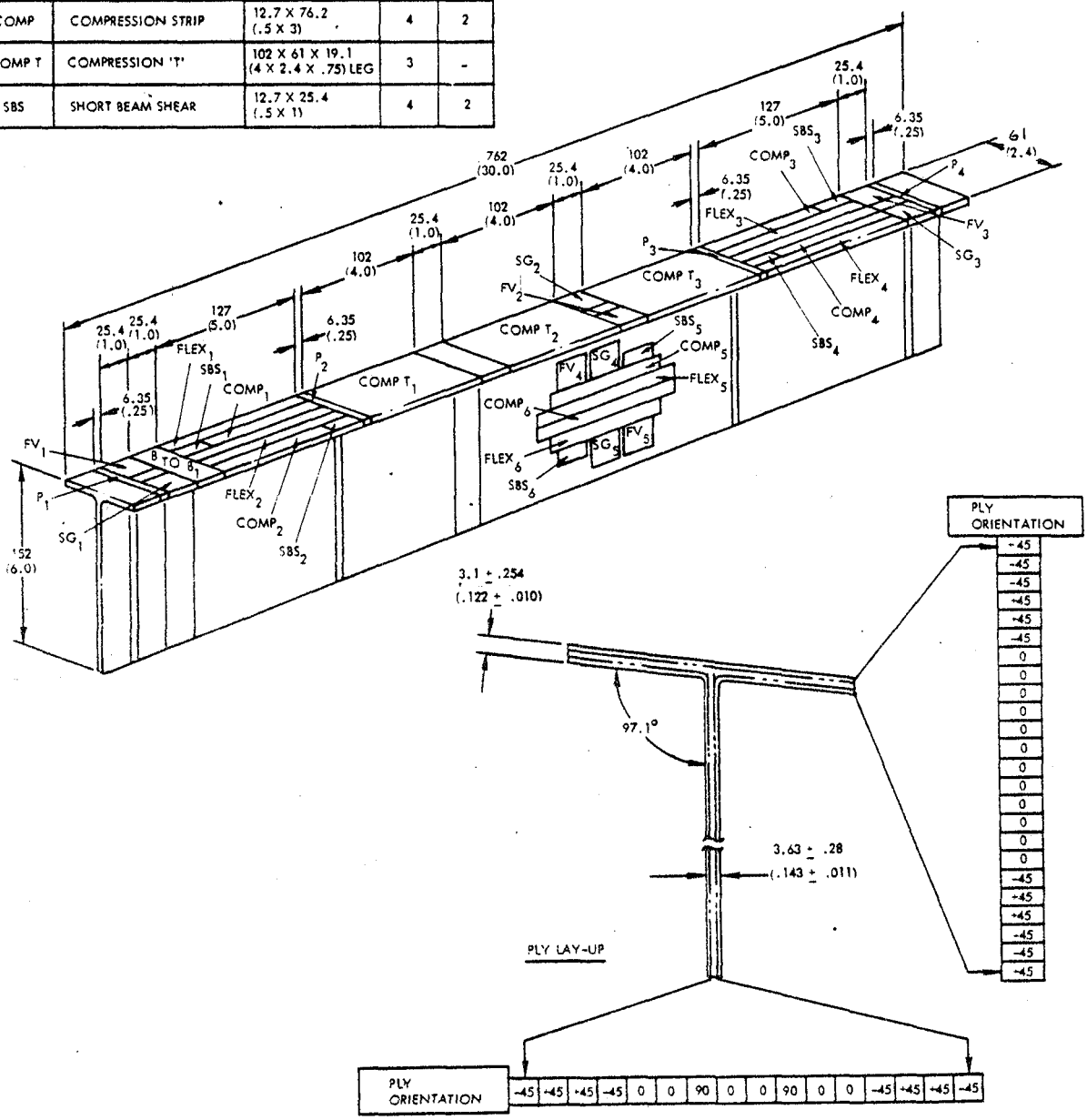

Figure 86. - Process development T test specimens.
(All dimensions in mm (in)).

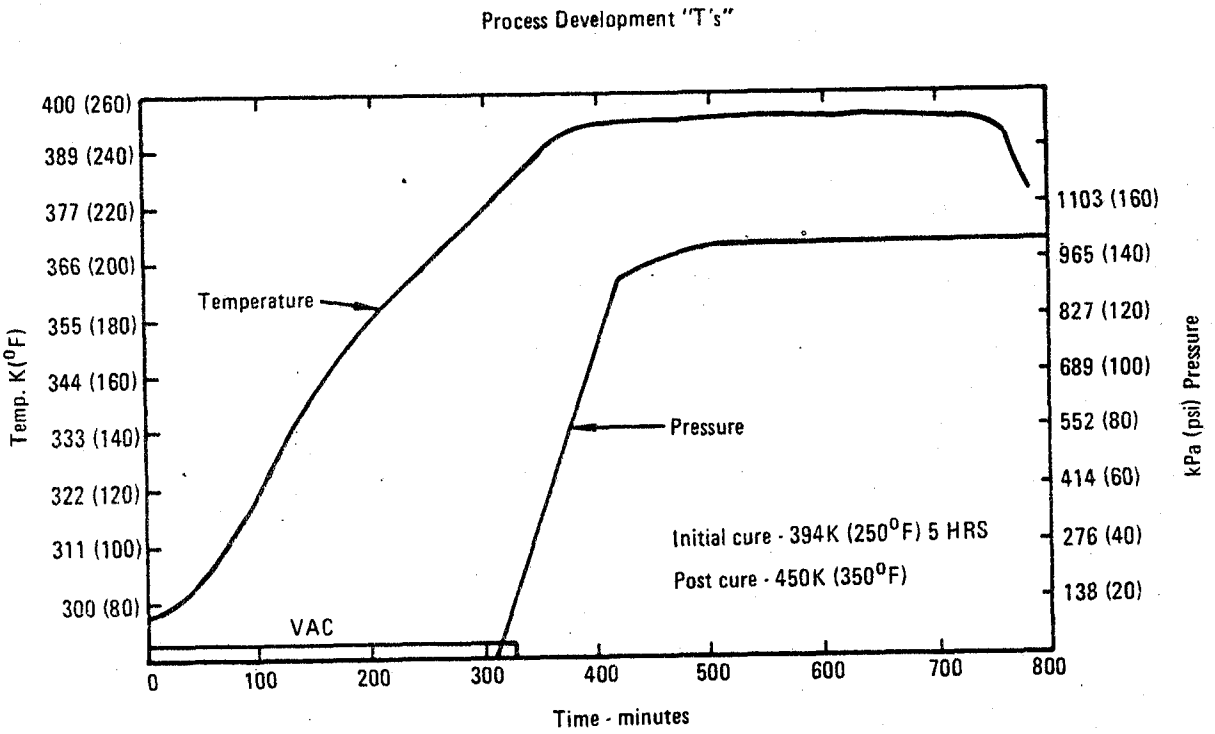

Figure 87. - Cure cycle.

locate porous pockets in the laminate. All three methods were used in examining the T's to determine porosity. Very limited porosity was indicated as shown in the table. The four cross sections that were cut out of each T, mounted in acrylic, polished and scanned with a 100x microscope, verified the limited porosity and found micro cracks. The amount of porosity found in the T was negligible; in fact, the solid laminate, free of porosity indicated the cure cycle and processing was producing a very good laminate. Micro-cracking did cause concern, but it was typical of that expected in a 12 ply, zero-degree lay-up.

A 90° ply was laid up in the middle of the zero-degree plies in T number 184, see Table 36. The effect was a considerable reduction in micro-cracks, but it did not completely eliminate all microcracks. No evidence was available that indicated the limited amount of microcracking found in the T's would be a problem. The addition of a 90° ply could reduce microcracking; if required, but no change wad made to the spar design.

Two specimens cut out of cross sections of the T were bonded back-to-back and pulled in tension to determine the interlaminar tension strength between the cap and web. A room temperature curing adhesive was applied to the aligned, back-to-back T specimens to form one tensile specimen. The web ends of the back-to-back specimen were loaded with spherically seated Templin grips. A specimen sustaining 181 kg (400 lb) was considered to be adequate considering the large amount of scatter in fillet radii and eccentricities in loading.

TABLE 36. - SUMMARY OF PROCESS DEVELOPMENT "T" SPECIMEN TEST RESULTS - SI UNITS
(1 of 2)

PROPERTY \ "T" NO		165	166	167	168	169	170	172	173	176	184
FIBERVOL. % [59-68]	1				64.2	67.5	63.5	65.1	61.8	68.1	63.6
	2	56.9	56.1	63	60.6	66.1	60.4	59.4	61.5	65.2	64.9
	3				64.0	61.3	59.1	57.3	64.0	64.8	65.1
	4	61.4	65.7	68.2	68.0	68.8	67.6	67.6	58.9	67.0	61.6
	5				62.0	67.5	60.4	61.4	61.5	61.4	60.4
SG [1.54-1.60]	1				1.554	1.584	1.559	1.563	1.541	1.486	1.560
	2	1.537	1.530	1.566	1.556	1.576	1.554	1.547	1.561	1.581	1.573
	3				1.572	1.567	1.555	1.531	1.557	1.570	1.551
	4	1.561	1.577	1.588	1.588	1.593	1.587	1.585	1.538	1.582	1.555
	5				1.558	1.586	1.548	1.550	1.554	1.553	1.551
POROSITY (1) CRACKS	1				LIM & C	LIM & C	LIM & C	LIM & C	LIM, VOID & C	NONE	LIM
	2	C	C	LIM	LIM & C	LIM & C	LIM & C	LIM & C	LIM & C	C	LIM & C
	3				LIM & C	C	C	LIM & C	LIM & C	NONE	LIM
	4	C	LIM C	LIM	LIM & C	C	LIM & C	LIM & C	LIM & C		LIM
BACK TO BACK [kN [1.8]					1.96	3.39	4.67	2.67	1.74	5.85	2.94
FLEXURAL MPa	1	634	641	820	652	645	696	717	765	517	393
	2	600	510	717	593	745	717	572	565	922	324
	3		669	600	703	710	689	621	724	662	483
	4	455	414	579	579	627	621	538	745	618	634
	5	296	379	372	372	379	359	359	345	372	393
	6	359	379	345	372	379	400	372	372	345	331
[662] COMP. STRIP MPa	1				765	855	676	724	752	786	738
	2				814	717	745	724	772	965	779
	3				793	627	869	717	786	669	669
	4				738	820	786	655	545	710	662
[414]	5				558	476	434	683	448	641	490
	6				483	648	462	476	524	490	483
COMP. "T"- kN [151]	1				177	176	178	147	172	169	197
	2				154	201	172	190	192	157	208
	3				155	179	178	167	183	128 *	194
SHORT BEAM SHEAR MPa	1	85	75	79	78	85	76	74	77	59	63
	2				68	67	64	83	73	61	72
	3	78	63	68	63	70	80	68	77	72	57
	4				76	75	81	72	57	74	80
	5	53	66	61	51	70	72	70	76	66	67
	6				61	65	62	69	82	68	67

"T" NOS. 165, 166 AND 167 WERE EXPERIMENTAL, OUTSIDE SPEC. TOLERANCES AND PARTIALLY TESTED.
"T" NOS. 163, 174 AND 185 WERE NOT ACCEPTABLE FOR TESTING. NOS. 171, 175, 177 - 183 WERE NOT "T's."
*END BROOMED.

(1) POROSITY: LIM - UP TO 1/2%
MICROCRACKS BETWEEN 0° PLIES: C - UP TO 2%

TABLE 36. - SUMMARY OF PROCESS DEVELOPMENT "T" SPECIMEN TEST RESULTS - CUSTOMARY US UNITS (2 of 2)

PROPERTY \ "T" NO		165	166	167	168	169	170	172	173	176	184
FIBERVOL. % [59-68]	1			*	64.2	67.5	63.5	65.1	61.8	68.1	63.6
	2	56.9	56.1	63	60.6	66.1	60.4	59.4	61.5	65.2	64.9
	3				64.0	61.3	59.1	57.3	64.0	64.8	65.1
	4	61.4	65.7	68.2	68.0	68.8	67.6	67.6	58.9	67.0	61.6
	5				62.0	67.5	60.4	61.4	61.5	61.4	60.4
SG [1.54-1.601]	1				1.554	1.584	1.559	1.563	1.541	1.586	1.560
	2	1.537	1.530	1.566	1.550	1.576	1.554	1.547	1.561	1.581	1.573
	3				1.572	1.567	1.555	1.531	1.557	1.570	1.551
	4	1.561	1.577	1.588	1.588	1.593	1.587	1.585	1.538	1.582	1.555
	5				1.558	1.586	1.548	1.550	1.554	1.553	1.551
POROSITY (1) CRACKS	1				LIM & C	LIM & C	LIM & C	LIM & C	LIM, VOID & C	NONE	LIM
	2	C	C	LIM	LIM & C	LIM & C	LIM & C	LIM & C	LIM & C	C	LIM & C
	3				LIM & C	C	C	LIM & C	LIM & C	NONE	LIM
	4	C	LIM C	LIM	LIM & C	C	LIM & C	LIM & C	LIM & C		LIM
BACK TO BACK lbs (400)					440	762	1050	600	392	1315	660
FLEXURAL ksi	1	92	93	119	945	93.6	101	104	111	75	57
	2	87	74	104	86	108	104	83	82	141	47
	3		97	87	102	103	100	90	105	96	70
	4	66	60	84	84	91	90	78	108	94	92
	5	43	55	54	54	44	52	52	50	54	57
	6	52	55	50	54	55	58	54	54	50	48
[-96] COMP STRIP ksi [-60]	1				111	124	98	105	109	114	107
	2				118	104	108	105	112	140	113
	3				115	91	126	104	114	97	97
	4				107	119	114	95	79	103	96
	5				81	69	63	99	65	93	71
	6				70	94	67	69	76	71	70
COMP "T" - lb [34000]	1				39800	39600	40000	33100	38700	37900	44300
	2				34600	45100	38600	38300	43200	35400	46900
	3				34800	40300	40000	37450	41200	28700*	43700
SHORT BEAM SHEAR ksi	1	12.3	10.9	11.5	11.3	12.3	11.0	10.7	11.2	8.5	9.2
	2				9.9	9.7	9.3	12.0	10.6	8.9	10.5
	3	11.3	9.2	9.8	9.1	10.1	11.6	9.9	11.1	10.4	8.2
	4				11.0	10.9	11.7	10.5	8.2	10.7	11.6
	5	7.7	9.5	8.9	7.4	10.2	10.5	10.1	11.0	9.5	9.7
	6				8.8	9.4	9.0	10.0	11.9	9.8	9.7

"T" NOS. 165, 166 AND 167 WERE EXPERIMENTAL, OUTSIDE SPEC. TOLERANCES AND PARTIALLY TESTED.
"T" NOS. 163, 174 AND 185 WERE NOT ACCEPTABLE FOR TESTING. NOS. 171, 175, 177 - 183 WERE NOT "T's."
*END BROOMED.

(1) POROSITY: LIM - UP TO 1/2%
MICROCRACKS BETWEEN 0° PLIES: C - UP TO 2%

Flexural test specimens cut out of the cap and web gave reasonably consistent test results. The web specimens 5 and 6 cut out of T numbers 166 through 184 were very close. The cap specimens, 1, 2, 3 and 4, had some scatter and fell off sharply when the 90° cross ply was added to specimen 184. No real conclusions could be reached from the flexural specimens, because of the difficulties in predicting the effects of edge conditions. The more uniform cross section of specimens 5 and 6 taken from the web did show consistent flexural strengths and indicated a good quality laminate.

Compression specimens were cut out of both the cap and web portions of the T's. These specimens were potted on both ends using a potting compound cured inside steel rings. The ends were machined flat and perpendicular to the specimens, and strain gages were attached to the test section at the center of the specimen for use in balancing the load in the test machine.

Compression test values for the compression strips exceeded the predicted values in all but three of the specimens. The average values for each group of specimens exceeded the predicted by approximately 10 percent, but scatter occurred in all of the T's. This scatter was reduced by revising the compression in test methods.

Three 0.1 m (4 in.) lengths of the cap with part of the web were cut out of each T and tested in compression. These specimens were prepared similar to the compression strips. Each end was potted using a room temperature curing potting compound and steel rings. The ends were machined flat and perpendicular to the specimen, and strain gages were attached to the midsection for use in balancing the load in the test machine. The actual test load for all specimens exceeded the predicted failure load except specimen three T number 176 (see table 36) which broomed on the ends and did not give a good compression test.

Short beam shear specimens were cut out of both the cap and web portions of the T and tested. Predicted test values for short beam shear specimens were not available, because of the difficulty in analyzing the edge effects of small, cross plied specimens. The test values were used for information in comparing test data from similar specimens.

Analysis of the data in table 36 could only be used as a guide to predict the test results from the full size spars. Overall, the average data for each T listed in the table indicated that the cure cycle and processing applied to T numbers 168, 169, 170, 172, 173, 176 and 184 would produce an acceptable spar. Tolerances permitted in the cure cycle and processing were applied during fabrication of these T's, and no effects on the mechanical or physical properties were identifiable from the test data.

4.3.1.4 Process and tool development: The steel box-rubber tooling concept for the tee was illustrated in figure 85. This tool simulated the tooling planned for molding the production spars, and the composite tee shown in figure 86 represented a section of the spar cap and web.

The small tool which was used to simulate the full-size tool action worked efficiently. Variations in the cure cycle, bleed procedure and rubber details were rapidly assessed by fabricating and testing T's made in this tool. As an example, the first six T's were too thick at the edge of the cap flange. This condition appeared to be caused by a step in the rubber which was planned to seal the edges and to prevent fiber wash. The step detail in the rubber was changed; the rubber was recast, and two more T's were made to find tune the rubber details and make acceptable flange edges. This and other changes were found by making the T's, and these changes were incorporated in the full size tool design.

Because of the mass of the full-scale tool which can be seen in figure 88 the final cure cycle was long as shown in figure 89 and cure is accomplished at 400K (260°F) a subsequent post cure outside the tool is then performed at 450K (350°F).

4.4 Quality Assurance

4.4.1 Laboratory tests.- The Quality Assurance Laboratory performed two basic functions during Phase II. (A) Batch acceptance testing to ensure that the graphite/epoxy material is acceptable to use, and B) testing of parts and tag-ends to support Engineering and Manufacturing in the various development and test programs.

A typical material batch acceptance test report is shown in table 37.

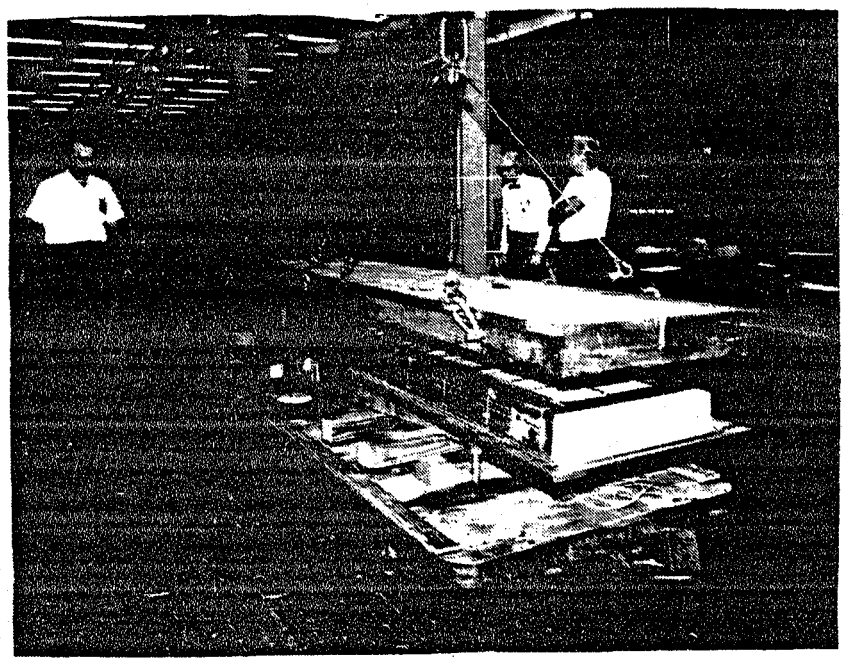

Figure 88. - Tool cover being lowered on base.

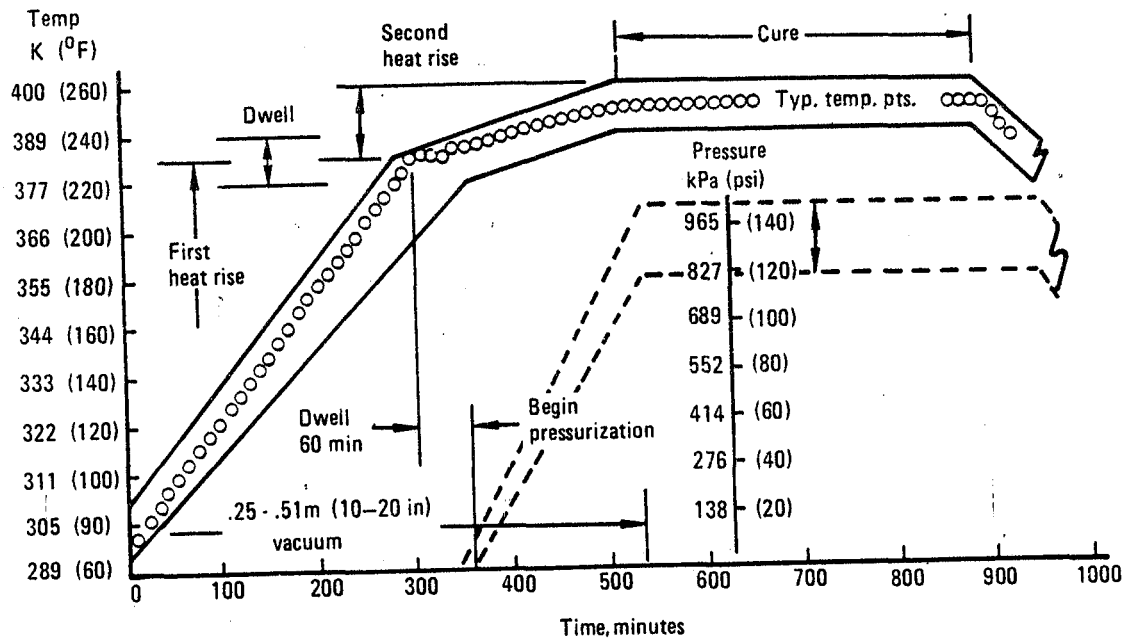

Figure 89. - Cure cycle for L-1011 ACVF spars.

4.4.2 Nondestructive inspection. Early in the Phase II effort, it became apparent that a set of baseline ultrasonic inspection standards would be required. A series of flat laminate panels 8, 12, 16, 20, 25, and 32 ply were fabricated (see figure 90). These laminates contained teflon 3.17 (0.125), 6.35 (0.250) and 12.77 mm square (0.50 in square) in the four locations shown in figure 90. The panels were inspected using a reflected thru-transmission ultrasonic technique to verify general panel quality. All panels were then sectioned, identified, and submitted to the Test Services Laboratory for evaluation. All standard tests were accomplished and an agreement reached between Engineering, Manufacturing, and Quality Assurance (NDI) that these standards would be used as baseline for all future work.

Throughout the Phase II effort, all laminates produced were submitted for ultrasonic inspection. These included: flat panels, ribs, and single stage cure cover specimens. Radiographic inspection was utilized on occasion to define the extent of matrix cracking and to verify the presence of foreign material.

All flat laminates fabricated for coupon testing were inspected using reflected thru-transmission ultrasonic techniques. C-Scan recordings were produced to provide permanent records of these inspections. Flat laminate coupons which were damaged; impact or saw cut, were reinspected during the test program. Penetrant inspection techniques were used on the saw cut specimens on completion of the test to evaluate damage growth.

TABLE 37. - T300/5208 BATCH ACCEPTANCE TEST RESULTS (SI UNITS) (1 of 2)

C22-1379/111 Specification Requirements		Results of Test					
		1	2	3	4	5	AVE
Areal wt	139-149 g/m^2	144	140	139	139		141
Infrared Spectrophotometric Analysis		Conforms					
Volatiles (60±5 minutes at 450K)	3% max	Edge 1.64	Center 1.58				1.61
Dry resin content	38-44%	43.4	42.6	44.0	42.8		43.2
Flow at 450K at 586 kPa	15-29%	20.3	21.7				21.0
Get Time at 450K	Info. only, minutes	20.3	21.2				20.8
Cured fiber volume 2mm panel	60-68%	68.0	67.8	67.9			67.9
Cured fiber volume 1mm panel	60-68%	67.9	67.4	67.9			67.7
Specific gravity 2mm panel	1.55-1.62	1.60	1.60	1.60			1.60
Specific gravity 1mm panel	1.55-1.62	1.59	1.60	1.60			1.60
Tensile strength, longitudinal at 297K	1172 MPa, min, ind.	1420	1434	1413			1422
Tensile modulus, longitudinal at 297K	138 GPa, min., ind.	154	145	143			147
Flexural strength at 297K	1448 MPa, min., ind.	1751	1827	1937			1838
Flexural modulus at 297K	124 GPa, min., ind.	133	130	137			133
Flexural strength at 356K	1379 MPa, min., ind.	1779	1662	1689			1710
Flexural modulus at 356K	110 GPa, min., ind.	132	138	126			132
Short beam shear at 297K	90 MPa, ind.	117	125	119			120
Short beam shear at 356K	83 MPa, ind.	103	99	101			101
Thickness per ply 2mm panel	0.117-0.142mm	0.117	0.119	0.119	0.117	0.119	0.118
Thickness per ply 1mm panel	0.117-0.142mm	0.117	0.117	0.122	0.117	0.122	0.119

NOTES: Batch 1015
Date 11-3-77
Lab Report 343951
min. ind. minimum individual

TABLE 37. - T300/5208 BATCH ACCEPTANCE TEST RESULTS (SI UNITS) (2 of 2)

Specification Requirements		Results of Test					
		1	2	3	4	5	AVE
Areal wt	139-149 g/m^2	144	140	139	139		141
Infrared Spectrophotometric Analysis		Conforms					
Volatiles (60±5 minutes at 350°F)	3% max	Edge 1.64	Center 1.58				1.61
Dry resin contents	38-44%	43.4	42.6	44.0	42.8		43.2
Flow at 350°F at 85 psi	15-29%	20.3	21.7				21.0
Gel Time at 350°F	Info. only, minutes	20.3	21.2				20.8
Cured fiber volume 0.080 in. panel	60-68%	68.0	67.8	67.9			67.9
Cured fiber volume 0.040 in. panel	60-68%	67.9	67.4	67.9			67.7
Specific gravity 0.080 in. panel	1.55-1.62	1.60	1.60	1.60			1.60
Specific gravity 0.040 in. panel	1.55-1.62	1.59	1.60	1.60			1.60
Tensile strength, longitudinal at 75°F	170 ksi, min., ind.	206	208	205			207
Tensile modulus, longitudinal at 75°F	20 x 10^6 psi, min., ind.	22.4	21.0	20.8			21.4
Flexural strength at 75°F	210 ksi, min., ind.	254	265	281			267
Flexural modulus at 75°F	18 x 10^6 psi, min., ind.	19.3	18.8	19.9			19.3
Flexural strength at 180°F	200 ksi, min., ind.	258	241	245			248
Flexural modulus at 180°F	16 x 10^6 psi, min., ind.	19.2	20.0	18.3			19.2
Short beam shear at 75°F	13 ksi, min., ind.	16.9	18.2	17.3			17.5
Short beam shear at 180°F	12 ksi, min., ind.	15.0	14.4	14.6			14.7
Thickness per ply 0.080 in. panel	0.0046-0.0056 in.	0.0046	0.0047	0.0047	0.0046	0.0047	0.0047
Thickness per ply 0.040 in. panel	0.0046-0.0056 in.	0.0046	0.0046	0.0048	0.0046	0.0048	0.0047

NOTES: Batch 1015
Date 11-3-77
Lab Report 343951
min. ind. minimum individual

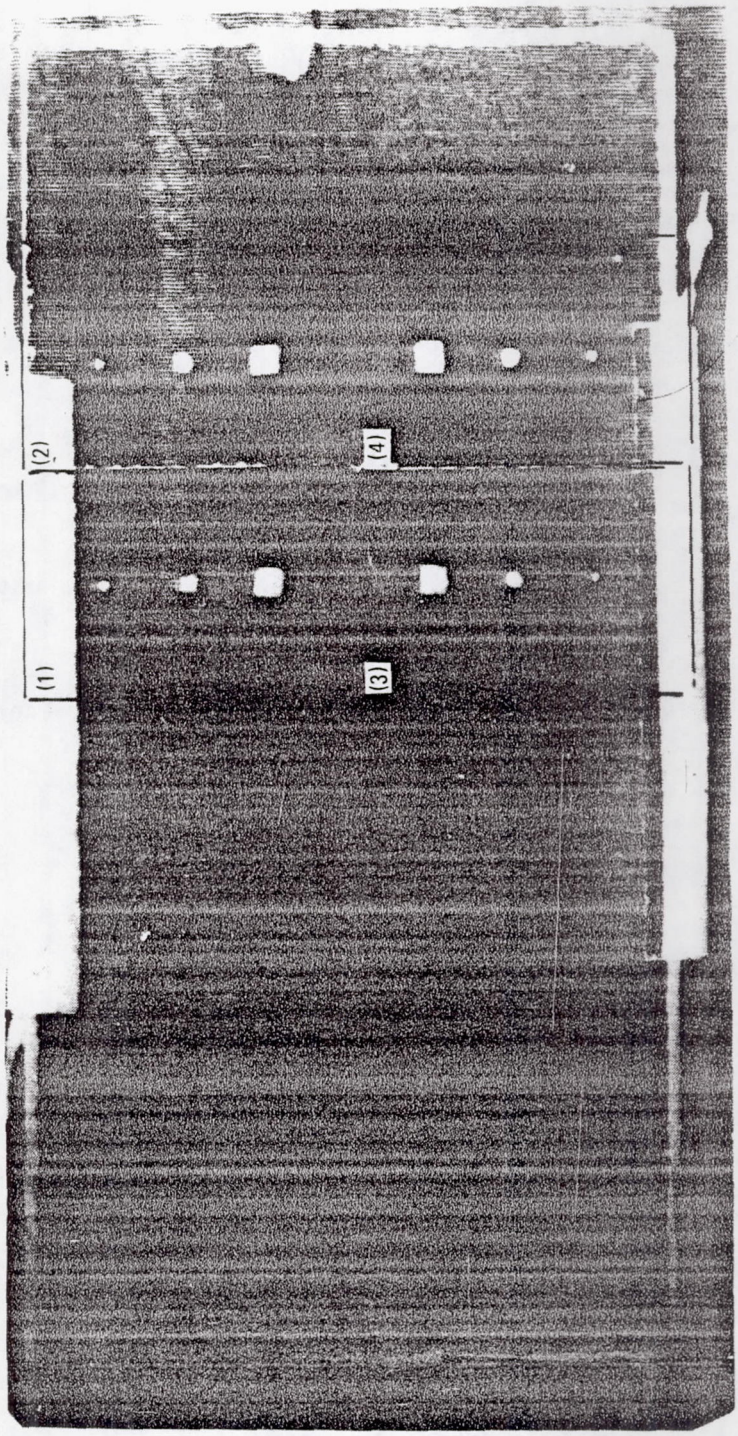

Figure 90. - Ultrasonic standards.

Due to the number of design iterations encountered during the rib development program, there were a number of variations in NDI techniques applied. The early bead stiffened ribs were inspected using reflected thru-transmission for the web area only. This was felt to be adequate to define general quality of these development parts. As the program progressed, the designs were modified to improve producibility and, with the improvement in the quality, the ultrasonic techniques were modified to provide complete coverage. The rib flanges were inspected using contact pulse-echo ultrasonic techniques and the results noted on the C-Scans of the web areas. These procedures were used throughout the remainder of the Phase II program.

Early single stage cover process development panels containing a single hat were ultrasonically inspected using reflected thru-transmission techniques. This limited the area inspected to that shown as "A" in figure 91; however, this was felt to be adequate for these development specimens.

Figure 92 shows the C-Scans produced using reflected thru-transmission ultrasonic inspection techniques on six of these early development specimens. As the quality of the cover specimens improved, it became necessary to expand the ultrasonic inspection procedures to provide one hundred percent coverage. Due to the configuration of the cover specimens, a combination of ultrasonic inspection techniques were employed (figure 91), reflected thru-transmission (skin and hat flange), immersed pulse-echo (hat crown and skin under hat), and contact pulse-echo for hat sidewalls. All cover specimens fabricated for the ancillary test program were inspected using this combination of ultrasonic techniques.

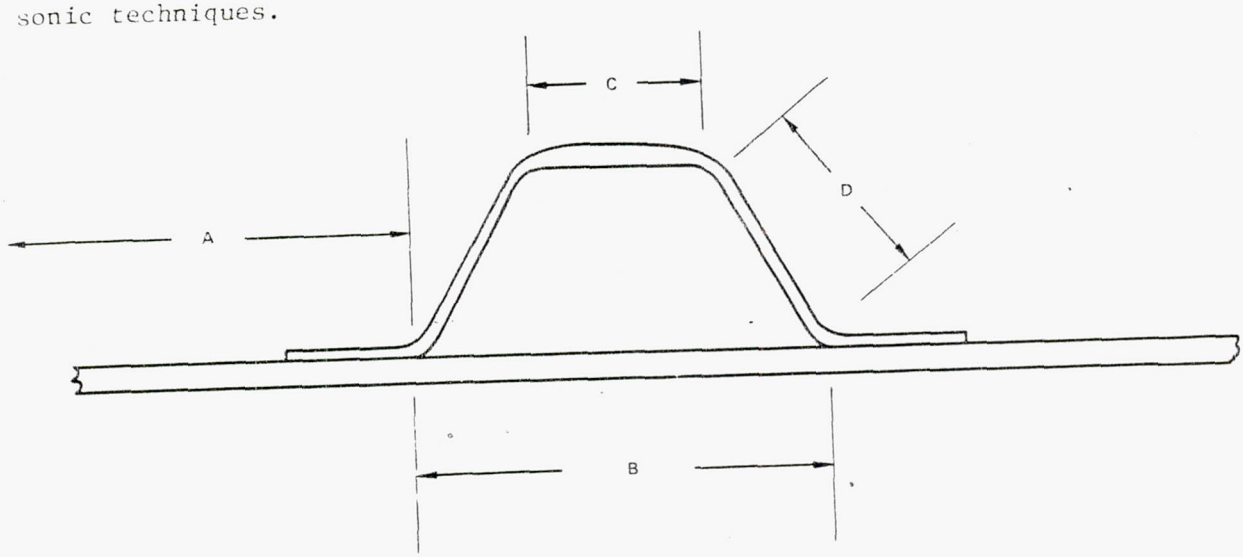

A = REFLECTED THRU TRANSMISSION: MULTIPLE GAIN SETTINGS FOR THE VARIOUS THICKNESSES INVOLVED 5 MHz TRANSDUCER

B = PULSE-ECHO: GATED ON BACKSURFACE 10 MHz FOCUSED TRANSDUCER

C = PULSE-ECHO: SAME AS B

D = PULSE-ECHO: HANDSCAN CONTACT 10 MHz TRANSDUCER

Figure 91. - Inspection techniques for cover panels.

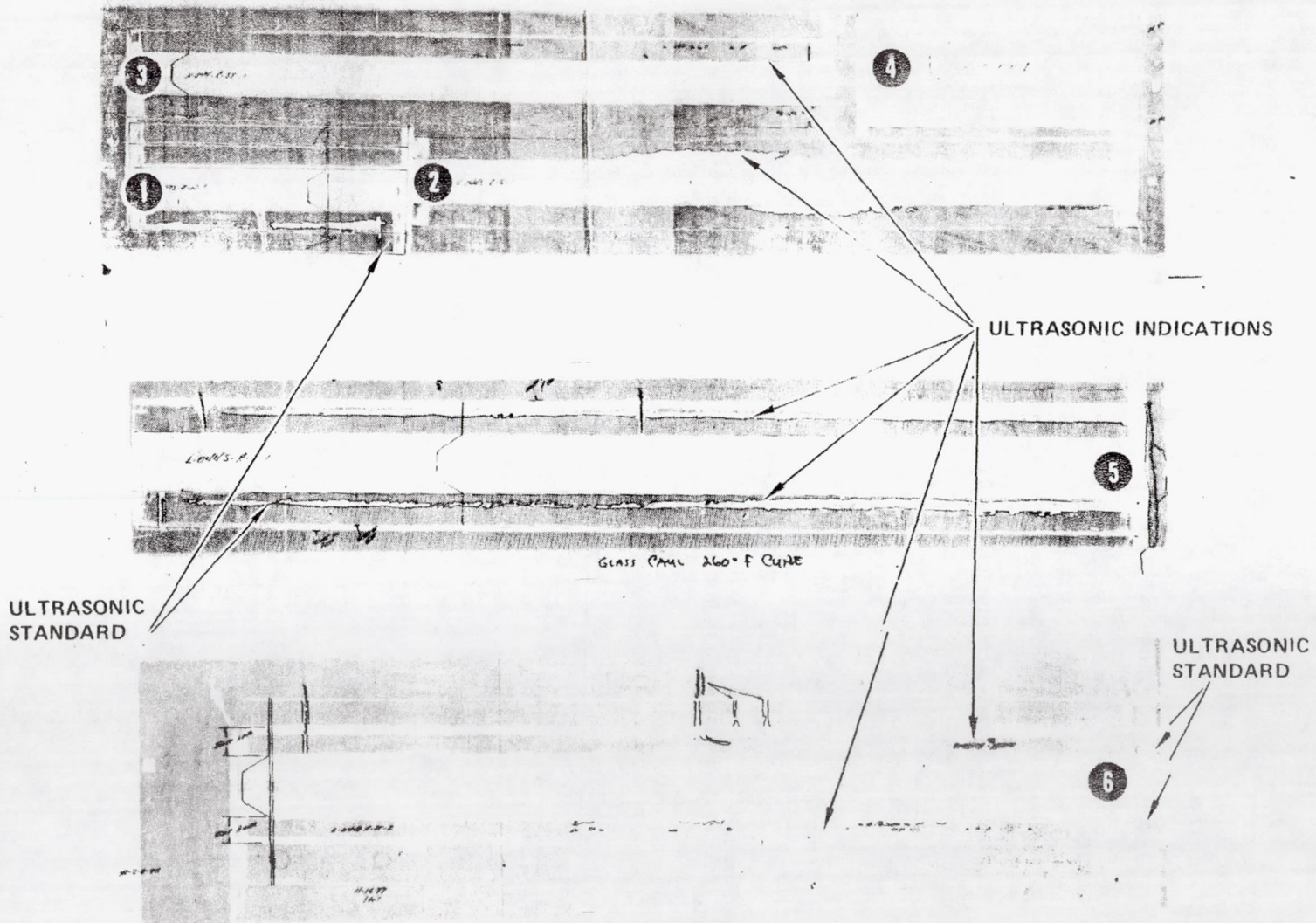

Figure 92. - Ultrasonic C-scans of single-stage cover specimens.

Portable ultrasonic inspection techniques were used to evaluate damage growth during tests conducted at Rye Canyon. These techniques were found to provide an accurate assessment of the extent of the damage and could be applied in a field environment.

Comprehensive visual and dimensional inspections of spar test components were conducted after the removal of resin flash and the process control specimens. Acceptance criteria utilized were those specified in the process bulletin and in engineering drawings. During Phase II very thorough 100% inspection was performed and documented on all test specimens fabricated.

Every part produced was nondestructively inspected using pulse-echo ultrasonic techniques. A backup technique using thru transmission ultrasonic dual transducers was utilized to further assess any indications found by the NDI inspector. Areas which still remained in question were verified by personnel qualified to MIL-STD-410D Level III.

All ultrasonic inspection was performed using approved procedures and calibration standards. Calibration targets were inserted in non-structural areas of the early specimens. Actual samples of caps, webs and stiffeners from specimen H-14 were modified by the Proficiency Development Laboratory to provide calibration standards for the H-20, H-23 and PRVT (Phase III) specimens.

4.4.3 Conformity certification . - FAA Conformity Certification was established by a Designated Manufacturing Inspection Representative (DMIR) on all parts established as ancillary test items.

5. CONCEPT VERIFICATION

The objectives of the concept verification tests were to verify the structural integrity of the most critical areas of the fin and to verify the analytical methods. In order to meet this objective, a series of tests were conducted on components of the cover, the spars, and the ribs. The selected areas were manufactured in conformance with all the engineering design, process and acceptance requirements. An FAA Statement of Conformity was issued prior to testing each test article, and each structural test was witnessed by a representative of the FAA.

Tests included static and spectrum fatigue specimens and were performed under various temperature and moisture conditions. These tests were used to demonstrate a consistent performance between subcomponents and design allowables derived from coupon and element data.

Moisture conditioning of subcomponents was to a minimum of 1 percent weight gain in 95 percent ± 5 percent relative humidity at 339K ±2.8K (150°F ± 5°F). The moisture weight gain was determined by weight-control coupons which accompanied the subcomponents. In some instances, some of the weight-control coupons were dried in a circulating-air oven at 366K (200°F) with a desiccant in order to determine the ambient moisture content prior to conditioning. The ambient moisture content was added to the weight gain recorded for the other weight-control coupons to determine that at least 1 percent moisture was present in the test component.

Failure loads and modes were predicted by analyses and were compared with the test results. The test results are summarized in table 38.

5.1 Truss Rib Test (H20A)

The purpose of this test was to verify the bending strength of the truss rib located at VSS 145.71. The testing was performed dry, at room temperature in the as-fabricated condition. All loadings were compression and were applied at approximately 267N/sec (60 lb/sec). There were four loading cases which are summarized in figure 93.

- Test sequence No. 1 represents a set-up to simulate an ultimate pressure loading of 13 134 N/m (75 lb/in) applied to the right side of the rib. No failure occurred with this loading arrangement.
- Sequence No. 2 is a similar loading arrangement to No. 1 except that due to the unsymmetrical geometry of the rib diagonals, the left side must also be tested. No failure occurred during this sequence.
- Test sequence No. 3 applied ultimate load to both sides of the rib simultaneously and again no failure was detected at ultimate pressure loading.

TABLE 38. - CONCEPT VERIFICATION TEST RESULTS (1 of 3)

Spec. No.	Size	Spec. Type	Load Type	Condition	DUL	Failure Mode		% DUL	Observed Failure Mode	Comments
						Calculated	Actual			
H20A	129.54 cm x 55.88 cm (51 in. x 22 in.)	Truss Rib Test	Static Bending	R.T.D.	Combined Loads	29 772 N/m (170 lb./in.)	29 246 N/m (167 lb./in.)	–	Flange Bending	
H20B1	60.96 cm x 182.88 cm (24 in. x 72 in.)	Rear Spar Test	Static Bending	R.T.D.	171 624 N/m (980 lb./in.)	243 426 N/m (1390 lb./in.)	278 452 N/m (1590 lb./in.)	163%	Shear at edge of lightning hole	
H20B2	60.96 cm x 182.88 cm (24 in. x 72 in.)	Rear Spar Test	Static Bending	355K Wet (180°F)	171 624 N/m (980 lb./in.)	234 670 N/m (1340 lb./in.)	309 975 N/m (1770 lb./in.)	181%	Shear at edge of lightning hole	
H21A1	60.96 cm x 60.96 cm (24 in. x 24 in.)	Spar Web Test	Static Shear	R.T.D.	231 308 N (52,000 lb.)	244 652 N (55,000 lb.)	262 445 N (59,000 lb.)	113%	Shear at edge of lightning hole	
H21A2	60.96 cm x 60.96 cm (24 in. x 24 in.)	Spar Web Test	Static Shear	R.T. Wet	231 308 N (52,000 lb.)	244 652 N (55,000 lb.)	284 686 N (64,000 lb.)	123%	Shear at edge of lightning hole	5 thermal cycles 219K (-65°F) to 355K (180°F) prior to test
H21B	60.96 cm x 60.96 cm (24 in. x 24 in.)	Spar Web Test	Fatigue Damage Tolerance	R.T.D.	231 308 N (52,000 lb.)	N.A.	268 673 N (60,400 lb.)	N.A.	Shear at edge of lightning hole	No damage growth in one lifetime
H23	60.96 cm x 182.88 cm (24 in. x 72 in.)	Front Spar Test	Static Bending	R.T.D.	228 541 N/m (1305 lb./in.)	274 074 N/m (1565 lb./in.)	294 213 N/m (1680 lb./in.)	129%	Shear at edge of lightning hole	
H24AT	63.5 cm x 55.88 cm (25 in. x 22 in.)	Truss Rib Attachment Test	Static Hinge Loads	R.T.D.	31 582 N (7100 lb.)	66 990 N (15,060 lb.)	86 740 N (19,500 lb.)	275%	Fasteners failed in double shear	No composite failure
H24AS	68.58 cm x 55.88 cm (27 in. x 22 in.)	Solid Web Rib Attachment Test	Static Hinge Loads	R.T.D.	22 997 N (5170 lb.)	62 275 N (14,000 lb.)	–	–	–	No failure at 68 947 N (15,500 lb.). Test suspended
			Fail Safe	R.T.D.	22 997 N (5170 lb.)	43 237 N (9720 lb.)	47 151 N (10,600 lb.)	205%	Tension in hinge lug	No composite failure

TABLE 38. - CONCEPT VERIFICATION TEST RESULTS (2 of 3)

Spec. No.	Size	Spec. Type	Load Type	Condition	DUL	Failure Mode		% DUL	Observed Failure Mode	Comments
						Calculated	Actual			
H24B1	78.74 cm x 27.94 cm (31 in. x 11 in.)	Rib Attachment Test	Static Actuator Loads	R.T.D.	70 816 N (15,920 lb.)	177 929 N (40,000 lb.)	–	–	–	No failure at 110 761 N (24,900 lb.) – capacity of loading system
			Fail Safe	R.T.D.	70 816 N (15,920 lb.)	133 447 N (30,000 lb.)	–	–	–	Element severed then loaded to 147 236 N (33,100 lb.) with no failure
H24C	78.74 cm x 55.88 cm (31 in. x 22 in.)	Rib Attachment Test	Static Actuator Loads	R.T.D.	±70 816 N (±15,920 lb.)	164 584 N (37,000 lb.)	–	–	–	No failure at 171 701 N (38,600 lb.) – capacity of loading system
H25	55.88 cm x 127 cm (22 in. x 50 in.)	Surface Attachment to Fuselage Test	Static Compression	R.T.D.	258 442 N (58,100 lb.)	346 961 N (78,000 lb.)	364 309 N (81, 900 lb.)	141%	Buckles delaminated stiffener	Initial buckling occurred at 77% of DUL
H25A	55.88 cm x 35.56 cm (22 in. x 14 in.)	Surface Attachment to Fuselage Test	Static Tension	R.T.D.	344 292 N (77,400 lb.)	600 510 N (135,000 lb.)	985 281 N (221,500 lb.)	286%	Net tension	Retest of H25 but in tension
H26A	17 78 cm x 127 cm (7 in. x 50 in.)	Stiffener Runout Test	Static Tension	+355K Wet (+180°F)	67 257 N (15,120 lb.)	110 761 N (24,900 lb.)	109 871 N (24,700 lb.)	159%	Fracture starting at fastener hole	Partial failure occurred at 93 413 N (21,000 lb.)
H26B	17 78 cm x 127 cm (7 in. x 50 in.)	Stiffener Runout Test	Fatigue	R.T.D.	67 257 N (15,170 lb.)	110 761 N (24,900 lb.)	–	–	–	Survived 2 lifetimes with no damage
			Residual Static	219K (-65°F)	67 257 N (15,120 lb.)	–	96 082 N (21,600 lb.)	142%	Hat/skin separation	
H27	53.34 cm x 190.50 cm (21 in. x 75 in.)	Surface Panel Stability Test	Static Compression	+355K Wet (+180°F)	258 442 N (58,100 lb.)	355 858 N (80,000 lb.)	311 376 N (70,000 lb.)	120%	Buckles delaminated stiffener	Initial buckling occurred at 93% of DUL

TABLE 38. - CONCEPT VERIFICATION TEST RESULTS (3 of 3)

Spec. No.	Size	Spec. Type	Load Type	Condition	DUL	Failure Mode		% DUL	Observed Failure Mode	Comments
						Calculated	Actual			
H27A	53.34 cm x 139.7 cm (21 in. x 55 in.)	Surface Panel Stability Test	Static Compression	R.T.D.	258 442 N (58,100 lb.)	355 858 N (80,000 lb.)	361 196 N (81, 200 lb.)	140%	Buckles delaminated stiffener	Retest of H27
H28	91.44 cm x 190.5 cm (36 in. x 75 in.)	Surface Panel Fail-Safe Test	Fatigue Damage Tolerance	R.T.D.	N.A.	N.A.	N.A.	N.A.	N.A.	Survived 1-1/2 lifetimes
H29	121.92 cm x 55.88 cm (48 in. x 22 in.)	Lightning Strike Test	Lightning Strike	R.T. Wet	N.A.	N.A.	N.A.	N.A.	Local resin burned away 3.81 cm (1-1/2 in. dia.) partially through thickness. Minor delam. surface ply	C-Scan showed no additional damage. Coupons will be cut for static tests

LEFT SIDE RIB CAP LOADS

Test Seq.	Crushing Rib Load N/m (lb/in.)
1	0
2	13 905 (79.4)
3	13 660 (78.0)
4	29 071 (166.0)

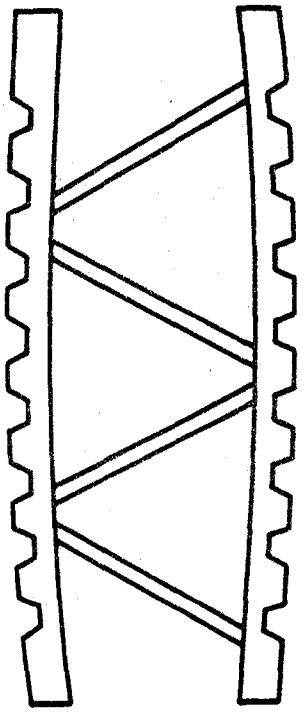

RIGHT SIDE CAP LOADS

Test Seq.	Crushing Rib Load N/m (lb/in.)
1	13 240 (75.6)
2	0
3	13 853 (79.1)
4	29 299 (167.3)

Figure 93. - H20A load summary.

- Test sequence No. 4 was designed as the failure run to ascertain the bending strength of the cap.

The rib was loaded successfully to ultimate load 13 137 N/m (75 lb/in.); however, upon reaching a load of 13 747 N/m (78.5 lb/in) or 105 percent DUL, a popping sound was heard which is believed to be the initiation of rib cap failure in the middle of the left side. This failure point is illustrated in comparison to the actual air foil pressure distribution in figure 94. Loading continued until final rib collapse occurred at 29 299 N/m (167.3 lb/in) or 223 percent DUL.

5.2 Rear Spar Tests (H20B)

The objective of this test was to verify the static strength of the rear spar and its attachment to the fuselage. Two identical H20B rear spar specimens were tested (figure 95). One specimen H20B2 was conditioned to a moisture content in excess of one percent by weight, heated to a temperature of 355K (180°F), and static tested. The other specimen H20B1 was tested dry at room temperature.

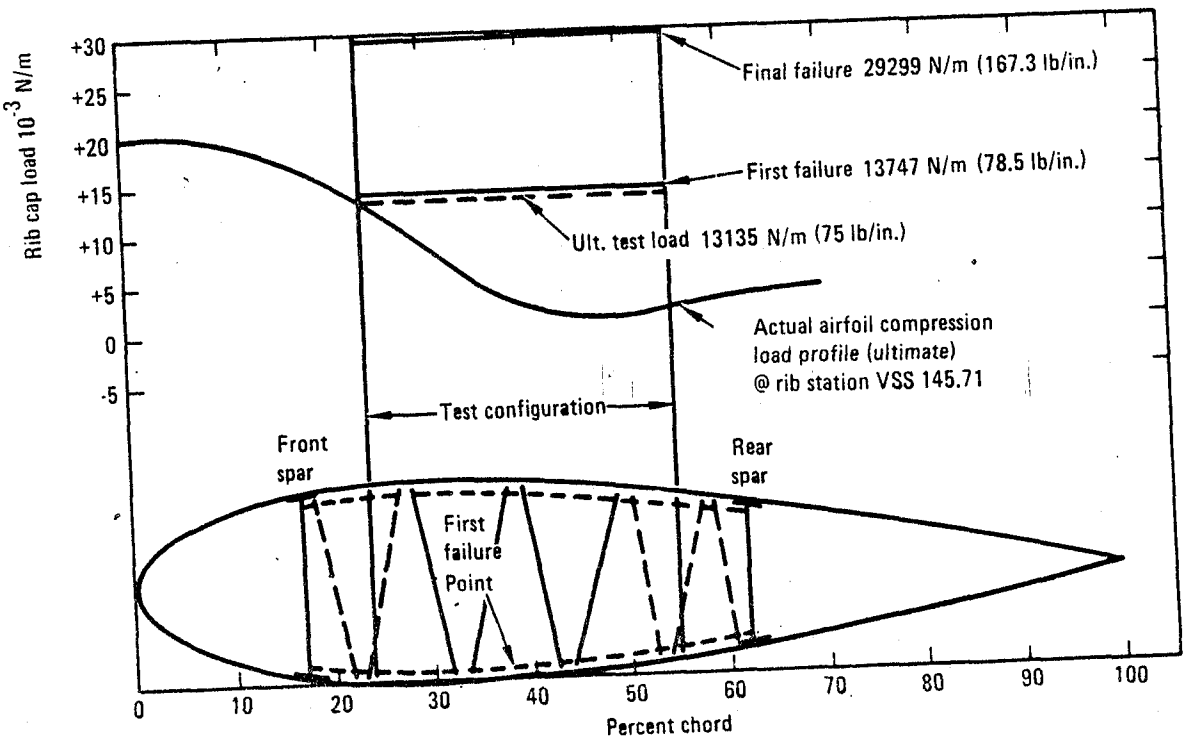

Figure 94. - H-20A pressure distribution - actual vs test.

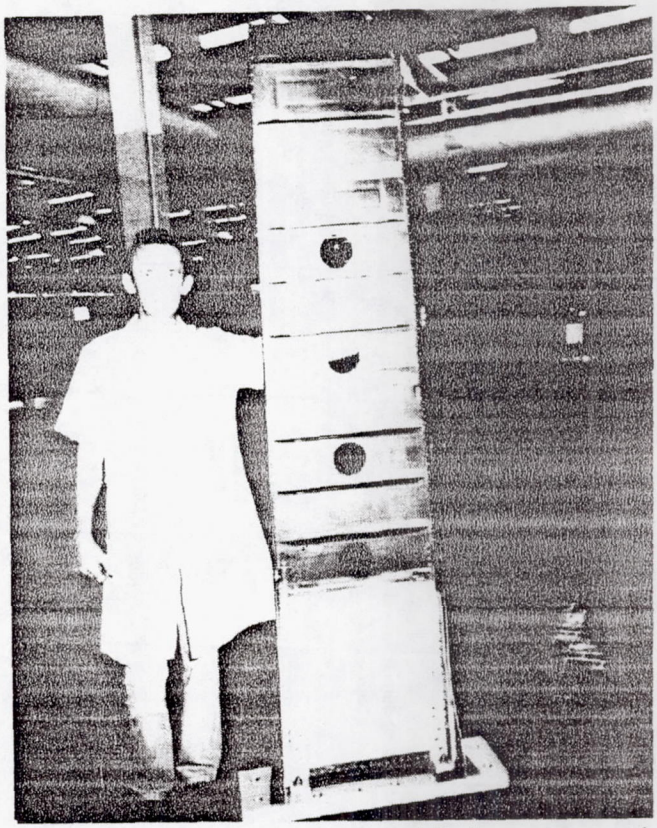

Figure 95. - H20B1 spar assembled test specimen.

5.2.1 Room temperature static (H20B1). - The objective of this test was to verify the static strength of the lower 2.54 m (100 in.) of the rear spar and its attachment to the fuselage.

The three loading conditions used to simulate the loads in the vertical fin box structure are shown in table 39. Loads were applied at four stations using eight tension jacks. Figure 96 shows the test set-up for the critical loading condition.

Loads were applied in 20 percent increments up to 100 percent of limit for each condition prior to applying design ultimate (150 percent of limit) loads. Load cases I and II being less critical than load case III, were loaded to 150 percent of limit prior to loading case III to failure. Case III was loaded to limit in 20 percent increments followed by 10 percent increments from limit to failure. Failure occurred at 244 percent of limit load. Failure occurred between VSS 96 and VSS 121, the highest strained area found when design ultimate loads were applied (see figure 97).

5.2.2 Hot wet static (H20B2). - The objective of this test was to verify the strength of the lower 2.54 m (100 in.) of the rear spar when saturated with 1 percent moisture and subjected to elevated temperatures.

TABLE 39. - LOAD SUMMARY FOR H20B1 AND H20B2

	Design		Load Case I			Load Case II (H20B1)			Load Case III		
V.S.S.	Cap Load N (lb.)	Shear Flow N/m (lb./in.)	Applied Jackload N (lb.)	Cap Load N (lb.)	Shear Flow N/m (lb./in.)	Applied Jackload N (lb.)	Cap Load N (lb.)	Shear Flow N/m (lb./in.)	Applied Jackload N (lb.)	Cap Load N (lb.)	Shear Flow N/m (lb./in.)
80	132 100 (29 700)			132 100 (29 700)			132 100 (29 700)			132 100 (29 700)	
88.12		96 300 (550)			91 400 (522)			96 300 (550)			59 000 (337)
96.25	113 000 (25 400)		0	99 200 (22 300)		22 700 (5 100)	97 400 (21 900)		-58 300 (-13 100)	113 000 (25 400)	
108.80		171 600 (980)			96 300 (550)			59 200 (338)			171 600 (980)
121.35	64 500 (14 500)		-22 200 (-5 000)	42 300 (9 500)		-24 900 (-5 600)	64 500 (14 500)		85 000 (19 100)	7 100 (1 600)	
132.97		147 100 (840)			147 100 (840)			113 000 (645)			12 800 (73)
144.58	44 500 (10 000)		106 300 (23 900)	-44 500 (-10 000)		56 500 (12 700)	0		6 200 (1 400)	0	
157.50		105 000 (600)			70 400 (402)			0			0
170.42	76 200 (5 900)		-32 900 (-7 400)			0	0		0	0	

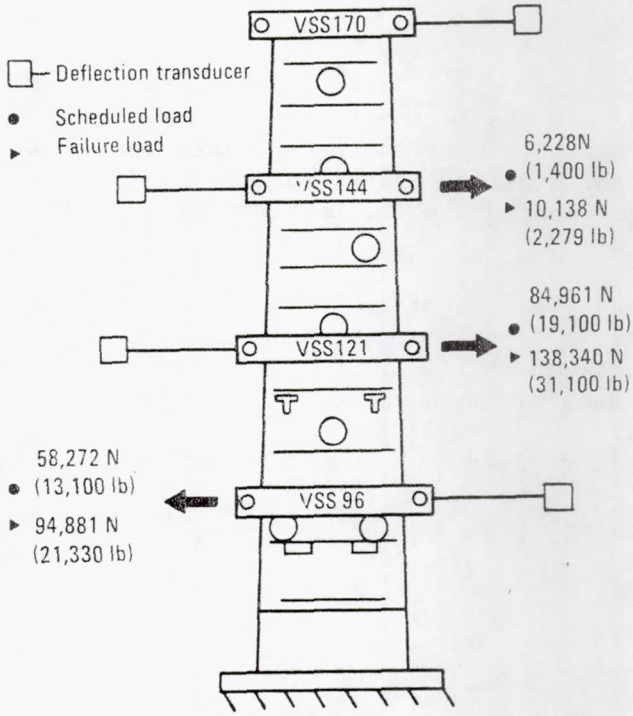

Figure 96. - H20B1 critical loading condition test set-up.

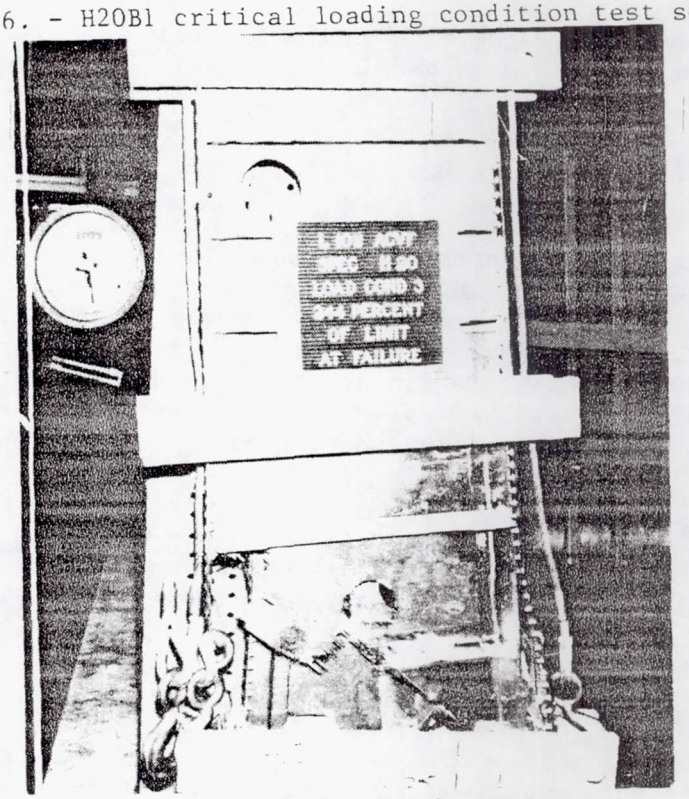

Figure 97. - H20B1 failed specimen.

Three loading conditions were used to simulate the loads in the vertical fin box structure. The spar was heated using hot air circulated as shown in figure 98 until the thermocouples on the specimen read 355K (180°F). Loads were applied at four stations using six tension jacks attached to the load bars through sealed openings in the environmental chamber and nylon film bag.

Cases I and III loads were identical to those previously applied to the H20B1 spar, however case II loads were changed to cover the higher shear flows in the spar web between VSS 80 and VSS 86.5 resulting from the final NASTRAN loads. These loads are summarized in table 40.

The loading schedule applied to the H20B2 spar was as follows:

- Load Case I — to 150 percent limit
- Load Case III — to 150 percent limit
- Load Case II — in table 53 to 150 percent limit
- Load Case III — to failure

Failure occurred at 272 percent of the critical Case III limit load, between VSS 96 and VSS 121, as shown in figure 99.

5.3 Spar Web Tests (H21)

A series of "picture frame" test panels simulating the highly-loaded lower shear web in the front spar were planned to demonstrate the structural integrity of the web, the unreinforced access hole and stiffener design. The area selected for testing was the spar web between VSS 90 and VSS 120. The highest shear in both front and rear spars occurred in this area, and the analysis indicated the lowest margin of safety in either front or rear spars existed in this area. Tests were planned to demonstrate static strength, dry, at room temperature, wet strength at room temperature and resistance to crack growth.

Three identical test panels with the same ply orientation, access hole and stiffener configuration as that in the front spar drawing were planned and scheduled for tests. The panel design is shown in figure 100.

5.3.1 Room temperature dry static (H21A-1). - The purpose of this test was to verify the dry, room temperature static strength of the spar web with an unreinforced access hole. This basic strength of an undamaged panel was planned to be used for comparison with the residual strengths of the damaged and humidity conditioned panels.

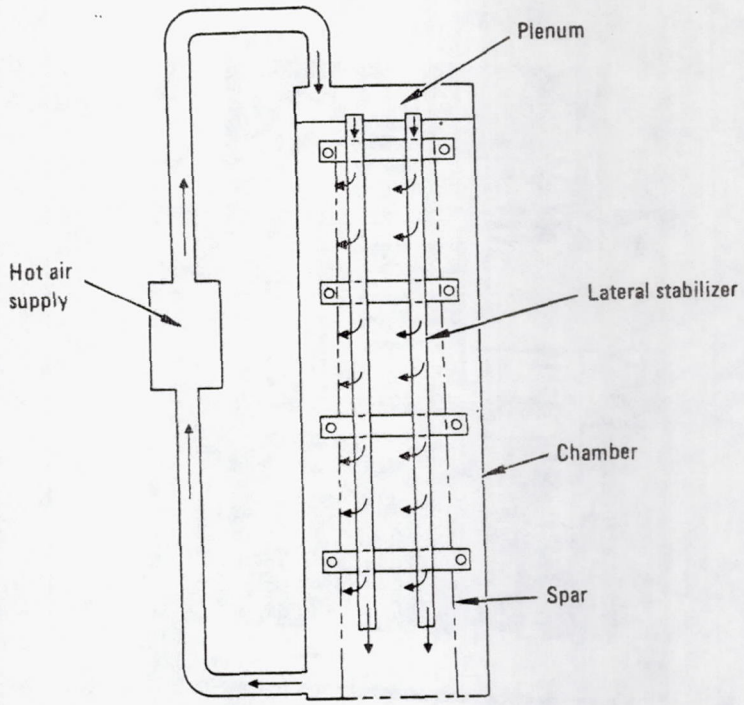

Figure 98. - Diagram of environmental chamber for H20B2.

TABLE 40. - DESIGN VS MODIFIED CASE II TEST LOADS

Load Changes for H20B2					
Design			Load Case II (H20B2)		
V.S.S.	Cap Load N (lb.)	Shear Flow N/m (lb./in.)	Applied Jackload N (lb.)	Cap Load N (lb.)	Shear Flow N/m (lb./in.)
80	132 600* (29 800)			132 600 (29 800)	
86.33		124 000 (708)			124 000 (708)
92.65	132 600* (29 800)		0	84 000 (18 900)	
107.00		153 200 (875)			131 700 (752)
121.35	64 500 (14 500)		70 300 (15 800)	0	
132.97		142 400 (813)			
144.58	44 500 (10 000)		0	0	
157.50		105 800 (604)			
170.42	26 200 (5 900)		0	0	

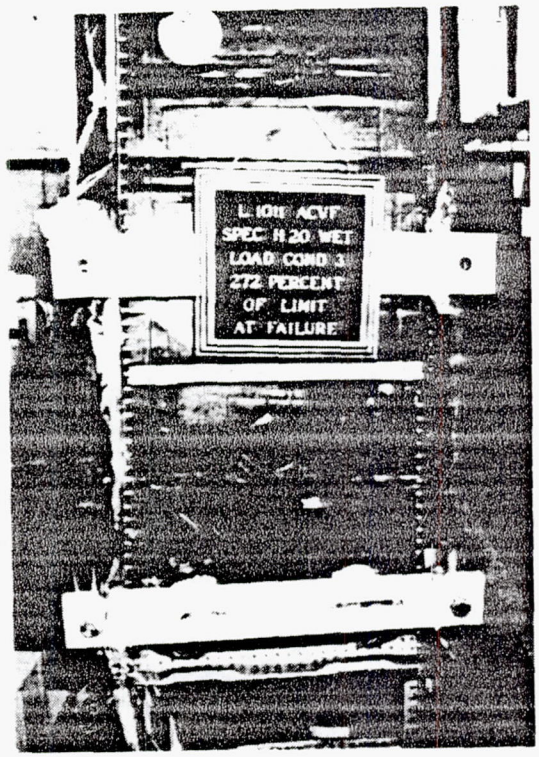

Figure 99. - Failed H20B2 specimen.

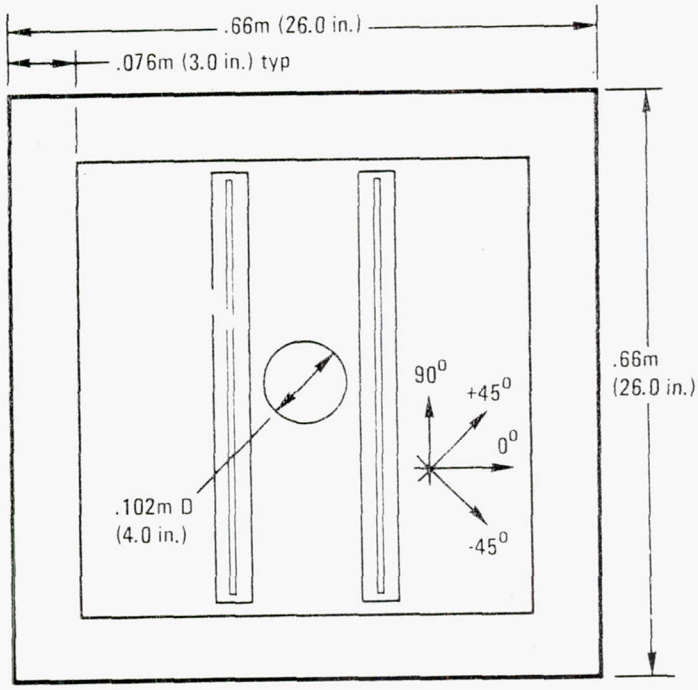

Figure 100. - H21 "picture frame" test panel.

H21A-1 was installed in the picture frame test fixture, instrumented and loaded incrementally until failure occurred at 263 353N (59,204 lb) or 170 percent of design limit load. This was less than the failure load of H21B which was expected to be slightly less than that for H21A-1. The failure load for the panel was, however, well within typical test scatter. Figure 101 shows the test set up, failure mode and selected strains in the access hole. Gage 11 read a compressive strain and gage 12 a tensile strain.

5.3.2 Hot wet static (H21A-2). - The purpose of this test was to verify that structural integrity of the proposed L-1011 ACVF spar web design would be maintained after environmental conditioning and subsequent moisture content increase of the panel. The configuration of this specimen was the same as that for H21A-1.

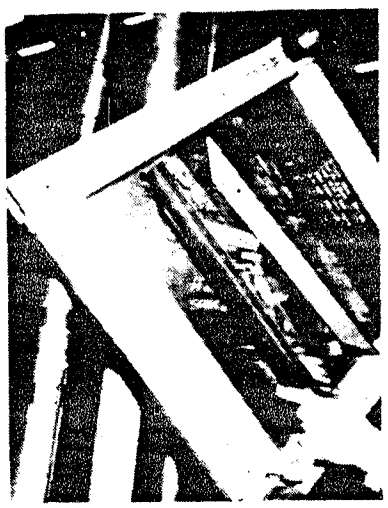

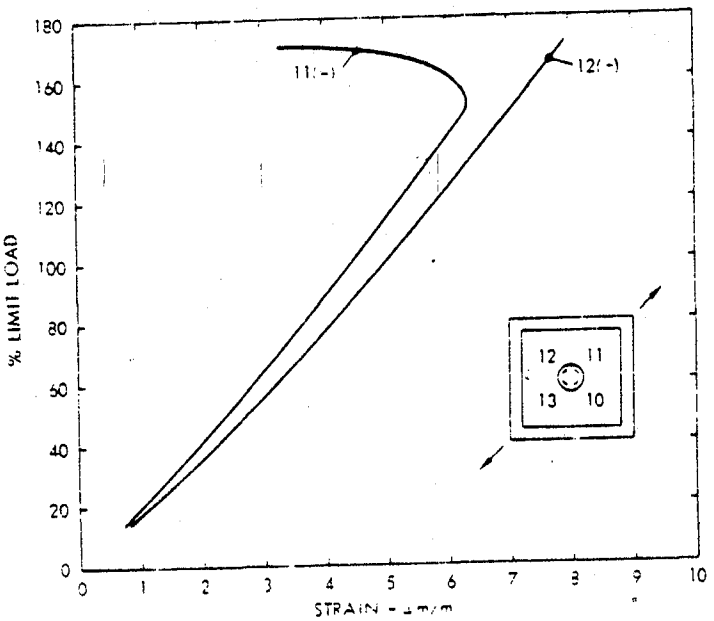

Figure 101. - Spar web failure mode and highest strains.

The specimen was conditioned for forty days in an environmental chamber at 344K (160°F) and 95 percent relative humidity. Both traveler specimens and desorption specimens were monitored for moisture content during this period. The traveler specimens, reflecting the moisture content in the test panel, showed a 1.57 percent weight increase during this period. The desorption specimens were dried over the same period and had an average 0.47 percent weight loss.

After environmental conditioning, this specimen was subjected to five thermal cycles. Each full cycle lasted 120 minutes and, during each cycle, the temperature ranged from 219 to 355K (-65 to 180°F). Figure 102 shows the thermal cycle and a schematic of the thermal cycling chamber.

Temperatures were monitored with six thermocouples attached to the specimen. Ultrasonic inspection of the specimen was performed after this thermal cycling and no damage was found. At this point, the specimen was installed in the test machine and limit load was applied. After unloading the fatigue specimen, the ultrasonic inspection was repeated and no damage was found. Finally the specimen was loaded to a failure load of 285 516N (64,200 lb) or 184 percent of load limit.

Final moisture content of H21A-2 as determined by drying out coupons cut out of the failed panel was 1.3 percent.

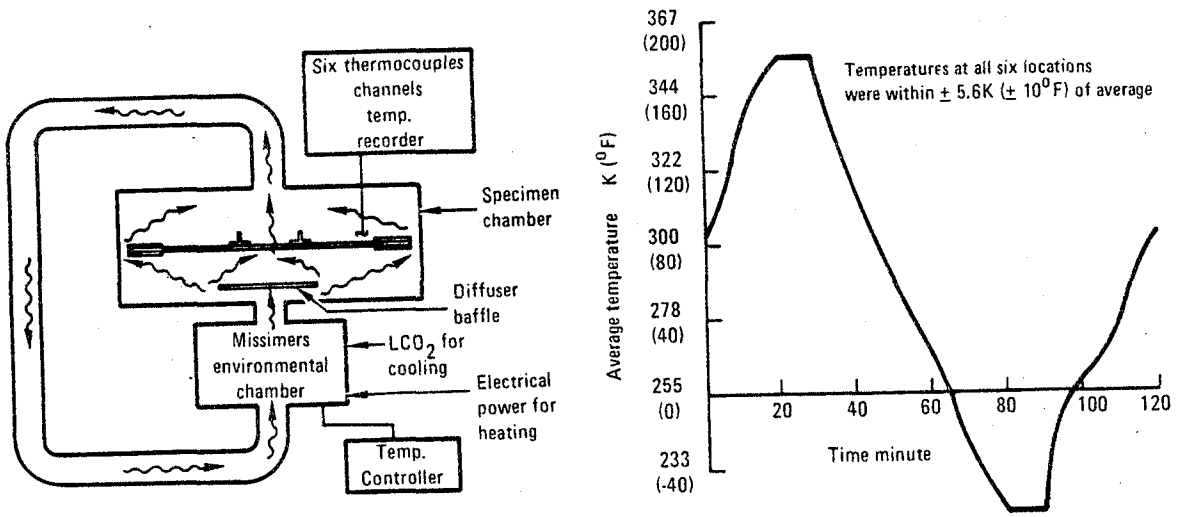

Figure 102. - Thermal chamber and thermal cycle.

5.3.3 Fatigue of spar web (H21B). - The purpose of this test was to demonstrate the resistance of unreinforced access holes in the all graphite spar web to crack growth during 1/2 life time.

The test included the application of one-half lifetime of the L-1011 flight load spectra to the H21B panel after a 6.4 mm (0.25 in.) saw cut was made in the edge of the access hole. After completion of the fatigue loading and inspection of the artificial crack, a residual strength test was conducted. Before testing, the panel was x-rayed using tetra bromethane (TBE) applied to the edge of the access hole.

The fatigue specimen in table 41 was applied to the panel. This spectrum is equivalent to one-half of a life time plus a limit load, 92 percent limit load and 77 percent limit load in flight number 18000.

After completing one-half lifetime of fatigue cycling, the panel was removed from the test machine and inspected. X-rays were made using TBE and compared to the x-rays made before fatigue cycling. Except for very faint lines extending approximately 2 mm (0.08 in.) in the ±45°, 0° and 90° directions from the tip of the artificially induced crack, no detectable damage was found. The test plan, for a residual strength test after one-half life time, was revised to put the panel back in the fatigue test machine and apply a second, one-half life time.

TABLE 41. - FATIGUE SPECTRUM FOR SPAR WEB TEST

% Limit Load	Load N (Kips)	N	ΣN	Flight					
				1	36	360	1 800	9 000	18 000
15	23.1 (5.2)	83 000	98 528	4	22				
23	35.6 (8.0)	12 430	15 528		24	8	3		
31	47.6 (10.7)	2 164	3 098		4	3	1	2	
38	58.7 (13.2)	638	934		1	2	3	4	1
46	71.2 (16.0)	164	296			3	1	2	
54	83.6 (18.8)	67	132			1	1	3	1
62	95.6 (21.5)	21	65				2		1
69	106.8 (24.0)	14	24				1	2	
77	119.2 (26.8)	5	10					2	1
81	125.4 (28.2)	1	5						1
85	131.7 (29.6)	1	4						1
88	136.1 (30.6)	1	3						1
92	142.3 (32.0)	1	2						1
100	154.8 (34.8)	1	1						1
Count				4	51	17	12	15	9
Multiplier				18 000	500	50	10	2	1

After completing the second one-half lifetime (equivalent to a total of 36,000 flights), the panel was removed from the test fixture and x-rayed again using TBE applied to the crack at the edge of the access hole. The x-ray made after one life time was identical to the x-ray made after one-half life time. No change could be seen in the condition of the crack. The faint lines radiating from the tip of the crack were identical to those seen in the x-ray made after one-half lifetime. Figure 103 shows the comparative x-rays.

The specimen was then tested to failure which occurred at 286 643 N (64,440 lb) or 173.5 percent of limit load. Failure occurred by apparent buckling of the web followed by delamination of the stiffeners from the web. The ratios of actual versus predicted values for failure at the cutout was 1.09 and the actual versus predicted buckling was 1.26.

No apparent degradation was observed in the strength of the specimen as compared to an uncracked, unfatigued specimen H21A-1.

5.4 Front Spar Test (H23)

The purpose of this test was to verify the static strength of the front spar between VSS 80.36 and VSS 145 and the attachments at the fuselage joint.

The test specimen included the lower 2.13 m (84 in.) of the composite spar, the metal parts attached to the spar, and the fittings and fasteners used to attach the base of the spar to the fuselage. This area of the front spar had the highest loads and the lowest margins of safety. Holes were drilled in the spar caps to simulate the hole pattern used to attach the covers and leading edge. A heavy base plate was also assembled to the specimen for attaching the specimen to the test fixture.

Four loading set ups and four load points simulated the loads in the spar web and spar caps. Molded rub attach angles, numbered R1, R2 and R3 were machined off to allow attachment of loading pads at VSS 96.87, VSS 121.35, and VSS 145.71. A fourth loading pad was attached to the upper end of the spar VSS 162.29. Design loads were applied by using four stepped conditions, i.e., one load set-up was used to apply shear and bending loads to one area and a second set-up was used to cover another area. The four load set-ups were needed to cover one design load case for the spar, because the spar was tested as a cantilever beam and loaded to simulate a spar in a box beam.

H23A was tested dry at room temperature, but design ultimate loads were increased ten percent to account for the predicted effect of moisture. Ultimate test loads were applied to the spar using the first three set-ups prior to loading the area of the spar with the lowest calculated margin of safety. This case simulated the design loads in the spar web between VSS 96.87 and VSS 121.35 and the spar cap loads between VSS 90 and VSS 96.87. Minimum margins of safety were predicted for the access holes between VSS 96.87 and VSS 121.35.

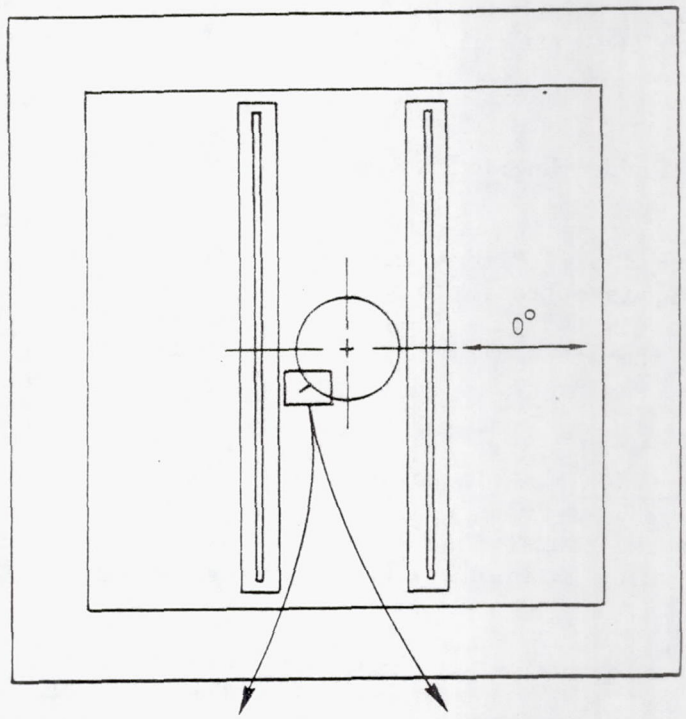

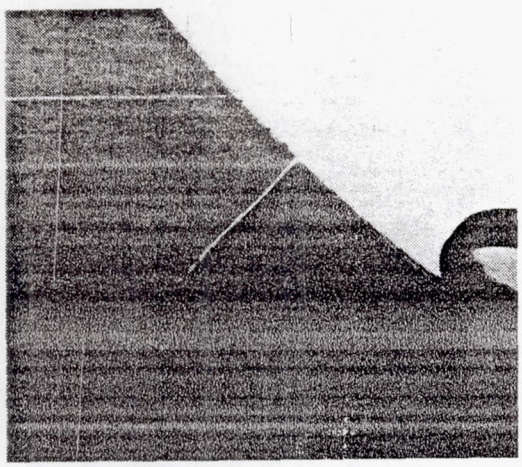

1/2 Lifetime

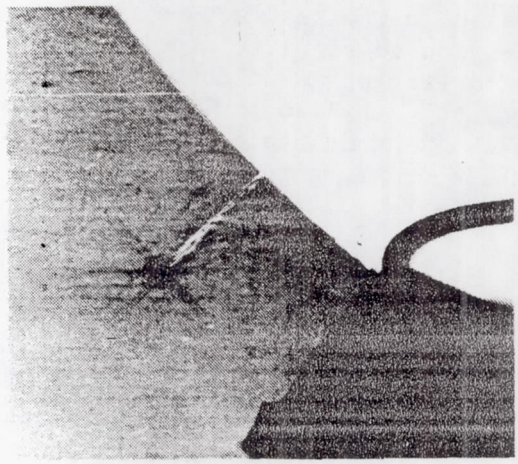

1 Lifetime

Figure 103. - X-rays of crack tip in access hole edge at 1/2 and 1 lifetime.

Loads were applied in ten percent increments until failure occurred between VSS 121.35 and VSS 96.87 at 194 percent of limit load. Selected strains measured during the critical, fourth loading set-up and the failure mode are shown in figure 104.

5.5 Rudder Hinge to Rib Attachment Tests (H24A)

These tests were designed to verify the static strength of the hinge to rib details. There are two specimens in the test program. The first, which is identified as H24AT, is a truss rib specimen representing the aft 0.76 m (2.5 ft) of the rib at VSS 145.71. The second specimen is a solid web rib specimen representing the aft 0.61 m (2 ft) of the rib at VSS 299.97 and is identified as H24AS.

5.5.1 Truss rib (H24AT). - The objective of this test was to verify the static strength of the H24AT truss rib hinge attachment which was a hinge-to-rib design detail for the truss ribs. The specimen was representative of the VSS 145.71 truss rib which carries the highest hinge loads. The specimen is shown in figure 105.

The truss rib test component was installed between two parallel 12.7 mm (0.5 in.) thick vertical steel reaction plates. The rib test component, as installed in the test set-up, was rotated 90° from its normal airplane fin orientation to simplify the loading arrangement. A triangular-shaped steel hinge fitting was used to transfer the hinge loads to the truss rib test component. A hydraulic loading jack was used to apply the test loads, and an Edison load maintainer was used to regulate and proportion the desired hydraulic pressure to the loading jack. The loading geometry provided a hinge load to jack load ratio of 1.559.

Three separate static tests of the H24AT truss rib were conducted. In Test No. 1, hinge test loads were applied to 67.8 percent of design ultimate load with no specimen damage. In Test No. 2, hinge test loads were applied to 100 percent of design ultimate load with no specimen damage. In Test No. 3, hinge test loads were applied until the component failed. Failure occurred at 274 percent of design ultimate load of 86 518N (19,450 lb). The primary failure occurred at the upper tang of the truss rib/hinge fitting attachment (figure 106).

The failure at the upper tang consisted of (a) shank failure of the two 6.35 mm (0.25 in.) diameter HiLok fasteners adjacent to the head of the pin, and (b) elongated holes in each of the structural members of the tang/hinge fitting attachment.

5.5.2 Solid web rig (H24AS). - The purpose of this test was to verify the static strength of the hinge to solid web rib design details. Four

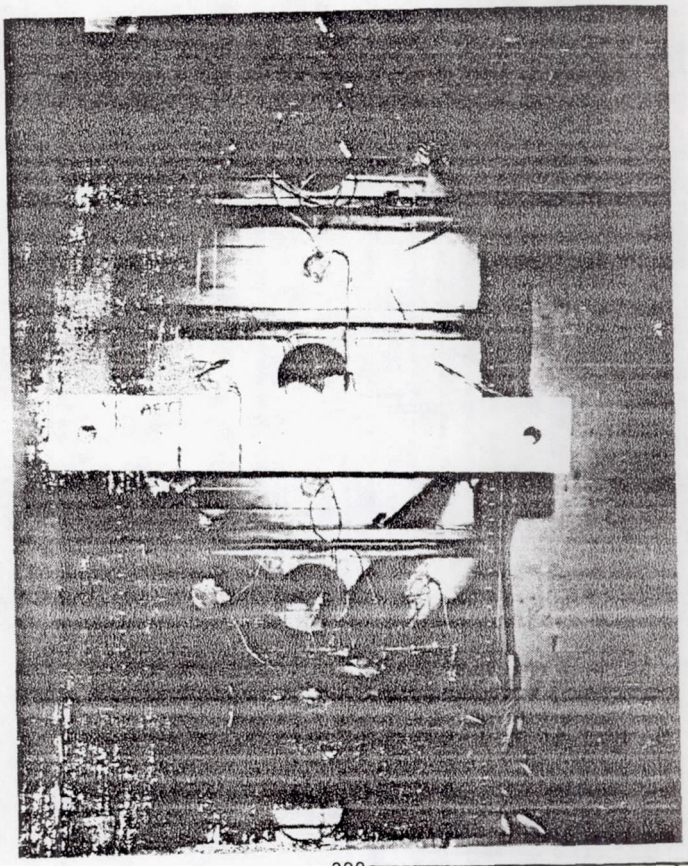

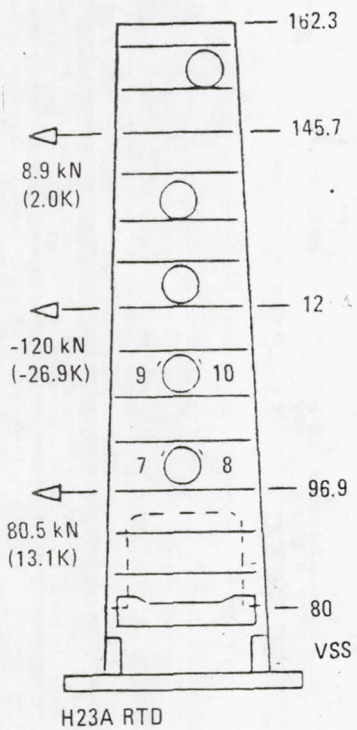

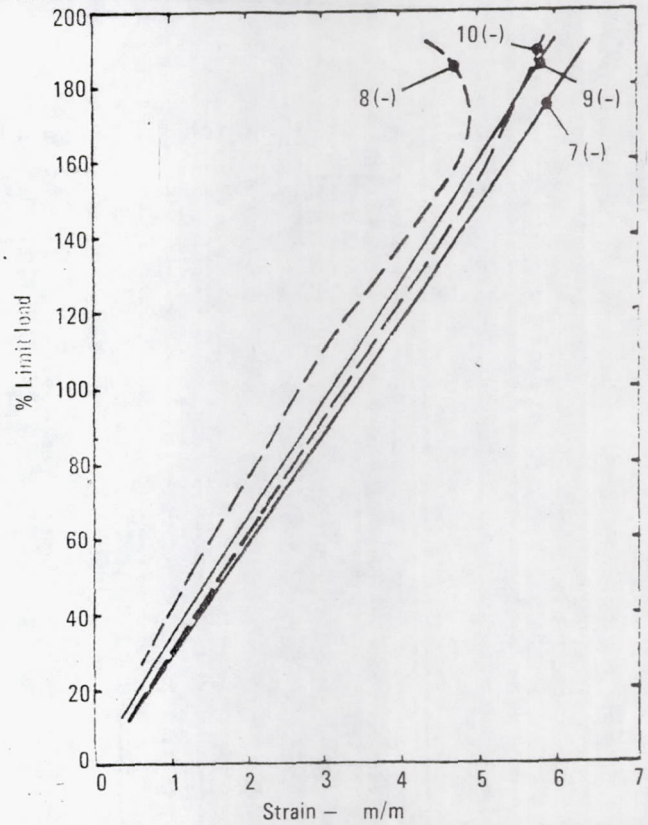

Figure 104. - Failure mode, ultimate loads and maximum strains for front spar.

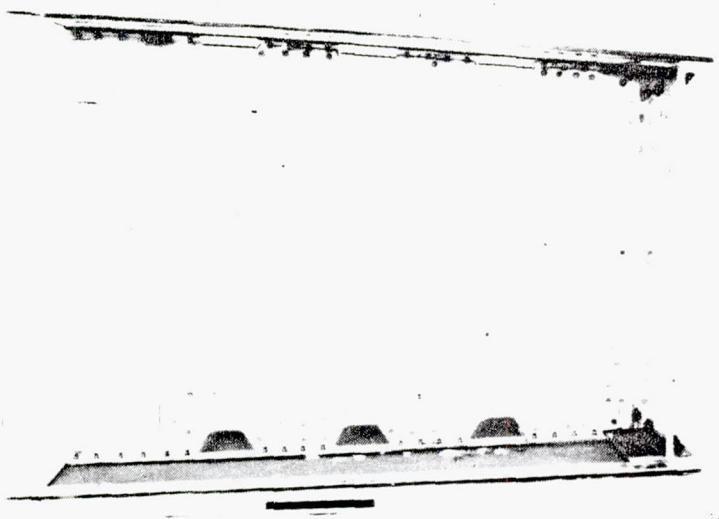

Figure 105. - Truss rib specimen.

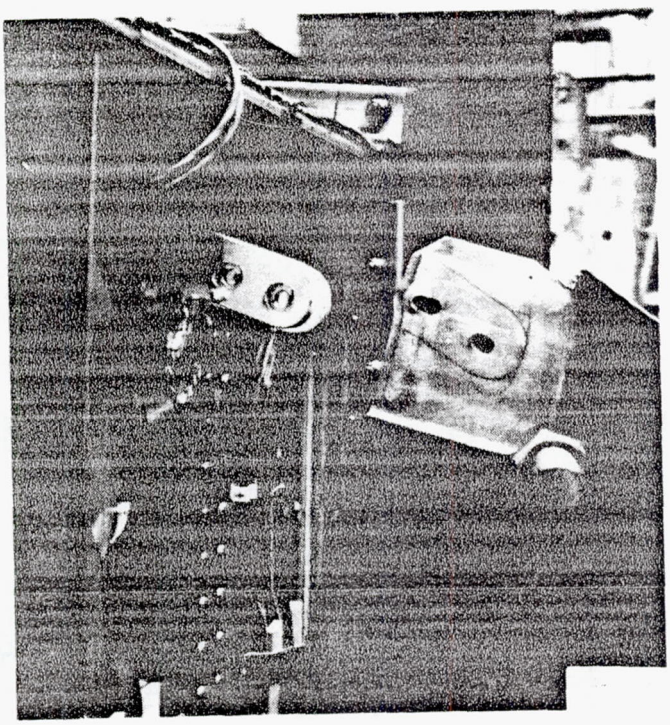

Figure 106. - Truss rib failure showing elongated holes at upper hinge attachment location.

separate tests of the H24AS solid web rib were conducted. For each of these tests, described below, the procedure consisted of continual loading to the maximum indicated load.

In Test No. 1, hinge test loads were applied to 100 percent of design ultimate load (P jack = 12 144 N (2.73 kips); hinge load = 22 686 N (5.1 kips)) with no specimen damage. In Test No. 2, hinge test loads were applied to 337 percent of design ultimate load (P jack = 40 906 N (9.196 kips); hinge load = 76 509 N (17.2 kips)) without specimen failure.

Since there was no failure in the above runs, the remaining tests were used to verify fail-safe integrity. In test number 3, eighteen fasteners were removed from the reinforcement angles on the tension hinge-load component side of the rib specimen. These fasteners, identified in figure 107, were 0.40 mm (5/32 in.) diameter protruding tension heat titanium hi-loks (HL 12V-5). Hinge test loadings was applied to 339 percent of design ultimate load (P jack = 41 177 N (9.257 kips),; hinge load = 76 999 N (17.31 kips)) without failure.

In Test No. 4, the eighteen fasteners were reinstalled in the reinforcement angles and the tension-loaded tang of the cruciform aluminum section at the rear spar was severed, leaving only the aluminum strap to transfer the tension hinge load component into the solid web rib. Hinge test loads were applied to 205 percent of design ultimate load (P jack = 24 875 N (5.592 kips); hinge load - 46 528 N (10.46 kips)) when failure occurred. Failure consisted of strap rupture at the cut location, followed by rupture of both the strap and the cruciform tang at the opposite end of the simulated hinge fitting. No other specimen damage was noted.

5.6 Actuator to Rib Attachment Tests (H24B & H24C)

These tests are identified as H24B and H24C. The purpose of these tests was to verify the static strength of the actuator to rib design. H24B was a test on a half width specimen of the rib, while H24C was a full width specimen.

5.6.1 Static test (H24B1). - The purpose of this test was to verify the static strength of the actuator fitting to rib details. The testing was performed dry, at room temperature, in the as-fabricated condition. The test specimen is shown in figure 108.

All loadings were tension and were continually applied at the rate of approximately 667 N/s (150 lb/sec). A summary of these loadings and their results are given in table 42.

The H24B1 Actuator to Rib Attachment was statically loaded to 157 percent of design ultimate load without failure. The load-carrying tee was then

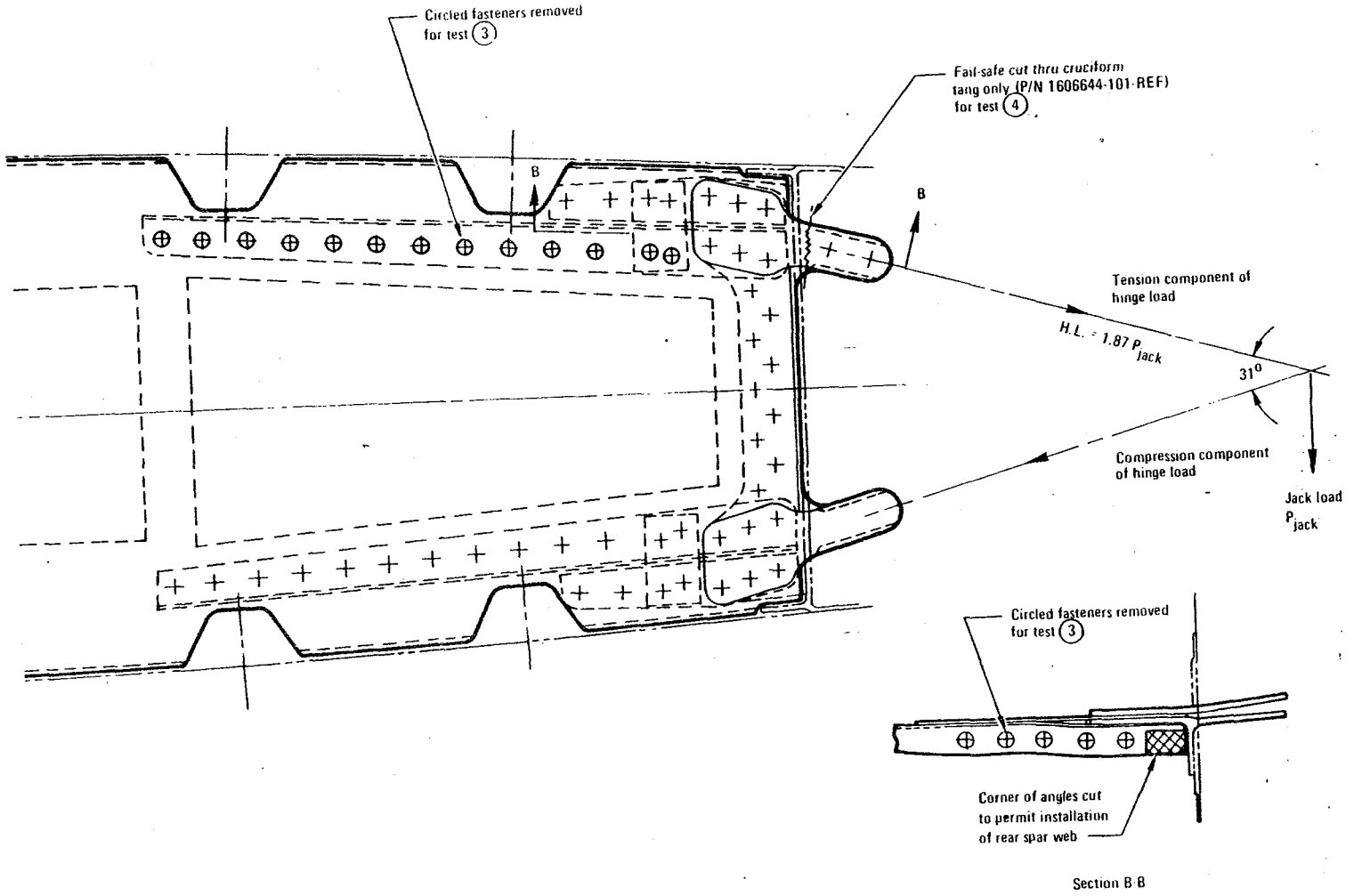

Figure 107. - Fail-safe test modifications - solid web rib specimen.

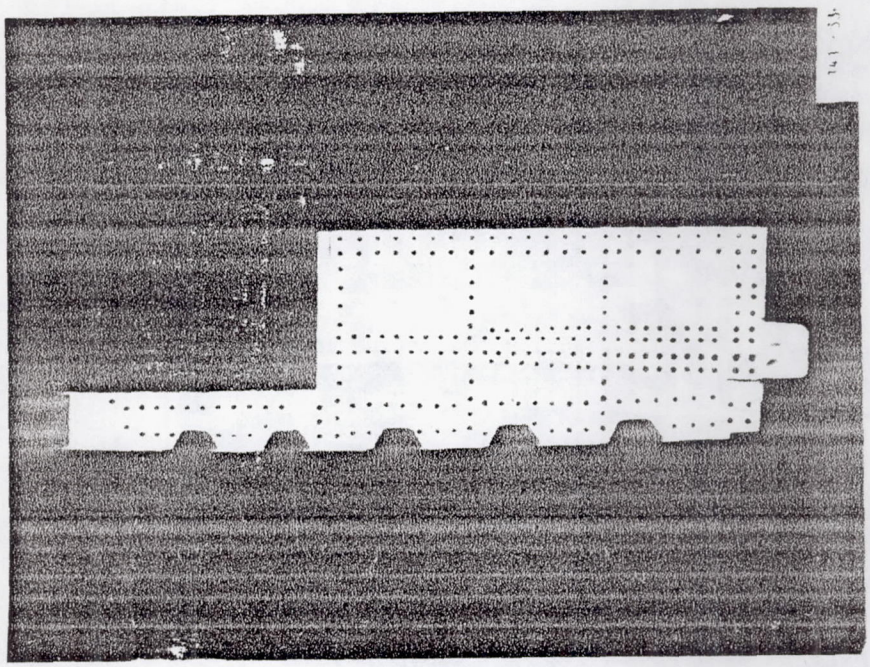

Figure 108. - Actuator rib test specimen.

TABLE 42. - LOADING SEQUENCE AND RESULTS FOR H24B1 TEST

Test Seq.	P_{MAX}	% Ult. Design	Remarks	Results
1	11 521N (2 590 lb.)	16	Prelim. Test #1	–
2	49 242N (11 070 lb.)	69	Prelim. Test #2	–
3	70 816N (15 920 lb.)	100	Prelim. Test #3	–
4	110 961N (24 945 lb.)	157	Failure run	No Failure
5	111 206N (25 000 lb.)	157	Fail-safe test 80% of P/N 1525371-101 Tee Severed	No Failure

severed between the 11th and 12th row of fasteners, (figure 109), and a fail-safe test was conducted. With the tee completely severed, a load of 208 percent of design ultimate was successfully applied without failure.

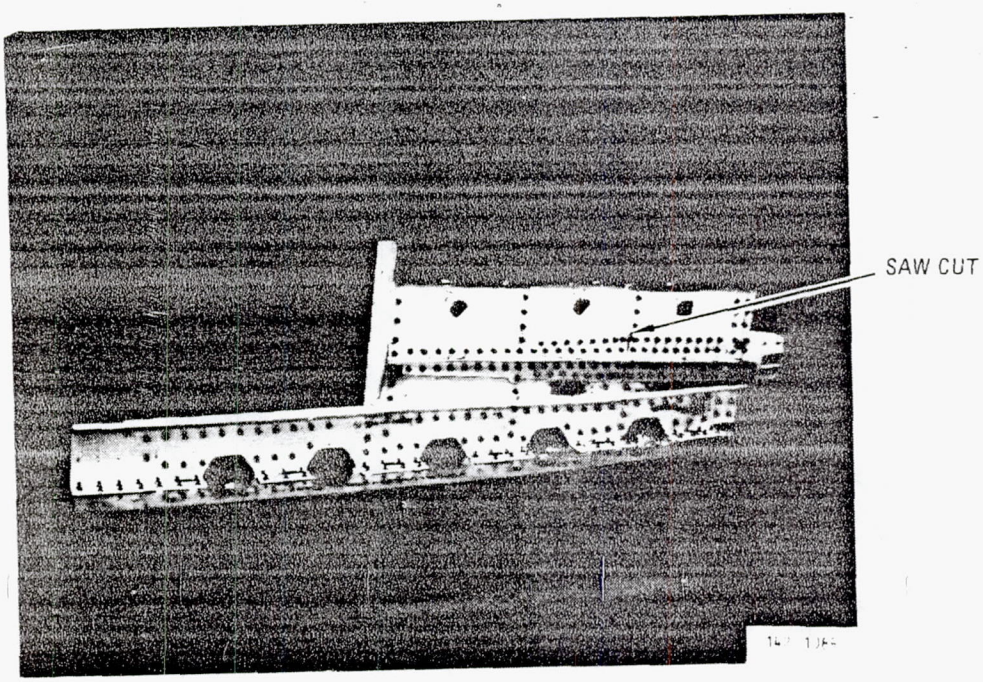

Figure 109. - Actuator rib test specimen after testing. (Note the saw cut severing the actuator attachment).

Following the testing, the specimen was removed from the reaction frame and disassembled. A cursory examination of the various components, including the holes and fasteners, showed that no damage other than the intentional saw cut across the actuator attachment, was sustained by the specimen.

5.6.2 VSS 97.19 actuator rib test (H24C). - The purpose of this test was to verify the strength of the actuator rib and to evaluate the shear web to rib cap joint design at VSS 97.19. The H24C test specimen, which consisted of a full rib assembly, is shown in figure 110.

Testing was performed dry, at room temperature. Loads were applied simultaneously to the two jacks. The lower jack, operating in tension loaded the left hand actuator attachment while the upper jack, operating in compression, was loading the right hand one (see the loading schematic at the bottom of table 43. A summary of the various test loadings and their results is also presented in the table.

The H24C Actuator Rib was statically loaded in excess of 247 percent of design ultimate without failure. The only damage was external and was confined to the slight bending of twelve 6.35 mm (0.25 in.) diameter pins used for attaching the loading jack trains to the two actuator attachments.

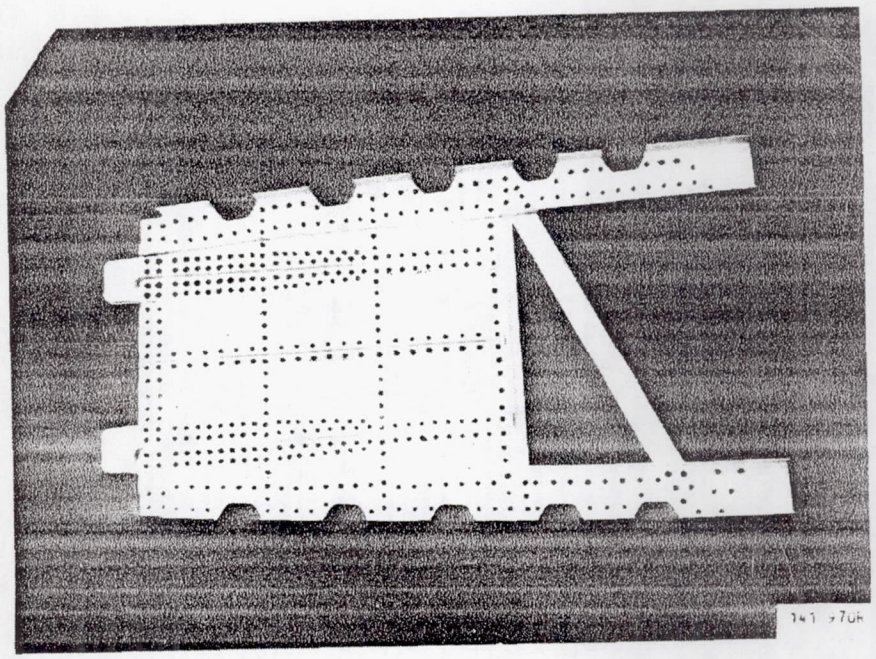

Figure 110. - Actuator rib test specimen.

5.7 Surface Attachment to Fuselage Tests (H25)

The objectives of this program were; (a) to verify the static strength of the fin to fuselage joint, and (b) to experimentally verify and visually observe the panel buckling characteristics. Two tests were conducted to meet these objectives. The first test, H-25 was a compression test, which satisfied objective (b). However, due to the non-uniform spanwise area of the panel, the full potential strength of the root-end joint was not established in this test. The second test, H25A was conducted in tension, dry, at room temperature in order to meet objective (a). Test specimen H25A consisted of the undamaged lower 0.66 m (26.0 in.) of test specimen H25. These are shown in figure 111.

5.7.1 Compression test (H25). - The purpose of this test was to verify the static strength of the fin to fuselage joint, and to observe the panel buckling characteristics using shadow moire. The test satisfied the objective of observing the panel buckling characteristics satisfactorily. However, at failure load, the static strength of the aforementioned joint was not satisfactorily verified.

TABLE 43. - SUMMARY OF STATIC TESTS OF ACTUATOR RIB SPECIMEN (H24C)

Test Seq.	Applied Jack Loads N (lb.) P_C	Applied Jack Loads N (lb.) P_T	Load Components P_{XR} N (lb.)	P_{XR} % D.U.L	P_{XL} N (lb.)	P_{XL} % D.U.L	P_Y N (lb.)	P_Y % D.U.L	Remarks
1	-34 785 (-7 820)	35 492 (7 979)	-34 701 (-7 801)	50	35 408 (7 960)	50	-4 906 (-1 103)	50	Preliminary Test – No Damage
2	-45 817 (-10 300)	53 379 (12 000)	-45 706 (-10 275)	66	53 250 (11 971)	75	-6 926 (-1 557)	71	Loaded to Design Limit – No Damage
3	-71 496 (-16 073)	74 699 (16 793)	-71 323 (-16 034)	103	74 517 (16 752)	103	-10 204 (-2 294)	104	Loaded to Design Ult. – No Damage
4	-171 701 (-38 600)	207 247 (46 591)	-171 283 (-38 506)	247	206 745 (46 478)	292	-26 454 (-5 947)	270	1 3
5	-171 701 (-38 600)	155 056 (34 858)	-171 283 (-38 506)	247	154 678 (34 773)	218	-22 806 (-5 127)	233	2

1 Intermittent loud popping noises starting at -102309N (-23 kip) level.

2 Specimen disassembled after final test. No visible damage other than the bent HLT 410-8 attachment pins.

3 Compression load cell bottomed out at 115654N (-26 kips). Post test analysis indicated, however, that a load of -171701N (-38.6 kips) had actually been applied.

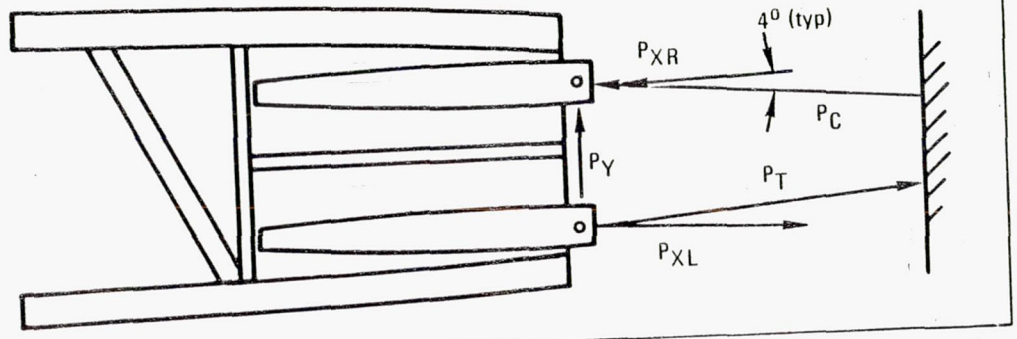

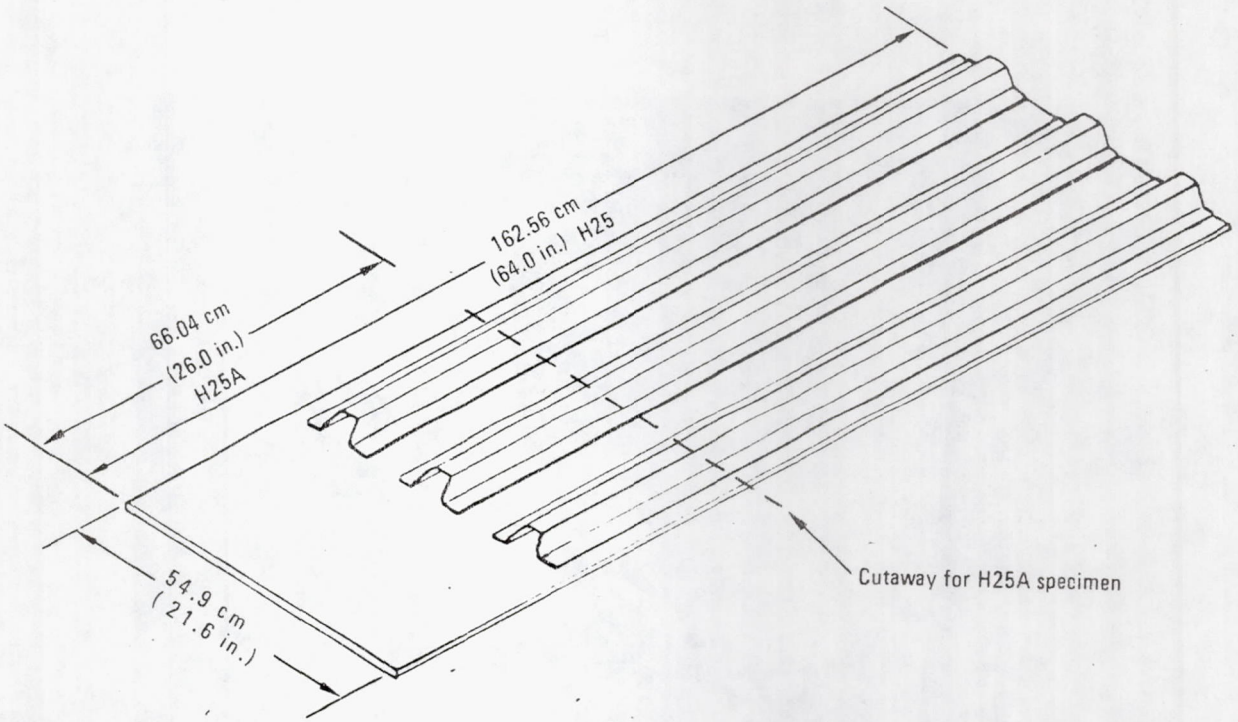

Figure 111. - Cover root end test specimens.

Test Specimen H25 was tested dry, at room temperature. The test panel was loaded three times prior to the final test. The loading sequence is summarized in table 44. Failure occurred at 364 354 N (81.91 kips) compression. The failure extended completely across the panel parallel to and about .038 m (1.5 in.) below the upper rib support (see figure 112). It should be noted that this upper rib support (at Station 51.72) actually appears at the bottom of the figure since the panel was station installed in the machine in an upside-down position.

TABLE 44. - H25 LOADING SEQUENCE

Test Seq.	Loads Applied	Comments
(1)	0 – 53 379N (0 – 12 kips)	To check gage polarity and initial slope of LVDT-generated deflection curves.
(2)	0 – 133 447N (0 – 30 kips)	To check out shadow moire setup and to determine secondary slope of deflection curves.
(3)	0 – 255 773N (0 – 57.5 kips)	Load increased to design ultimate, in 44 482N (10 kips) increments, then reduced to 44 482N (10 kips).
(4)	44 482 – 364 354N (10 – 81.91 kips)	Panel loaded to failure at approximately 13 345N/second (3 kips/second).

Figure 112. - Closeup of cover root end specimen failure.

The shadow moire' pattern at 360 306 N (81 kips) is shown in figure 113. In general, there was a slightly unsymmetrical skin buckling pattern which was compatible with the geometry of the test panel. The maximum skin buckling between stiffeners was approximately 2.54 mm (0.1 in.) inward (toward the stiffener side).

5.7.2 Tension test (H25A). - The purpose of this test was to verify the static strength of the fin to fuselage joint. This test was proposed as a result of the inadequacy of test H25 to satisfy the above objective. The specimen consisted of the lower, undamaged portion of the H25 specimen (see figures 114 and 115).

The following two tension tests were conducted on Test Panel H-25A under normal room temperature and laboratory air conditions: (A) A preliminary loading from zero the design limit of 226 859 N (51 kips) was applied in order to check out the loading system, the reaction structure, and the gages. (B) The panel was loaded from zero to failure at a loading rate of approximately 6 672 N/s (1.5 kips/sec).

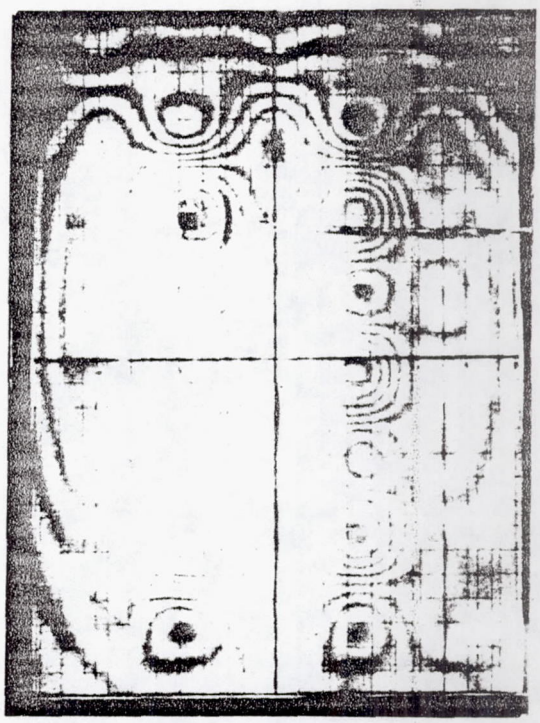

Figure 113. - Shadow moire pattern at 360 306 N (81 kips).

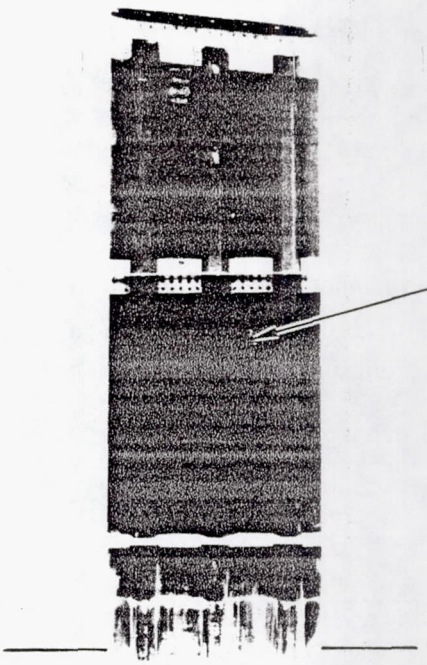

Figure 114. - Compression panel following failure
Loading fixtures have been removed.

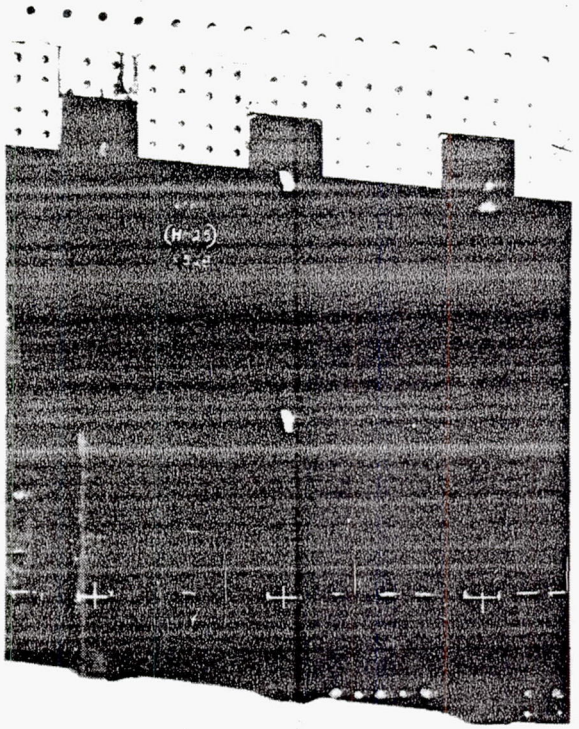

Figure 115. - Closeup of root end tension test segment after removal from the compression panel.

The joint failed in tension at 985 281 N (221.5 kips) or 286 percent of design ultimate, along the upper edge of the tapered splice plate at the first row of fasteners. Figure 116 shows an enlarged view of the root-end joint area failure.

5.8 Stiffener Runout at Front Spar Tests (H26)

The objective of this program was to verify the static and fatigue strength of the stiffener runout at the front spar.

The test article was a single hat stiffened panel with runout arrangement typical for that at the front spar. Two articles were build; one (H26A) for static testing and the second (H26B) for fatigue testing.

5.8.1 Static test (H26A). - The purpose of this test was to verify the static strength of the stiffener runout at the front spar under extreme environmental conditions. The test was designed to demonstrate the capability of the stiffener runout to carry ultimate load at both 219 K (-65°F) and 355 K (180°F) with high humidity. Figure 117 shows the test specimen mounted in the tensile machine, surrounded by the environmental chamber.

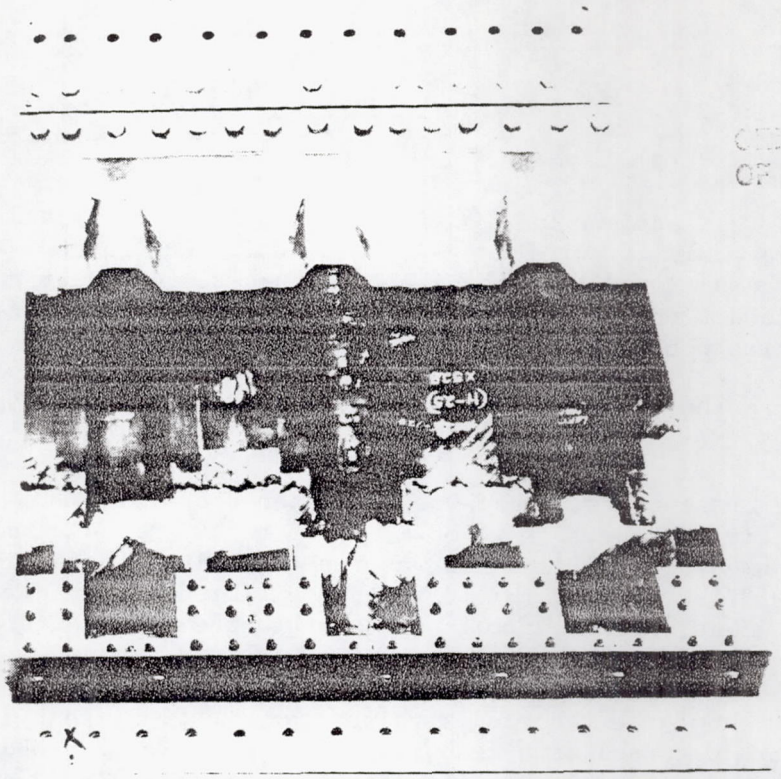

Figure 116. - Closeup of failed tension panel after removal from test fixture.

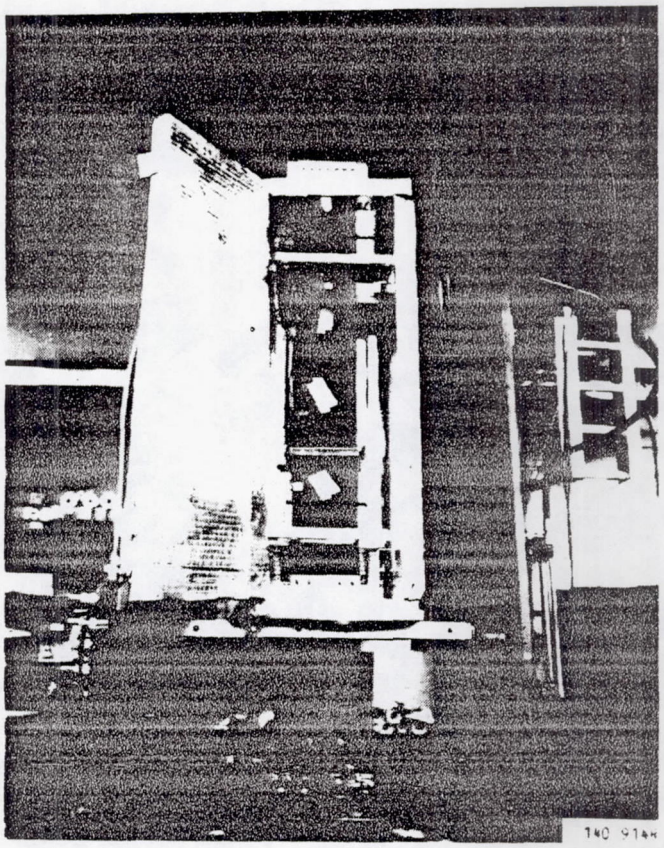

Figure 117. - Stiffener runout specimen in environmental chamber.

The static test article was conditioned at 339K (150°F) and 95 - 100 percent relative humidity for 16 days. Moisture pickup in the skin was 1 percent. This preconditioned test specimen was then tested under two different environmental conditions to design ultimate load without evidence of failure. The first test was conducted at 219 K (-65°F) with the specimen loaded in tension to 67 257 N (15,120 lb). The second test was conducted at 355K (+180°F) at 95 to 100 percent relative humidity, with the specimen loaded in tension to 67 257 N (15,120 lb).

In both of these tests, there was no evidence of failure. The specimen was again subjected to the 355K (+180°F) at 95 to 100 percent relative humidity environmental condition and was run to failure in tension. Failure occurred at 109 871 N (24,700 lb) or 163 percent of design ultimate load. Failure initiated at a fastener hole adjacent to the rib. Figures 118 and 119 show the failure from both the hat and skin sides.

Figure 120 shows the recorded strains near the front spar just prior to failure. Failure occurred at a measured stress level of 286 MPa (41,500 psi). The average notched allowable strength for this laminate is 292 MPa (42,400 psi).

5.8.2 Fatigue test (H26B). - The objective of this test was to verify the durability of the stiffener runout at the front spar, and to obtain the residual static strength after two lifetimes of fatigue loading.

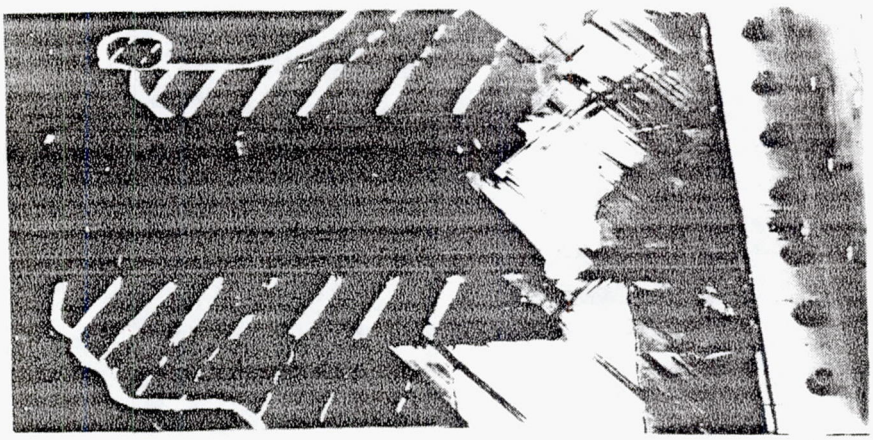

Figure 118. - Closeup of H-26A failed area as viewed From the hat side of the specimen.

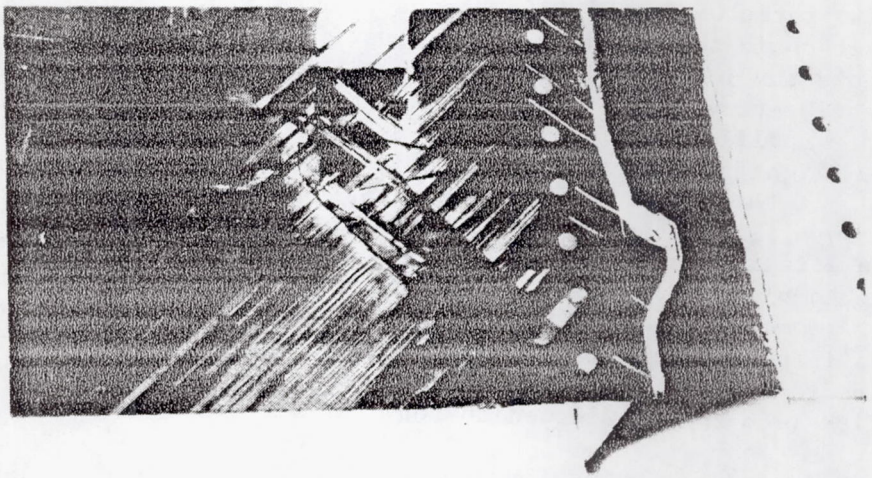

Figure 119. - Closeup of stiffener runout failed area as viewed from the skin side.

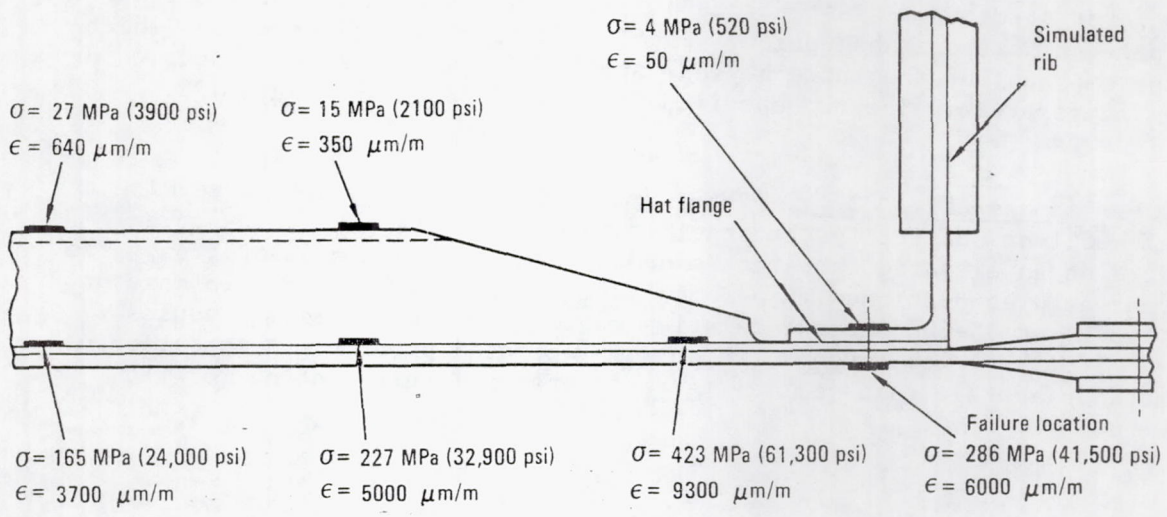

Figure 120. - Stress and strain levels at failure load stiffener runout.

A load spectrum equivalent to two lifetimes (72 000 flights) was randomly applied at a stress ratio of R = -1.0. The spectrum is shown in table 45. The spectrum is set up in two portions. The first is the 1800 flight tape. This tape represents the loads applied in every flight (1), and the loads which occur less frequently every 36, 360 and 1800 flights. Thus in one lifetime these load sets are applied 36,000, 1000, 100 and 20 times respectively. The loads in the 1800 flight tape are fully randomised so that it is possible for a 360 flight load set to occur in two consecutive flights. The second portion is the growth flight tape which contains the highest loads that occur only 4 times in a lifetime or less. These loads are applied after 36,000 flights have been completed from the 1800 flight tape. The fatigue test was conducted dry, at room temperature. At the end of the 72 000 flights, the test specimen was inspected visually and no external damage was apparent. Next, an environmental chamber was placed about the panel. The temperature was lowered to 219K (-65°F) and allowed to soak for one hour.

The panel was loaded to failure in tension, which occurred away from the joint, at 90 082 N (21,600 lb) or 143 percent design ultimate load. The failure was a combination tension failure (across the skin) and shear failure (between the hat and the skin). Figure 121 shows the failed surface after the residual test.

5.9 Surface Panel Stability Tests (H27)

The purpose of these tests was to verify the static compressive strength of the cover structure. Test H27 is a 3-bay test at an elevated temperature and 1 percent moisture absorption. Panel H27A is a two bay specimen, which is a subcomponent of the three bay H27 specimen. Test H27A was conducted dry, at room temperature. The two specimens are illustrated in figure 122.

5.9.1 3 bay test (H27). - The purpose of this test was to determine the initial buckling and verify the static compression strength of the cover structure at an elevated temperature and 1 percent moisture absorption. The specimen was preconditioned in a Bemco Environmental Chamber for 18 days at 339K (150°F) at 95-100 percent relative humidity prior to test. Results obtained from traveler coupons, which were weighted prior to preconditioning, indicated an average gain of 1.01 percent total moisture content for the panel.

TABLE 45. - FATIGUE TEST SPECTRUM

% Limit Load	N	ΣN	1800 Flight Tape				Growth Flight Tape		
			1	36	360	1 800	9 000	18 000(1)	36 000(2)
15	166 000	197 020	4	22					
23	24 860	31 020		24	8	3			
31	4 328	6 160		4	3	1	2		
38	1 279	1 832		1	2	3	4	1	1
46	328	553			3	1	2		
54	134	225			1	1	3	1	
62	43	91				2		1	1
69	28	48				1	2		
77	9	20					2		1
81	3	11						1	1
85	3	8						1	1
88	3	5						1	1
92	1	2							1
100	1	1							
Cycle Count			4	51	17	12	15	6	8
Multiplier			36 000	1 000	100	20	4	2	1

(1) The 18000th growth flight tape includes the 9000 growth flight cycles (21 total cycles).

(2) The 36000th growth flight tape includes the 9000th and 18000th growth flight cycles (29 total cycles).

The panel was tested, at 335K (180°F) with 95-100 percent relative humidity, in two parts. First the panel was loaded up to design ultimate load of 258 442 N (58,100 lb), which showed some initial buckling in the skin at 240 120 N (54,000 lb) of compressive load. Next, the panel was tested to failure which occurred at 311 376 N (70,000 lb) or 120 percent of ultimate load. Failure occurred in the lower bay of the 3 bay panel. Examination of the panel indicated that a skin/hat separation had occurred with subsequent rapid failure of the hats and skins (see figure 123).

The remaining undamaged portion of the panel was ultrasonically inspected and determined to be suitable for retesting as a 2-bay panel. This smaller panel became H27-A and was tested to provide additional information under compressive loading.

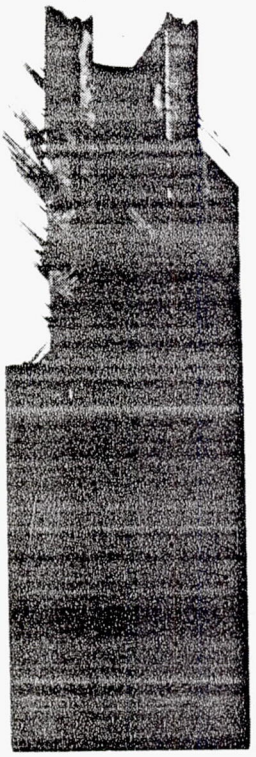

Figure 121. - H26B failed surface.

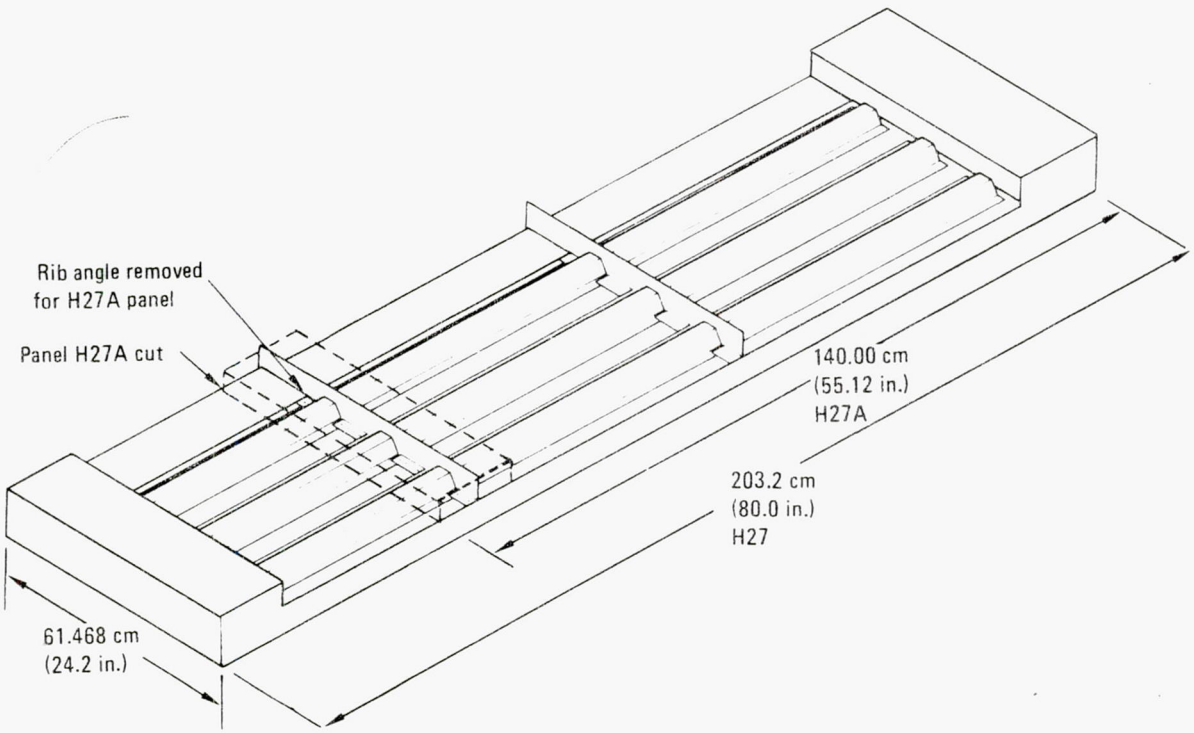

Figure 122. - Schematic of stability test specimens.

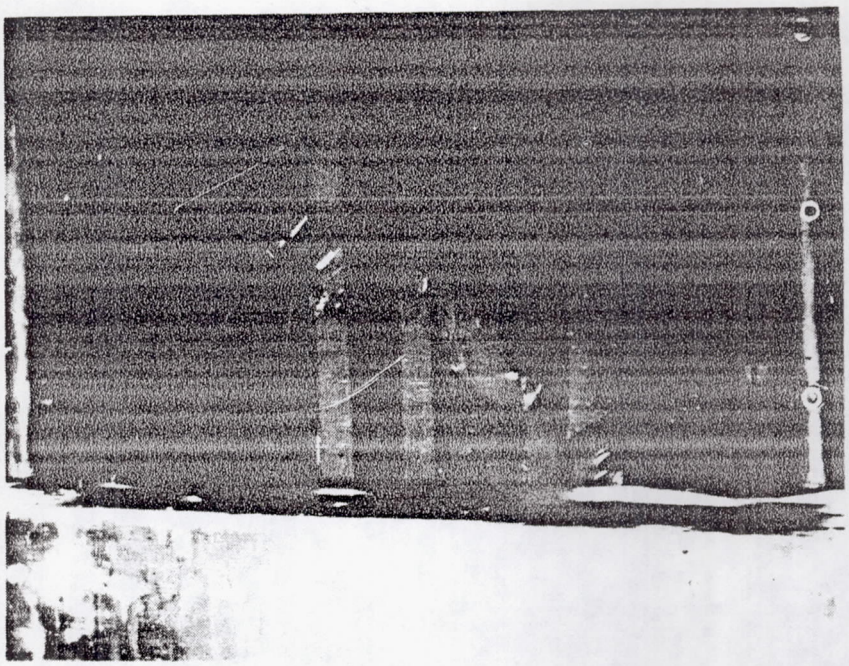

Figure 123. - H27 failed specimen.

5.9.2 2 bay test (H27A). - The purpose of this test was to verify both the static compressive strength and stability of a 2-bay, 3-hat graphite epoxy surface panel containing a single rib attachment. This test was conducted dry, at room temperature. There were two test sequences conducted. During the first test run, the specimen was loaded (in compression) in 44 482 N (10,000 lb) increments up to design unit load of 169 477 N (38,100 lb) and to design ultimate load of 258 442 N (58,100 lb).

In the second test run, the specimen was loaded to failure at a rate of approximately 133 447 N/min (30,000 lb/min). Failure occurred at 363 277 N (81,668 lb) or 141 percent of design ultimate load, in the upper bay adjacent to the potted end. The failure is shown in figure 124.

The test results showed that some initial buckling occurred at approximately 249 100 N (56,100 lb) load, although one buckle did occur at 174 370 N (39,200 lb). This one buckle did not show any further rapid divergence beyond the initial buckling up to the failing load. Figure 125 shows the moiré pattern of skin deformation 356 730N (80,200 lb), 138% DUL just prior to failure.

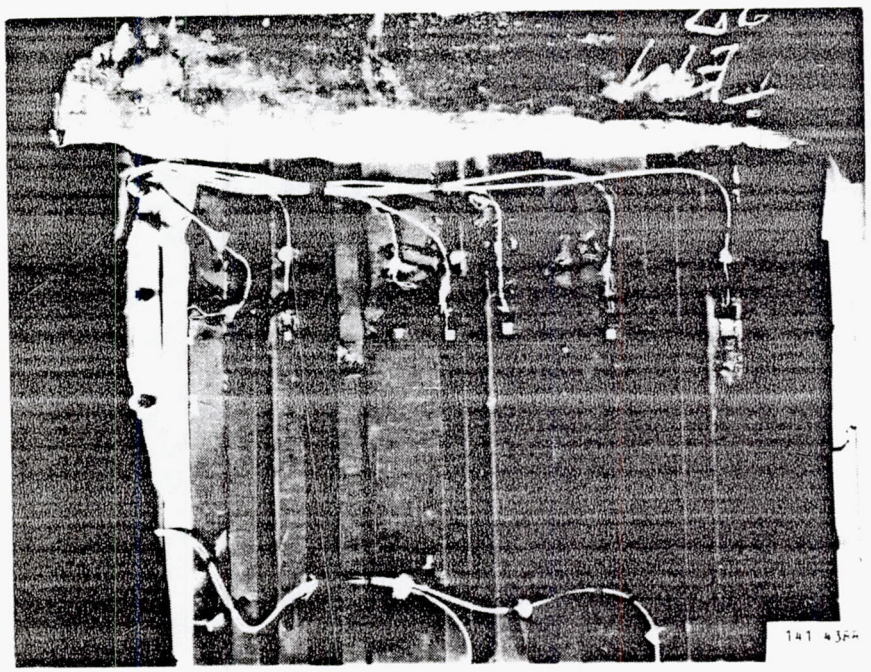

Figure 124. - H27A failed specimen.

5.10 Surface Panel Fail-Safe Test (H28)

The purpose of this test was to establish the crack propagation rates and fail-safe features of the hat-stiffened cover design. The specimen consisted of a panel with five stiffeners and covers, 15 three rib bays in length and is shown in figure 126.

Endurance testing to the surface panel was a completely reversed type of loading with a strain range ratio of R = -1.0. Endurance loads were applied to the test specimen by means of a closed loop electro-hydraulic servo system. Programming of the test loads was accomplished by a pre-recorded magnetic tape system operating through a servo controller. The servo controller provides the output analog signals to drive the hydraulic servo valve. The hydraulic servo valve meters the high pressure hydraulic fluid to the appropriate hydraulic actuator ports, thereby loading the test specimen. A load cell in the hydraulic actuator loading train provides the feedback signal to the servo controller to match the pre-recorded programming signals. The prerecorded magnetic tape contains all the loading cycles in 1800 flights and is programmed as shown in table 45. A second separate

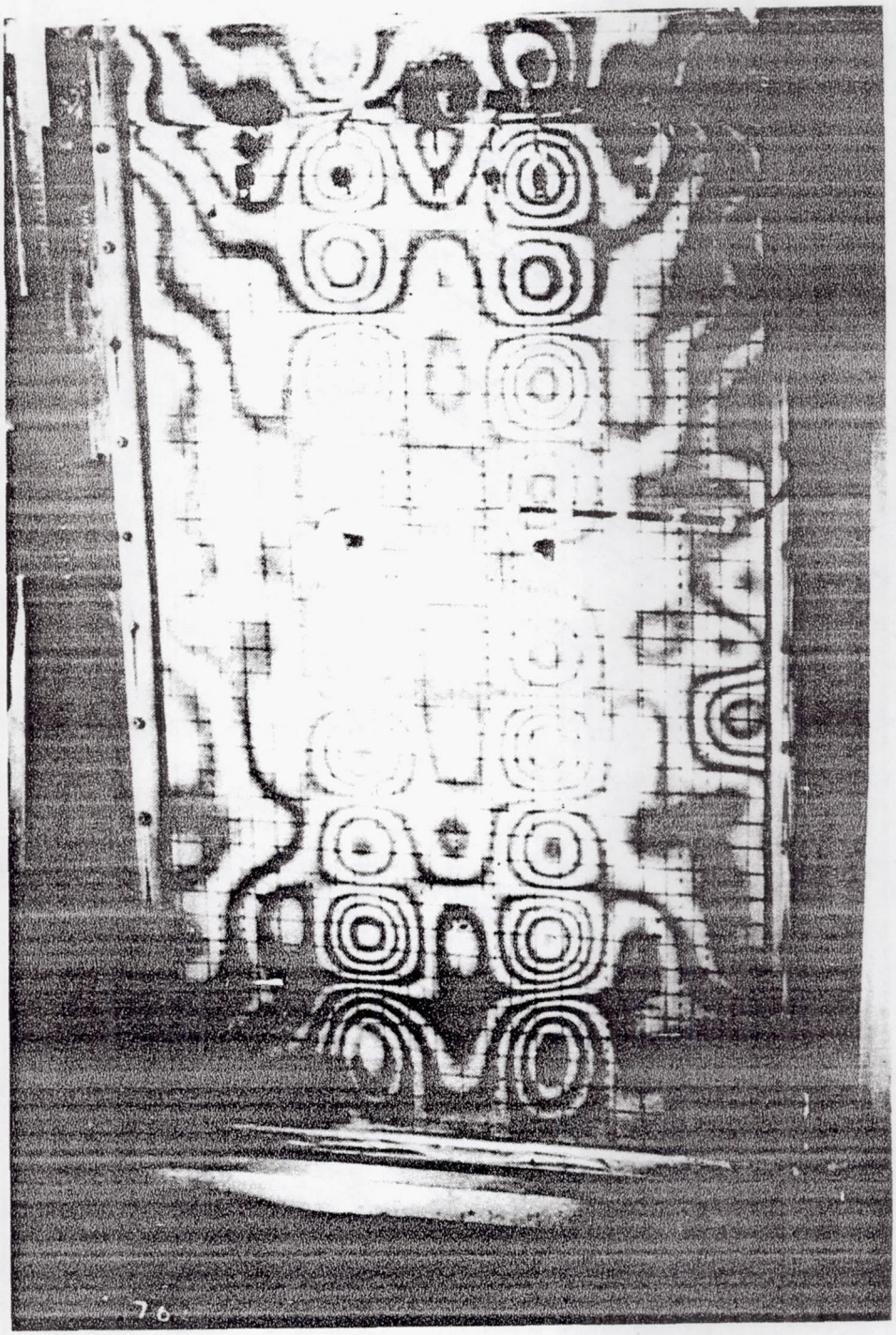

Figure 125. - Moiré pattern of skin deformation at 138% DUL 356 730N (80,200 lb) compression load just prior to failure.

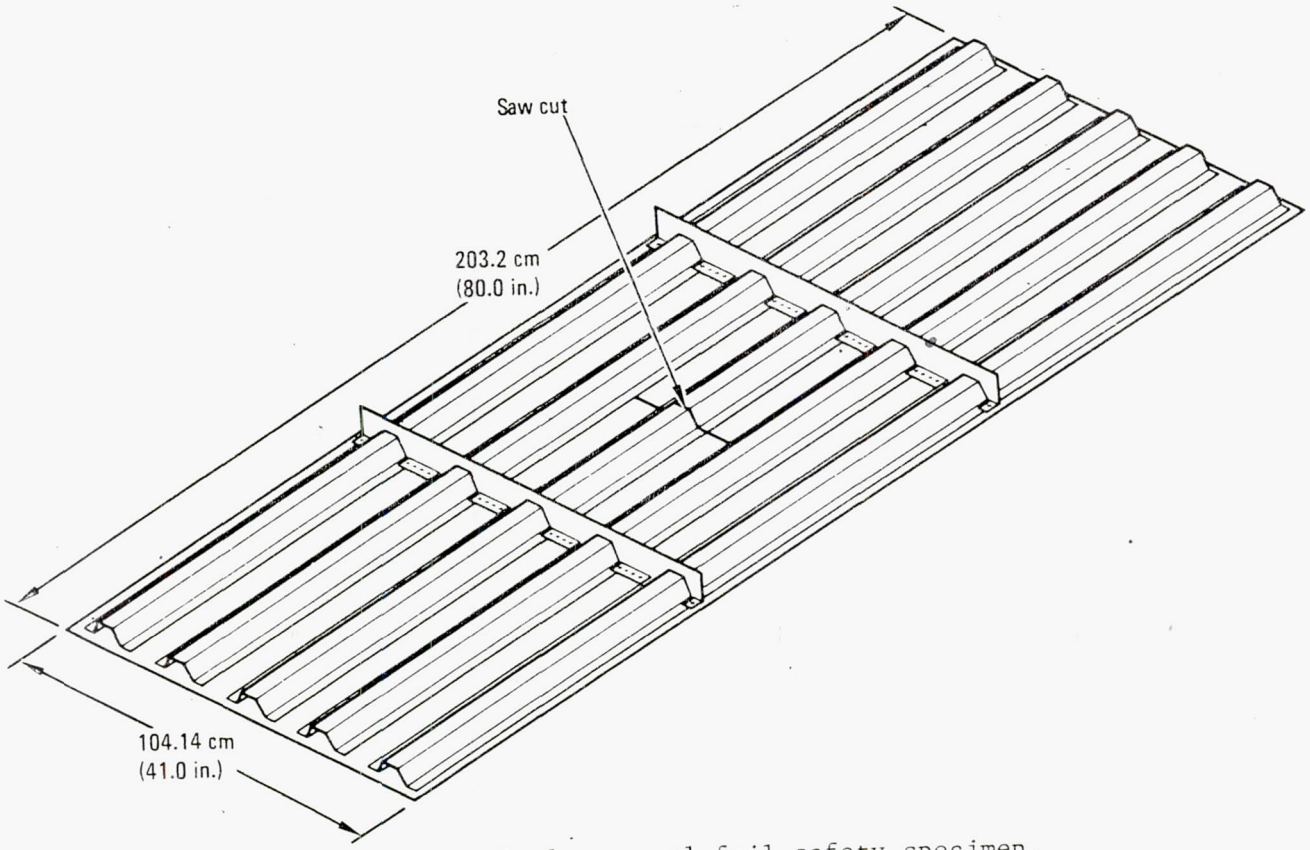

Figure 126. - Surface panel fail safety specimen.

magnetic tape contains the pre-recorded 9 000, 18 000 and 36 000 growth flight loading cycles. The growth flight loading cycles both in magnitude and quantity are also shown in table 45. These tapes are played back through the servo system in the proper order to produce the desired test loading history spectra.

An initial saw cut was made in the skin only under the center hat section of the panel. This saw cut was 6.223 cm (2.45 in.) in length and is shown schematically in figure 127.

The following section details the significant occurrences of each segment of the 1-1/2 lifetimes of endurance testing:

- Flight Interval 0-9 000 - During this flight interval no crack growth was observed.

- Flight Interval 9 000 + Growth (1/4 Lifetime) - A portable ultrasonic NDI inspection was accomplished adjacent to the saw cut ends prior to application of the growth flight cycles. The growth flight cycles (29 total), including the maximum cycle up to limit load, were applied to the specimen and no damage was noted. A post test portable NDI ultrasonic inspection was conducted and confirmed the observed results. The saw cut was extended out to 0.088 m (3.45 in.) to include the flange element of the hat section (see figure 126).

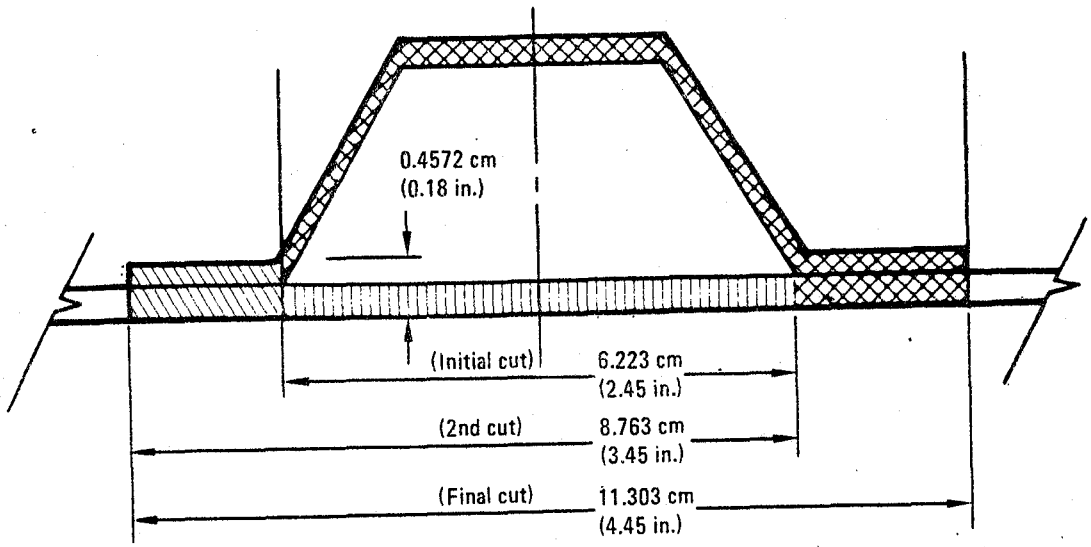

Figure 127. - Cross section of hat/skin elements showing The areas cut during the test.

- Flight Interval 9 000 - 18 000 - During this flight interval, two small hairline cracks occurred at the end of the saw cut in the hat flange-to skin transition area fillet. These cracks did not grow after they developed and were attributed to the fillet as being a strain-rich area. No other cracking was observed during this period.

- Flight Interval 18 000 + Growth (One-half lifetime) - Portable ultrasonic inspection techniques were used prior to, and after, the application of the basic 18 000 flights. During the application of the final cycles of the growth flight, a loud, sharp report was heard. The testing was not stopped at this point and was allowed to complete the load application. The post-test inspection revealed an approximately 9.5 mm (3/8 in.) crack/delamination area had occurred in the hat sidewall stemming from one corner of the saw cut. No external damage in that area was observed.

- Flight Interval 18 000 - 27 000. - During this flight interval, the hat sidewall damage extended to the crown area of the hat. This occurred in the span of 3 600 flights (21 600 flights total) and was approximately 33 mm (1.3 in.) in length. The propagation did not extend beyond the hat crown and little or no growth was observed for the remaining 5 400 flights (27 000 flights total).

- Flight Interval 27 000 to 36 000. - During this flight interval, little or no extension of crack was observed on the hat sidewall. The hat crown successfully arrested the sidewall crack growth for over one-quarter lifetime of 14 400 flights. At the end of 26 000 flights, the specimen again was ultrasonically inspected using the portable equipment. A previously reported hat flange-to-skin delamination area now indicated that no delamination was present. A smaller diameter probe was used and this indicated that no delamination was present. The previously used larger diameter probe was picking up the hat flange-to-skin transition area and thereby giving a false indication of delamination. The NDI inspection of the hat sidewall indicated approximately 2.54 mm (0.1 in.) of additional growth beyond the areas defined by using a surface "tapping" method. The total true length of the sidewall crack is approximately 35.6 mm (1.4 in.) long.

- Flight Interval 36 000 to 45 000. - After completion of the ultrasonic inspection at 36 000 flights the saw cut was extended through the remaining hat flange and skin area out to .11 m (4.45 in.) total length. In addition, the two sidewalls and hat crowns were also severed. This completely removed the center hat element and skin section from being loaded during the subsequent testing. This additional cut is shown schematically in figure 126. Testing proceeded without incident for the additional one-quarter lifetime with no evidence of crack initiation or growth.

- Flight Interval 45 000 to 54 000. - During this flight interval at 46 800 flights, a crack developed, starting from one corner of the saw cut and progressing along the 45° ply. This crack started on the hat side of the panel. This crack grew rapidly during the course of the 1800 flights to a length of 10.1 mm (.40 in.) long. A second crack, running parallel to the first crack, also developed and rapidly grew to 6.35 mm (0.25 in.) long. After an additional 3600 flights, the crack growth had rapidly diminished to only approximately .51 mm (.02 in.) of additional length. No cracks had developed on the opposite side of the panel indicating that these cracks may have been in the surface plies only. Testing continued to a total of 54 000 flights without apparent increase in crack growth.

- Flight Interval 54 000 + Growth. - A portable NDI inspection was accomplished prior to the application of the maximum growth flight cycles. This inspection confirmed the cracks in the skin panel that developed at the 46 000 flight interval were only a surface ply delamination and the cracks did not extend through the skin.

  During the application of the maximum growth flight cycles, the panel failed during the compression portion of the cycle. During these load cycle applications, the limit load tension and compression are applied to the test panel. It was during the application of the maximum cycle that the panel failed in compression. The panel had

withstood 101 percent limit load in the tension portion of the cycle and the initial failure started at 92.8 percent (60 000 lb) and finally ruptured at 97 percent of limit load (-62 700 lb). The initial failure was caused by localized skin buckling in the vicinity of the intentional flaw. This local instability caused the skin to separate from the hat flange and subsequent rapid failure of the remaining section of the test panel.

5.11 Lightning Strike Tests (H29)

The purpose of these tests were to verify the resistance of the ACVF structure to a lightning sweep strike. The lightning strike tests were performed at Lightning and Transients Research Institute in St. Paul, Minnesota.

Two panels were tested. The first was used to investigate attachment effects and the second, larger panel, was tested in the wind tunnel for swept stroke and restrike effects. The panels are shown in figure 128.

Both stationary and swept lightning strike tests were carried out on the test samples and both test waveforms included: (a) an initial low continuing current, (b) a high rate of rise initial restrike current, and (c) a high current restrike component in combination with (d) an intermediate current typical of natural discharges to aircraft.

Figure 129 shows the damage from the second swept stroke test, which appeared to be the worst case. The damage appeared in all cases to extend only a few layers into the panel and no damage was detected on the backside of the panel. The panels have been ultrasonically inspected and there is no damage detectable outside the areas of visual damage.

6. CONCLUSIONS

An advanced composite vertical fin has been designed which has met the requirements of the contract. The fin box is at least 20% lighter than the metal box, in fact 27.4%. At least 40% by weight of the constituent parts had to be fabricated from advanced composite materials. In fact 78.3% of the box is fabricated from graphite/epoxy material.

The Producibility Study and the process development has lead to a highly producible design. The cost-effectiveness will be verified in Phase IV.

The test program has verified the structural integrity of the design concepts selected and the analysis methods used in the design.

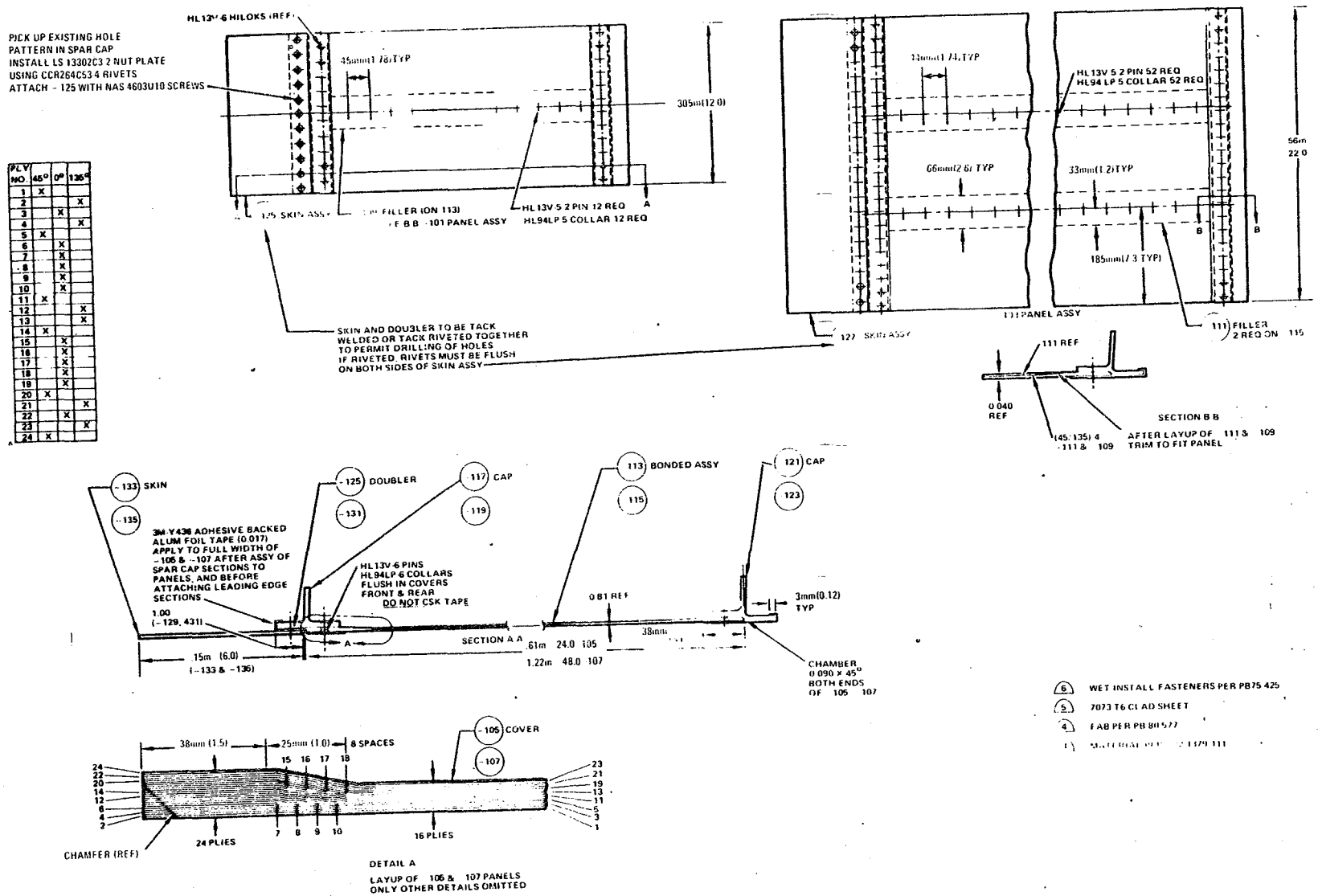

PLY NO.	45°	0°	135°
1	X		
2			X
3		X	
4			X
5	X		
6		X	
7		X	
8		X	
9		X	
10		X	
11	X		
12			X
13			X
14	X		
15		X	
16		X	
17		X	
18		X	
19		X	
20	X		
21			X
22		X	
23			X
24	X		

Figure 128. - H29 lightning strike test panels.

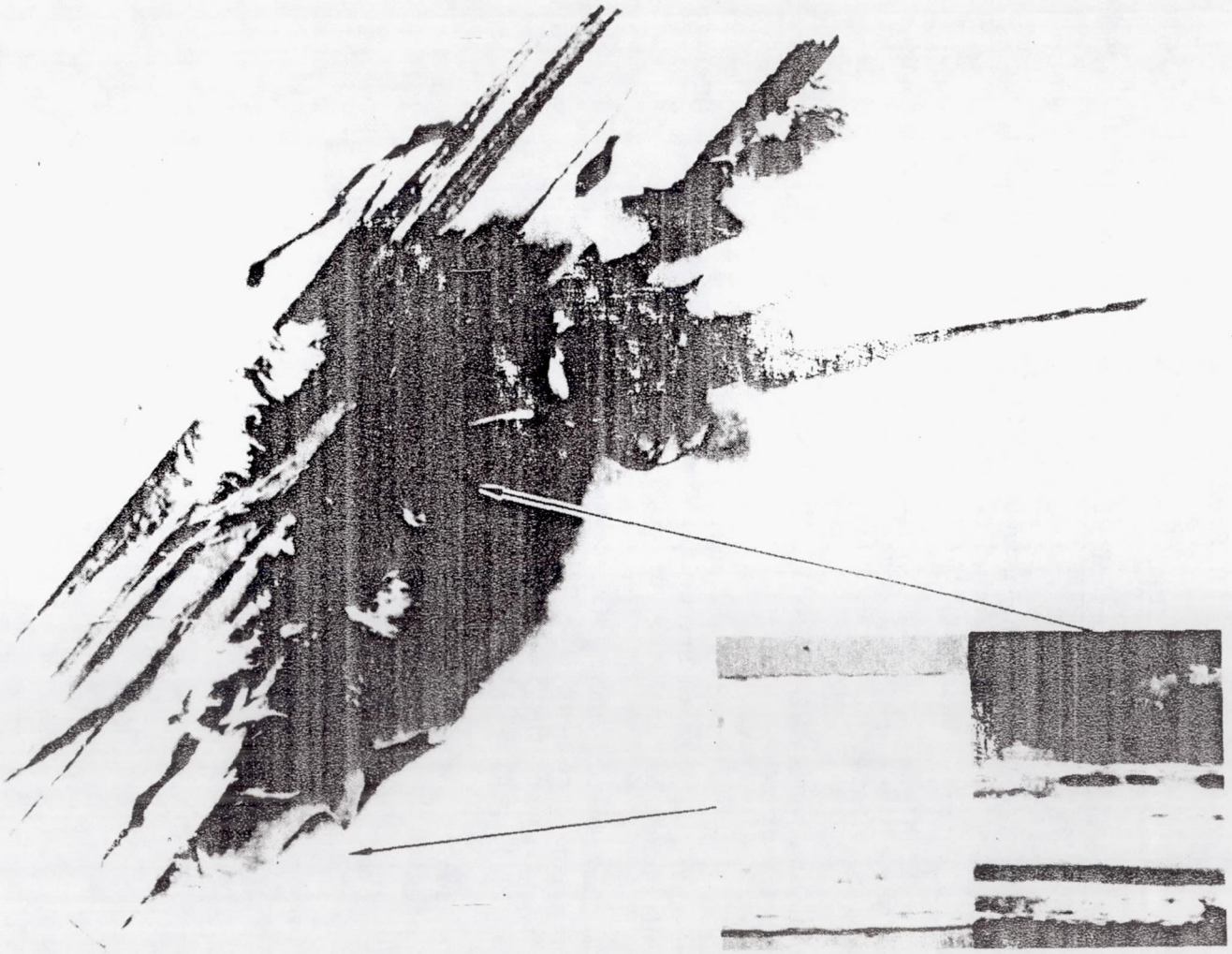

Figure 129. - Surface damage from swept stroke test, and section photographs.

REFERENCES

1. NASA CR-144986 Phase I - Final Report, Engineering Development, May 1976.

2. Timoshenko and Gere, Theory of Elastic Stability, McGraw Hill Second Edition, 1961.

3. "Military Standardization Handbook, Metallic Materials and Elements for Aerospace Vehicle Structures," MIL-HDBK-5C, Volumes 1 and 2 including changes dated 15 December, 1978.

4. Anderson, M.S.; Hennessy, K.W.; Heard, W.L. Jr.; "Addendum to Users Guide to VIPASA; NASATM X-73914, June 1976.

The following papers were written based on the work conducted during this phase of the program:

Jackson, A.C.; "Design and Analysis of L-1011 Composite Fin Covers," presented at SME 4th Structural Composite Manufacturing Applications Conference, Los Angeles June 1978.

Van Hamersveld, John: "Extensive Cost Reduction Studies - Composite Empennage Component - L-1011 Commercial Airliner," Science of Advanced Materials and Process Engineering Series Vol. 23 SAMPE, Anaheim CA May 1978, pgs. 94 thru 112.

Jackson, A.C.; "Development of Graphite Epoxy covers for L-1011 Advanced Composite Vertical Fin," National SAMPE Technical Conference Series Vol 12, "Materials 1980" Seattle WA, pgs. 414 thru 423, Oct 1980.

Van Hamersveld, John; "Process Development - Cocured Composite Empennage Cover - Utilizing Low Resin Content Graphite Material," presented at the SAMPE Technical Conference Seattle, WA, Oct 1980.

APPENDIX

Allowables Test Specimen Configurations

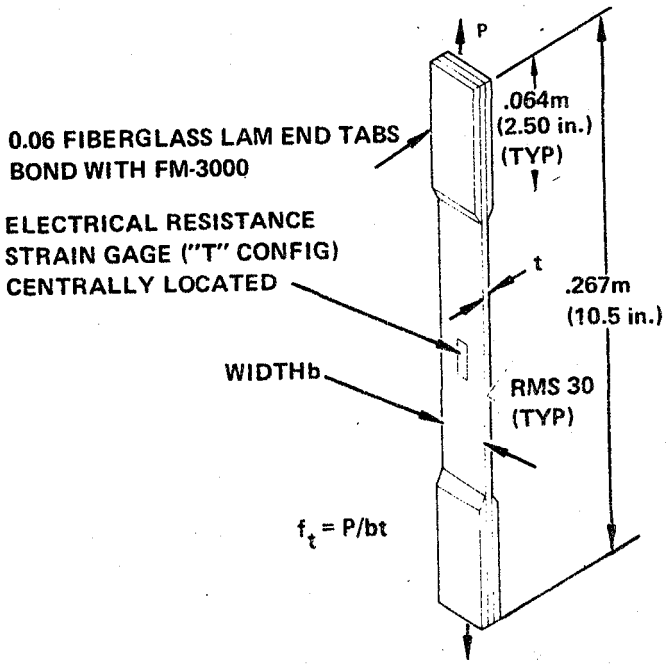

NOTE *

b = 12.7mm (0.5 in.) FOR UNIDIRECTIONAL TENSION SPECIMEN
b = 25.4mm (1.0 in.) FOR CROSSPLY TENSION AND COMPRESSED SPECIMENS

FIGURE A1. CROSSPLY TENSION AND COMPRESSION AND UNIDIRECTIONAL TENSION COUPON

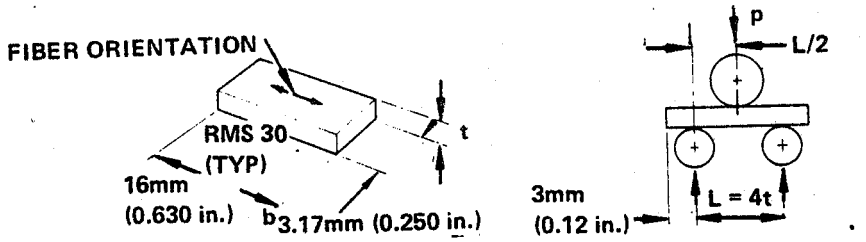

FIGURE A2. 0° INTERLAMINAR SHEAR TEST

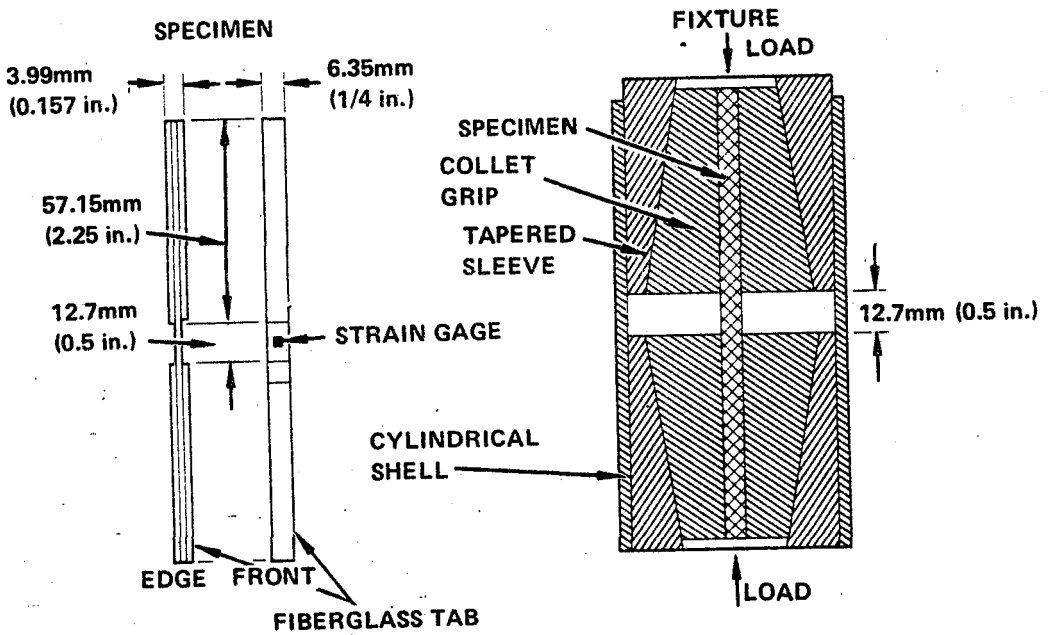

FIGURE A3. CELANESE COMPRESSION TEST SPECIMEN AND FIXTURE

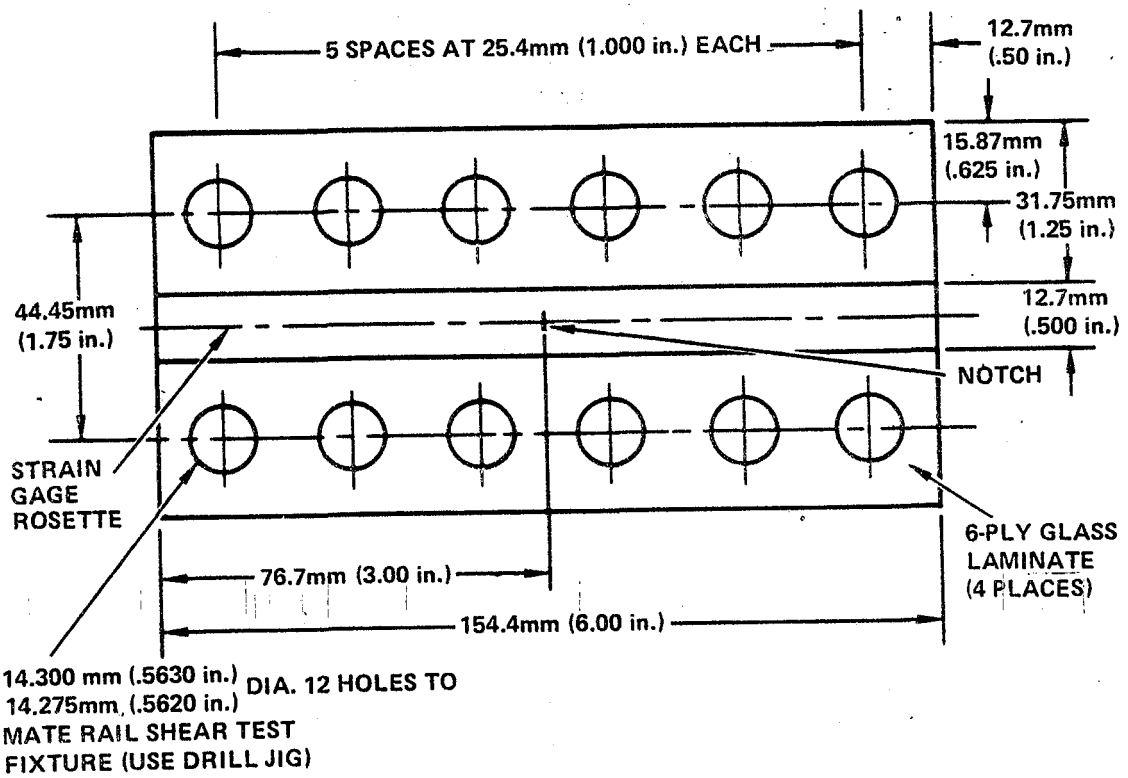

FIGURE A4. IN-PLANE SHEAR SPECIMEN

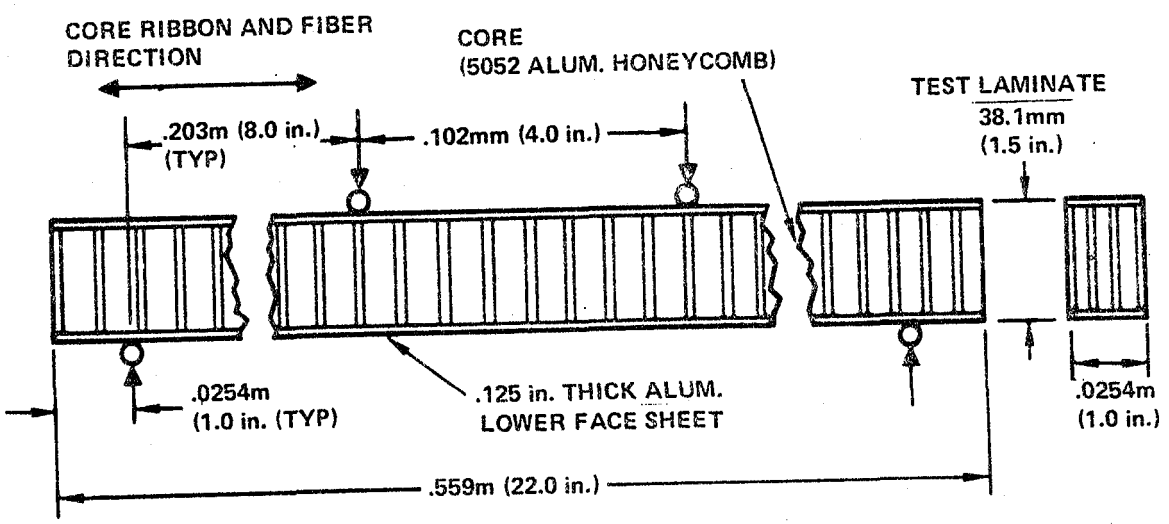

FIGURE A5. SANDWICH BEAM COMPRESSION TEST